Technische Universität München
TUM School of Engineering and Design

The carbon footprint of stationary lithium-ion battery energy storage systems

Anupam Gajanan Parlikar, M.Sc.

Vollständiger Abdruck der von der TUM School of Engineering and Design der Technischen Universität München zur Erlangung des akademischen Grades eines

Doktors der Ingenieurwissenschaften (Dr.-Ing.)

genehmigten Dissertation.

Vorsitz:		Prof. Dr. sc. Marcelo Lobo Heldwein
Prüfende der Dissertation:	1.	Prof. Dr.-Ing. Andreas Jossen
	2.	Prof. Dr. rer. nat. Holger Hesse
	3.	Prof. Dr.-Ing. Ulrich Wagner

Die Dissertation wurde am 30.10.2024 bei der Technischen Universität München eingereicht und durch die TUM School of Engineering and Design am 25.02.2025 angenommen.

Abstract

The viability of modern human civilization is incumbent on our ability to harness energy to fulfill various needs. Breaking away from millennia of reliance on carbonaceous energy sources is crucial to avoid anthropogenic global warming. Decarbonization is a gradual transition to renewable energy sources, which are essentially emissions-free in their operation phase. The intermittency of power generation from renewable energy sources inevitably requires flexibility in the energy system - especially in the electricity grid. Energy storage is an indispensable flexibility measure to achieve high renewable energy penetration and its effective integration. Electricity is the most versatile energy vector, making electrical energy storage an important part of the solution. Lithium-ion Battery Energy Storage System (BESS) technology is the forerunner among commercialized energy storage technologies. It is imperative that the carbon footprint of this technology and its decarbonization potential across all its lifecycle phases be quantifiable and known. In this thesis, a comprehensive and consistent mathematical framework to quantify the carbon footprint of energy storage applications is developed. Open-source python-based simulation programs Energy System Network (ESN) and Simulation of Stationary Energy Storage Systems (SimSES) have been developed and co-developed in this thesis to implement this framework. This framework enables the quantification of the carbon footprint of energy storage applications, the efficient allocation of energy storage capacity, and its emissions-optimal operation, among other functions. This is demonstrated through the case studies performed in this thesis.

Kurzfassung

Die Lebensfähigkeit der modernen Zivilisation hängt von unserer Fähigkeit ab, Energie zu nutzen. Um die anthropogene globale Erwärmung zu vermeiden, ist es entscheidend, von kohlenstoffhaltigen Energiequellen abzurücken. Der Übergang zu erneuerbaren, emissionsfreien Energiequellen ist ein schrittweiser Prozess. Aufgrund der Unregelmäßigkeit der erneuerbaren Stromerzeugung ist Flexibilität im Energiesystem, insbesondere im Stromnetz, notwendig. Energiespeicherung ist entscheidend für die Integration und Nutzung erneuerbarer Energien. Die elektrische Energiespeicherung, insbesondere die Lithium-Ionen-Batteriesysteme (BESS), spielt eine zentrale Rolle. Es ist wichtig, den CO_2-Fußabdruck dieser Technologie und ihr Dekarbonisierungspotenzial zu kennen. Diese Arbeit entwickelt ein mathematisches Rahmenwerk zur Quantifizierung des CO_2-Fußabdrucks von Energiespeicheranwendungen. Die Open-Source-Simulationsprogramme Energy System Network (ESN) und Simulation of Stationary Energy Storage Systems (SimSES) wurden hierfür entwickelt. Dieses Rahmenwerk ermöglicht die Quantifizierung des CO_2-Fußabdrucks, die effiziente Allokation von Speicherkapazitäten und deren emissionsoptimierten Betrieb, wie die Fallstudien in dieser Arbeit zeigen.

Contents

List of Publications

Peer-reviewed journal paper contributions (lead author)

a Parlikar, A.; Troung, C.N.; Jossen, A.; Hesse, H.: *The carbon footprint of island grids with lithium-ion battery systems: An analysis based on levelized emissions of energy supply*, in: *Renewable and Sustainable Energy Reviews (149)*, doi.org/10.1016/j.rser.2021.111353, 2021

b Parlikar, A.; Schott, M.; Godse, K.; Kucevic, D.; Jossen, A.; Hesse, H.: *High-power electric vehicle charging: Low-carbon grid integration pathways with stationary lithium-ion battery systems and renewable generation*, in: *Applied Energy (333)*, doi.org/10.1016/j.apenergy.2022.120541, 2023

c Parlikar, A.; Tepe, B.; Möller, M.; Hesse, H., Jossen, A.: *Quantifying the carbon footprint of energy storage applications with an energy system simulation framework - Energy System Network*, in: *Energy Conversion and Management (304)*, doi.org/12.3456/en12345678, 2024

Self-written sections of peer-reviewed lead author journal paper contributions are partially contained in this doctoral thesis without further reference in the text.

Peer-reviewed conference paper contributions (lead author)

a Parlikar, A.; Hesse, H.; Jossen, A.: *Topology and Efficiency Analysis of Utility-Scale Battery Energy Storage Systems*, in: *Atlantis Highlights in Engineering (4), 13th International Renewable Energy Storage Conference (IRES 2019)*, www.atlantis-press.com/article/125923324, 2019

b Parlikar, A.; Collath, N.; Tepe, B.; Hesse, H.; Jossen, A.: *The Lifetime Carbon Footprint of Lithium-Ion Battery Systems in Exemplary Applications*, in: *Energy Proceedings, 15th International Conference on Applied Energy (ICAE 2023)*, doi.org/10.46855/energy-proceedings-10893, 2023

Selection of conference contributions

a Parlikar, A.; Möller, M.; Hesse, H.; Jossen, A.: *Efficient and scalable system design for stationary battery energy storage systems*, in: *9th Energy Colloquium of the Munich School of Engineering: Shaping a Sustainable Energy Future*, Munich, Germany, Poster, 2019

b Parlikar, A.; Jossen, A.; Hesse, H.: *System Thermal Modelling of Utility-scale Stationary Battery Energy Storage Systems*, in: *12th Advanced Battery Power Conference*, Canceled due to COVID-19, Poster, 2020

c Parlikar, A.; Truong, C.N.; Jossen, A.; Hesse, H.: *Influence of Battery Energy Storage Systems on the Carbon Footprint of Energy Systems*, in: *10th Energy Colloquium of the Munich School of Engineering: Energy Research in Bavaria*, Online, Oral Presentation, 2020

d Parlikar, A.; Collath, N.; Hesse, H.; Jossen, A.: *Thermal Modelling of Utility Scale Stationary Battery Energy Storage Systems: Analysis of Energetic and Environmental Performance*, in:

13th Advanced Battery Power Conference, Online, Poster, 2021

e Parlikar, A.; Schott, M.; Kucevic, D.; Hesse, H.; Jossen, A.: *Battery-Assistance vs. Grid Reinforcement for High-Power EV Charging: An Emissions Perspective*, in: *11th Energy Colloquium of the Munich School of Engineering: Energy Sciences for Europe's Green Deal*, Online, Oral Presentation, 2021

f Parlikar, A.; Jossen, A.; Hesse, H.: *Quantifying the Decarbonization Potential of Energy Storage in the Energy Transition: Techno Environmental Modelling and Simulation of Energy Storage and Energy Systems*, in: *2022 LUCS & PACE Summer School: From Energy Systems to Energy Justice*, Sundvollen, Norway, Oral Presentation, 2022

g Parlikar, A.; Jossen, A.; Hesse, H.: *Stationary Battery Energy Storage Systems: Low-Carbon Integration Pathways in Grid Applications*, in: *16th International Renewable Energy Storage Conference (IRES) 2022*, Düsseldorf, Germany, Poster, 2022

h Parlikar, A.; Jossen, A.; Hesse, H.: *Quantifying the Decarbonization Potential of Energy Storage*, in: *6th Herbstworkshop "Energiespeichersysteme" der Technischen Universität Dresden*, Online, Oral Presentation, 2022

i Parlikar, A.; Collath, N.; Tepe, B.; Hesse, H.; Jossen, A.: *The Lifetime Carbon Footprint of Lithium-Ion Battery Systems in Exemplary Applications*, in: *15th International Conference on Applied Energy (ICAE) 2023*, Doha, Qatar, Oral Presentation, 2023

Peer-reviewed journal paper contributions (co-author)

a Kucevic, D.; Tepe, B.; Englberger, S.; Parlikar, A.; Mühlbauer, M.; Bolhen, O.; Jossen, A.; Hesse, H.: *Standard battery energy storage system profiles: Analysis of various applications for stationary energy storage systems using a holistic simulation framework*, in: *Journal of Energy Storage (28)*, doi.org/10.1016/j.est.2019.101077, 2020

b Möller, M.; Kucevic, D.; Collath, N.; Parlikar, A.; Dotzauer, P.; Tepe, B.; Englberger, S.; Jossen, A.; Hesse, H.: *SimSES: A holistic simulation framework for modeling and analyzing stationary energy storage systems*, in: *Journal of Energy Storage (49)*, doi.org/10.1016/j.est.2021.103743, 2022

Peer-reviewed conference contributions (co-author)

a Tepe, B.; Jablonski, S.; Parlikar, A.; Hesse, H.; Jossen, A.: *Vehicle-to-X service provision for various modes of e-transportation with consideration of the influence on lithium-ion battery utilization*, in: *Energy Proceedings, International Conference on Applied Energy (ICAE 2023)*, doi.org/10.46855/energy-proceedings-10897, 2023

Abbreviations

Please note that the list below is based on the main part of this thesis and does not fully cover the abbreviations used in the papers. Each paper itself includes an individual list.

AC . . . . Alternating Current

BA . . . . Battery-Assisted
BESS . . . . . . Battery Energy Storage System
BMS . . . . Battery Management System
BOL . . . . Beginning-of-Life
BTM . . . . Behind-the-meter

CO_2 . . . . Carbon Dioxide

DC . . . . Direct Current
DOC . . . . Depth of Cycle
DOD . . . . Depth of Discharge

ECM . . . . Equivalent Circuit Model
EFC . . . . Equivalent Full Cycle
EMS . . . . Energy Management System
EOL . . . . End-of-Life
EPR . . . . Energy-to-Power Ratio
ESN . . . . Energy System Network
EV . . . . Electric Vehicle

FCR . . . . Frequency Containment Reserve
FTM . . . . Front-of-the-meter

GHG . . . . greenhouse gas
GR . . . . Grid Reinforcement
GWP . . . . . . Global Warming Potential

HPC . . . . High-Power Charging
HVAC . . . . . . Heating, Ventilation, Air Conditioning

LAM . . . . Loss of Active Material
LCA . . . . Life Cycle Analysis
LEC . . . . Load Energy Consumption

LEES . . . . . . Levelized Emissions of Energy Supply
LFP . . . . Lithium Iron Phosphate
LLI . . . . Loss of Lithium Inventory

OCV . . . . Open Circuit Voltage

PER . . . . Power-to-Energy Ratio
PV . . . . Photovoltaic Solar

SimSES . . . . . Simulation of Stationary Energy Storage Systems
SOC . . . . State of Charge
SOCI . . . . State of Carbon Intensity
SOE . . . . State of Energy
SOF . . . . State of Function
SOH . . . . State of Health
SOP . . . . State of Power
SOS . . . . State of Safety

TMS . . . . Thermal Management System

Formula Symbols

Please note that the list below is based on the main part of this thesis and does not fully cover the symbols used in the papers. Each paper itself includes an individual list.

CI_t^{ch} . . . . Carbon intensity of the charging energy at time t

CI_t^{ES} . . . . . . Effective carbon intensity of the available energy in the energy system at time t

$CI_t^{gen,i}$ . . . . . . Carbon Intensity of the i^{th} generation component at time t

CI_t^{gen} . . . . . . Carbon intensity for the generation component at time t

CI_t^{gr} . . . . Carbon Intensity of the grid component at time t

c_p^{batt} . . . . Specific heat capacity of the battery

c_p^{ia} . . . . Specific heat capacity of the internal air (ia)

E_{ch} . . . . Energy charged

E_{dch} . . . . Energy discharged

ε^{gen} . . . . Total emissions for the generation component

$\varepsilon^{gen,EOL}$ . . . . . End-of-life emissions for the generation component

$\varepsilon^{gen,exp}$ . . . . . . Export emissions for the generation component

$\varepsilon^{gen,op}$ . . . . . . Operation phase emissions for the generation component

$\varepsilon_t^{gen,op,i}$ . . . . . Operation phase emissions for the i^{th} generation component at time t

$\varepsilon^{gen,prod}$ . . . . . Production phase emissions for the generation component

ε^{gr} . . . . Total emissions for the grid component

$\varepsilon^{gr,EOL}$ . . . . . End-of-life emissions for the grid component

$\varepsilon^{gr,exp}$ . . . . . . Export emissions for the grid component

$\varepsilon^{gr,op}$ . . . . Operation phase emissions for the grid component

$\varepsilon_t^{gr,op}$ . . . . Operation phase emissions for the grid section at time t

$\varepsilon^{gr,prod}$ . . . . . . Production phase emissions for the grid component

ε^{LEC} . . . . Load Energy Consumption (LEC) emissions for the load component

$\varepsilon_t^{LEC,k}$ . . . . . . Load Energy Consumption emissions for the k^{th} load component at time t

ε^{load} . . . . Total emissions for the load component

$\varepsilon^{load,op}$ . . . . . . Operation phase emissions for the load component

$\varepsilon_t^{load,op,k}$ . . . . . Operation phase emissions for the k^{th} load component at time t

ε^{st} . . . . Total emissions for the storage component

E_n . . . . Nominal energy capacity

E_n^t . . . . Nominal energy capacity at time t

E_{st} . . . . Energy stored in storage medium

$\varepsilon^{st,EOL}$ . . . . . . End-of-life emissions for the storage component
$\varepsilon^{st,exp}$ . . . . . . Export emissions for the storage component
$\varepsilon^{st,op}$ . . . . Operation phase emissions for the storage component
$\varepsilon_t^{st,op,j}$ . . . . . . Operation phase emissions for the j^{th} storage component at time t
$\varepsilon^{st,prod}$ . . . . . . Production phase emissions for the storage component
E_t . . . . Energy content at time t
η_{ch} . . . . Charging efficiency
η_{dch} . . . . Discharging efficiency
$\eta_t^{gen,i}$ . . . . Efficiency of the i^{th} generation component at time t
η_{PE} . . . . Power conversion efficiency of power electronics
η_{rt} . . . . Roundtrip efficiency

f_L . . . . Load fraction of power electronics

I . . . . Current
I_r . . . . Rated current
I_t . . . . Current at time t

m_{batt} . . . . Mass of the battery unit
m_{ia} . . . . Mass of the internal air

P . . . . Power
$P_{conv}^{batt-ia}$ . . . . . Rate of convection heat transfer between battery and internal air (ia)
P_{loss}^{batt} . . . . Power loss of the battery unit
$P_t^{ch,loss}$ . . . . . . Charging loss power at time t
$P_t^{dch,loss}$ . . . . . Discharging loss power at time t
$P_t^{gen,i}$ . . . . . . Power generated by the i^{th} generation component at time t
$P_t^{gen,loss}$ . . . . . Loss power during generation at time t
$P_t^{gr,exp}$ . . . . . . Power exported to the grid component at time t
$P_t^{gr,imp}$ . . . . . . Power imported from the grid component at time t
$P_t^{gr,loss}$ . . . . . . Loss power from the grid at time t
P_{hvac} . . . . Thermal power of the HVAC system
P_{conv}^{ia-il} . . . . . . Rate of convection heat transfer between the internal air (ia) and the inner layer (il) of the housing wall
P_{PE}^{in} . . . . Input power of power electronics
$P_t^{load,c}$ . . . . . . Net power consumed by the load component at time t
$P_t^{load,k}$ . . . . . . Power consumed by the k^{th} load component at time t
$P_t^{load,loss}$ . . . . . Power loss within the load component at time t
P_t^{load} . . . . Gross power supplied to the load component at time t
P_{PE}^{out} . . . . Output power of power electronics
P_r . . . . Rated power
$P_t^{st,ch,j}$ . . . . . . Charging power of the j^{th} storage component at time t
$P_t^{st,dch,j}$ . . . . . Power discharged by the j^{th} storage component at time t

Q_{dch} . . . . Charge discharged
Q_n . . . . Nominal charge capacity
Q_n^t . . . . Nominal charge capacity at time t
Q_t . . . . Charge content at time t

R_t . . . . Internal resistance at time t

T_{batt} . . . . Temperature of the battery
T_{ia} . . . . Temperature of the internal air (ia)

V_n . . . . Nominal voltage
V^{OC} . . . . Open circuit voltage
V_t . . . . Terminal voltage at time t

1 Introduction

1.1 Motivation

Energy is the basis of modern human civilization, enabling humans to alter their environments to suit their needs and counter adversity. The ever-increasing sophistication and efficiency in harnessing energy from an increasingly complex variety of sources have all tightened human control over energy flow. Human civilization has progressed from being limited by the capabilities of human and animal muscle effort to unleashing chemical energy locked up in carbonaceous energy sources. The mainstay of the energy supply system remains chemical energy from carbonaceous fossil fuels. Energy modeling studies conducted by the International Energy Agency forecast peak fossil fuel consumption in 2030 [1]. Combustion of carbonaceous fuels releases reaction products such as Carbon Dioxide (CO_2) and acidic oxides of sulfur and nitrogen into the atmosphere. Grave environmental problems, such as global warming, sea level rise, extreme weather events, and acidification, are attributed to the presence of these substances in the atmosphere [2]. The 2015 Paris Agreement reached at the United Nations Climate Change Conference held in Paris, France, stipulates stringent action from member states of the UN to mitigate and sharply cut down on greenhouse gas (GHG) emissions to limit the average global temperature rise to 2°C relative to pre-industrial times by the turn of the century in 2100 [3]. Global GHG emissions growth has slowed in the last decade despite a higher rate of global economic growth. The remaining carbon budget for anthropogenic CO_2 emissions to limit global warming to 1.5, 1.7, and 2 °C is estimated to be around 275, 625, and 1150 gigatons, respectively [4].

Electricity is the most versatile energy vector of the energy system. The 21^{st} century has witnessed an ever-accelerating global transition to renewable energy sources, with each year in the last 22 years setting a new record in annual renewable capacity additions. In 2023, renewable capacity additions jumped nearly 50% to 510 GW [5]. At the Climate Change Conference 2023 held in Dubai, United Arab Emirates, more than 130 national governments agreed to collaborate to triple the global installed renewable energy capacity to over 11 000 GW by 2030 [6]. With the advent of cost-competitive electricity produced by fluctuating renewable energy sources such as Photovoltaic Solar (PV) solar and wind turbines, the economic hurdles in the way of large-scale adoption of these technologies are set to gradually disappear [7–9]. Renewable energy sources can directly decarbonize the electricity sector, reducing the reliance on fossil-fuel-based conventional electricity generation. The electrification of other sectors of the energy system promises to extend the decarbonization of the electricity sector to other applications, resulting in a major shift of the energy demand from other sectors to the electricity grid. Furthermore, there is an increasing strain on electricity transmission systems worldwide due to an ever-increasing number of consumers with a rising per capita consumption [10].

As power generation from renewable energy sources such as PV solar and wind turbines is intermittent and often difficult to predict with a high degree of accuracy, the power fluctuations introduce further instability into the grid [11, 12]. A very large proportion of the nameplate capacity, represented by PV solar generators, goes offline after sunset, leaving the deficit to be fulfilled by wind turbines, conventional generators, and other grid participants. Often, a substantial amount of energy is curtailed, i.e., not supplied to the grid to prevent oversupply [5]. Hence, mere en-masse replacement of conventional generators with renewable generators is not the solution, as power is not available on tap and is subject to meteorological conditions. This compels energy system operators to continue relying on reserve conventional generation capacity to smooth out the fluctuations and supply energy in periods of lull and ensure that the delicate balance between power generation and demand is maintained at all instants of time [10]. A variety of low-carbon flexibility options are required to smooth out the mismatch between load and demand at all times. Effective and interconnected transmission networks with sufficient capacity, limited bottlenecks, and smart networking technologies to enable efficient energy flows are also a part of the solution. Demand-side measures to incentivize consumers to react to the power generation rather than vice-versa also contribute to greater flexibility. Modern power plants running on carbon-neutral carbonaceous fuels and hydrogen also have a role to play. High ramp rates, good part-load efficiencies, and low response times are necessary to complement renewable energy sources. Signs of inflexibility in the power system are amply visible today - these include difficulty in balancing the demand and supply, higher than necessary curtailments of renewable energy generation, price volatility in the energy markets, and negative market prices [13]. Energy storage is an indispensable flexibility measure and is slated to play a pivotal role in stabilizing the grid in the upcoming times [14].

Electricity is an energy form without an inherent storage possibility. Storing electrical energy relies on several broad categories of energy conversion and storage technologies, such as thermal, mechanical, chemical, electrochemical, electrostatic, and electromagnetic systems. With the right set of converters, electrical energy can be converted and stored in one of the forms of energy that can be stored. Storing electrical energy in an electrochemical system is relatively straightforward and efficient as it requires few auxiliary systems. In addition, these systems are also relatively good at retaining the stored energy in a standby state under standard operating conditions [15]. Lithium-ion battery technology is the leading electrochemical storage technology today owing to its relatively high round-trip efficiency, high energy and power densities, as well as superior lifetime performance [16, 17]. Stationary lithium-ion BESSs are a reliable solution in integrating renewable energy sources in the electricity grid and provide greater flexibility to maintain grid stability [18, 19]. Stationary BESSs can provide a number of vital ancillary services to the electricity supply system, such as - frequency control, voltage control, load balancing, and peak shaving, among others [16, 20, 21]. These advantages mean that battery storage was the fastest-growing energy technology in the power sector in 2023. With nearly 42 GW of added capacity globally, a 100% growth in deployed volumes year-on-year was observed in 2023. To achieve the lofty target of tripling renewable capacity by 2030, as agreed at the Climate Change Conference 2023, stationary BESS capacity must increase roughly sevenfold in the same period [22].

Owing to the same set of advantages that makes lithium-ion battery technology a forerunner for stationary BESSs, the technology is also a forerunner in the decarbonization and electrification of the mobility sector [22]. All types of Electric Vehicles (EVs) on the electrification spectrum, ranging from plug-in hybrids to fully electric EVs, rely on high-performance lithium-ion batteries as a/the source of motive energy. Global stocks of EVs crossed 40 million in 2023, with 14 million added in 2023 alone, representing a 35% year-on-year increase and a sixfold increase over 2018 sales volumes. This represents nearly one out of five new cars sold globally in 2023 [23]. The impending electrification of the mobility sector as part of the energy transition also introduces its own challenges. The first one pertains to the shifting of energy demand from the oil and gas sector to the electricity grid. At the same time, the second is related to the handling of the expected volumes of decommissioned EV traction batteries [24, 25]. Li-ion batteries undergo degradation over time and usage. This manifests itself in the form of two visible phenomena at the system level - capacity fade, which refers to the permanent loss in charge capacity of electric vehicle batteries, and power fade, which refers to the decrease in generated output power due to an increase in cell internal resistance [26]. However, these battery packs can still be utilized for less-demanding 'second-life' stationary energy storage applications, where subpar energy and power densities are not the central design considerations [27, 28]. A bibliometric study of highly cited research publications on the topic of grid-connected lithium-ion BESSs found that the most consequential directions for future research included performance improvements, cost optimization, mitigation of grid instability, and the investigation of End-of-Life (EOL) scenarios [29].

A key implication of the preceding discussion is that it is crucial to quantify and ascertain the extent to which energy storage systems aid in the decarbonization process of the energy system, enabling us to stay within the remaining carbon budget. This need embodies the central motivation for this work. This work studies the lifecycle carbon footprint of lithium-ion BESSs as the pre-eminent energy storage technology. A systematic mathematical framework has been developed due to a paucity of coherent and consistent methodologies to quantify the lifetime carbon footprint of energy storage systems in general. Through a diverse set of case studies on stationary BESS applications, the capabilities and significance of this methodology are demonstrated. The developed framework and associated metrics can just as well be applied to other energy storage technologies.

1.2 Thesis scope and outline

This publication-based thesis comprises nine chapters, which touch upon various aspects of the modeling and evaluation of the carbon footprint of stationary lithium-ion BESSs. In total, six research articles have been included in this thesis, of which five are part of the main body of the manuscript, while one is placed in the appendix for ready reference. Figure 1.1 graphically depicts the structure of this thesis while indicating the main topics dealt with in each of the chapters.

Chapter 2 presents the fundamental theoretical concepts that the later chapters build upon. This includes a general description of lithium-ion BESSs and the evaluation methodologies used to describe their performance. Furthermore, the chapter discusses the idea of second-life batteries and looks at typical stationary BESS applications. Chapter 3 discusses some aspects of the methodology employed in this work to model battery systems (section 3.1) and energy systems (section 3.2). It also introduces the two main simulation programs (SimSES and ESN) used in the creation of the case studies presented in this thesis.

Chapter 4 presents the research article titled *Topology and Efficiency Analysis of Utility-Scale Battery Energy Storage Systems*. This chapter presents the findings of simulative investigations on the factors that influence the efficiency of utility-scale BESSs. These factors include the application, i.e., the load profile, the power electronics topology, and the battery parameters. The BESS applications illustrated here are industrial peak shaving and frequency regulation.

Chapter 5 makes up the central aspect of this thesis and encompasses the research article titled *Quantifying the carbon footprint of energy storage applications with an energy system simulation framework - Energy System Network*. This article introduces ESN, the open-source energy system simulation program that has been instrumental in conducting the studies discussed in this thesis. Two accompanying case studies demonstrate the procedure to obtain the carbon footprints for the chosen applications - energy arbitrage and home energy systems.

Chapter 6 comprises the research article titled *The carbon footprint of island grids with lithium-ion battery systems: An analysis based on levelized emissions of energy supply.* This chapter presents a methodology to ascertain the effect of and the effectiveness of energy storage integration on the carbon footprint of isolated energy systems. To this end, two novel new metrics are introduced, Levelized Emissions of Energy Supply (LEES), and R - the reduction in emissions per additional unit of energy storage.

Chapter 7 consists of the research article *High-power electric vehicle charging: Low-carbon grid integration pathways with stationary lithium-ion battery systems and renewable generation.* This article explores the carbon footprint of battery-assisted high-power charging stations for EVs. A practical new state variable for BESSs, the State of Carbon Intensity (SOCI), is introduced in this chapter. The role of the energy management strategy in reducing the carbon footprint of the localized energy system is also explored.

Chapter 8 comprises the research article titled *The Lifetime Carbon Footprint of Lithium-Ion Battery Systems in Exemplary Applications.* This article unearths the major factors influencing the carbon footprints for three potential lifecycle pathways for lithium-ion batteries - stationary BESS, EV batteries, and second-life batteries. The carbon footprint of repurposed batteries is also examined in this article.

Chapter 9 sums up the findings of this thesis and concludes with a discussion on a wide array of connected potential research directions that could build upon and branch off from the work presented in this thesis.

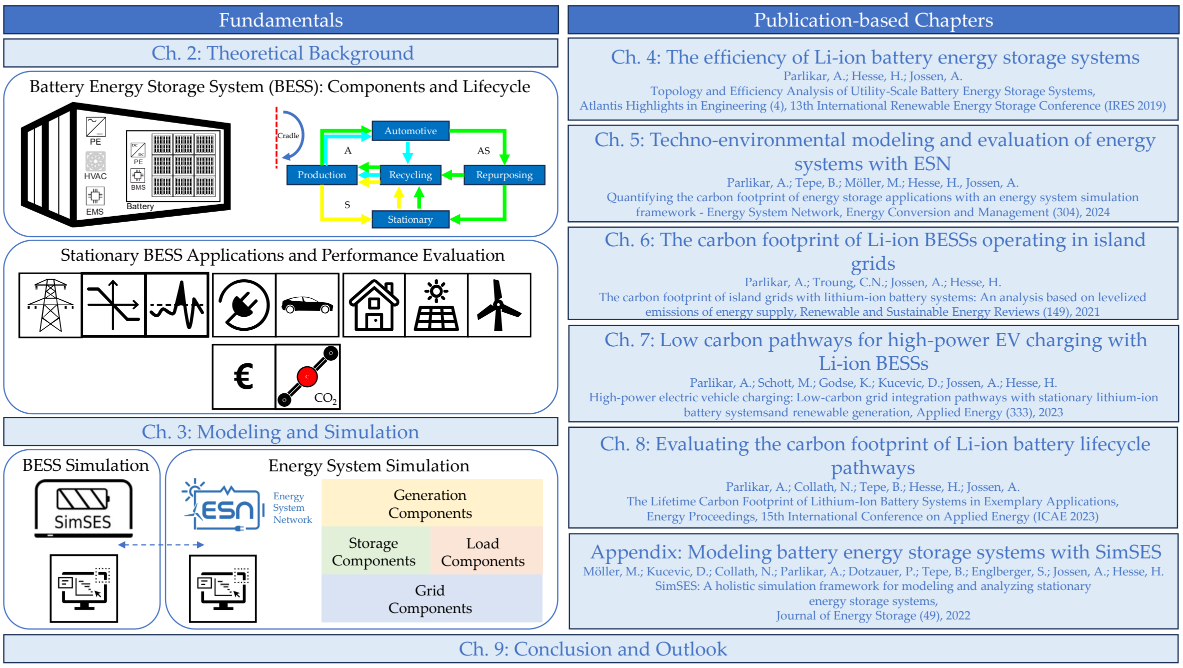

Figure 1.1: Outline of this thesis. Chapters 2 and 3 (on the left) provide context and theoretical background for the publication-based chapters (on the right).

2 Theoretical background

This chapter introduces the fundamentals of BESSs and the prevalent performance evaluation methodologies. Section 2.1 presents a general description of BESSs, which includes a discussion of the major components in a BESS and battery degradation. This is followed by a discussion on some useful technical quantities relevant to the contents of the subsequent sections and chapters. Section 2.2 discusses techno-economic and techno-environmental performance evaluation methodologies for BESSs. The topic of discussion moves on to battery repurposing and second-life batteries (SLBs). The salient aspects of this battery usage concept are discussed in section 2.3. Section 2.4 provides the reader with an overview of typical stationary BESS applications.

2.1 Battery energy storage systems

Lithium-ion batteries offer high energy and power densities, thus enabling a wide variety of energy storage applications wherein volume and weight are the predominant constraints [30]. These applications include EVs and portable electronic devices, and now increasingly stationary BESSs [31]. Lithium-ion batteries generally have a longer cycle life relative to other rechargeable battery technologies, enabling them to undergo a large number of charge-discharge cycles before experiencing significant capacity degradation [32]. These batteries also exhibit very low self-discharge rates, leading to excellent charge retention over longer periods when not in use [33]. Lithium-ion battery cells operate at higher voltage ranges as compared to rechargeable batteries with aqueous electrolytes. Higher voltage ranges are advantageous for certain applications where energy density, power density, and efficiency are crucial [34]. This technology is also highly energetically efficient, with relatively low energy losses during charge and discharge cycles. Lithium-ion batteries can be charged and discharged at high current rates. This rate capability is essential for applications requiring fast charging or discharging, such as in EVs and certain consumer electronics [32, 35]. Lithium-ion batteries are completely maintenance-free over their lifespan. Safety is critical to lithium-ion battery technology, and manufacturers implement various safety features to prevent issues such as thermal runaway or short-circuit [36].

A cell is the smallest possible indivisible unit of a battery. The cell represents a redox system that generates a voltage across its terminals due to the redox reaction taking place within it [37]. Batteries can be classified as primary or secondary, depending on whether the dominant redox reaction can be reversed by passing an external electrical current in the opposite direction. The redox reaction in a secondary cell can be reversed; these cells are therefore termed rechargeable cells. Some prominent examples of secondary cells include lead-acid, nickel-cadmium, nickel metal hydride, and lithium-ion batteries [38]. A lithium-ion cell is a special type of secondary cell wherein no chemical conversion of the materials participating in the redox reaction occurs. The redox reaction taking place, in this case, is an intercalation mechanism that shuttles lithium ions between the lattice structures of an anode material and a cathode material [36]. Common anode materials include graphite, silicon, or a blend of both [39]. Cathode materials used today are primarily inorganic mixed metal oxides or phosphates of lithium with transition metals [40]. Depending on the exact anode and cathode materials, several lithium-ion battery chemistries have been successfully commercialized in the three decades since the invention of this battery type. The three most commercially successful cathode materials are lithium nickel manganese cobalt oxides ($LiNi_xMn_yCo_{1-x-y}O_2$), lithium nickel cobalt aluminium oxides ($LiNi_xCo_yAl_zO_2$, with x + y + z = 1), and lithium metal phosphates ($LiMPO_4$, where M is commonly iron (Fe), manganese (Mn), or a blend of these metals) [40, 41]. The most common geometrical cell formats are cylindrical, pouch, and hard-case prismatic. Each of these three cell form factors offers various advantages and some accompanying disadvantages. System designers must identify a suitable cell format that can meet their requirements [42].

The case studies presented in this study work primarily with Lithium Iron Phosphate (LFP) batteries due to their wide range of advantages and suitability for stationary applications [43, 44].

2.1.1 Components of a Battery Energy Storage System (BESS)

BESSs used in stationary applications consist of a number of sub-systems [45, 46]. The exact form and capabilities of the various components vary to some extent based on the specific characteristics and requirements of the application. The following subsystems are typically installed in a BESS, and the functions of these sub-systems are described in the subsequent paragraphs. Figure 2.1 exhibits the typical components of a BESS.

- Battery (racks, modules, cells)
- Power electronics
- Energy management system
- Battery management system
- Thermal management system including Heating, Ventilation, Air Conditioning (HVAC)
- Enclosure/Housing

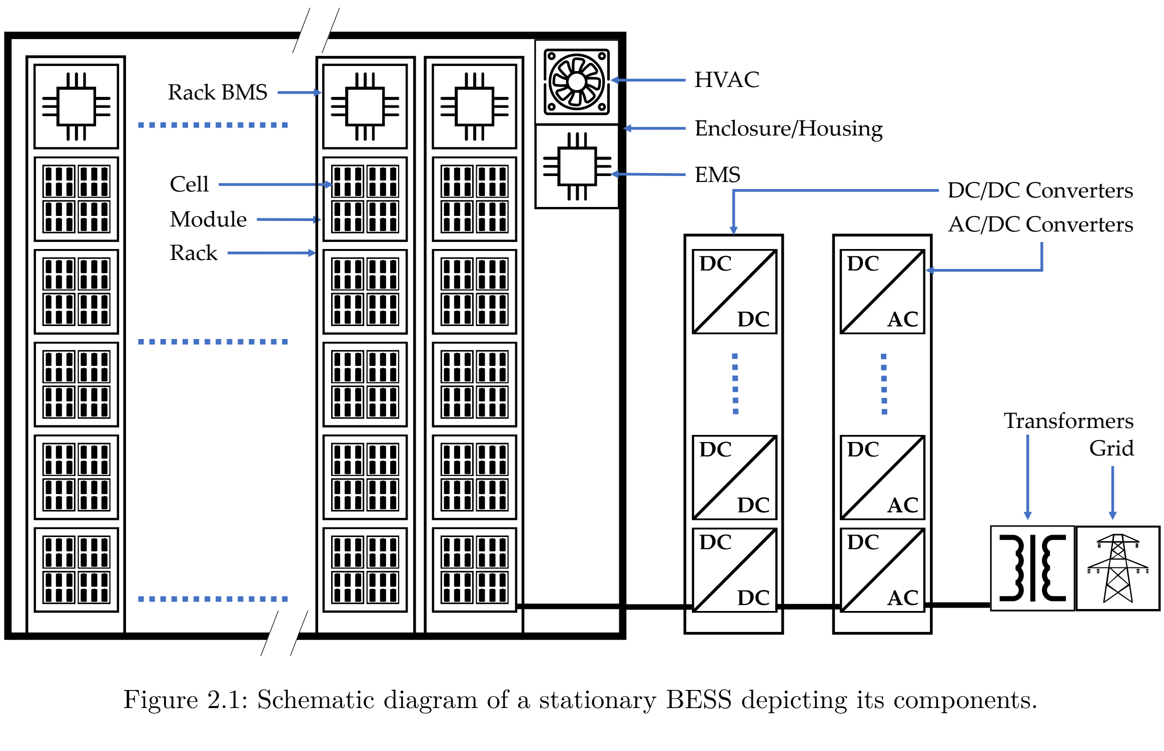

Figure 2.1: Schematic diagram of a stationary BESS depicting its components.

Battery: The battery in a BESS comprises multiple racks connected in series and/or parallel. Each rack consists of several modules connected in series and/or parallel. Each module, in turn, comprises many individual cells connected in series/parallel. The actual connection architecture of each module and rack depends on the target voltage level and power capability, among other considerations. Each rack also houses the Battery Management System (BMS), cabling, cooling, and venting required for the modules [47, 48]. A fresh battery pack inevitably suffers from intrinsic cell-to-cell parameter variations. Consequently, module-to-module parameter variations originate from deviations in the cell fabrication and assembly processes [49–51]. Such variations are further aggravated due to several extrinsic operational factors such as local temperature gradients inside a battery pack, deviations in current distribution, cycle depths, and contact resistances, which cause a further heterogeneous non-uniform degradation [49, 52]. In this thesis, the topology of the battery is inferred within the simulation models from the system requirements to enable an improved emulation of the battery characteristics. For simplicity and due to simulation constraints, the cell-to-cell parameter variations are disregarded in this work. All cells are assumed to behave identically throughout their service lives.

Power electronics: The power conversion system, which includes the power electronics, serves as the bidirectional interface between the grid and the battery and is indispensable in managing the flow of electrical energy between the battery and the grid. The power electronics convert the Direct Current (DC) from the battery into Alternating Current (AC) for the grid and vice versa. On the Alternating Current (AC) side, they maintain the voltage and frequency the grid requires. On the Direct Current (DC) side, they adapt to the battery voltage across its voltage range [53]. The exact topology to achieve the requisite power conversion in a specific application is determined with a suitable combination of AC/DC and DC/DC converters. The design process considers the load characteristics and other requirements of the application to arrive at an efficient and cost-effective configuration [54, 55].

Energy management system: The Energy Management System (EMS) is a top-level controller acting as the information interface between the BESS and the energy system. An EMS monitors and manages the operation of the BESS while tracking its energy content and determines when the battery charges or discharges. The EMS relies on specific algorithms to determine the scheduling of the BESS for a particular application. These algorithms often use forecasts and real-time data for generation and load power. This data is often augmented with other data streams, such as energy prices and grid frequency, if required for decision-making. These algorithms use rule-based or optimization-based strategies to determine power targets and operation schedules for BESSs. Irrespective of the type of strategy used, the EMS operation is guided by the realization of either financial, technical, or other hybrid targets [56, 57].

Battery management system: The BMS is one of the key enablers of the widespread adoption of lithium-ion battery technology. The BMS ensures safe battery operation by enforcing safety limits on voltage, current, and temperature values. It measures and, where necessary, computes or estimates battery parameters such as the current, voltage, temperature, the State of Charge (SOC), and the State of Health (SOH). The BMS is responsible for data acquisition and data logging. An indispensable function is balancing the sub-units within each module or each pack/rack in the system to prevent the parameters from drifting apart and affecting system performance [58–60].

Thermal management: Thermal management of lithium-ion battery systems during operation is crucial for both safety and overall performance. Lithium-ion batteries must be maintained within their optimal temperature ranges to achieve a longer lifespan. The cooling/heating system aims to keep the batteries within the specified safe operation temperature ranges. Excessive heating of the batteries can lead to accelerated capacity and power fade and, at worst, thermal runaway and fires/explosions. Cooling systems are used to cool the components in warm climates and to counteract the heat evolution in the components during operation. On the other hand, operation at very low temperatures, especially during charging, can cause lithium plating within the batteries. Heating systems are, therefore, also required to maintain the systems within the optimal temperature range. The Thermal Management System (TMS) controls the operation of the cooling system in accordance with inputs from the BMS and the EMS. Both passive and active thermal management systems are used in commercial systems today. Primary examples of passive thermal management methods include passive convection and phase-change materials. Examples of active thermal management methods include forced air convection and liquid-based systems [61–64]. In the present work, air-cooling is employed to bring about convective heat transfer, with a simplified model used to emulate the functioning of the HVAC.

Enclosure/Housing: The housing shields the sensitive components in the BESS, including the battery racks, power electronics, and other electronic components, from adverse environmental conditions. The standard shipping container is a widespread housing option and ensures efficient and safe operation for large-scale BESSs. These containers are weather-resistant and equipped with heating/cooling systems to ensure climate control and protect the batteries and other components from snow, rain, and extreme temperatures. Additionally, the containers are modular, highly scalable, and suitable for marine, rail, and road transport, often making this type of housing the preferred option to house BESS components [47, 65–67]. In the present work, the standard 20 ft. and 40 ft. shipping containers are used as the enclosure for the BESS.

All the aforementioned BESS components are modeled and simulated with the software program Simulation of Stationary Energy Storage Systems (SimSES), which has been discussed in greater detail in chapter 3.

2.1.2 Battery degradation and lifetime

Lithium-ion batteries experience a deterioration in their functionality over their service lifetimes due to a number of side reactions and degradation mechanisms. Some of these side reactions and degradation mechanisms are active at all times, including during rest periods, while others occur during cell operation (charging or discharging). The degradation mechanisms are largely classified into two degradation modes, based on the impact they have on the cell - Loss of Lithium Inventory (LLI) and Loss of Active Material (LAM) [68]. Degradation mechanisms that cause LLI lead to the consumption of lithium ions in parasitic reactions, rendering them incapable of participating in the primary intercalation process. These include Solid Electrolyte Interphase (SEI) layer growth, lithium plating, and electrode particle cracking with electrical isolation. Degradation mechanisms that lead to LAM include particle cracking with loss of electrical contact, surface film formation, and loss of lithium intercalation sites due to other structural disordering. These degradation modes cause a discernible capacity and power fade, with LLI primarily responsible for capacity fade and LAM contributing to both capacity and power fade [26].

Lithium-ion battery degradation is a crucial factor in lifetime estimation, which is a central aspect of techno-economic and techno-environmental analyses of BESSs. Several types of degradation models are available in the literature spanning all battery modeling scales - from the material/electrode level to the pack/system level [69]. At the material/electrode level, the so-called pseudo-2D (p2D) models and the single particle models (SPM) are often used to model cell degradation [68]. These models are computationally intensive and not suitable for simulating battery systems consisting of hundreds or thousands of individual cells spanning large time horizons [70]. Cell-level degradation models employ an Equivalent Circuit Model (ECM) approach with time-variant elements. These models shift their gaze from the electrochemical phenomena taking place inside the cells to the measurable electrical quantities such as voltage, impedance, and current at the cell terminals [69].

Semi-empirical cell degradation models are typically parameterized with extensive cell capacity and resistance measurements gathered from extensive degradation experiments. In most models, the total degradation is categorized into calendric and cyclic degradation. Underpinning these models is the assumption that the contributions of the calendric and cyclic components are path-independent and that their superposition yields the total degradation [71–75]. Some studies investigating the validity of this assumption find that a path dependence on the order of the stress factors indeed exists, thereby indicating that the superposition assumption is not perfect [76, 77]. A large discrepancy is, however, not expected. In this work, semi-empirical cell degradation models developed by Naumann et al. for the LFP lithium-ion cell chemistry have been used in the various case studies [72, 73]. The superposition of calendric and cyclic aging is considered a valid assumption, and the degradation is considered to be path-independent. Figure 2.2 depicts the two overarching degradation mechanisms and the stress factors contributing to each.

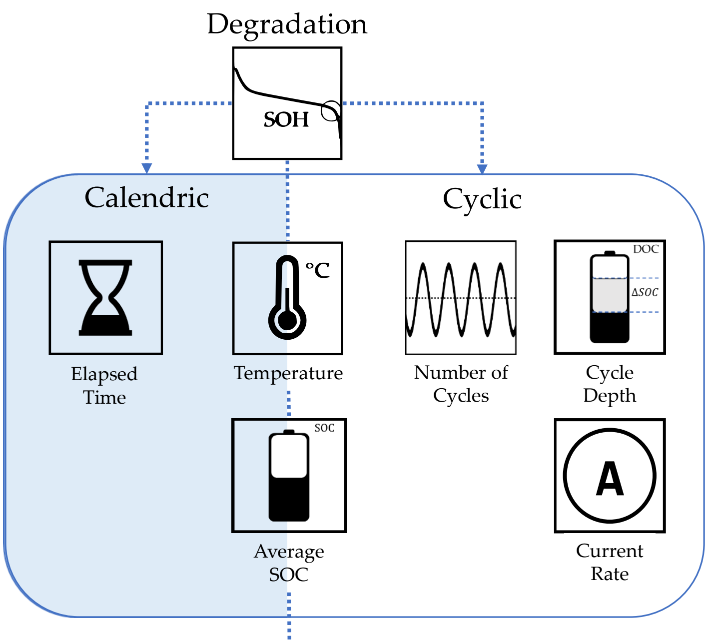

Figure 2.2: Overview of the most prominent operating conditions and factors influencing the rate of cell degradation - both calendric and cyclic.

2.1.3 Technical quantities

This subsection presents the relevant technical quantities required to model and evaluate the performance of BESSs. Some of these quantities are related to the battery system configuration and are fixed at the outset. Other quantities describe the state of the system during operation and are dynamic in nature.

Rated power: The rated power (P_r) of a lithium-ion BESS is the value of power that can be drawn continuously from the battery without leading to any unexpected degradation or failure. This is computed as the product of the rated current capability (I_r) and the nominal voltage (V_n) of the battery (eq. 2.1) [78].

$$P_r = I_r \cdot V_n \tag{2.1}$$

Energy capacity: The nominal or rated energy capacity (E_n) of the battery system at the Beginning-of-Life (BOL) is the amount of energy that can be drawn out of the battery under standard operating conditions. This is given by the product of the nominal charge capacity (Q_n) of the battery at BOL and the nominal voltage, V_n (eq. 2.2). The actual energy capacity of the battery at time t, E_n^t, decreases with the actual charge capacity (Q_n^t) due to degradation [78].

$$E_n = V_n \cdot Q_n \tag{2.2}$$

Energy-to-power ratio: The Energy-to-Power Ratio (EPR) is the ratio of the nominal energy capacity (E_n) to the rated power, P_r. This quantity essentially indicates the discharge duration at rated power. System configurations with larger Energy-to-Power Ratio (EPR) values are chosen if longer discharge durations are necessary to fulfill the requirements of an application. In some cases, the reciprocal of the EPR, termed as the Power-to-Energy Ratio (PER), is also used to convey information about the charge/discharge characteristics of the BESS (eq. 2.3) [79, 80].

$$EPR = \frac{1}{PER} = \frac{E_n}{P_r} \tag{2.3}$$

Normalized values of rated power and the energy capacity with respect to the system mass are termed the specific power and specific energy or the gravimetric power and energy densities, respectively. If the normalization of the rated power and the energy capacity is carried out with respect to the system volume, the resulting quantities are referred to as the volumetric energy and volumetric power densities, respectively [81]. Considering these quantities is especially crucial in automotive and other mobile and portable applications, as mass and volume constraints influence the design process to a greater extent than in stationary applications.

C-rate: The C-rate is the ratio of the current (I) at which a battery is charged or discharged to its charge capacity, Q_n^t (eq. 2.4) [35]. The E-rate is an analogous concept to the C-rate and describes the rate at which energy is transferred to or from a battery system relative to its energy capacity. The E-rate is the ratio of the power at which a battery is charged or discharged (P) to its energy capacity, E_n^t (eq. 2.5) [82]. During the service period, the effective values of these quantities increase due to capacity degradation.

$$C - rate = \frac{I}{Q_n^t} \tag{2.4}$$

$$E - rate = \frac{P}{E_n^t} \tag{2.5}$$

Equivalent Full Cycle (EFC): The ratio of the charge throughput in the discharge process to the charge capacity of the battery represents the number of Equivalent Full Cycles (EFCs). In cases where the total charge throughput, including both the charge and discharge processes of a cycle, is considered, twice the charge capacity is used as the denominator in this ratio [83]. EFCs can also be determined in terms of the energy throughput (eq. 2.6) [82], as a ratio of the discharged energy (E_{dch}) to the energy capacity, E_n^t.

$$EFC = \frac{E_{dch}}{E_n^t} \tag{2.6}$$

Energy efficiencies: The charging and discharging efficiencies for a BESS are based on an expanded scope to include all the other components present in a BESS. The charging efficiency of a BESS, η_{ch}, is defined as the ratio of the actual energy stored in the batteries (E_{st}) to the total charging energy supplied at the system interface, E_{ch} as measured from a given initial state. This value is dynamic and depends on the individual efficiencies of all components and their part-load characteristics. This considers energy conversion losses encountered in the batteries themselves, the power electronics, and the energy consumption of the auxiliary components (eq. 2.7). [84, 85]

$$\eta_{ch} = \frac{E_{st}}{E_{ch}} \tag{2.7}$$

The discharging efficiency of a BESS, η_{dch}, is defined as the ratio of the discharged energy available at the system interface (E_{dch}) to the actual energy stored in the batteries, E_{st} as measured from a given initial state. This value is also dynamic and depends on the individual efficiencies of all components and their part-load characteristics (eq. 2.8). [84, 85]

$$\eta_{dch} = \frac{E_{dch}}{E_{st}} \tag{2.8}$$

The roundtrip efficiency of a BESS, η_{rt}, is a measure of how efficiently the system can store and retrieve energy over a complete cycle, i.e. the system has identical initial and final states. It is mathematically expressed as the ratio of the energy output during discharge (E_{dch}) to the energy input during charging, E_{ch} (eq. 2.9). [84, 85]

$$\eta_{rt} = \frac{E_{dch}}{E_{ch}} = \eta_{ch} \cdot \eta_{dch} \tag{2.9}$$

Self-discharge rate and Coulombic efficiency: The time rate of reversible natural loss of charge in a lithium-ion battery as a function of the SOC and temperature is termed as the battery self-discharge rate. This rate is influenced by various parasitic side reactions that all lead to a loss of stored charge in the battery [86]. The self-discharge rates for lithium-ion batteries are generally low [33]. The battery self-discharge rate is expressed as a percentage of the nominal charge capacity lost per unit of time. In this thesis, the self-discharge of batteries is assumed to be zero as a simplification. The Coulombic efficiency indicates the extent of charge conservation within a lithium-ion battery [87]. It is the ratio of the discharged charge capacity to the charged charge capacity of the battery [88, 89]. In this thesis, as a simplification, the Coulombic efficiency is considered equal to 1, as lithium-ion batteries exhibit very high Coulombic efficiencies after the initial formation cycles [90].

The next set of quantities to discuss are the *state variables*. State variables assume values that vary with time and describe the state of the system at each point in time. They convey important operation information about the battery system.

State of Charge (SOC): The SOC of a lithium-ion battery is the ratio of the charge content of the battery at the present time, Q_t, to the present charge capacity of the battery, Q_n^t. It is expressed as a percentage or a ratio (eq. 2.10) [91, 92]. The State of Energy (SOE) for a battery is the ratio of the energy content of the battery at the present time, E_t, to the present energy capacity of the battery, E_n^t. The State of Energy (SOE) is expressed as a percentage or a ratio (eq. 2.11). Since a lithium-ion battery does not exhibit a constant voltage across its voltage range, equal charge throughput at different SOC levels does not correspond to an equal energy throughput. Hence, the value of the SOE is often slightly different from the SOC [91, 92]. Although not identical, the two terms are often used interchangeably, especially at the system level. In the present work, the SOC indicates the available fraction of the energy storage capacity at any given time.

$$SOC_t = \frac{Q_t}{Q_n^t} \tag{2.10}$$

$$SOE_t = \frac{E_t}{E_n^t} \tag{2.11}$$

Depth of Discharge (DOD): The Depth of Discharge (DOD) for a battery is the ratio of the charge discharged (Q_{dch}) to the charge capacity of the battery at the present time, Q_n^t. It describes the extent to which a battery has been discharged. While the DOD is often used to describe the state of a battery at a given point in time, the Depth of Cycle (DOC) is used to describe the cycle depth of the cycles a BESS is subjected to during operation (eqs. 2.12, 2.13) [82, 83, 93].

$$DOD_t = \frac{Q_{dch}}{Q_n^t} \tag{2.12}$$

$$DOD_t = 1 - SOC_t \tag{2.13}$$

State of Health (SOH): The SOH is an indicator of the overall level of degradation witnessed by the battery leading up to the present time. The most common definition of SOH is based on the ratio of the charge capacity of the battery at the present time (Q_n^t) to the nominal charge capacity at BOL, Q_n. The rise in internal resistance is also used in some definitions of the SOH (eq. 2.14) [91, 92]. This thesis uses the capacity-related definition of the SOH in the subsequent chapters.

$$SOH = \frac{Q_n^t}{Q_n} \tag{2.14}$$

Other state variables are found in the literature but are not used within the context of this thesis. The State of Power (SOP) is an indicator of the maximum value of power that the battery can safely charge or discharge at the present time. It is usually expressed as the product of the voltage at the present time and the corresponding maximum permissible current under consideration of constraints such as SOC and temperature [91]. The State of Function (SOF) is a binary quantity that expresses the ability of the battery to fulfill a particular power request in its current state [94]. The State of Safety (SOS) is a safety-related state variable that quantifies the safety of a BESS as inversely proportional to the concept of abuse [95]. In chapter 7, a new state variable, the State of Carbon Intensity (SOCI), is introduced.

2.2 Battery performance evaluation and metrics

Performance metrics are crucial indicators of the performance of any technology, either for comparison with other technologies or to assess the extent of fulfillment of core system objectives. Evaluating and estimating system performance is one of the central objectives behind the modeling and simulation of battery systems. Furthermore, performance metrics enable system engineers to improve design and optimize certain aspects. Performance metrics are also valuable tools for identifying future research direction. The performance evaluation of energy storage systems, which are a part of the larger energy system, can be carried out on lines similar to the performance evaluation of energy systems [96].

Energy storage systems, like all engineering systems, are expected to perform satisfactorily on three major heads:

1. Technical
2. Economic
3. Environmental

The ideal aim of technology development is tangible positive developments on all three heads and not solely technical and economic viability. Until now, an improved environmental footprint has only been viewed as an optionality, not an obligation - making a worse environmental footprint possible if the economics were favorable.

Techno-economic is the most prevalent form of performance evaluation for BESSs. Depending on the nature of the metric, it may also be of interest for system designers to consider not just the absolute values of some metrics but also the values of these metrics relative to other conditions and system configurations. While performing performance evaluation studies, it is also important to consider the influence of the choice of system boundaries for the evaluation [97]. Performance indicators and metrics are usually highly dependent on the system configuration and on the specific application. In the following subsections, techno-economic and techno-environmental performance evaluation methodologies are discussed. This work focuses on the techno-environmental performance evaluation of BESSs.

2.2.1 Techno-economic evaluation

Techno-economic evaluation is crucial in the project-planning phase of a BESSs, as the business case for a BESS hinges on a favorable assessment of the technical and economic performance in the considered use case. Conducting techno-economic evaluations for various competing solutions helps in the decision-making process to arrive at a suitable system technology and configuration. Techno-economic performance evaluation metrics for BESSs encompass a wide range of indicators. Some of these are discussed in the following paragraphs.

The Net Present Value (NPV) is the difference between the present values of all cash inflows and cash outflows over the service life of the BESS. This metric is useful in determining the profitability of a BESS. A positive value indicates the profitability for the project [98]. The Internal Rate of Return (IRR) is the value of the interest rate that makes the NPV of the project exactly equal to zero. This criterion is useful in conducting feasibility studies for projects and determining the extent of their economic viability [98]. The Return on Investment (ROI) is the ratio of the net return, which includes the revenue, avoided costs, energy costs, and maintenance costs, to the total capital expenditure, which includes the initial investment and the capital requirements for replacements over the operation period. [99] The Levelized Cost of Storage (LCOS) is a concise metric based on the Levelized Cost of Energy (LCOE) metric used to study the techno-economic characteristics of power generation components. The metric represents the per-unit cost of energy storage over the entire lifetime of the technology, considering all capital costs, operation and maintenance costs, and residual value at EOL [100]. Alternatively, the LCOS can be defined as the fictitious average electricity price fetched by each unit of discharged energy over the lifetime of the storage system to break even financially [101].

Other techno-economic evaluation metrics have also been used in the published literature to ascertain the economic viability of energy storage projects operating in various applications. These include the payback period, the discounted payback period, the net present cost (NPC), the equivalent annual cost (EAC), and the levelized cost of energy (LCOE) [98]. The LCOE metric has also been extended to include storage in addition to the generation technology [102]. The levelized cost of delivery (LCOD) is a variant of LCOE, which is also closely related to the LCOS [103].

2.2.2 Techno-environmental evaluation

The techno-environmental performance evaluation of lithium-ion BESSs involves assessing the technical and environmental aspects of these systems throughout their life cycle. This evaluation is key to understanding the overall environmental impact, carbon footprint, and resource efficiency of lithium-ion battery technology [104]. Techno-environmental evaluation is not as widespread as its techno-economic counterpart. Studies spanning across the entire value chain are necessary for informed decision-making, but there is a growing discussion in the scientific community about the carbon footprint of battery systems over their entire lifecycle [105]. Life Cycle Analysis (LCA) provides a holistic view of the environmental footprint of lithium-ion batteries and helps identify areas for improvement in terms of emissions reduction and resource efficiency. Understanding the energy intensity of production helps identify opportunities for efficiency improvements and the use of renewable energy sources in manufacturing. Efficiency improvements determine how effectively the battery can store and release energy, impacting its overall effectiveness in real-world applications [106, 107]. Proper EOL management is essential for minimizing the environmental impact and maximizing the recovery of valuable materials for reuse [108]. The environmental impacts across all stages of the battery life cycle, including raw material extraction, production, use, and EOL should be considered [108]. Transportation-related emissions also contribute to the overall environmental footprint of lithium-ion batteries. In this work, the scope of the techno-environmental performance evaluation is restricted to one impact category - the Global Warming Potential (GWP) footprint or the carbon footprint.

Battery production

The battery production process is a complex chain of sub-processes, which includes the extraction of raw materials, synthesis of active materials, cell manufacturing, and pack assembly. Cell manufacturing encompasses a further set of sub-processes, such as electrode production, cell production, and cell conditioning. Electrode production includes the mixing of active materials with conductive carbon, binders, additives, and various aqueous/non-aqueous solvents. Mixing is followed by coating the active materials on their respective current collectors, before drying to vaporize the solvents. The coated current collector sheets are then calendered, slit, and subjected to a final drying process. Cell production takes place in a highly controlled atmosphere in a dry room. It consists of electrode cutting, stacking with separators, adding contacts, enclosing in a sturdy material, and filling cells with an electrolyte. The produced cell is subsequently subjected to conditioning in which cell formation, aging, and requisite quality control occur. Cell manufacturing is followed by pack assembly, wherein cells are connected in modules and packs with a BMS to monitor cell operation and safety. [109] As all the sub-processes involved in battery production are highly energy-intensive processes, a certain embodied energy is associated with the battery being produced. The carbon footprint of the embodied energy attributed to the production phase can, therefore, be attributed to the production phase of the battery.

Battery operation

The operation phase of a battery system is the longest phase in the lifecycle of a battery. No direct environmental impacts are anticipated during the battery operation phase. This phase is nonetheless relevant for determining the carbon footprint or the GWP of the entire lifecycle. The presence of a battery system in the energy system introduces additional energy losses during energy conversion. The carbon footprint associated with the lost energy is attributed to the operation phase of the battery. Battery characteristics influence this evaluation to a large extent. These characteristics include charging/discharging efficiencies and cyclic/calendric degradation rate. The source of the charging energy and, by implication, its carbon intensity both influence the carbon footprint of the operation phase. [110–112]

Battery EOL

The final phase of the battery lifecycle also plays a role in the lifecycle carbon footprint. Three recycling processes for lithium-ion batteries are currently widely discussed in the literature. These are pyrometallurgy, hydrometallurgy, and direct recycling. Depending on the exact process, some pretreatment is always required. The batteries are deep discharged to prevent uncontrolled energy release due to short-circuiting during crushing or shredding. The black mass is separated from other components in the shredded mix. Pyrometallurgy is the most technically mature process, albeit with low aluminum and lithium recovery rates. Hydrometallurgy and direct recycling can recover aluminum and lithium from the battery mass, although the technology readiness level is still not as high for these processes. If the purity level of the recovered material is comparable to that of the virgin material, a closed-loop circular process approach can be employed in the production process. In this case, an environmental credit is associated with recycling, as the recycled product effectively replaces fresh raw material extraction and other associated processes. This essentially reduces the carbon footprint of the production process. [109]

Thus, the lifetime GWP or carbon footprint of a battery across its lifecycle comprises the GWP footprints of each of the individual lifecycle phases.

System boundaries and functional unit

The system boundaries dictate which physical components, processes, and lifecycle phases are included within the scope of the evaluation. Cradle-to-gate evaluations in reviewed studies include the environmental impacts associated with the cells/battery systems from the extraction of raw materials (cradle) to the point when it leaves the factory gate [112]. This analysis considers all stages of production, including raw material extraction, transportation, manufacturing, and packaging, but excludes the product use phase and EOL disposal. In contrast, several studies also perform cradle-to-grave evaluations to evaluate the environmental impacts associated with cells/battery systems throughout the entire lifecycle, from raw material extraction (cradle) to disposal or EOL (grave) [106, 111]. This evaluation considers all lifecycle stages, including raw material acquisition, manufacturing, distribution, use, and EOL. If closed-loop recycling is the EOL process of choices, the recovered material can be reintroduced back into the production phase (cradle). This essentially closes the loop, enabling an evaluation possibility for circular product lifecycle approaches [113]. The term 'cradle-to-cradle' evaluation has gained popularity in cases where closed-loop recycling is evaluated [114]. Some studies perform evaluations that leave out certain lifecycle phases - such as the use phase or the EOL phase, focusing on the manufacturing and other phases [107, 109, 115]. This thesis considers cradle-to-grave evaluations, with recycling credits, wherever applicable, to consider circularity. The importance of selecting a suitable functional unit for conducting techno-environmental evaluations and its impact on the results is recognized in the community [116]. Diverse effects and influencing factors can be captured and subsequently normalized down the unit of service or product represented by the functional unit. This step enhances the comparability of alternatives possible by boiling down the information to the functional unit. Selecting a functional unit for a service, product, or device intrinsically depends on the system boundaries and the temporal boundaries of the evaluation [117].

The environmental impact per usable/nominal storage capacity is a functional unit that captures the performance of the batteries in terms of specific energy and the environmental footprints of the manufacturing and recycling processes [109, 110, 112]. The environmental impact per unit of lifetime energy delivered/stored/output is a more comprehensive metric, as it conveys the effect of the calendar and cycle lives, as well as the efficiency of the battery [106, 107, 111, 112]. The Energy Stored on Energy Invested (ESOI) is defined as the ratio of electrical energy stored by the storage device over its lifetime to the amount of primary embodied energy (cradle-to-gate) required to produce the device. This metric is useful in determining which storage technologies are the most durable and energetically cheapest to manufacture. The Levelized Embodied Energy is defined as the ratio of the cradle-to-gate embodied energy to the total energy stored by the system during a pre-defined levelization period at a set capacity factor. This quantity is also equal to the reciprocal of the ESOI [118]. The Lifecycle Emissions (LCE) denotes the amount of lifecycle emissions to store 1 kWh of electricity in battery systems. The LCE consists of two contributions - emissions due to the manufacturing of the battery systems and emissions due to the losses during charging and discharging [107]. The Energy Payback Time (EPBT) is defined as the time in years during which the energy storage system will have discharged energy equal to the embodied energy required to produce it [119].

Other metrics include an extended variant of the Energy Returned on Energy Invested (EROI) framework, which includes energy storage systems in the calculations [120]. Thus, identifying the carbon footprint of batteries is crucial for understanding their contribution to global warming and for making informed decisions about the environmental impact of energy storage solutions. Evaluating the role of lithium-ion batteries in the overall energy system helps optimize their deployment and maximize benefits for grid stability and renewable energy integration.

The state-of-the-art reveals that GWP footprint analyses and evaluations for energy systems lack granularity on both temporal and component aspects across all lifecycle phases. The operation phase of the energy storage system, in particular, is analyzed using imprecise lumped parameters. The temporal variations in the operating conditions, such as the carbon intensity of the electricity grid and the variations in efficiency, are often not considered. There is also a dearth of quantities and metrics to describe and capture all relevant information, thereby hindering more detailed and rigorous analyses. This thesis develops a detailed analytical and mathematical framework for calculating the GWP footprints of all components of an energy system across all lifecycle phases, with a detailed breakdown of the emissions into several emissions categories (Chapter 5). To this end, some useful quantities and metrics are introduced, which enhance the informational content of an emissions analysis by assigning meaning and names to involved quantities. In Chapter 6, a techno-environmental evaluation metric, Levelized Emissions of Energy Supply (LEES), is introduced. In Chapter 7, a new state variable, the State of Carbon Intensity (SOCI), is introduced and defined. This new state variable is key to quantifying the carbon footprint of the stored energy, and in calculating the carbon footprint of the battery operation phase.

2.3 Second-life batteries

EV traction batteries gradually degrade with time and use in service and may no longer meet the performance requirements for powering an EV due to capacity fade and power capability fade [121]. A fading capacity leads to a reduced operational range of the vehicle, causing range anxiety for the owner [122, 123]. A decreasing power capability directly affects the acceleration/regenerative braking capability of the vehicle [122–124]. Such batteries are widely deemed inadequate for automotive service and are taken out of service once their capacities have degraded below a specified threshold (typically 70 - 80% of the original value) [17, 45, 122, 125]. Automotive battery repurposing refers to giving a second life to used batteries originally designed for automotive applications [126]. Repurposing decommissioned automotive batteries helps prolong the use phase of the battery lifecycle before needing to be recycled. These batteries are especially attractive for stationary energy storage applications where the reduced specific energy and power values are not as critical to the operation [127].

An optimal reuse of automotive batteries in stationary applications requires repurposing of the decommissioned battery packs. The packs are then installed in the stationary application either as-is or after disassembly, sorting, and reassembling at the module or cell level [128]. Theoretically, the full potential of repurposing/remanufacturing can be tapped if batteries are disassembled to single cells and regrouped into battery packs after sorting, based on their current SOH and electrical properties [129]. This is practically challenging due to the construction methods used and the testing effort required. Specific sub-systems such as the power electronics, the EMS, the cooling system, and the housing would most likely need to be replaced to make the automotive batteries suitable for service in a stationary application. Remanufacturing is another term used in the literature, which is distinctly different from repurposing [128]. In remanufacturing, only the units limiting the pack performance are replaced with new or similarly aged units to enhance pack performance to acceptable standard levels [130].

Installation of second-life batteries in stationary applications is strongly dependent on the battery price and the duration of operation over which revenue can be generated for these services. As the costs of new lithium-ion cells have been falling owing to rising volumes, questions have arisen regarding the economic viability of second-life batteries vis-á-vis new batteries. Studies have shown that these developments notwithstanding, the economic viability for second-life batteries can be realized in suitable applications with the help of correct sizing methodologies [27, 45]. Figure 2.3 presents a schematic depiction of the entire lifecycle of a battery with three application pathways. The repurposing process for decommissioned automotive batteries used in second-life applications is also depicted.

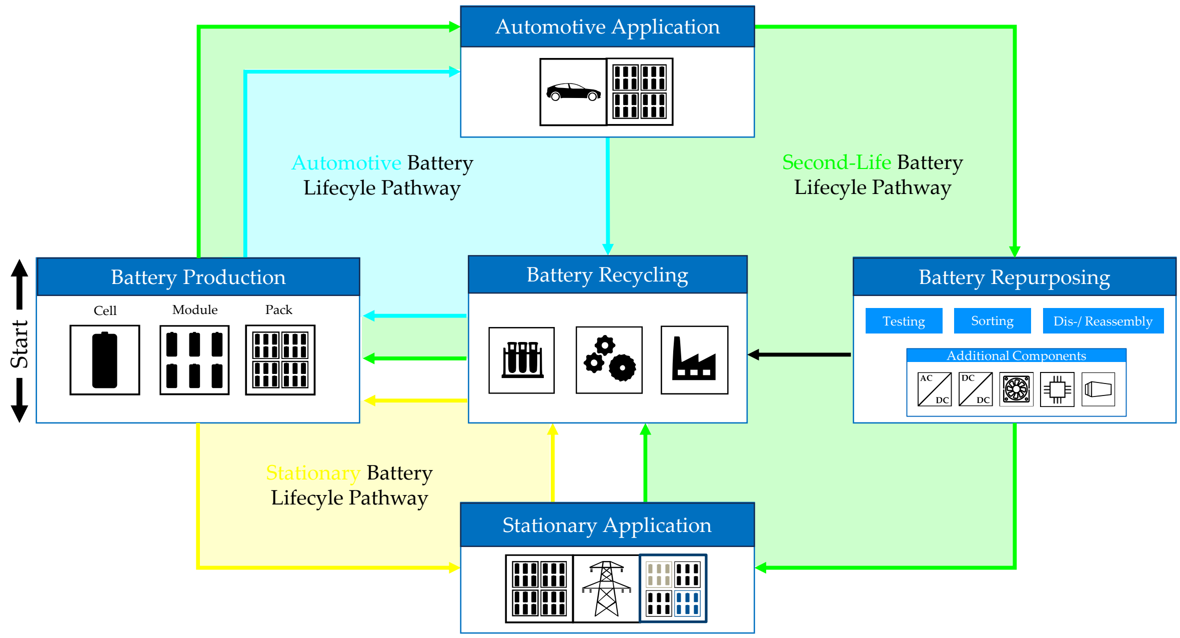

Figure 2.3: Lifecyle of a battery and the three prevalent application pathways - stationary application, automotive application, and the cascaded second-life pathway.

In chapter 8, the carbon footprint of second-life batteries is investigated compared to solely automotive or stationary usage.

2.4 Stationary applications

Battery storage applications today include transportation, consumer electronics, stationary systems, and portable tools, which are highly varied and broad [131–133]. The scope of this thesis restricts itself primarily to grid-connected and off-grid stationary battery applications. Grid-connected applications can further be classified as Front-of-the-meter (FTM) or as Behind-the-meter (BTM) applications [134].

In FTM applications, energy storage systems are typically deployed at the utility or grid level rather than behind the meter at individual homes or businesses. These systems are integrated into the larger electricity grid infrastructure and are often used for grid stabilization, peak shaving, renewable energy integration, and other grid support services [135]. FTM systems are also typically larger than BTM systems. BTM refers to energy systems or technologies located on the customer's side of the utility meter. These systems are installed at residential, commercial, or industrial sites [136, 137]. Stationary BESSs are also suited to provide grid services at all voltage levels in the electricity grid [138]. In the following subsections, some of these applications are discussed, and the subsequent chapters related to each of these applications are indicated.

Peak shaving

Demand peak shaving is an increasingly prevalent BTM service that a BESS is extremely well-placed to provide due to favorable attributes, such as fast response times, high energy efficiency, and durability [139–141]. Industrial and commercial electricity consumers with very high intermittent load peaks are required to pay not just for the amount of energy consumed but also for the maximum power demand at their sites in their annual or monthly billing cycles [142]. The peak shaving operation is performed with BESS by discharging stored energy during periods of peak demand in parallel with the grid power, essentially lowering the power drawn from the grid. The BESS is then charged during idle periods with relatively low overall site power demands [143]. The operator of the peak shaving BESS can thus save costs related to the maximum power demand and must only pay for the energy extracted from the grid at lower values of power [144]. While the motivation for peak shaving is often financial, such systems can also be used to strengthen grid infrastructure at locations with disproportionately high intermittent loads, such as electric vehicle (EV) fast-charging stations, or to provide relief to a strained local distribution grid. This is essentially akin to deferral of investments for grid reinforcement. All such systems reduce the peak instantaneous power demand that the grid has to fulfill and spread it over a larger period of time [145].

In chapter 4, the efficiency of a utility-scale BESS providing a peak shaving service at an industrial site is investigated.

Frequency regulation

Frequency regulation is an ancillary service in the electricity grid that is critical to system stability. Within the European context, the Frequency Containment Reserve (FCR) is designed to address sudden and unexpected imbalances between electricity generation and consumption, which can lead to deviations in the grid frequency. Such imbalances can be caused by unforeseen events such as sudden changes in demand, unexpected power plant outages, or fluctuations in renewable energy generation. FCR requires low response times to react to grid frequency deviations but provides participants with certain degrees of freedom [146, 147]. The full activation power must be attained within 30 seconds to prevent further disruptions and to maintain grid operation within an acceptable frequency range [148]. Upward reserves are activated when there is an unexpected increase in demand or a decrease in generation, leading to a frequency drop. Downward reserves are activated when there is a sudden decrease in demand or an increase in generation, causing a frequency rise. While adhering to the operation guidelines, FCR services can be provided by a variety of resources, including conventional power plants, energy storage systems, demand response programs, and other flexible grid participants.

The FCR product operates dynamically, with frequent activation and deactivation of reserves as the grid experiences fluctuations in supply and demand [149]. BESSs offer low response times, typically in the milliseconds to seconds range. The provision of frequency containment reserve with BESSs is an integral part of grid management today and helps mitigate the increasingly intermittent nature of power generation [150, 151]. A minimum permissible energy capacity to power (E/P) ratio is prescribed to ensure system availability to provide a minimum duration of reserves in both directions, as prescribed by the ENTSO-E (European Network of Transmission System Operators for Electricity) [152].

In chapter 4, the efficiency of a utility-scale BESS providing frequency regulation services is investigated. In chapter 8, the provision of FCR is chosen as an exemplary stationary application to investigate the carbon footprints of the three possible BESS lifecycle pathways.

Energy arbitrage

Energy arbitrage refers to the practice of buying and storing energy when prices are low and selling it when prices are high, thereby taking advantage of price differentials [153]. This strategy is commonly employed with energy storage systems, such as a BESS, due to their relatively high round-trip efficiencies and excellent ramp-rate capabilities. Depending on the regulatory environment, energy storage systems can participate in energy markets, including wholesale and ancillary service markets, to enhance revenue through arbitrage. Energy arbitrage relies on identifying and capitalizing on variations in electricity prices between low-demand (off-peak) and high-demand (peak) periods and determining an optimal schedule for the BESS, thus making price and demand forecasting capabilities of paramount importance [154]. The business case for the energy arbitrage application rests largely on favorable energy efficiency and battery degradation characteristics for the chosen BESS [155]. It is important to note that any profit earned in every transaction (consisting of buy and sell) is greater than the total marginal costs incurred during the transaction. These marginal costs cover the energy losses and the battery cyclic degradation. Incurred costs due to battery calendric degradation and auxiliary system consumption can be considered fixed costs, as they are present at all times, irrespective of the energy transactions [156].

In chapter 5, one of the two case studies presented investigates the carbon footprints of two different variants of energy arbitrage with a BESS.

Residential storage

Residential BESSs and rooftop solar installations are becoming increasingly popular as homeowners seek to reduce their reliance on traditional grid power, lower energy costs, and contribute to environmental sustainability [157]. The downward price trends for rooftop solar PV systems and lithium-ion BESSs, coupled with imminent future advancements in battery technology and regulatory support, are expected to increasingly favor the case for this application [158, 159]. Battery storage enhances the ability to store excess energy for later use. Proper sizing ensures that the system meets the household's energy needs and may allow for excess energy generation that can be stored or fed back to the grid [160]. Suitable EMS strategies coordinate solar generation, battery storage, and household consumption to meet the required energy demand while simultaneously maximizing self-consumption and minimizing battery degradation and the levelized cost of energy (LCOE) [161]. Excess electricity generated by rooftop solar panels or drawn from the grid during off-peak hours is stored in the battery system. Most residential BESS are equipped with power inverters that convert DC electricity from solar panels or the stored energy in the battery (also DC) into AC electricity, which most homes use. Smart management systems regulate when the battery charges and discharges based on several factors, including energy demand, energy prices, and battery health. Systems are often automated to optimize energy savings and battery life [162]. Storing excess energy generated during peak solar production times and using it during peak demand to avoid high electricity costs. This allows homeowners with solar panels to maximize the use of the energy they generate rather than selling it back to the grid at a lower price than what they would pay to buy it back later. This mechanism makes the value proposition for residential storage even more attractive, and in the long-term, policy incentives may become less relevant [163]. Although economically profitable, the environmental benefit with respect to the carbon footprint warrants a closer look [164].

In chapter 5, one of the two case studies presented investigates the carbon footprints of four distinct home energy system configurations with and without PV solar generation and battery storage.

Island grid

Island grids are isolated or autonomous energy systems operating independently from larger interconnected power systems. They are typically found in remote or off-grid locations without direct connection to a larger electricity grid. BESSs can fulfill a crucial role in the resilience, stability, and efficiency of island grids [165, 166]. Island grids rely on local resources for power generation, often incorporating renewable energy sources such as solar or wind. Energy storage helps balance the intermittent nature of renewables, storing excess energy when generation exceeds demand and supplying stored energy during periods of low generation. Island grids must maintain stable frequency and voltage levels, which can be challenging due to variations in renewable energy output and load fluctuations [167]. BESSs can offer fast response capabilities for frequency regulation and voltage control, helping to stabilize the grid during sudden changes in demand or generation. Island grids often face peak demand periods, and meeting these peaks can be challenging with limited generation capacity [168]. BESSs can be used for peak shaving and discharging stored energy during periods of high demand to reduce the need for additional generation capacity. BESSs can provide flexibility and controllability, allowing operators to optimize energy storage strategies based on real-time conditions, load forecasts, and economic considerations. Proper sizing and configuration of the battery system are essential to ensure optimal performance, considering the island's energy demand, renewable generation capacity, and desired storage duration [169].

In chapter 6, a new techno-environmental performance evaluation methodology is presented based on the BESS application of the island grid. A new metric Levelized Emissions of Energy Supply (LEES) is introduced, and the carbon footprint of such systems is discussed.

Battery-assisted electric vehicle charging

A successful ramp-up of the energy transition in the road transport sector hinges not only on the extent of public charging infrastructure coverage but also on reducing charging times. The availability of public charging infrastructure within a certain radius from any point is crucial to alleviate range anxiety, as not all EV users have access to home charging [170]. Low charging times ensure that longer trips can be completed within their planned schedules. While advances in lithium-ion battery technology now permit fast charging with high current rates, leading to reduced charging times, this solves only the EV side of the puzzle. Several challenges are expected in order to realize broad charging infrastructure coverage and fast charging with the present electricity grid. The current grid design does not account for large electric loads in the form of EVs connecting to and disconnecting from the grid at multiple locations without a pre-notified schedule [171]. As a consequence, not all locations connected to the electricity grid are designed to handle large fluctuating electric loads [172]. Also, in the absence of high utilization factors for these locations, grid operators might need to levy large sums in the form of peak demand charges, making it economically unattractive for charging operators to set up new installations [173].

A possible solution is battery-assisted high-power charging. Also known as a buffer-storage, this BTM application involves a stationary BESS installed on-site next to the charging infrastructure [174]. The BESS is discharged in times of peak EV charging power demand to augment the power capacity of the grid connection. The BESS is charged in periods of low charging demand when grid capacity is available in addition to the charging power demand. The BESS is able to successfully meet large peak loads while avoiding hefty demand charges and deferring grid investments until higher grid utilization rates can be achieved at that location [175]. The BESS is sized to be able to cover peak charging power demand with sufficient energy capacity to sustain the requisite discharging power over periods of peak demand [176].

In chapter 7, the carbon footprint of battery-assisted high-power charging is investigated. The modeling and simulation of this application are discussed in detail. A novel state variable - the State of Carbon Intensity (SOCI) is introduced, and the influence of various EMS strategies on the LEES value of the charging energy supplied to EVs is studied.

3 Modeling and simulation

This chapter discusses the modeling techniques and simulation methodologies used to simulate lithium-ion battery systems within the broader context of energy systems. Section 3.1 presents a short discussion on battery modeling before proceeding on to the specifics of battery simulation with SimSES, an open-source simulation program for modeling lithium-ion battery systems. The simulation procedure for lithium-ion battery systems, including modeling second-life batteries with SimSES, is outlined. As a BESS does not operate in isolation but rather as a part of energy systems, modeling energy systems is an indispensable step in conducting system-level evaluations. Section 3.2 discusses the central features of energy system modeling, followed by a deeper discussion on the modeling procedure in ESN, an open-source simulation program to model energy systems. This section also presents the components of an energy system, followed by a discussion on the simulation procedure and the programmatic coupling between SimSES and ESN.

3.1 Modeling lithium-ion battery systems

In the domain of battery system simulation, the depth of simulation detail varies significantly based on the intended application, ranging from extremely detailed electrochemical models to highly simplified economic analyses. MATLAB, Simulink, Python, OpenModelica, and even spreadsheeting software offer highly customizable development environments to create battery models that cater to a broad range of requirements. Some well-known tools discussed in the reviewed literature include Homer, StorageVET, BLAST, SAM, and PermodAC, which are available to assess various aspects of battery systems operating in stationary applications. A wide spectrum of modeling approaches points to diverse simulation requirements, ranging from detailed performance simulations to broader system-level and economic evaluations. And yet, while these tools individually offer useful capabilities, none offers a comprehensive and flexible suite of simulation capabilities [177]. The need for a holistic simulation framework like SimSES and the shortcomings of the prevalent tools are discussed in detail in the appendix. Section 3.1.1 presents some salient features of the battery system modeling procedure with SimSES. Section 3.1.2 discusses the simulation setup process, while section 3.1.3 discusses the simulation of second-life batteries with SimSES.

3.1.1 Battery modeling with Simulation of Stationary Energy Storage Systems (SimSES)

This section discusses the modeling procedure for a lithium-ion battery system with the open-source simulation program SimSES[1]. SimSES offers a holistic energy storage system modeling approach, which covers all the major components of a BESS described in section 2.1.1. The stationary BESS applications discussed in section 2.4 are simulated with a SimSES instance running within ESN - an

[1] Link to the SimSES Gitlab code repository hosted by LRZ.

energy system simulation tool (described in section 3.2.1). The following paragraphs discuss specific aspects of the modeling approach employed within SimSES. A detailed publication introducing SimSES and its features is presented in the appendix.

Battery model: A parameterized ECM is deployed in SimSES to emulate the electrical-thermal behavior of an individual lithium-ion cell. The model consists of a voltage source and a series-connected internal resistance. The voltage source is based on an Open Circuit Voltage (OCV) curve, which links the cell voltage to its SOC. The OCV curve and the internal resistance values can be obtained from detailed characterization tests for each cell type. Physical properties such as the mass, specific heat capacity, and the surface convection coefficient are obtained from the cell datasheet and literature sources. Depending on data availability, the OCV and the internal resistance of a cell can be modeled as functions of temperature, SOC, or other factors such as the SOH. This data is accessed by SimSES through multidimensional lookup tables, with linear interpolation to obtain the necessary values. The parallel and series connection topology necessary for the BESS is obtained based on the application boundary conditions, the individual cell charge capacity, and the nominal voltage. The battery is modeled on a big-cell modeling approach to avoid the computational complexity and effort of simultaneously simulating thousands of cells. The electrical and thermal properties of an individual cell are scaled up to reflect those of the connected topology. The cell-to-cell variations discussed in section 2.1.1 are not considered further in this thesis, and all cells are considered to be identical. The terminal voltage at time t, V_t is given by eq. 3.1. V^{OC} represents the OCV. I_t and R_t represent the current (signed) and internal resistance values at time t respectively.

$$V_t = V^{OC} - I_t \cdot R_t \tag{3.1}$$

Power electronics model: AC/DC converters enable the conversion of AC power on the grid side to DC power on the battery side, and vice-versa. On the other hand, DC/DC converters facilitate energy conversion between dissimilar DC voltage levels. The power electronics components in SimSES are modeled with the help of efficiency curves that specify the converter efficiency values at the corresponding load values. This data is obtained from literature sources and manufacturers' datasheets. By accounting for the efficiency of power conversion processes, SimSES can estimate the system efficiency and thermal behavior. Although SimSES offers the possibility of including both AC/DC and DC/DC converters in a BESS simulation, only AC/DC converters are used for BESS configurations simulated in this thesis. Eq. 3.2 represents the power calculation at the output (P_{PE}^{out}) with respect to the input (P_{PE}^{in}) terminals of the power electronics device. η_{PE} represents the power conversion efficiency as a function of the load fraction f_L.

$$P_{PE}^{out} = P_{PE}^{in} \cdot \eta_{PE}(f_L) \tag{3.2}$$

BMS model: The BMS model within SimSES monitors cell operation and if required, enforces limits on the permissible current. The model operates in conjunction with the ECM and continuously monitors critical cell parameters, ensuring the limits on the allowed charging and discharging C-rate values, operating temperatures, and available energy are complied with. This functionality is indispensable for the safe operation and normal degradation of lithium-ion batteries.

EMS model: The EMS model in SimSES generates power targets for the BESS, based on the requirements for the chosen BESS application. SimSES can also receive externally-determined power targets and operate the BESS in accordance with these. The EMS determines how the storage interacts with the grid, responds to demand, and optimizes its performance for various applications. SimSES can implement various operation strategies designed for specific applications or objectives. These strategies can range from basic power following, where the storage system aims to match a predefined power profile, to more complex strategies like peak shaving, frequency regulation, or optimizing for profit, such as energy arbitrage. The parameters and rules governing the operation strategy can be tailored to specific research questions or project requirements.

Housing model: The housing model in SimSES emulates the physical enclosure in which the battery and associated components are installed. External environmental conditions, such as the ambient temperature and solar irradiation, significantly influence the efficiency and degradation of the BESS. A standard shipping container is often used for utility-scale and commercial BESSs due to the associated advantages such as modularity, scalability, and transportability. The container model in SimSES includes the insulation properties of the container wall, and its impact on the heat transfer to/from the ambient environment can also be observed. The housing model allows the simulation results to reflect seasonal variations and geographical differences in climate, which are critical for designing and operating a BESS. SimSES offers two container options for utility-scale BESSs - the 20 ft. container and the 40 ft. container. The physical and thermal characteristics of the container, including its wall layers and insulation properties, can be customized to reflect different types of enclosures.

Electro-thermal system model: The thermal behavior of the BESS model can also be investigated with SimSES. The correct system thermal model and housing type combination is coupled with the electrical simulation based on the simulated scenario. In the basic configuration, the operation of the BESS can be simulated with an invariable constant battery temperature and no thermal interactions with the surroundings. Simulating the BESS operation with passive convective heat exchange with a constant temperature environment is also possible. The components are not subjected to solar irradiation or other environmental effects. The third configuration enables the simulation of a BESS installed in one of the two standard shipping container housing types. The container can be subjected to location-dependent ambient temperature and solar irradiation profiles. The system thermal model integrates all other thermal components to simulate the heat transfer dynamics within the BESS. This model solves a system of differential equations to predict the temperatures of the storage technologies, internal air, and other components after each simulation timestep. It accounts for heat generation due to losses in energy conversion, heat exchange between components and the environment, and the HVAC system.

In eq. 3.3, T_{batt} is the temperature of the battery unit. m_{batt} refers to the mass of the battery units, and c_p^{batt} represents its specific heat capacity. P_{loss}^{batt} is the rate of heat dissipation within the battery due to losses in the energy conversion process, whereas $P_{conv}^{batt-ia}$ is the rate of convective heat transfer from the battery unit to the internal air in the enclosure.

$$m_{batt} \cdot c_p^{batt} \cdot \frac{dT_{batt}}{dt} = P_{loss}^{batt} - P_{conv}^{batt-ia} \tag{3.3}$$

In eq. 3.4, T_{ia} is the temperature of the internal air in the enclosure. m_{ia} refers to the mass of the internal air, and c_p^{ia} represents its specific heat capacity. $P_{conv}^{batt-ia}$ is the convective heat transfer rate from the battery unit to the internal air in the enclosure, P_{hvac} is the thermal power of the HVAC system, and P_{conv}^{ia-il} is the convective heat transfer rate from the internal air to the inner layer of the housing wall.

$$m_{ia} \cdot c_p^{ia} \cdot \frac{dT_{ia}}{dt} = \sum P_{conv}^{batt-ia} - P_{hvac} - P_{conv}^{ia-il} \tag{3.4}$$

The detailed mathematical framework can be found in the appendix, which presents the central publication introducing SimSES.

3.1.2 Simulating a BESS with SimSES

Setting up a simulation within the SimSES environment begins with the definition of the duration of the simulation, the timestep, the BESS configuration, the simulation parameters, and the input data. The config files (.ini) in the project folder serve as the interface to the program. The BESS configuration includes the type of lithium-ion cell, the power electronics model for AC/DC conversion, the thermal management system, and other system components. This modular setup allows for a wide range of possible BESS configurations. The EMS operation strategy plays a pivotal role in dictating how the storage system interacts with the grid and responds to energy demands. These strategies can range from built-in strategies within SimSES to custom approaches designed by the user to create the charge-discharge schedule. The requisite time-series profiles, such as those for the load demand, renewable generation, and energy prices, can be specified for use in the simulated scenario. After the configuration step, the simulation can be run. SimSES calculates and stores the various system states at each simulation step. After the simulation is completed, SimSES runs an analysis of the simulation results to generate the technical performance evaluations, which provide insights into the system efficiency and degradation over time, among other metrics.

3.1.3 Modelling second-life batteries with SimSES

Second-life batteries can be simulated in stationary applications with SimSES. The relevant information pertaining to the state of the second-life batteries can be specified in the config file. One of the parameters to be specified is the start SOH, which is typically expressed as a fraction and is a measure of the residual capacity of the battery as it begins its second life. The share of calendric and cyclic degradation in the already degraded capacity must also be specified to enable the initialization of the degradation functions. The next important parameter to specify is the increase in the internal resistance of the battery at the start of its second life compared to its original value. A higher internal resistance affects the efficiency and heat generation of the battery during operation as compared to a new battery. The simulation can be started after specifying the system configuration and other simulation parameters as in any other simulation.

3.2 Modeling energy systems

As a BESS operates within the confines of an energy system, modeling the energy system is inevitable. Energy system modeling and simulation is a central aspect of energy engineering that enables decision-makers to simulate and investigate the dynamics behind the consumption and generation of energy. Top-down energy system models are top-level and deal with the aggregated aspects of the energy sectors - energy demand, energy supply, and their relation to macroeconomic aspects of the economy. Bottom-up energy system models, in contrast, exhibit a high degree of technological detail and do not consider macroeconomic aspects [178]. The general trend in energy system model development points to an unmistakable preference for bottom-up optimization-based models, with flexibility in all modeling aspects - time horizon, temporal, and spatial resolution, being highly sought after [179]. While the questions energy system modeling attempts to answer have not changed, large energy system models covering the entire energy system ought to give way to leaner frameworks consisting of agile models that enable specific questions relating to the changing requirements of today to be answered [180].

Energy system models involve energetic components such as demand, generation, transmission, and storage. These components are intercoupled through a mathematical framework of governing equations and constraints to investigate relevant aspects of system behavior through scenario generation and simulations. The immediate context provided by the energy system in which a BESS operates is crucial for determining its carbon footprint. Although many energy system modeling tools and simulation programs exist today, none of them offer detailed modeling and high-resolution capabilities to quantify the carbon footprint of BESS operating in energy systems. Thus, the necessity for an agile bottom-up model with flexible modeling aspects was identified to enable specific questions relating to the carbon footprint of energy storage systems to be addressed [181]. To address this necessity, Energy System Network (ESN) was developed to enable many research aspects in this thesis to be answered. Chapter 5 presents a detailed literature review on available energy system modeling tools and a deeper discussion on the rationale for a new energy system simulation program focusing on energy storage.

3.2.1 Energy system modeling with Energy System Network (ESN)

This section discusses the modeling procedure for an energy system with the open-source simulation program ESN[2]. Within ESN, an energy system is modeled as an interconnected framework that integrates various energy system components to simulate and analyze the behavior and performance of localized energy systems. A particular focus is on their carbon footprint. ESN employs a modular approach, inspired by the programming approach of SimSES, that allows the simulation of several energy system configurations.

Energy system: An energy system within ESN is defined as a self-contained simulation unit representing a single node that fulfills an energy balance. This conceptualization of an energy system includes a combination of energy system components, including generation, storage, grid connection, and load components. These components operate in tandem to ensure the energy supply meets the specific demands of a particular application or scenario. The energy flows between the components are managed by an EMS to achieve specific objectives as defined in the operation strategy. Figure 3.1 provides an overview of the energy system components and the EMS.

[2] Link to the ESN Gitlab code repository hosted by LRZ.

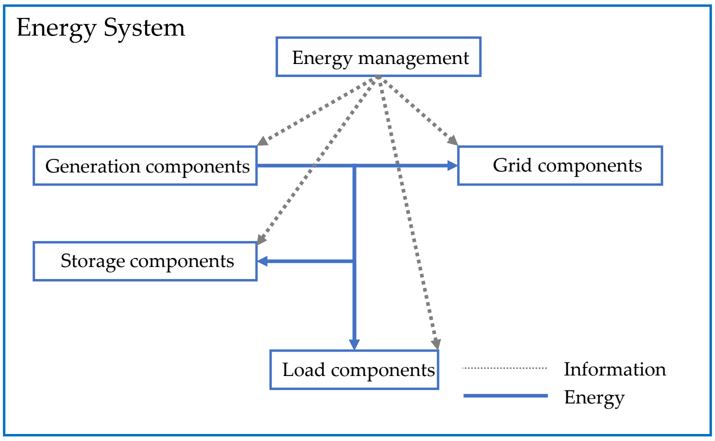

Figure 3.1: Schematic overview of an energy system with the energy system components and the Energy Management System (EMS) presiding over their operation. The energy system components are connected to one another at a common node in the energy system, and an energy balance must be fulfilled at this node.

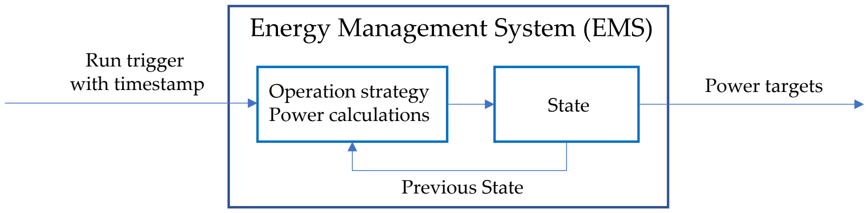

Figure 3.2: Schematic diagram of the Energy Management System (EMS) and its operation principle. Based on the operation strategy, the EMS generates power targets for all energy system components.

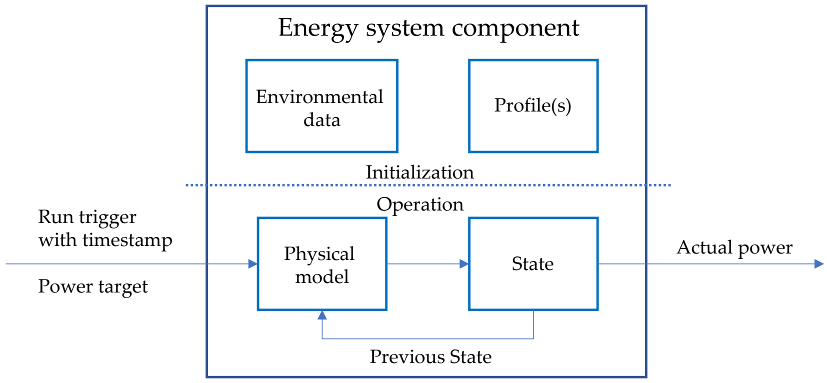

Figure 3.3: Schematic diagram of an energy system component, i.e., a generation, grid, storage, or a load component. Each energy system component receives a power target from the EMS and attempts to fulfill it within the bounds of its physical limits and other constraints.

Energy system components: In an energy system, generation components play a central role - producing the power to meet the energy demand of a load. Generation technologies include conventional generators and non-conventional or renewable energy generators. Conventional generators include thermal power generation technologies such as coal, natural gas, nuclear power plants, and diesel generators. Renewable sources of power generation include solar, wind, and hydropower plants. Within ESN, generation components simulate power generation systems, including renewable sources like solar PV and wind turbines. Grid components play a critical role in energy system simulation models by representing the infrastructure and elements that facilitate the transmission and distribution of electricity within a power system. Within ESN, grid components represent grid connections or grid sections that facilitate the import and export of power to and from the larger grid. Storage components are an integral part of the energy system simulation model, providing the capability to store excess energy for later use, balance supply and demand, and enhance the overall flexibility and reliability of the system. Storage components model the characteristics of energy storage systems, such as a BESS. Load components in ESN represent the electricity demand from various sectors. Load components approximate power consumers within the energy system, including residential, commercial, or industrial loads, and EV charging demands. They capture the consumption patterns through load profiles. Figure 3.3 depicts the schematic structure of an energy system component, whereas figure 3.2 depicts the schematic structure of the EMS.

Detailed handling of the carbon footprints of generation, grid, storage, and load components is a key feature of ESN. The total carbon footprint attributable to each component over the simulation period is the sum of the carbon footprints of individual lifecycle phases such as production, operation, and EOL. The following expressions give the carbon footprint for a generation component over the simulation period (assuming this is also equal to its service lifetime). ε^{gen} is the total carbon footprint of the generation component over the simulation period. This comprises of the carbon footprints of the production phase, $\varepsilon^{gen,prod}$, the operation phase, $\varepsilon^{gen,op}$, and the EOL phase, $\varepsilon^{gen,EOL}$. The carbon footprint attributable to the exported energy ($\varepsilon^{gen,exp}$) is subtracted from the total carbon footprint of the component and allocated to external actors (eq. 3.5).

$$\varepsilon^{gen} = \varepsilon^{gen,prod} + \varepsilon^{gen,op} + \varepsilon^{gen,EOL} - \varepsilon^{gen,exp} \tag{3.5}$$

The total operation phase emissions, $\varepsilon^{gen,op}$, can be calculated as shown in eq. 3.6. Here, CI_t^{gen} refers to the carbon intensity of the generated energy before losses at time t and is equal to the combustion emissions per kWh of electricity for conventional generation components. For generation components such as the PV solar system and wind turbines, CI_t^{gen} is zero. $P_t^{gen,loss}$ is the loss power at time t. Δt is the chosen simulation timestep.

$$\varepsilon^{gen,op} = \sum_{t=start}^{end} \left(CI_t^{gen} \cdot P_t^{gen,loss} \right) \cdot \Delta t \tag{3.6}$$

The following expressions describe the carbon footprint for a grid component over the simulation period (assuming this is also equal to its service lifetime). The total emissions for the grid component, ε^{gr}, are calculated as the sum of the production phase emissions, $\varepsilon^{gr,prod}$, the operation phase emissions, $\varepsilon^{gr,op}$, and the end-of-life emissions, $\varepsilon^{gr,EOL}$, minus the emissions attributable to the exported energy,

$\varepsilon^{gr,exp}$ (eq. 3.7).

$$\varepsilon^{gr} = \varepsilon^{gr,prod} + \varepsilon^{gr,op} + \varepsilon^{gr,EOL} - \varepsilon^{gr,exp} \tag{3.7}$$

The operation phase emissions, $\varepsilon^{gr,op}$, can be calculated as shown in eq. 3.8. Here, CI_t^{gr} refers to the carbon intensity of the grid energy at time t. $P_t^{gr,loss}$ is the loss power at time t. Δt is the chosen simulation timestep.

$$\varepsilon^{gr,op} = \sum_{t=start}^{end} \left(CI_t^{gr} \cdot P_t^{gr,loss} \right) \cdot \Delta t \tag{3.8}$$

The following expressions give the carbon footprint for a storage component over the simulation period (assuming this is also equal to its service lifetime). Similar to the calculations presented earlier for the other components, the total emissions for the storage component, ε^{st}, are calculated as the sum of the production phase emissions, $\varepsilon^{st,prod}$, the operation phase emissions, $\varepsilon^{st,op}$, and the end-of-life emissions, $\varepsilon^{st,EOL}$, minus the emissions attributable to the exported energy, $\varepsilon^{st,exp}$ (eq. 3.9).

$$\varepsilon^{st} = \varepsilon^{st,prod} + \varepsilon^{st,op} + \varepsilon^{st,EOL} - \varepsilon^{st,exp} \tag{3.9}$$

The operation phase emissions, $\varepsilon^{st,op}$, can be calculated as shown in eq. 3.10. Here, CI_t^{ch} refers to the carbon intensity of the charging energy at time t, which is often equal to the effective carbon intensity of the energy available in the energy system, CI_t^{ES} (eq. 3.11). The State of Carbon Intensity (SOCI) is a novel state variable introduced specifically to quantify the carbon footprint of the energy stored in a storage component (eq. 3.12) and is also useful in calculating the value of $\varepsilon^{st,op}$. A detailed treatment of SOCI can be found in chapter 7. $P_t^{ch,loss}$ and $P_t^{dch,loss}$ are the loss powers during the charging and discharging processes, respectively, at time t. Δt is the chosen simulation timestep.

$$\varepsilon^{st,op} = \sum_{t=start}^{end} \left(CI_t^{ch} \cdot P_t^{ch,loss} + SOCI_t \cdot P_t^{dch,loss} \right) \cdot \Delta t \tag{3.10}$$

$$CI_t^{ES} = \frac{\sum_{i=1}^{m} P_t^{gen,i} \cdot CI_t^{gen,i} + CI_t^{gr} \cdot P_t^{gr}}{\sum_{i=1}^{m} P_t^{gen,i} + P_t^{gr}} \tag{3.11}$$

$$SOCI_{t+1} = \frac{SOCI_t \cdot SOC_t + \Delta SOC \cdot CI_t^{ch}}{SOC_{t+1}} \tag{3.12}$$

The following expressions give the carbon footprint for a load component over the simulation period. In contrast to the energy system components presented thus far, the total emissions for the load component, ε^{load}, are calculated as the sum of the Load Energy Consumption (LEC) emissions, ε^{LEC} and the operation phase emissions, $\varepsilon^{load,op}$ (eq. 3.13). P_t^{load} is the gross power supplied to the load component at time t. It comprises the actual power consumed by the load component, $P_t^{load,c}$, and the loss power of the load component, $P_t^{load,loss}$ (eq. 3.14).

$$\varepsilon^{load} = \varepsilon^{LEC} + \varepsilon^{load,op} = \sum_{t=start}^{end} \left(P_t^{load} \cdot CI_t^{ES}\right) \cdot \Delta t \tag{3.13}$$

$$P_t^{load} = P_t^{load,c} + P_t^{load,loss} \tag{3.14}$$

ε^{LEC} and $\varepsilon^{load,op}$ are calculated as follows with the help of $P_t^{load,c}$, $P_t^{load,loss}$, and CI_t^{ES} as given in eq. 3.15 and eq. 3.16. The LEC emissions are those emissions associated with the energy consumed by the load component.

$$\varepsilon^{LEC} = \sum_{t=start}^{end} \left(P_t^{load,c} \cdot CI_t^{ES}\right) \cdot \Delta t \tag{3.15}$$

$$\varepsilon^{load,op} = \sum_{t=start}^{end} \left(P_t^{load,loss} \cdot CI_t^{ES}\right) \cdot \Delta t \tag{3.16}$$

An energy balance among all the components must be satisfied within each energy system at each timestep. This ensures that the total energy is conserved and accounted for (eq. 3.17). On the left-hand side of eq. 3.17, $P_t^{gen,i}$ represents the power generated by the i^{th} generation component at time t, $P_t^{st,dch,j}$ represents the power discharged by the j^{th} storage component at time t, and $P_t^{gr,imp}$ is the power imported from the grid component at time t. On the right-hand side, $P_t^{load,k}$ represents the power consumed by the k^{th} load component at time t, $P_t^{st,ch,j}$ represents the charging power of the j^{th} storage component at time t, and $P_t^{gr,exp}$ is the power exported to the grid component at time t.

$$\sum_{i=1}^{l} P_t^{gen,i} + \sum_{j=1}^{m} P_t^{st,dch,j} + P_t^{gr,imp} = \sum_{k=1}^{n} P_t^{load,k} + \sum_{j=1}^{m} P_t^{st,ch,j} + P_t^{gr,exp} \tag{3.17}$$

Similarly, a CO_2 emissions balance also applies to each energy system while considering the correct system and temporal boundaries for each component. Consequently, CO_2 emissions can be allocated to each component under the respective emissions categories (eq. 3.18). On the left-hand side of eq. 3.18, CI_t^{gr} represents the carbon intensity of the grid component at time t, $CI_t^{gen,i}$ represents the carbon intensity of the i^{th} generation component at time t, while $\eta_t^{gen,i}$ is the efficiency of this generation component. On the right-hand side, $\varepsilon_t^{gr,op}$ represents the operation emissions of the grid component at time t, $\varepsilon_t^{gen,op,i}$ represents the operation emissions of the i^{th} generation component. $\varepsilon_t^{st,op,j}$ represents the operation emissions of the j^{th} storage component, while $\varepsilon_t^{LEC,k}$ and $\varepsilon_t^{load,op,k}$ represent the LEC emissions and the operation emissions respectively of the k^{th} load component.

$$P_t^{gr,imp} \cdot CI_t^{gr} + \sum_{i=1}^{l} \frac{P_t^{gen,i}}{\eta_t^{gen,i}} CI_t^{gen,i} = \varepsilon_t^{gr,op} + \sum_{i=1}^{l} \varepsilon_t^{gen,op,i} + \sum_{j=1}^{m} \varepsilon_t^{st,op,j} + \sum_{k=1}^{n} (\varepsilon_t^{LEC,k} + \varepsilon_t^{load,op,k}) \quad (3.18)$$

3.2.2 Simulating an energy system with ESN

Modeling an energy system within the ESN environment is achieved by specifying the desired simulation configuration through the config files (.ini) in the project folder. The first step is specifying the general simulation data, including the simulation duration and timestep. Configuring the EMS is the next step, along with defining several parameters related to the chosen operation strategy. The user chooses whether to use rule-based or optimization-based strategies for energy management. Rule-based strategies operate based on predefined rules under certain conditions, while optimization-based strategies use mathematical optimization to determine power targets for all components. Examples of rule-based strategies available in ESN include *SimpleDeficitCoverage* (prioritizes energy system components to meet load demand) and *SimplePeakShaving* (manages peak power demands using storage components). Examples of optimization-based strategies in ESN include *RHOptimization* (employs a rolling horizon optimization problem to minimize emissions) and *ArbitrageOptimization* (optimizes the dispatch schedule of BESS for energy arbitrage). The next step is specifying the energy system components and their parameters within the energy system. Attributes such as the peak generation power, energy capacity, and peak demand power for all the components are defined in this step. The next step involves specifying the time-series profiles for generation, load demands, and other variable attributes like grid carbon intensity. The lifecycle emissions data for each component is configured to enable comprehensive carbon footprint analysis across the production, operation, and EOL phases.

Subsequently, the simulation can be executed using the specified energy system configuration, energy management strategy, and simulation setup. ESN simulates and stores the resulting system states at each timestep. The program analyzes the simulation results once the simulation has concluded. The system performance can be analyzed using various performance indicators computed by the program. For detailed user documentation on ESN, readers are urged to check the repository website[3], which includes configured examples with extensive descriptions of the config files. Chapter 5 presents a detailed description of the mathematical framework underpinning ESN and the methodology to quantify the carbon footprint of all energy system components.

3.2.3 Coupling ESN and SimSES

The integration of the simulation program SimSES (discussed earlier in section 3.1.1) with ESN enhances the capability to simulate and analyze the BESS performance within localized energy systems. The coupling of these two programs leverages the strengths of each to provide a comprehensive simulation program for the simulation, evaluation, and optimization of energy storage systems and their interactions with the broader energy system. The coupling allows for the simulation of various scenarios, assessing how different configurations of energy storage systems can meet energy demands, support renewable energy integration, and minimize carbon emissions in localized energy systems.

SimSES provides an in-depth technical simulation of energy storage systems, primarily lithium-ion BESSs. Its modular design allows for the flexible configuration of BESSs for a wide range of ap-

[3] Link to the ESN Gitlab code repository hosted by LRZ.

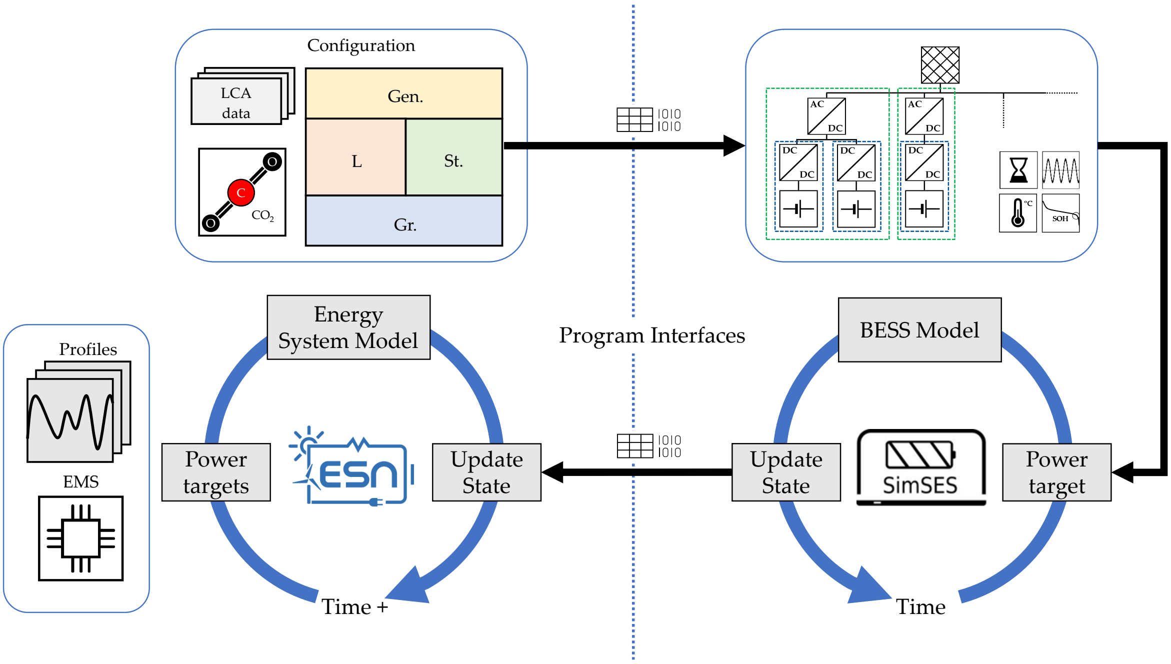

Figure 3.4: Graphical depiction of the integration of ESN and SimSES. ESN interacts and exchanges information with SimSES via multiple program interfaces. Configuration information, state information, and results are shared between the programs at each timestep or at the start/end of a simulation run.

plications. This capability is crucial for understanding the performance, efficiency, and degradation patterns of the BESS under various operational conditions. SimSES can thus emulate the behavior and performance of storage systems to a high degree of detail by simulating these technical aspects. ESN complements SimSES by focusing on the carbon footprint and environmental impact of energy storage and other components within localized energy systems. It takes a comprehensive view, considering the operational phase and the production and EOL stages of system components. The detailed CO_2 emissions analysis in ESN helps identify strategies to minimize the environmental footprint of energy storage systems. Figure 3.4 depicts the integration of SimSES and ESN through the program interfaces that allow the exchange of information.

4 The efficiency of Li-ion battery energy storage systems

A significant portion of the energy losses in a BESS is attributed to conversion losses within the power electronics and the battery system. There is a need for a deeper understanding of these components. Some major factors that influence the efficiency include the characteristics of the application in which these systems are operated, the topology of power electronics, and the specific parameters of the batteries themselves. This study discusses several performance indicators to aid the analysis, such as system efficiency, temporal and active charge-based utilization ratios, and system availability. These metrics serve as essential tools for assessing the operational efficiency and behavior of a BESS across different scenarios. The analysis of two specific grid-related applications — peak shaving and primary control reserve (PCR) — highlights how the efficiency and performance of a BESS can vary significantly based on their operation. Peak shaving, characterized by infrequent but high-power energy requests, contrasts with the frequent, low-power energy demands of PCR. This distinction underlines the necessity of tailoring the BESS design and operation to suit specific application needs, emphasizing that a one-size-fits-all approach is insufficient.

The highlights of this article include:

- Application characteristics and their impact on the efficiency of lithium-ion BESSs
- The influence of power electronics topologies and load distribution strategies on the efficiency of BESSs
- The effect of battery parameters, such as State of Health (SOH) and internal resistance, on the efficiency and operation of a BESS

It is found that the choice of the power electronics topology and load distribution strategy can substantially affect the conversion efficiency of BESS, especially in applications characterized by low active charge-based and high temporal utilization ratios. The findings suggest that the operational strategy for BESSs must be carefully considered to improve efficiency, especially when incorporating aged batteries, which pose additional challenges due to capacity fade and increased resistance. A pressing need for holistic system models that can comprehensively account for all components of a BESS is identified.

Author contributions
Anupam Parlikar was the principal author of this study, handling the conceptualization, data curation, formal analysis, simulative investigations, visualization, and writing the original draft and subsequent revisions. Holger Hesse contributed through formal analysis, provided supervision, assisted with visualization, partook in the manuscript's review and editing, and assisted in securing funding. Andreas Jossen was instrumental in acquiring funding, providing resources, offering supervision, and revising the manuscript. This article is a result of the collaborative efforts of all authors.

Topology and Efficiency Analysis of Utility-Scale Battery Energy Storage Systems

Anupam Parlikar, Holger Hesse, and Andreas Jossen

Atlantis Highlights in Engineering (4), 13th International Renewable Energy Storage Conference (IRES 2019), 2019

Permanent weblink:
https://www.atlantis-press.com/proceedings/ires-19/125923324

ATLANTIS PRESS

Atlantis Highlights in Engineering, volume 4

13th International Renewable Energy Storage Conference (IRES 2019)

Topology and Efficiency Analysis of Utility-Scale Battery Energy Storage Systems

Anupam Parlikar*, Holger Hesse†, Andreas Jossen‡
Institute for Electrical Energy Storage Technology (EES), Technical University of Munich (TUM)
Munich, Germany
Email: *anupam.parlikar@tum.de, †holger.hesse@tum.de, ‡andreas.jossen@tum.de

***Abstract*—Energy storage is an important flexibility measure to stabilize and secure the electrical energy supply system. Lithium-ion battery energy systems (BESS) are, owing to their characteristics, uniquely poised to support and augment the functioning of the energy supply system. It is crucial to identify and analyze the factors which play a role in their efficient and effective operation. This paper identifies and analyses three such major factors - application scenarios, power electronics with power distribution strategies, and battery parameters which influence the efficiency of a BESS. The applications analyzed are primary control reserve and peak shaving. Two Power electronics topologies and their load distribution strategies are presented, with their influence on the conversion efficiency being evaluated subsequently. Two commercial lithium-ion technologies - a Lithium Iron Phosphate cathode/Graphite anode cell and a Lithium Nickel Manganese Cobalt Oxide cathode/Graphite anode cell are also simulated for two states of health (SOH). The aged cells are considered to possess a capacity equal to 80% of original nominal capacity and a cell resistance twice that of the new cells. It is found that the system conversion efficiency can be greatly improved in applications with low active charge-based and high temporal utilization ratios by deploying a suitable power electronics topology and load distribution strategy. For applications with high active charge-based and low temporal utilization ratios, the battery resistance and the serial-parallel combination play an important role.**

***Index Terms*—energy storage, lithium-ion battery, efficiency, battery energy storage system**

I. Introduction

With the global advent of cost-competitive electricity produced by fluctuating renewable energy sources such as photovoltaic solar and wind turbines [1]–[3], the economic hurdles in the way of large-scale adoption of these technologies are set to gradually disappear. At the same time, increasing grid-penetration ratios pose significant challenges to the maintenance of grid stability and power quality [4], [5]. A variety of flexibility options will have to be pressed into service to be able to smooth out the mismatch between load and demand at all times [6]. Energy storage, being one such flexibility measure, is slated to play a pivotal role in the stabilization of the grid in the upcoming times [7].

Stationary Lithium-ion battery energy storage systems (BESS) are increasingly being seen as a reliable solution to the challenge posed by the acute requirement of flexibility measures aiding the grid to maintain its stability. Stationary BESS can provide a number of vital ancillary services to the electricity supply system such as - frequency control, voltage control, load balancing, peak shaving, among others [8]–[11]. Lithium-ion BESS technology is the leading battery energy storage technology in current times owing to its relatively high round-trip efficiency, high energy and power density as well as superior lifetime performance [10], [12].

This paper aims to highlight some of the factors influencing the efficiency of a stationary BESS. Section II discusses the components of a modern stationary BESS and the influence of components on the efficiency of the system. This is followed by section III, in which definitions of performance indicators employed in this paper are presented. Section IV-A discusses the dependence of the efficiency on the kind of service being provided by a BESS, with a further focus on two grid-related applications. The section IV-B discusses the influence of the cells used on the system efficiency, whereas the subsequent section IV-C investigates the influence of the power electronics components on the efficiency of the system.

II. State-of-art

A typical stationary BESS, depicted in fig. 1, generally comprises of the following sub-components [9], [13]:

1) Battery system:
   a) Cell
   b) Module
   c) Rack
2) Power Electronics
   a) DC/DC converter(s)
   b) AC/DC converter(s)
3) Auxiliary components
   a) Energy Management System (EMS)
   b) Battery Management System (BMS)
   c) Thermal Management System (TMS)

The individual lithium ion cells are combined in series to form strings, two or more of which are combined in parallel to form modules. These modules are further combined as per requirements to yield racks or packs at the desired voltage level. The power electronics come into the picture at this stage, where a DC/DC converter can used to further step up the DC terminal voltage of the rack/pack before being connected to an AC/DC converter that then interfaces with the grid, depending on the voltage level, either directly, or with a transformer in between. The DC/DC converter is often optional, but when used it enables the battery system to be

ATLANTIS PRESS
Atlantis Highlights in Engineering, volume 4

used across a wider range of its voltage curve, as lower terminal voltages can also be stepped up to match those required by the AC/DC converter. This greater usable range comes at the cost of efficiency losses across the DC/DC converter, which, depending on the particular system, might be acceptable in light of the wider operating voltage range. The DC/DC converter and transformer are not considered further in this work. The energy conversion processes that enable the

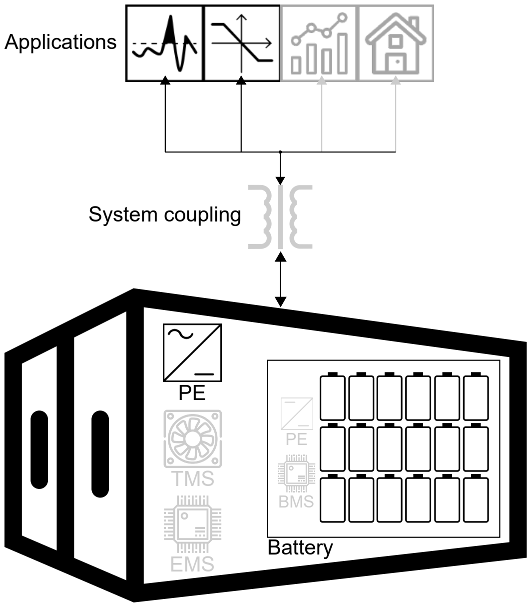

Fig. 1: Schematic diagram of a typical stationary battery energy storage system (BESS). Greyed-out sub-components and applications are beyond the scope of this work.

storage of electrical energy in the form of chemical energy take place within the power electronics and the battery system. The energy management, battery management, and thermal management systems can be termed as auxiliary components, and are responsible for controlling and ensuring the safe operation of the BESS. The large portion of losses in the first two components are the conversion losses. The remaining losses such as the standby losses and consumption by other components constitute the system losses. Schimpe et al [14] present a further breakdown of the conversion losses and system losses into detailed individual loss mechanisms within each sub-system. They list a total of 18 loss mechanisms, and present a detailed analysis with the help of an electro-thermal modeling framework. It is found that the conversion losses in the power electronics and the battery system are significant. The framework is based on the results of a container BESS named *Energy Neighbor* [15], developed at the Technical University of Munich as part of a research project *EEBatt*. Patsios et al [16] also confirm that the conversion losses in the battery system and power electronics) are significant and warrant a closer look. Not only does the the choice of size, layout and operating strategy of sub-components play an important role in application in determining the overall round-trip efficiency of the system, but also the service being rendered by a BESS [17]. This paper highlights the relation between the conversion losses and aspects such as the application scenario and system configuration. Evaluation of system losses (such as standby losses, power consumption by auxiliary components) is not a part of this work.

III. Definitions of performance indicators

In this section, definitions of performance indicators used in the subsequent sections of this paper are presented.

A. *Efficiency*

The efficiency (η_{system}) of a battery energy storage system is defined as the ratio of the time integral of the discharging power to the time integral of the charging power over a complete cycle such that the initial and final states of charge (SOCs) are identical [14]. The system necessarily encounters dissipative losses at all times in all the components, and especially during the charge and discharge processes. The value of η_{system} therefore, lies between 0 and 1, as the discharged energy is always less than the charging energy.

$$\eta_{system} = \left. \frac{\int_{0}^{t_1} P_{discharge}(t) \cdot dt}{\int_{t_1}^{t_2} P_{charge}(t) \cdot dt} \right|_{SOC_0 = SOC_{t_2}} \tag{1a}$$

$$= \left. \frac{E_{discharged}}{E_{charged}} \right|_{SOC_0 = SOC_{t_2}} \tag{1b}$$

$$E_{charged} = E_{discharged} + E_{loss,total} \Big|_{SOC_0 = SOC_{t_2}} \tag{1c}$$

$$E_{loss,total} = \sum_{i=1}^{n} E_{loss,c,i} + \sum_{i=1}^{n} E_{loss,s,i} \Big|_{SOC_0 = SOC_{t_2}} \tag{1d}$$

where:
.. η_{system} is the system efficiency
.. $E_{discharged}$, $E_{charged}$ represent the energy discharged and charged respectively
.. $E_{loss,c/s,i}$ represents the energy lost in the ith component due to conversion (c) and system (s) losses respectively
.. n is the total number of components for which the losses are evaluated
For the purpose of this work, only the conversion losses are considered, i.e. it is assumed that the sum of system losses $\Sigma E_{loss,s,i}$ is effectively zero. This assumption implies that the efficiency definition applied in this paper refers to the conversion efficiency of the system.

B. *Temporal utilization ratio*

The temporal utilization ratio τ_t is defined in [14] as the ratio of the sum total of the time during which the BESS is in operation to the total time of the simulation. This indicator is particularly useful to compare load profiles against each other with respect to the degree of activity seen by a BESS.

The quantity τ_t can therefore assume values between 0 and 1, depending on how often the system is summoned into service.

$$\tau_t = \frac{t_{operation}}{t_{simulation}} \tag{2a}$$

where:
.. τ_t is the temporal utilization ratio
.. $t_{operation}$ is the total time of operation of the BESS
.. $t_{simulation}$ is the duration of simulation

C. Active charge-based utilization ratio

The active charge-based utilization ratio $\tau_{Q,a}$ is defined as the ratio of sum of absolute values of charge throughput of the BESS in charge and discharge directions during the non-idle time periods to the sum of the absolute charge throughout in the two directions at a C-rate of 1 C within the same periods. A C-rate of 1 is that value of current which can completely charge/discharge a battery in a duration of 1 hour. The quantity $\tau_{Q,a}$ provides an indication of how demanding a particular load profile is with respect to the battery capacity. In contrast to the temporal utilization ratio τ_t, the active charge-based utilization ratio $\tau_{Q,a}$ is useful to compare load profiles against each other with respect to the intensity of activity demanded of a BESS. From the definition, it is then clear that $\tau_{Q,a}$ may assume a value between 0 and the sum of maximum permissible charge and discharge C-rates. Schimpe et al [14], on the other hand, present a related performance indicator which compares the actual battery charge throughput to that due to cycling the battery continuously at 1C throughout the duration of simulation.

$$\tau_{Q,a} = \frac{Q_{throughput}}{\tilde{Q}_{throughput,1C}} \tag{3a}$$

where:
.. $\tau_{Q,a}$ is the active charge-based utilization ratio
.. $Q_{throughput}$ is the total absolute charge throughput of the BESS
.. $\tilde{Q}_{throughput,1C}$ is the theoretical total absolute charge throughput of the BESS at 1C

D. System availability

In the discipline of systems engineering, the system availability and reliability are measures to quantify the likeliness of the system operating as expected under the given service conditions in a time frame of interest. It quantifies the actual performance of the system vis-a-vis its expected performance. The BESS may fail to perform as expected in cases wherein the C-rates, SOC values or temperatures tend to step out of the permissible range. The system may also reject requests in the case of failure/degradation of components resulting in impaired or zero capabilities [18]. Here we define two sub-indicators under this category:

1) Qualitative system availability: The qualitative system availability $s_{qualitative}$ is defined as the ratio of the number of successfully completed energy requests (charge, discharge, or both) to the total number of requests made to the BESS within the time frame of interest. This quantity can assume values between 0 and 1.

$$s_{qualitative} = \frac{n_{fulfilled}}{n_{requested}} \tag{4a}$$

where:
.. $s_{qualitative}$ is the qualitative system availability factor
.. $n_{fulfilled}$ is the number of energy service requests (charge, discharge or both) successfully fulfilled by the system
.. $n_{demanded}$ is the total number of energy service requests (charge, discharge, or both) received by the BESS

2) Quantitative system availability: The quantitative system availability factor is defined as the ratio of the actual quantity of energy exchanged (charge/discharge, or both) with the energy supply system to the quantity of energy exchange requested within the time frame under consideration. This ratio can assume values between 0 and 1, implying complete incapability and total fulfillment respectively. Values in between point to partial fulfillment.

$$s_{quantitative} = \frac{E_{fulfilled}}{E_{requested}} \tag{5a}$$

where:
.. $s_{quantitative}$ is the quantitative system availability factor
.. $E_{fulfilled}$ is the actual energy service (charge, discharge or both) fulfilled by the system
.. $E_{demanded}$ is energy service (charge, discharge, or both) requested of the BESS
For grid applications such as peak shaving, the request to discharge is of prime interest, and the system availability of a BESS providing such a service would be based on the number of discharge requests successfully honored. For other applications such as primary control reserve (PCR), the requests to both charge as well as discharge the system in response to frequency fluctuations are of interest, and the system would be mandated to fulfill all requests with a system availability of 1, in order to stay within the regulatory bounds.

IV. Factors influencing efficiency

To illustrate the dependence of the conversion efficiency on the system configuration and the application scenario in which the system is operated, simulations are run with the stationary battery energy storage system simulation tool SimSES [19], which has been developed at the Technical University of Munich. The definition of efficiency presented in the section III, and especially the conversion efficiency is used in evaluations presented in the subsequent sections.

A. Application scenario

Two applications of large-scale stationary BESS in the electrical energy supply system are considered to highlight

ATLANTIS PRESS
Atlantis Highlights in Engineering, volume 4

the dependence of conversion losses on the characteristics of the application. The applications considered are:

1) Peak Shaving (PS)
2) Primary Control Reserve (PCR)

The peak shaving (PS) application is known to subject the BESS to infrequent bursts of high-intensity energy requests, whereas the primary control reserve (PCR) application is the opposite in the sense that it subjects the BESS to frequent low-intensity energy requests throughout the time frame of consideration. In summary, the PS application exhibits a low τ_t and a high $\tau_{Q,a}$ value, while on the contrary, the PCR application exhibits a high value of τ_t and a low value of $\tau_{Q,a}$. In applications that exhibit high $\tau_{Q,a}$ values, the conversion losses in the batteries tend to be higher, whereas applications with simultaneously high τ_t and low $\tau_{Q,a}$ tend to suffer disproportionately high conversion losses in the power electronics, which fare sub-optimally under part-load conditions.

Two base case systems are defined to simulate BESS operation in the peak shaving and primary control reserve applications. The system configuration considered for each case is listed in table I. The voltage at the battery system terminals is 650 V in each case. The battery system is then connected to a bi-directional AC/DC converter whose DC operating range is 600-750 V. The system is then interfaced to the 400 V AC distribution grid. The system layout is described as ns mp, implying n cells in series, and m such combinations of n cells connected in parallel. This layout scheme is depicted in figure 2. The two applications chosen serve to underline the influence of the application on the individual components of the system conversion efficiency. A one size fits all design ideology is, hence not suitable for the deployment of stationary BESS in grid applications. The following sections depict how each application requires a BESS system design which is sensitive towards the unique demands of the application.

TABLE I: BESS system parameters

	Scenario	
	Peak Shaving	Primary Control Reserve
Energy capacity	350 kWh	2.8 MWh
Power rating	700 kW	1.4 MW (qualified)
Power Electronics	AC/DC bidirectional	AC/DC bidirectional
Cell chemistry	LFP/C	LFP/C
Form factor	Cylindrical 26650	Cylindrical 26650
System layout	204s 179p	204s 1430p
Cell state	New	New

1) Peak Shaving: Deployment of battery energy storage systems to provide the so-called peak shaving service is fast gaining ground. Industrial and other commercial users with very high intermittent load peaks are required to not just pay for the amount of energy consumed, but also for the maximum power demand at their sites in their annual or monthly billing cycles. In order to avoid high power-related costs, peak shaving is a frequently implemented solution [20].

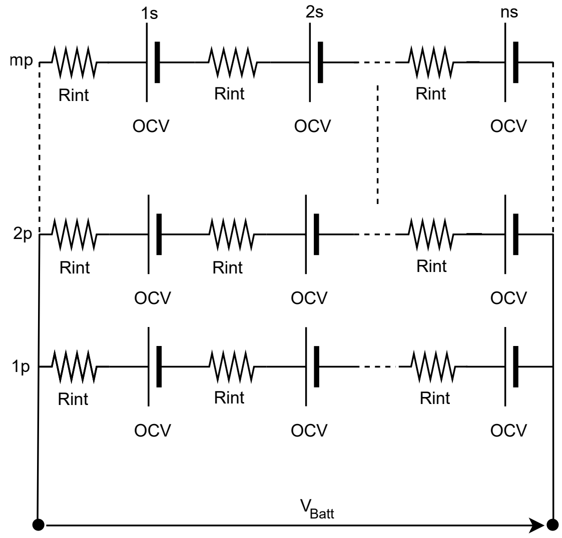

Fig. 2: System layout with n cells in series and m such strings in parallel (ns mp). OCV stands for open circuit voltage and Rint stands for internal resistance. Each cell is modelled as a voltage source with a series resistance.

Mature fossil-based technologies such as diesel generators and gas turbines installed on-site (captive power plants) are being replaced by BESS, owing to their precise and accurate response to demand, low response times, suitable ramp rates and relatively high efficiencies [10], [12]. These demand peaks are shaved off by the BESS at relatively higher C-rates than those normally witnessed in the PCR application. The BESS then charges in idle periods with relatively low C-rates. The operator of the peak shaving BESS can thus save costs related to the maximum power demand, and must only pay for the energy extracted from the grid at lower values of power [21]. While the motivation for peak shaving is often economic in nature, such systems can be also be used for strengthening of grid infrastructure at locations with disproportionately high intermittent loads such as at electric vehicle (EV) fast-charging stations, or to provide relief to a strained local distribution grid. All such systems reduce the peak instantaneous power demand that the grid has to fulfill, and spreads it over a larger period of time [22], [23].

For the purpose of this work, a synthetic load profile based on that of an industrial client is created with a high number of sharp peaks per day. The operation of the system described in table I is simulated for one year with a sample rate of 5 minutes in the exemplary peak shaving application. The peak load is 1.31 MW, while the minimum load is 95 kW. The average load during the simulated period is 211.69 kW. The temporal utilization ratio of this profile is 0.1930, meaning that the system is active for 19.30% of the simulated period. The grid connection to this load center, owing to specific

ATLANTIS PRESS

Atlantis Highlights in Engineering, volume 4

constraints, can only supply a maximum power of 630 kW. The BESS is operated in this scenario such that it caters to the residual demand over and above what the grid connection can supply. This limit, 630 kW in this case is termed as the peak shaving limit. The system operates within a C-rate range of 1 C for charging and 1.8867 C for discharging. The simulation results also reveal that the system is able to shave the peaks off by supplying the demanded power with a qualitative and quantitative system availability of 1 (i.e. 100%). An evaluation of the active charge-based utilization ratio reveals that the system operates with a $\tau_{Q,a}$ of 0.6961, which is relatively high. The conversion losses of the system over the simulated duration of one year are depicted on the right side in figure 4. It is clear that the conversion losses in the battery are significant and make up the largest proportion of losses in this application. While the conversion losses in the power electronics are comparable, there is not much room for improvement as the system operates near its rated capacity for a large portion of the operating time as shown on the left side of figure 3.

2) Primary Control Reserve: Operation of stationary BESS in provision of primary control reserve with consideration of its unique requirements has been investigated in scientific circles [24]–[28]. To simulate the operation of a stationary BESS in the PCR application, certain regulatory conditions have to be fulfilled. The minimum permissible energy capacity to power (E/P) ratio is governed by the regulatory framework to ensure guaranteed system readiness to provide a minimum prescribed duration of positive and negative reserves. A theoretical minimum ratio of 1 is required to fulfill the 30-minute criterion prescribed by the ENTSO-E (European Network of Transmission System Operators for Electricity) [29], but this ratio is not practically viable, as the storage system cannot charge or discharge energy at this ratio. An E/P ratio of 2 is therefore chosen to simulate the operation of a BESS in the PCR application. For such a system, the permissible SOC range in which the BESS may operate is then 25 - 75 %. Based on the grid frequency time series for the year 2017, the stationary BESS demand power profile is developed (see fig. 3). This profile has a temporal utilization ratio τ_t of 0.7999, which implies that the system remains in active operation for nearly 80% of the considered time period. In comparison to the temporal utilization ratio of around 19% for the PS application, the system is used much more frequently in the PCR application.As the grid frequency signal does not show any strong patterns, the BESS operation is simulated for the 15^{th} of each month of 2017, based on the frequency fluctuations and requested system response. The sample rate of these simulations is 1 second. The conversion efficiencies for the system described in table I are evaluated for the 12 sample days.

Figure 5 depicts the conversion losses in the power electronics and the battery system for the simulated days in 2017. Two cases are picked from these results for further discussion - the simulated sample days with the best and worst power electronics conversion efficiencies. The best conversion efficiency among the 12 sample days is observed on the 15^{th} of November, and the worst is observed on the 15^{th} of July, with the average value lying between them. From the C-rate distributions depicted in figure 5 for the 15^{th} of November (bottom right) and the 15^{th} of July (bottom left), it can be inferred that the BESS undergoes cycling under very gentle conditions in the PCR application. With a temporal utilization ratio τ_t of 0.8528 and active charge-based utilization ratio $\tau_{Q,a}$ of 0.0319, the simulation for the 15^{th} of November sees conversion losses of around 19% in the power electronics. On the other hand, with a τ_t of 0.7104 and a $\tau_{Q,a}$ of 0.0206, the conversion losses in the power electronics are nearly 29% on the 15^{th} of July. The system is operated under part-load conditions in both the cases for most of the time. Part-load operation at low C-rates while leading to low conversion losses in the battery system due to low currents flowing through the internal resistance, also implies higher losses in the power electronics components, which exhibit best conversion efficiencies at their nominal power ratings. The above results can also be explained from the C-rate distributions of the simulation for the 15^{th} of November, which has a higher average C-rate as compared to the simulation for the 15^{th} of July, which exhibits a lower average C-rate in the simulated time period. The two system availability ratios remain at 1 (100%) in all the sample days, indicating satisfactory performance of the system. It can thus be inferred that the power electronics conversion efficiency improves with rising values of $\tau_{Q,a}$. This was also apparent from the section on peak shaving, in which the system exhibited a very high value of active charge-based utilization ratio.

B. Battery system

From the results presented in subsection IV-A1 on the applicability of batteries in the peak shaving application, it is clear that the conversion losses in the battery play an important role in applications with relatively higher C-rates. To investigate the dependence of these losses on the cell parameters such as resistance and the cell capacity, three additional scenarios are simulated. In addition to the LFP/C 26650 cell, a commercial NMC/C 18650 cell is also simulated. Both the cell types are simulated twice - once considering the cells as 'new' - i.e. with 100% capacity and low internal resistance, the second set of simulations treats the cells as 'old' with only 80% of capacity and twice the internal resistance as compared to the new cells. For around 20% capacity loss, the resistance rise for the LFP/C cells is around 70% [30], while the resistance rise for the NMC/C cells is around 85% [31]. The assumption of 100% rise considered here is taken as a worst case scenario. Based on the objectives of the investigation, the use of various battery models such as empirical models, physico-chemical models and equivalent circuit models is prevalent [33]–[36] in scientific circles. Physico-chemical models are the closest to the underlying electrochemical processes taking place within the cell, whereas the equivalent circuit models, although quite popular in their usage, present a higher degree of abstraction, employing electrical circuit analogies to approximate

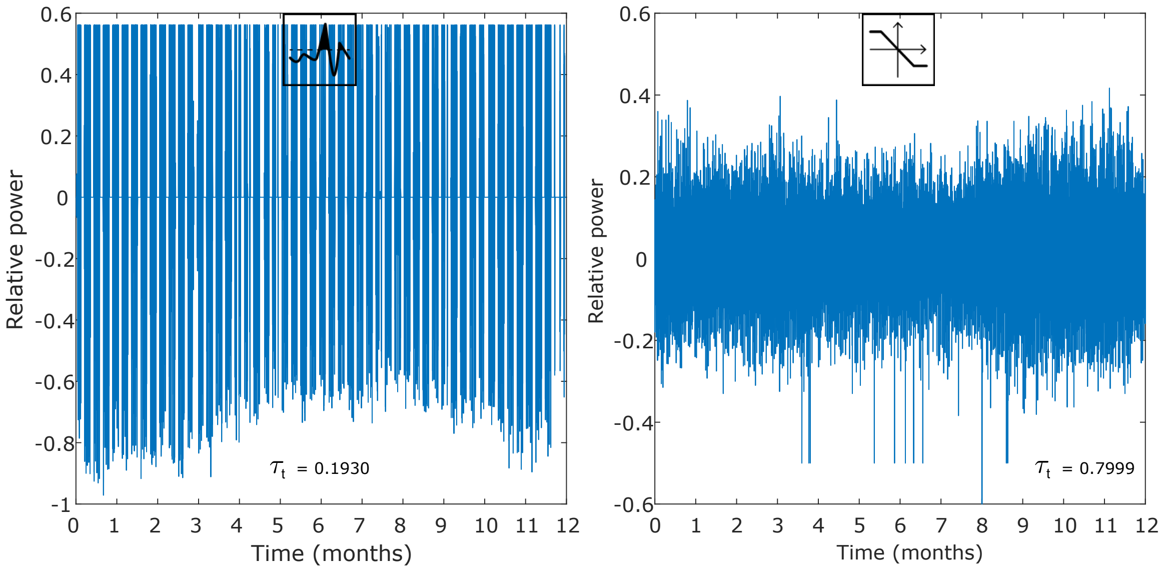

Fig. 3: Power profiles for the peak shaving (left) and primary control reserve (right) and applications (normalized with respect to the respective system power ratings).

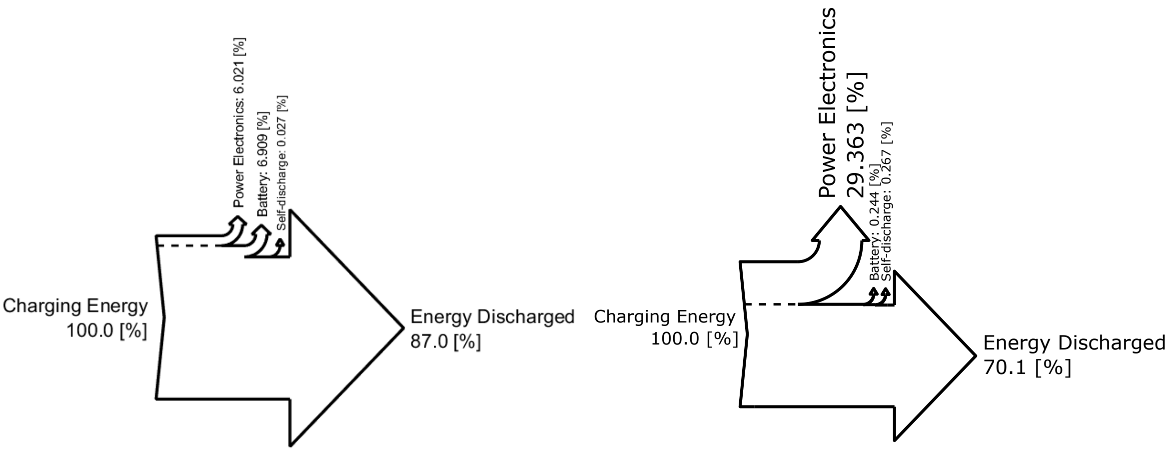

Fig. 4: Conversion losses in peak shaving (left) and primary control reserve (right) applications.

the physical processes. The empirical and data-based models are the farthest away from physical reality and are purely mathematical in nature.

1) Equivalent circuit model: As the dynamic response of the cell under load is not of prime interest in these analyses, the so-called Rint [36], [37] equivalent circuit model is deemed sufficient to assess the losses in the cells. The Rint model visualizes the battery as a series combination of a resistance with a voltage source (which represents the open circuit voltage). The values of the open circuit voltage are read out from a look-up table depending on the state of charge. The values of the internal resistance are also read out from look-up tables depending on the direction of power flow, the temperature and the state of charge. The open circuit voltage curves for both the cells and the Rint model (inset) are depicted in figure 6. The cell model (open circuit voltage and resistances) is scaled up to the module and rack level with the help of scaling factors. A number of commercial lithium-ion cells have been characterized and tested in the scientific community to model their electro-thermal and aging behavior with sufficient

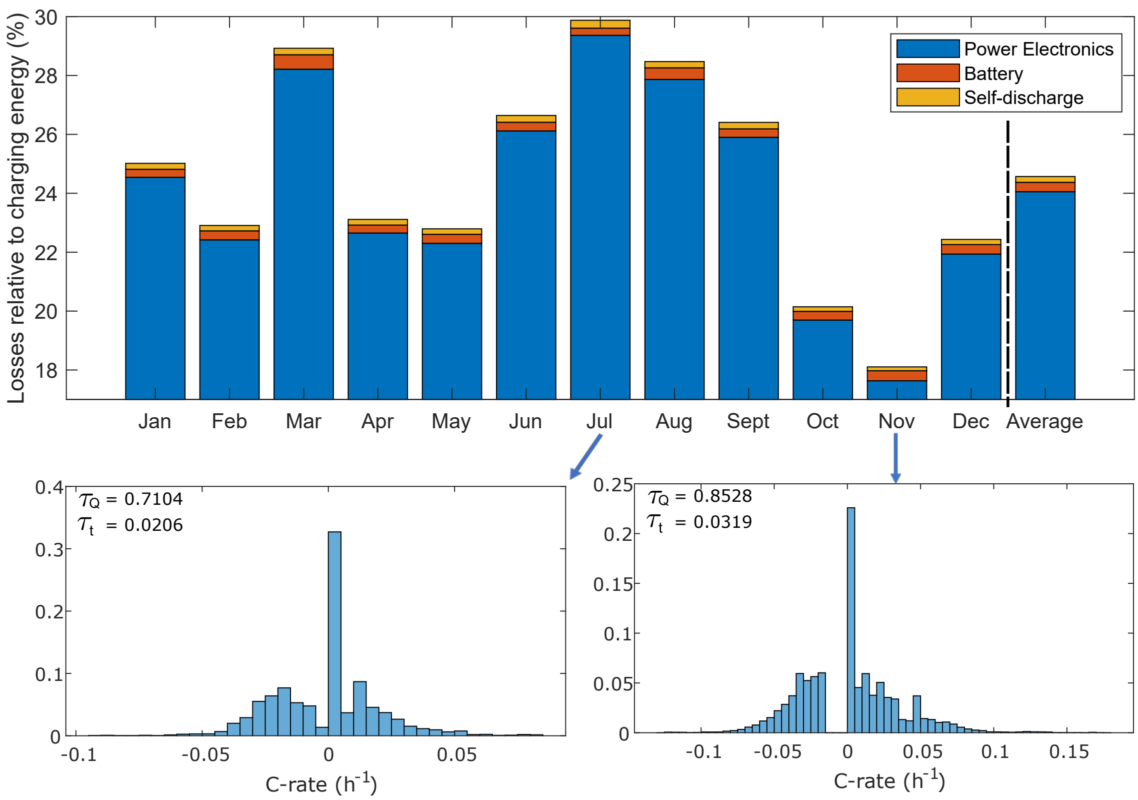

Fig. 5: Conversion losses during operation in PCR application (top). Distribution of system C-rates on 15 July (bottom left). Distribution of system C-rates on 15 November (bottom right).

accuracy [38]–[41]. The simulations carried out in this paper use two Rint equivalent circuit battery models (ECM) based on full cell characterizations of the LFP 26650 [19], [42], [43], and the NMC 18650 [31] cells. The dependence of the resistance of the LFP cells on the temperature and state of charge in the process of charging and discharging is depicted in figure 6. The dependence of the NMC cell resistance on the state of charge is also depicted in figure 6.

2) 0D lumped parameter thermal model: In conjunction with the Rint ECM model, the thermal behavior of the system is modeled as a 0D lumped parameter model at the cell level, and scaled up to the system level. The heat transfer processes considered include the internal heat generation on account of the dissipative losses in the internal resistance, and the heat exchange with the ambient air. The reversible heat exchanges due to the chemical reactions is not taken into account. The heat exchange with the ambient air is modeled as natural convection. The rise in temperature can be obtained from the energy balance equation for these two processes:

$$\Delta T = (\dot{Q}_{loss} + A \cdot h \cdot (T_{amb} - T_1))/(m \cdot c_p) \tag{6a}$$

$$T_2 = T_1 + \Delta T \tag{6b}$$

For the NMC/C cells in the peak shaving operation, the system configuration is 181s 276p for the same system energy and power ratings as the base case system. The number of cells in series is lower than in the LFP/C based system due to the higher open circuit voltage of the NMC/C cells. Due to the lower capacity of the NMC/C cells, it is imperative that a greater number of strings be connected in parallel as compared to the LFP/C case. Although the NMC/C cells exhibit resistance values which are higher, due to the difference in the system layout - 204s 179p for LFP/C vs. 181s 276p for NMC, the simulations reveal that the system with NMC/C cells sees a lower proportion of conversion losses in the battery system due to lower equivalent resistance values. It is seen from fig. 7 that the aged cells with lower capacities and higher resistances show a higher proportion of conversion losses in the battery. The self-discharge in proportion is negligible over the simulated period, as lithium-ion batteries in general exhibit favorable self-discharge characteristics. The conversion losses take the form of heat dissipation, and entail additional efforts to expel the heat out of the vicinity of the battery in order to keep it within its recommended temperature limits. The heating effect also causes faster aging of the cells, which

ATLANTIS PRESS

Atlantis Highlights in Engineering, volume 4

TABLE II: Cell parameters. 'n' stands for new, and 'a' stands for aged. (* approximate values from literature, further investigation necessary [32].)

	Cells			
	LFP-n	LFP-a	NMC-n	NMC-a
Charge capacity (As)	10800	8640	7020	5616
Max. continuous charge current (A)	3	3	1.95	1.95
Max. continuous discharge current (A)	20	20	3.9	3.9
Max. charge voltage (V)	3.6	3.6	4.2	4.2
Min. discharge voltage (V)	2	2	3	3
Mean internal resistance at 25°C (mΩ)	47.5	95	67.1	134.2
State of health (SOH)	100%	80%	100%	80%
Mass of cell (g)	85	85	47.5	47.5
Surface area (m^2)	0.0064	0.0064	0.0037	0.0037
Heat transfer coefficient (W/m^{2}K)	15	15	15	15
Specific heat capacity coefficient (J/kgK)	925.52	925.52	823*	823*
Form factor	26650	26650	18650	18650

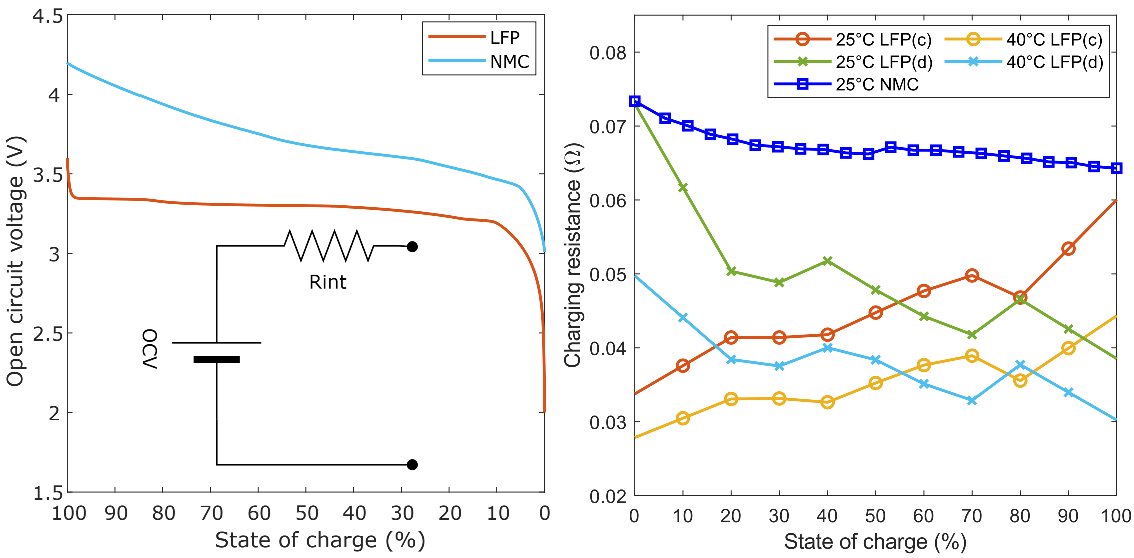

Fig. 6: Open circuit voltage curves (left) for the the LFP/C and NMC/C cells, with a schematic of the Rint cell model (inset). Dependence of ohmic resistance on state of charge and temperature (right). The symbols in brackets c and d stand for charging and discharging respectively.

further lead to a rise in resistance and capacity degradation. This forms a vicious cycle that causes the battery to age at increasingly faster rates. The temperature evolution over the simulation period of one year for the 4 batteries is depicted in fig. 7. It is seen that the batteries reach significantly high intermittent temperatures during the operation, which is attributed to the lack of a cooling system in the simulation. In a real-world situation, active cooling measures would be

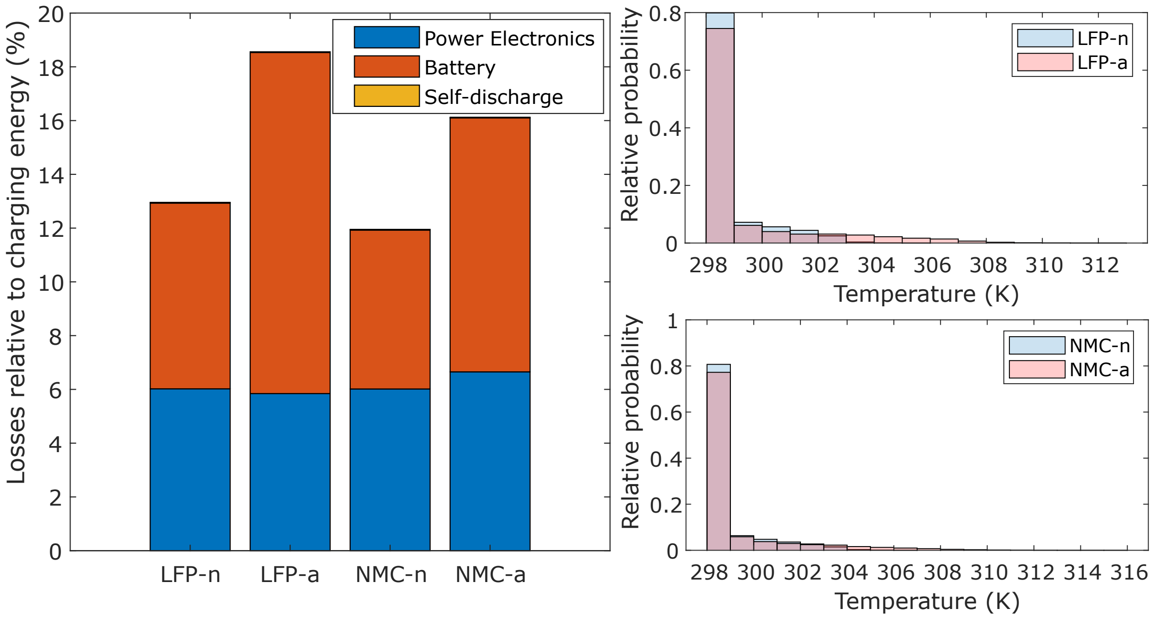

Fig. 7: Conversion losses with new (n) and aged (a) LFP and NMC cells in the peak shaving application (left). Temperature (in K) of simulated cells over duration of simulation in the absence of cooling measures (right).

undertaken by the thermal management system (TMS) to keep the cells within their normal temperature ranges. For the NMC/C cells, the high intermittent temperatures are also attributed to the low specific heat capacity of the cells, which needs further investigation.

With aged batteries, it is of particular interest to investigate if the system availability is maintained despite the faded capacity and higher resistance. As the chosen application does not exhibit very wide peaks which need to be shaved, the battery system does not undergo high depth-of-discharge (DOD) cycles. As a result, the lower capacity of the batteries does not impede the system availability. The lower terminal voltage due to the increased resistance also does not affect the system availability, as the batteries are able to supply power at higher currents to meet the power request at a lower terminal voltage. This results in even higher battery conversion losses, which is apparent from figure 7.

C. Power electronics

Several power electronics topologies are used to interface the battery system to the grid. The most common among these, depending on whether there is a DC/DC voltage conversion stage between the batteries and the AC/DC conversion, are termed as single-stage and the two-stage topologies [17], [44]. Load distribution strategies also play an important role in the final choice of the power electronics components used and their interconnection. While some systems rely on load distribution strategies which do not introduce large SOC deviations among strings, some [45] rely on strategies that actively balance the widely divergent SOCs by distributing the power dynamically among the strings.

The inverter/rectifier model used for simulations in this work is based on a full characterization of a commercially available bi-directional converter such that the losses in both directions at various load levels are modeled in the form of a look-up table [14]. Scaling factors are used to adjust the model to the power rating of simulated system. The PE topology used to simulate the BESS operation in section IV-A is depicted in fig. 8. In this topology, each battery string is connected to a separate bidirectional AC/DC converter. The load distribution strategy operates the individual converters such that the power demand at the system coupling point is uniformly fulfilled by all the strings. For this topology the following relations hold true:

$$P_{nominal,sys} = n * P_{nominal,converter} \tag{7a}$$

$$P_{t,sys} = x * n * P_{nominal,converter} \tag{7b}$$

$$0 \leq x \leq 1 \tag{7c}$$

where:

.. $P_{nominal,sys}$ is the rated power of the system

.. $P_{nominal,converter}$ is the rated power of each individual converter

.. n is the total number of converters in the topology

.. x is the load factor at time t

To illustrate the effect of the power electronics topology on the system conversion efficiency, the 15th of July (depicted in fig. 5), representing the worst case among the 12 days

Atlantis Highlights in Engineering, volume 4

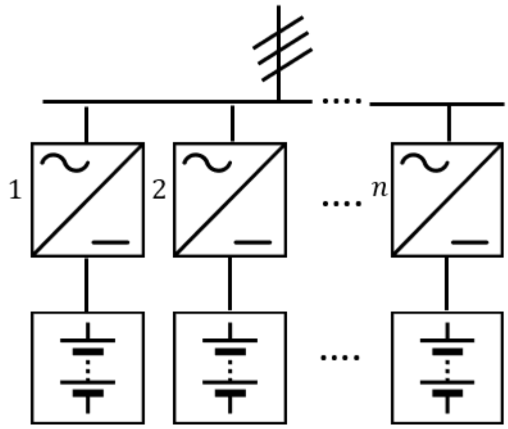

Fig. 8: Dedicated string converter topology operating with the uniform load distribution strategy.

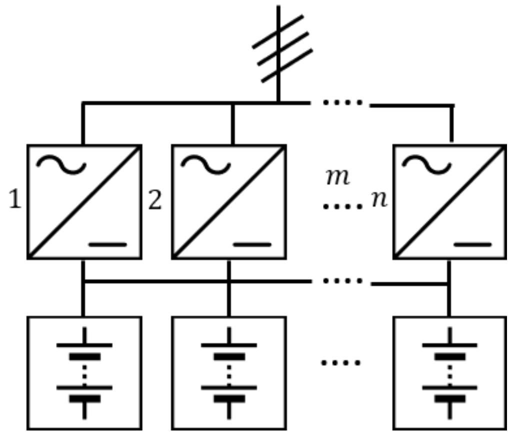

Fig. 9: Converter topology with common DC bus operating with the incremental load distribution strategy.

simulated, is considered as a base case. It has been discussed that these high conversion losses are caused due to prolonged part-load operation. A second converter topology, in which all the battery strings are connected in parallel to the array of AC/DC bidirectional converters is now considered. The strings no longer possess dedicated converters in this topology, but there are now several converters which can be sequentially brought online to match the power demand. This topology is depicted in figure 9. For this topology, the following relations for the system power hold true:

$$P_{nominal,sys} = n * P_{nominal,converter} \tag{8a}$$

$$P_{t,sys} = m * P_{nominal,converter} + x * P_{nominal,converter} \tag{8b}$$

$$0 \leq m \leq n \tag{8c}$$

$$0 \leq x \leq 1 \tag{8d}$$

where:
.. m is the number of converters being operated at the specified upper threshold
.. x is the load factor of the $(m+1)^{th}$ converter at time t

It is important to state here that the relations presented in equations (7) and (8) are valid if all the individual converters are identical. For the case with dissimilar converters, the equations can still be used with some minor adjustments.

Schimpe et al [17] have evaluated the relative losses arising due to the operation of the grid coupling components namely the DC/DC bidirectional converter, AC/DC bidirectional converter and the transformer. Two-stage and single stage topologies are also evaluated, with the incremental topology investigated in connection to a prototype system. A simulation framework has been developed to investigate the effect of such an incremental inverter topology on the system conversion efficiency with a variable number of converters. The chosen base case is now simulated with the topology depicted in fig. 9, with the number of inverters n being varied from 2 to 10. For the base case simulated earlier, $n = 1$. As can be seen in figure 11, the additional benefit of each extra inverter diminishes with the number of inverters, while the mean conversion efficiency across the power range (shown on the secondary y-axis) eventually flattens out. While these results may make it seem like it is in the system designer's interest to keep increasing the number of converters indefinitely to obtain even better mean efficiencies, caution is advised due to the likeliness of the economic and environmental costs per kW of rated capacity making such an implementation prohibitive. Which implies monetary and energetic gains in efficiency, could be nullified due to higher investment costs of BOS components. A comprehensive and focused analysis of these questions needs to be carried out in order to arrive at a clearer conclusion. The conversion efficiency curve for the topology depicted in figure 9, operating under the incremental load distribution strategy is calculated across the entire load range. Efficiency curves for topologies consisting of 1 to 10 converters are depicted in figure 10. The efficiency values for all cases converge towards the end of the power range as then all converters are operating at rated power. The deployment of such a topology yields the best results during operation at low relative power values.

V. Conclusion and outlook

Rising electricity production from variable renewable energy sources such as solar and wind energy, while making the energy from the world's most versatile energy vector greener, has also brought unique challenges into the picture which, if not addressed in a timely fashion, threaten the quality and security of power supply across the world. Lithium-ion battery energy storage systems, the technology which is expected to provide relief to the systems need to be designed and analyzed comprehensively to equip them better to tackle the challenges efficiently and effectively. It has been shown how the conversion efficiencies of the major components of a BESS

ATLANTIS PRESS

Atlantis Highlights in Engineering, volume 4

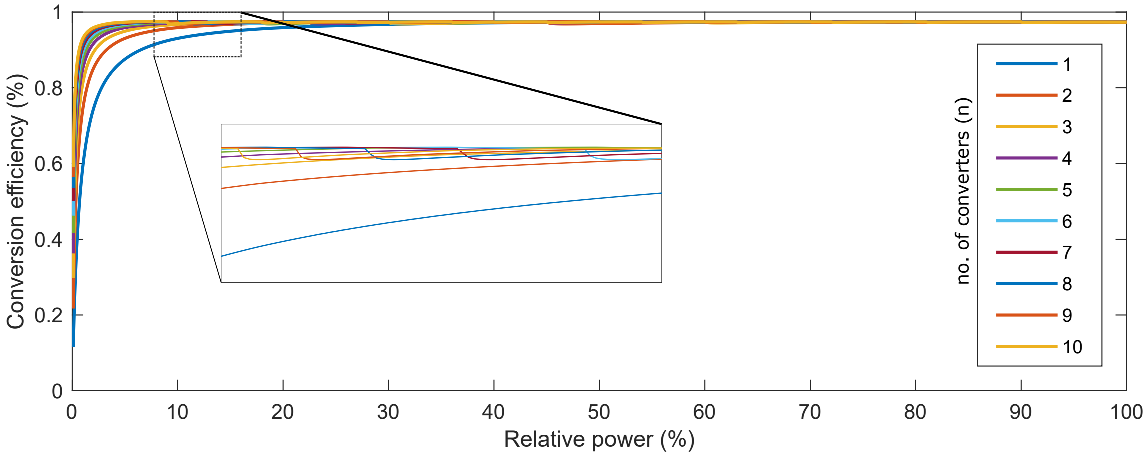

Fig. 10: Efficiency curves for the topology with incremental load distribution strategy (for topologies with number of converters $n = 1$ to $n = 10$). The inset image depicts the second and third converters C2 and C3 respectively coming online for a topology with 10 converters.

.

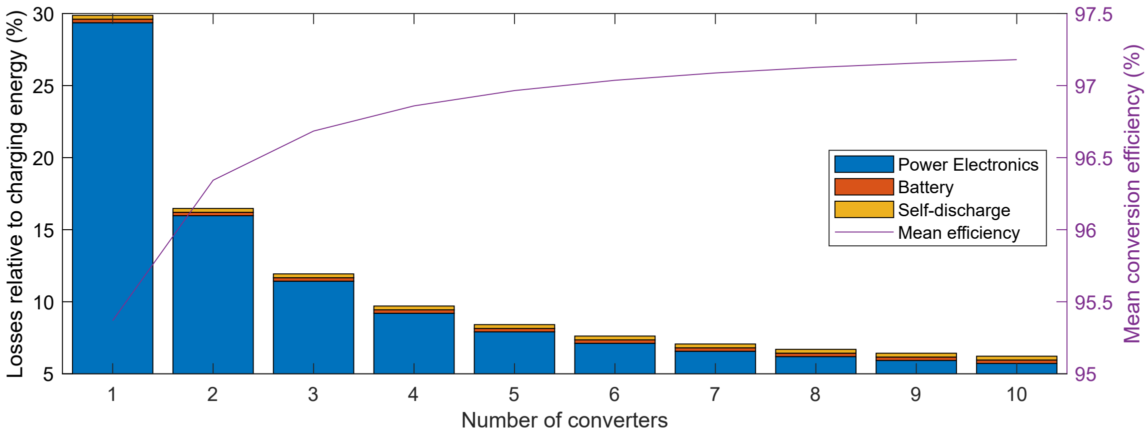

Fig. 11: Reduction in conversion losses in power electronics for the worst case by increasing the number of converters (stacked bar graph, left axis). Mean conversion efficiency of topology across load range (line graph, right axis).

- the power electronics and the batteries play a major role in the overall round trip efficiency of the system. It is also clear that the system losses need to be studied and modeled further in a holistic manner in order to be able to evaluate and quantify these losses for stationary BESS with minimal effort. Power electronics topologies, the type of coupling with the batteries, and their load distribution strategies are instrumental in certain applications with lower average C-rates, while being of lesser significance in others with higher average C-rates. It has also been shown how the possible usage of second-life batteries can affect the system efficiency and availability in particularly demanding applications such as peak shaving. It is imperative to mention here that aged batteries are not always able to shave off some of the highest and widest peaks completely due to the rise in resistance and degradation in capacity over time. A thorough investigation into the sizing methodologies for second-life batteries in existing applications in order to ensure maximum possible system availability is also necessary.

Based on the area of interest and the properties to be investigated, there are a variety of models in use today which simulate the electrochemical, thermal, mechanical and energetic performance [46]. System level stationary BESS models with varying levels of details have been proposed in the literature [47], which aim to address the scaling up of the system from a single cell model to a module and rack level model. These models focus primarily on the core component of the BESS, which is the battery system and the battery management system (BMS). The power electronics and the auxiliary components such as the energy management system (EMS), the thermal management system (TMS) are not coupled to the core battery system, consequently the influence thereof is not immediately apparent. Other models [14] which include the auxiliary components do not address the complexities encountered in the scaling process to keep the computational effort within acceptable bounds. A holistic system model framework is needed to provide a rigorous treatment to each aspect of the stationary BESS. Such a framework will not only enable faster design and development of Lithium-ion battery energy storage systems, but also the analysis of the influence of variation in application scenarios, individual sub-system configurations and attributes on the overall system efficiency. The economic and environmental appeal of stationary energy storage systems as a viable technology to support further integration of renewable energy sources into the energy system can be enhanced with such evaluations. The authors intend to take a closer look at the aforementioned areas of research in subsequent works.

VI. Acknowledgments

This research is funded by the German Federal Ministry for Economic Affairs and Energy (BMWi), via the research project EffSkalBatt (grant number 03ET6148A), and overseen by Project Management Juelich (PtJ). The authors would also like to thank Daniel Kucevic for making the PCR load profile available, and Yulong Zhao, who helped implement the NMC/C model in SimSES. Stefan Englberger provided us with some of his self-created graphic symbols. The sankey diagram plotting tool for MATLAB has been created by James Spelling [48]. The cliparts in figure 1 were created by their respective owners [49].

References

[1] Harry Wirth. Recent facts about photovoltaics in germany.

[2] Rebecca Jones-Albertus, David Feldman, Ran Fu, Kelsey Horowitz, and Michael Woodhouse. Technology advances needed for photovoltaics to achieve widespread grid price parity. *Progress in Photovoltaics: Research and Applications*, 24(9):1272–1283, 2016.

[3] Ranjit Deshmukh, Grace C. Wu, Duncan S. Callaway, and Amol Phadke. Geospatial and techno-economic analysis of wind and solar resources in india. *Renewable Energy*, 134:947–960, 2019.

[4] Amirhossein Sajadi, Luka Strezoski, Vladimir Strezoski, Marija Prica, and Kenneth A. Loparo. Integration of renewable energy systems and challenges for dynamics, control, and automation of electrical power systems. *Wiley Interdisciplinary Reviews: Energy and Environment*, 8(1):e321, 2019.

[5] William Zappa, Martin Junginger, and Machteld van den Broek. Is a 100% renewable european power system feasible by 2050? *Applied Energy*, 233-234:1027–1050, 2019.

[6] J. Cochran, M. Miller, O. Zinaman, M. Milligan, D. Arent, B. Palmintier, M. O'Malley, S. Mueller, E. Lannoye, A. Tuohy, B. Kujala, M. Sommer, H. Holttinen, J. Kiviluoma, and S. K. Soonee. Flexibility in 21st century power systems.

[7] Michael Child, Claudia Kemfert, Dmitrii Bogdanov, and Christian Breyer. Flexible electricity generation, grid exchange and storage for the transition to a 100% renewable energy system in europe. *Renewable Energy*, 139:80–101, 2019.

[8] Patrick T. Moseley and Jürgen Garche. *Electrochemical energy storage for renewable sources and grid balancing*. Elsevier, Amsterdam, 2015.

[9] Holger Hesse, Michael Schimpe, Daniel Kucevic, and Andreas Jossen. Lithium-ion battery storage for the grid—a review of stationary battery storage system design tailored for applications in modern power grids. *Energies*, 10(12):2107, 2017.

[10] Furquan Nadeem, S. M. Suhail Hussain, Prashant Kumar Tiwari, Arup Kumar Goswami, and Taha Selim Ustun. Comparative review of energy storage systems, their roles, and impacts on future power systems. *IEEE Access*, 7:4555–4585, 2019.

[11] Ruben Hidalgo-Leon, Diego Siguenza, Carola Sanchez, Jonathan Leon, Pablo Jacome-Ruiz, Jinsong Wu, and Diego Ortiz. A survey of battery energy storage system (bess), applications and environmental impacts in power systems. In *2017 IEEE Second Ecuador Technical Chapters Meeting (ETCM)*, pages 1–6. IEEE, 16.10.2017 - 20.10.2017.

[12] Aoxia Kevin Chen, Yaswanth Nag Velaga, and Pankaj K. PK. Sen. Future electric power grid and battery storage. In *2019 IEEE Texas Power and Energy Conference (TPEC)*, pages 1–6. IEEE, 07.02.2019 - 08.02.2019.

[13] G. Pistoia. *Lithium-ion batteries: Advances and applications / [editor] Gianfranco Pistoia*. Elsevier, Amsterdam, first edition edition, 2014.

[14] Michael Schimpe, Maik Naumann, Nam Truong, Holger C. Hesse, Shriram Santhanagopalan, Aron Saxon, and Andreas Jossen. Energy efficiency evaluation of a stationary lithium-ion battery container storage system via electro-thermal modeling and detailed component analysis. *Applied Energy*, 210:211–229, 2018.

[15] Cong Nam Truong, Michael Schimpe, Maik Naumann, Andreas Jossen, and Holger C. Hesse. Impact of sub-components on the overall performance of stationary battery systems: Insights on the prototype energy neighbor: 28-29 nov. 2017. 2017.

[16] Charalampos Patsios, Billy Wu, Efstratios Chatzinikolaou, Daniel J. Rogers, Neal Wade, Nigel P. Brandon, and Phil Taylor. An integrated approach for the analysis and control of grid connected energy storage systems. *Journal of Energy Storage*, 5:48–61, 2016.

[17] Michael Schimpe, Nick Becker, Taha Lahlou, Holger C. Hesse, Hans-Georg Herzog, and Andreas Jossen. Energy efficiency evaluation of grid connection scenarios for stationary battery energy storage systems. *Energy Procedia*, 155:77–101, 2018.

[18] Helder Lopes Ferreira, Raquel Garde, Gianluca Fulli, Wil Kling, and Joao Pecas Lopes. Characterisation of electrical energy storage technologies. *Energy*, 53:288–298, 2013.

[19] Maik Naumann. *Techno-economic evaluation of stationary battery energy storage systems with special consideration of aging*. Doctoral, 2018.

[20] Rodrigo Martins, Holger Hesse, Johanna Jungbauer, Thomas Vorbuchner, and Petr Musilek. Optimal component sizing for peak shaving in battery energy storage system for industrial applications. *Energies*, 11(8):2048, 2018.

[21] Alexandre Oudalov, Rachid Cherkaoui, and Antoine Beguin. Sizing and optimal operation of battery energy storage system for peak shaving application. In *2007 IEEE Lausanne Power Tech*, pages 621–625. IEEE, 01.07.2007 - 05.07.2007.

[22] Jason Leadbetter and Lukas Swan. Battery storage system for residential electricity peak demand shaving. *Energy and Buildings*, 55:685–692, 2012.

[23] O. Veneri, L. Ferraro, C. Capasso, and D. Iannuzzi. Charging infrastructures for ev: Overview of technologies and issues. In *2012 Electrical Systems for Aircraft, Railway and Ship Propulsion*, pages 1–6. IEEE, 16.10.2012 - 18.10.2012.

[24] Daniel-Ioan Stroe, Vaclav Knap, Maciej Swierczynski, Ana-Irina Stroe, and Remus Teodorescu. Operation of a grid-connected lithium-ion battery energy storage system for primary frequency regulation: A battery lifetime perspective. *IEEE Transactions on Industry Applications*, 53(1):430–438, 2017.

[25] Johannes Fleer and Peter Stenzel. Impact analysis of different operation strategies for battery energy storage systems providing primary control reserve. *Journal of Energy Storage*, 8:320–338, 2016.

[26] Maciej Swierczynski, Daniel Ioan Stroe, Ana Irina Stan, and Remus Teodorescu. Primary frequency regulation with li-ion battery energy storage system: A case study for denmark. In *2013 IEEE ECCE Asia Downunder*, pages 487–492. IEEE, 03.06.2013 - 06.06.2013.

[27] Yann G. Rebours, Daniel S. Kirschen, Marc Trotignon, and Sbastien Rossignol. A survey of frequency and voltage control ancillary

services—part i: Technical features. *IEEE Transactions on Power Systems*, 22(1):350–357, 2007.

[28] Yann G. Rebours, Daniel S. Kirschen, Marc Trotignon, and Sbastien Rossignol. A survey of frequency and voltage control ancillary services—part ii: Economic features. *IEEE Transactions on Power Systems*, 22(1):358–366, 2007.

[29] ENTSO - E. Operations handbook.

[30] Maik Naumann, Cong Nam Truong, Michael Schimpe, Daniel Kucevic, Andreas Jossen, and Holger C. Hesse. *SimSES: Software for techno-economic Simulation of Stationary Energy Storage Systems: 28-29 November 2017*. VDE, Berlin, Germany, 2018.

[31] Simon F. Schuster, Martin J. Brand, Christian Campestrini, Markus Gleissenberger, and Andreas Jossen. Correlation between capacity and impedance of lithium-ion cells during calendar and cycle life. *Journal of Power Sources*, 305:191–199, 2016.

[32] E. Peter Roth. Thermal abuse performance of moli, panasonic and sanyo 18650 li-ion cells: Final report to nasajsc.

[33] Jinhao Meng, Guangzhao Luo, Mattia Ricco, Maciej Swierczynski, Daniel-Ioan Stroe, and Remus Teodorescu. Overview of lithium-ion battery modeling methods for state-of-charge estimation in electrical vehicles. *Applied Sciences*, 8(5):659, 2018.

[34] Fida Saidani, Franz X. Hutter, Rares-George Scurtu, Wolfgang Braunwarth, and Joachim N. Burghartz. Lithium-ion battery models: a comparative study and a model-based powerline communication. *Advances in Radio Science*, 15:83–91, 2017.

[35] J. Li, N. Lotfi, R. G. Landers, and J. Park. A single particle model for lithium-ion batteries with electrolyte and stress-enhanced diffusion physics. *Journal of The Electrochemical Society*, 164(4):A874–A883, 2017.

[36] Hongwen He, Rui Xiong, and Jinxin Fan. Evaluation of lithium-ion battery equivalent circuit models for state of charge estimation by an experimental approach. *Energies*, 4(4):582–598, 2011.

[37] Alexandros Nikolian, Joris de Hoog, Karel Fleurbay, Jean-Marc Timmermans, Omar Noshin, Peter van de Bossche, and Joeri van Mierlo. Classification of electric modelling and characterization methods of lithium-ion batteries for vehicle applications. 2014.

[38] Dian Wang, Yun Bao, and Jianjun Shi. Online lithium-ion battery internal resistance measurement application in state-of-charge estimation using the extended kalman filter. *Energies*, 10(9):1284, 2017.

[39] Johannes Schmalstieg, Stefan Käbitz, Madeleine Ecker, and Dirk Uwe Sauer. A holistic aging model for li(nimnco)o2 based 18650 lithium-ion batteries. *Journal of Power Sources*, 257:325–334, 2014.

[40] Madeleine Ecker, Nerea Nieto, Stefan Käbitz, Johannes Schmalstieg, Holger Blanke, Alexander Warnecke, and Dirk Uwe Sauer. Calendar and cycle life study of li(nimnco)o2-based 18650 lithium-ion batteries. *Journal of Power Sources*, 248:839–851, 2014.

[41] Noshin Omar, Mohamed Abdel Monem, Yousef Firouz, Justin Salminen, Jelle Smekens, Omar Hegazy, Hamid Gaulous, Grietus Mulder, Peter van den Bossche, Thierry Coosemans, and Joeri van Mierlo. Lithium iron phosphate based battery – assessment of the aging parameters and development of cycle life model. *Applied Energy*, 113:1575–1585, 2014.

[42] Maik Naumann, Michael Schimpe, Peter Keil, Holger C. Hesse, and Andreas Jossen. Analysis and modeling of calendar aging of a commercial lifepo4/graphite cell. *Journal of Energy Storage*, 17:153–169, 2018.

[43] M. Schimpe, M. E. von Kuepach, M. Naumann, H. C. Hesse, K. Smith, and A. Jossen. Comprehensive modeling of temperature-dependent degradation mechanisms in lithium iron phosphate batteries. *Journal of The Electrochemical Society*, 165(2):A181–A193, 2018.

[44] Sergio Vazquez, Srdjan M. Lukic, Eduardo Galvan, Leopoldo G. Franquelo, and Juan M. Carrasco. Energy storage systems for transport and grid applications. *IEEE Transactions on Industrial Electronics*, 57(12):3881–3895, 2010.

[45] Michael Schimpe, Christian Piesch, Holger Hesse, Julian Paß, Stefan Ritter, and Andreas Jossen. Power flow distribution strategy for improved power electronics energy efficiency in battery storage systems: Development and implementation in a utility-scale system. *Energies*, 11(3):533, 2018.

[46] Venkatasailanathan Ramadesigan, Paul W. C. Northrop, Sumitava De, Shriram Santhanagopalan, Richard D. Braatz, and Venkat R. Subramanian. Modeling and simulation of lithium-ion batteries from a systems engineering perspective. *Journal of The Electrochemical Society*, 159(3):R31–R45, 2012.

[47] Matthieu Dubarry, George Baure, Carlos Pastor-Fernández, Tung Fai Yu, W. Dhammika Widanage, and James Marco. Battery energy storage system modeling: A combined comprehensive approach. *Journal of Energy Storage*, 21:172–185, 2019.

[48] James Spelling. drawsankey function for matlab, available on matlab central. access link: https://ch.mathworks.com/matlabcentral/fileexchange/26573-drawsankey.

[49] Freepik, Pause08, Eucalyp, and Smashicons. Cliparts from www.flaticon.com. licensed with creative commons by3.0.

5 Techno-environmental modeling and evaluation of energy systems with ESN

This article presents a systematic methodology to assess the carbon footprint of energy storage systems, with a particular focus on BESSs within localized energy systems. The core of this work is the development and deployment of Energy System Network (ESN), a simulation program designed to model and analyze the carbon footprint across various configurations of energy systems. The program employs a comprehensive approach that combines energy system modeling with streamlined LCA techniques. ESN is available as open-source software hosted on a public GitLab repository[4]. This accessibility encourages transparency and collaboration among researchers and other users, allowing for modifications and extensions to suit specific research needs or policy analyses.

ESN is designed as a holistic simulation program for energy systems, capable of modeling interactions between multiple energy system components. These components include generation, grid connections, storage, and load. The primary aim is to assess the carbon footprint of these systems, offering detailed, component-wise, and time-resolved emissions modeling. Each energy system is treated as a node with its own energy balance, managed through an Energy Management System (EMS). The EMS uses algorithms to regulate energy flows based on predefined rules or optimization strategies. The framework uses a combination of physical models, time-series data, and environmental metrics to simulate the operation and impacts of each component. This includes detailed emissions modeling throughout the life cycle phases—production, operation, and end-of-life of the components. The underlying rationale behind the creation of ESN is an earnest attempt to achieve the following:

- A coherent and unambiguous carbon emissions modeling framework for localized energy systems with energy storage
- Consistent and reproducible comparisons of the carbon footprints of energy storage systems operating in localized energy system configurations

Two illustrative case studies are presented to demonstrate the application and capabilities of the ESN framework. The first explores energy arbitrage strategies using lithium-ion batteries, examining their effects on carbon emissions. The second case study assesses the carbon footprint of home energy systems, comparing scenarios with varying levels of integration of solar PV and battery storage. The case studies attempt to answer the following:

- Can the battery application energy arbitrage support grid decarbonization, and how can this be quantified?
- How can the decarbonization impact of residential battery storage systems and rooftop solar generation in home energy systems be quantified?

The findings from the case studies highlight the potential of energy storage systems, particularly when integrated with renewable energy sources, to support the decarbonization of energy systems. The ESN framework aids in identifying optimal configurations and strategies that minimize the carbon footprint

[4] Link to the ESN Gitlab code repository hosted by LRZ.

of localized energy systems.

The open-source nature of ESN is a significant contribution to enhancing transparency, comparability, and reproducibility in the assessment of the carbon footprint of energy storage applications. Some reflections on the limitations of the current study and prospective avenues for future research are discussed at the end of the article. A deeper dive into life cycle analyses with better primary data and a closer examination of the evolving grid carbon intensity could be of special relevance to the community.

Author contributions

Each author contributed significantly to different aspects of this work. Anupam Parlikar was the lead author, handling the conceptualization, data curation, formal analysis, investigation, methodology development, software design, visualization, and both the original draft and revision of the writing. Benedikt Tepe was involved in data curation, formal analysis, investigation, and visualization and contributed to both the original writing and its subsequent revisions. Marc Möller contributed greatly to the software development and also played an important role in the review and editing of the manuscript. Holger Hesse contributed through formal analysis, secured the funding, provided supervision, assisted with visualization, and partook in the manuscript's review and editing. Andreas Jossen was instrumental in acquiring funding, providing resources, offering supervision, and revising the manuscript.

Quantifying the carbon footprint of energy storage applications with an energy system simulation framework - Energy System Network

Anupam Parlikar, Benedikt Tepe, Marc Möller, Holger Hesse, and Andreas Jossen

Energy Conversion and Management 304 (2024), 118208, 2024

Permanent weblink:
https://doi.org/10.1016/j.enconman.2024.118208

Energy Conversion and Management 304 (2024) 118208

Contents lists available at ScienceDirect

Energy Conversion and Management

journal homepage: www.elsevier.com/locate/enconman

Research paper

Quantifying the carbon footprint of energy storage applications with an energy system simulation framework — Energy System Network

Anupam Parlikar [a,*], Benedikt Tepe [a], Marc Möller [a], Holger Hesse [b], Andreas Jossen [a]

[a] Technical University of Munich (TUM), School of Engineering and Design, Department of Energy and Process Engineering, Chair of Electrical Energy Storage Technology (EES), Arcisstr. 21, 80333 Munich, Germany

[b] Kempten University of Applied Sciences, Faculty of Mechanical Engineering, Institute for Energy and Propulsion Technologies, Bahnhofstr. 61, 87435 Kempten, Germany

ARTICLE INFO

Keywords:
Energy system
Battery energy storage system
Energy System Network
Carbon footprint
Levelized Emissions of Energy Supply (LEES)
LEES
State of Carbon Intensity (SOCI)

ABSTRACT

Energy storage is a crucial flexibility measure to temporally decouple power generation from power demand and is touted as the missing link in realizing a decarbonized energy system based on renewable energy. Energy storage capacity buildup at all levels of the global energy system is expected to accelerate the decarbonization process. To this end, a coherent mathematical framework to ascertain the carbon footprint of localized energy systems with energy storage is indispensable. This article presents an open-source energy system simulation program — Energy System Network (ESN). A variety of energy system configurations can be simulated with the Python program, which incorporates key energy system components such as generation, grid, storage, and loads. ESN features an integrated bottom-up approach that combines energy system modeling with streamlined life cycle assessment techniques to quantify the carbon footprint of all components in a localized energy system. The lifecycle phases of each component, including production, operation, and end-of-life treatment, can be considered. Carbon footprint values are obtained for two demonstrative case studies with lithium-ion battery applications: energy arbitrage and home energy systems. The metric Levelized Emissions of Energy Supply (LEES) has been used to evaluate the carbon footprint of each application. An unconventional energy arbitrage strategy designed to exploit the grid carbon intensity spreads instead of the energy price spreads manages to achieve a LEES value about 17% lower than the conventional variant. The influence of rooftop solar generation, battery energy storage system, and the energy management strategy on the LEES values for a home energy system is explored. A maximum LEES reduction of over 37% vis-á-vis the base scenario was observed with optimal energy management for the solar generation and the battery system. The open-source availability of ESN can contribute to transparency, comparability, and reproducibility in carbon footprint assessments of localized energy systems with energy storage.

1. Introduction

The rapid expansion of renewable energy sources is a central feature of the transition toward a decarbonized energy landscape [1]. Energy system simulation models allow for analyzing system behavior and performance under different scenarios, considering factors such as energy sources, grid characteristics, system configurations, and energy management strategies. Energy system models are indispensable for understanding and analyzing complex energy systems. Through scenario analyses, policymakers, energy planners, and other stakeholders can obtain detailed insights into system behavior for optimal resource allocation [2]. A localized energy system comprises a combination of actors, which can be grouped into generation, storage, grid connection, and load components. These components operate in tandem to ensure energy supply and meet the specific needs of a particular application.

Energy storage is becoming increasingly crucial in integrating intermittent renewables, meeting peak electricity demand, and maintaining grid stability. Stationary lithium-ion BESSs are the leading technology due to their high energy density, efficiency, service life, and scalability [3,4]. With a favorable downward cost trend that further accentuates their attractiveness, the capacity buildup and deployment of these systems both continue to grow [5,6]. It is imperative to understand and quantify their environmental impact, particularly in terms of their carbon footprint. The carbon footprint of an energy storage system comprises the total greenhouse gas emissions associated with

* Corresponding author.
E-mail addresses: anupam.parlikar@tum.de (A. Parlikar), benedikt.tepe@tum.de (B. Tepe), marc.moeller@tum.de (M. Möller), holger.hesse@tum.de (H. Hesse), andreas.jossen@tum.de (A. Jossen).

https://doi.org/10.1016/j.enconman.2024.118208
Received 14 November 2023; Received in revised form 15 January 2024; Accepted 12 February 2024
Available online 20 February 2024

Abbreviations

BESS	Battery Energy Storage System
CO_2	Carbon Dioxide Equivalent
CO_2eq	Carbon Dioxide Equivalent
DEC	Discharge Energy Consumption
DOC	Depth of Cycle
EFC	Equivalent Full Cycle
EMS	Energy Management System
EOL	End-of-Life
ESN	Energy System Network
EV	Electric Vehicle
GEC	Grid Energy Consumption
GENEC	Generation Energy Consumption
GWP	Global Warming Potential
HES	Home Energy System
LCA	Life Cycle Assessment
LEC	Load Energy Consumption
LEES	Levelized Emissions of Energy Supply
PV	Photovoltaic Solar
SimSES	Simulation of Stationary Energy Storage Systems
SOC	State of Charge
SOCI	State of Carbon Intensity
SOH	State of Health

Parameters

CF^{gen}	Capacity Factor of generation component
$CI^{gen,exp,fix}$	Fixed component of the carbon intensity of the exported energy from a generation component
$CI^{gr,exp,fix}$	Fixed component of the carbon intensity of the exported energy with a grid component
$CI^{st,exp,fix}$	Fixed component of the carbon intensity of the exported energy discharged from a storage component
CI_t^{ch}	Carbon intensity of charging energy for BESS at time t
$CI_t^{st,exp}$	Carbon intensity of exported discharge energy from the storage at time t
$CI_t^{ES,exp}$	Carbon intensity of the export energy at time t
CI_t^{ES}	Carbon intensity of the energy at the central node of the energy system at time t
$CI_t^{gen,exp}$	Carbon intensity of the energy exported from the generation component at time t
CI_t^{gen}	Carbon intensity of the generation component at time t
$CI_t^{gr,exp}$	Carbon intensity of the energy exported with the grid component at time t
CI_t^{gr}	Effective carbon intensity of the grid mix at time t
$E^{s,EV}$	Energy supplied to the EV over the simulation period
$E^{s,H}$	Energy supplied to the household over the simulation period
$E_l^{st,dch}$	Total energy discharged by the storage technology over its service life
E_t^{st}	Energy content of the storage component at time t
$P^{gen,rated}$	Rated peak power of generation component
$P^{gr,peak}$	Peak power of the grid component
$P_t^{gen,can-run}$	Total power generation of all can-run generation components at the time t
$P_t^{gen,exp}$	Exported generation power from generation component at time t
$P_t^{gen,load,i}$	Directly consumed power generated by generation component i at the time t
$P_t^{gen,loss}$	Loss power of generation component at time t
$P_t^{gen,must-run}$	Total power generation of all must-run generation components at the time t
P_t^{gen}	Generation power of generation component at time t
$P_t^{gr,exp}$	Grid component export power at time t
$P_t^{gr,load}$	Grid power directly supplied to the load at time t
$P_t^{gr,loss}$	Power lost in the grid section during transmission at time t
P_t^{gr}	Total grid power entering the system boundaries at time t
$P_t^{load,c}$	Power consumed by end-application in a load component at time t
$P_t^{load,loss}$	Load loss power at time t
P_t^{load}	Load demand power at time t
$P_t^{residual}$	Residual power after factoring in total must-run generation power at the time t
$P_t^{st,ch}$	Storage component charging power at time t
$P_t^{st,dch,load,i}$	Directly consumed power discharged from storage component i at the time t
$P_t^{st,dch}$	Storage component discharging power at time t
$SOCI_t$	State of Carbon Intensity (SOCI) at time t
SOC_t	SOC at time t
Δt	Simulation timestep
η_t^{gen}	Generation component efficiency at time t
η_t^{gr}	Grid component energy efficiency at time t
$\eta_t^{st,ch}$	Storage component charging efficiency at time t
$\eta^{st,ch}$	Storage component average charging efficiency
$\eta_t^{st,dch}$	Storage component discharging efficiency at time t
$\overline{DOC}$	Mean DOC over simulation period
$\overline{SOCI}$	Mean SOCI over simulation period
$\overline{SOC}$	Mean SOC over simulation period
ε^{BESS}	Total emissions of the BESS over simulation period
ε^{DEC}	Total Discharge Energy Consumption (DEC) emissions for the load over simulation period
ε^{GENEC}	Total Generation Energy Consumption (GENEC) emissions for the load over simulation period

all its life cycle phases, which include production, operation, and end-of-life treatment. Calculating the carbon footprint requires accounting for numerous factors, including the energy mix used for charging the storage systems, energy losses during charge and discharge processes, storage degradation over time, and energy consumed for the production and recycling processes [7].

Estimating the carbon footprint is essential to informed decision-making in terms of the deployment of battery systems. A rigorous and

$\varepsilon^{\mathrm{LEC}}$	Total Load Energy Consumption (LEC) emissions over simulation period
$\varepsilon^{\mathrm{gen,EOL}}$	End-of-Life (EOL) phase emissions of the generation component
$\varepsilon^{\mathrm{gen,en}}$	Total energy emissions for energy from on-site generation components
$\varepsilon^{\mathrm{gen,exp}}$	Export emissions of the generation component
$\varepsilon^{\mathrm{gen,op}}$	Operation phase emissions of the generation component
$\varepsilon^{\mathrm{gen,prod}}$	Production phase emissions of the generation component
$\varepsilon^{\mathrm{gr}}$	Total attributable emissions for the grid section over simulation period
$\varepsilon^{\mathrm{load,op}}$	Operation phase emissions attributable to the load over the entire simulation period
$\varepsilon^{\mathrm{load}}$	Total emissions attributable to the load over the entire simulation period
$\varepsilon^{\mathrm{st,EOL}}$	EOL phase emissions of the storage component
$\varepsilon^{\mathrm{st,exp}}$	Total export emissions of energy discharged from a storage component over simulation period
$\varepsilon^{\mathrm{st,op}}$	Total operation phase emissions for the storage component
$\varepsilon^{\mathrm{st,prod}}$	Production phase emissions of the storage component
$\varepsilon^{\mathrm{st}}$	Total emissions of the storage component over simulation period
$\mathrm{b}_t^{\mathrm{st}}$	Binary variable to prevent simultaneous charging and discharging of the storage component at time t
$\mathrm{c}_t^{\mathrm{IDM}}$	Energy price on the Intraday Market at time t
h	Optimization time horizon h
m	Number of generation components in the energy system
n	Number of storage components in the energy system
p	Number of load components in the energy system
t	Time t
l^{gen}	Expected service lifetime of generation component in years

comprehensive analysis that captures the unique characteristics and application scenarios is indispensable. Various simulation models exist for modeling different aspects of the energy system with varying amounts of focus on battery systems, some of which have been published in open-source form. The following paragraphs briefly discuss the features of some existing energy system modeling tools.

Python for Power System Analysis (PyPSA) is an open-source toolbox developed in Python that provides functionalities for modeling, simulating, and optimizing power systems using power flow calculations and multi-period optimization. It is mainly used to create models of power networks, which include generators, power lines, and rudimentary storage systems. PyPSA can define and impose global constraints on Carbon Dioxide (CO_2) emissions during the optimization process. CO_2 emissions limits for different generation units can be specified by considering emissions factors associated with specific technologies [8]. EnergyPLAN is an open-source energy system modeling tool that facilitates the analysis and optimization of energy systems — from localized to national energy systems. Its main features include scenario analysis, renewable energy integration, energy system optimization, and multi-sectoral modeling. It also enables the specification of CO_2 emission factors for different energy generation technologies and sectors. The tool uses generic energy storage models. Carbon capture and storage can also be considered [9,10].

Calliope is an energy simulation Python tool designed to model and simulate national and urban scale energy systems designed to work with a variety of supply, transmission, storage, and demand technologies. The focus of performance evaluation is economic in nature. The program always solves an optimization problem to obtain the schedule for the energy system, and there is no possibility to run user-defined operation strategies. Time-resolved handling of the CO_2 emissions calculation for all components, especially for storage, is not supported [11,12]. Tools for Energy Model Optimization and Analysis (TEMOA) is another open-source modeling framework for performing energy system analyses and optimizations [13,14]. Temoa is a linear optimization problem that minimizes the costs of energy supply through the use of energy technologies and raw materials, such as coal or biomass, over defined time horizons. Quantification of C02 emissions from energy sources is also possible, albeit component-wise, and bottom-up time-resolved handling of the CO_2 emissions, especially for storage technologies, does not seem possible. The emissions can be limited via constraints of the linear optimization problem. TEMOA is an energy system optimization tool, i.e., it does not let users define their own energy management strategies [13,14].

urbs is a Python-based generator for linear energy system optimization models. The tool does not support user-defined energy management strategies, and the modeling capabilities for energy storage are elementary. The tool also does not support a very extensive CO_2 emissions calculation, especially for energy storage [15,16]. Oemof.solph is another open-source tool that can model and optimize energy systems as a Python package. In the optimization, a minimization of emissions can be defined as a constraint. According to the developers, the higher-level oemof (open energy modeling framework) can also minimize CO_2 emissions from biomass power plants [17,18]. The Framework for Integrated Energy System Assessment (FINE) is another Python-based open-source framework that enables the analysis and optimization of integrated energy systems. FINE can simulate energy systems ranging from localized to international. Entire electricity and natural gas grids can also be simulated. In addition, FINE models storage systems to a somewhat greater extent of detail than PyPSA and EnergyPLAN. Users can define CO_2 emission factors for different energy generation technologies, and in addition to economic optimization, they can also minimize CO_2 emissions [19,20].

GridLAB-D is a C++-based open-source power distribution system simulation and analysis tool that enables the simulation of electrical distribution networks, including storage and distributed energy resources. The tool does not provide built-in features dedicated to emissions modeling, although limited analyses to analyze certain scenarios are possible [21,22]. HOMER (Hybrid Optimization of Multiple Energy Resources) is a tool for analyzing and optimizing hybrid renewable energy systems. Its central capabilities include system optimization to determine cost-effective configurations, modeling renewable resources and loads, simulation and optimization of energy storage options, economic analysis, and the ability to conduct sensitivity analysis and explore different scenarios. Multiple commercial variants that deal with specialized aspects of energy system modeling are available: HOMER Pro, HOMER Grid, and HOMER Front. Homer Pro enables the calculation of CO_2 emissions based on specific emissions of the individual energy sources [23–25]. The System Advisor Model (SAM) is a tool that can be used to model renewable energy systems. SAM includes models for PV systems, storage systems of different types, and industrial processes. The models can be used directly in the desktop application and via application programming interfaces (APIs). CO_2 emissions can only be calculated in SAM in the Biomass Power model. Beyond that, no CO_2 calculations are carried out [26,27].

Distributed Energy Resource Value Estimation Tool (DER-VET™) is another option for the simulation and optimal design of microgrids, storage systems, and distributed energy resources (DERs). The open-source tool is based on the StorageVET® tool, which can simulate storage systems in particular. CO_2 emissions are currently not modeled by DER-VET. However, integration of emissions modeling into the DER-VET optimization problem is planned, according to the developers [28]. Component-Oriented Modeling AND Optimization (COMANDO) is a framework for the design and operation of energy systems. Within COMANDO, an energy system is defined as a collection of different connected components. The tool solves optimization problems for the design and operation of energy systems. In contrast to other open-source tools, COMANDO does not rely solely on a linearization of the optimization problem but can also include dynamics and non-linear expressions. COMANDO does not allow user-defined energy management or customized energy system components. There is also no provision for a detailed CO_2 emissions calculation for components and for energy storage [29,30]. The Performance Simulation Model for Photovoltaic Solar (PV)-Battery Systems (PerMod), an open-source project, allows comparison of the energy efficiency of different grid-connected PV battery systems. This MATLAB-based tool can map different loss mechanisms of grid-connected PV storage systems. Accordingly, it enables a detailed simulation of households with home PV storage systems. Emissions modeling is not a part of the program [31].

A further Python-based optimization model for capacity expansion and unit commitment is ficus. This model focuses on determining the optimal size of system components, including energy storage, and their optimal operation scheduling. There is no provision to add user-defined operation strategies. The storage model used is generic. There is no known functionality to calculate the CO_2 emissions [32,33]. DRAF, short for Demand Response Analysis Framework, is an open-source tool for local multi-energy systems focusing on demand response, as the name suggests. DRAF is an optimization tool that employs linear and mixed-integer linear programming techniques. User-defined energy management strategies that rely on other optimization techniques or strategies that are rule-based cannot be implemented in DRAF. DRAF also includes elmada, a tool that can generate the grid carbon intensity profiles for European countries. The tool also relies on generic battery models which do not consider degradation. From the surveyed literature, the degree of detail in modeling the component-wise CO_2 emissions, especially for energy storage, could not be ascertained [34, 35].

Two storage-centric simulation programs were also studied. The Battery Lifetime Analysis and Simulation Tool (BLAST) is a software tool specifically for analyzing and simulating battery systems. With BLAST, users can perform electrical and thermal simulations to assess the performance and lifetime of batteries. For example, BLAST-Lite is open-source and used in SAM to model storage systems. BLAST does not include a calculation of CO_2 emissions [36]. Simulation of Stationary Energy Storage Systems (SimSES) is a Python-based open-source tool that can simulate storage systems in various applications. SimSES does not offer emissions modeling capabilities. SimSES is used to model storage systems in ESN through a programmatic integration [37].

The reviewed energy system modeling tools are, for the most part, optimization tools that solve a particular form of sizing or scheduling problem. Applications and use cases that require very specific constraints and rules are difficult to simulate, thus restricting flexibility. The battery models employed in most tools are also generic in nature and not detailed enough. None of the tools reviewed offer specific capabilities to quantify and simulate the CO_2 emissions of energy storage systems operating in localized energy systems in a component-wise and time-resolved fashion. The specialized battery simulation tools, such as BLAST, SAM, and SimSES are well suited for modeling the electrical and thermal behavior of battery cells and storage systems but are limited in their ability to model the CO_2 emissions. These findings are corroborated by multiple review papers studying energy system models used in the scientific community [38–41]. Detailed tabular comparisons of the features of various energy system models were found in the reviewed literature, and the reader is referred to these excellent studies [34,38,39,41]. Studying the time-resolved carbon footprint of specific BESS applications in localized energy systems with detailed models is not possible with the reviewed energy system and energy storage models alone. This article presents Energy System Network (ESN),[1] a program to simulate localized energy systems with inherent bottom-up time-resolved capabilities to calculate the CO_2 emissions footprints of energy system components. ESN provides a platform to enable custom energy management strategies and specialized energy system components for any application as time series simulations. With seamless SimSES[2] integration allowing for detailed battery system modeling, ESN offers advanced simulation capabilities to simulate energy storage applications within localized energy systems. A reviewed study provides five modeling recommendations for the carbon footprint of energy storage systems [42]. ESN coupled with SimSES can aid users with four of the five recommendations pertaining to the inclusion of life cycle phases, energy management, and system components in such studies. The program is distributed as open-source code hosted on a Gitlab repository and is built with an object-oriented programming approach in Python.

Scope and outline

This article presents the simulation framework underpinning ESN, while attempting to shed light on the following research questions:

1. How can a coherent and unambiguous carbon emissions modeling framework for localized energy systems with energy storage be implemented such that the results are component-wise and time-resolved?
2. How can the carbon footprints of such localized energy system configurations providing a given service be compared consistently and reproducibly?

The use of this framework is demonstrated through case studies. An attempt is made to address the following research questions through the simulation of two battery storage system applications, energy arbitrage, and home energy systems:

1. Can the battery application energy arbitrage directly support grid decarbonization, and how can this be quantified?
2. How can the decarbonization impact of residential battery storage systems and rooftop solar generation in home energy systems be quantified?

The contents of this article are structured as follows. Section 2 presents the simulation framework behind ESN with the emissions modeling methods for all energy system component classes. The two case studies are presented in Section 3, accompanied by a discussion on the simulation setup and the simulation results. In Section 4, a summary of the current and possible future capabilities of ESN is presented along with the key findings and limitations of the case studies.

2. Simulation framework

This section presents the simulation framework behind ESN and the mathematical framework underpinning it. The simulation program is, in principle, designed to model multiple energy systems interacting with one another, i.e. an energy system comprised of multiple smaller energy systems. In its current state, ESN supports scenarios that can be modeled as a single energy system.

[1] https://gitlab.lrz.de/open-ees-ses/energy_system_network
[2] https://gitlab.lrz.de/open-ees-ses/simses

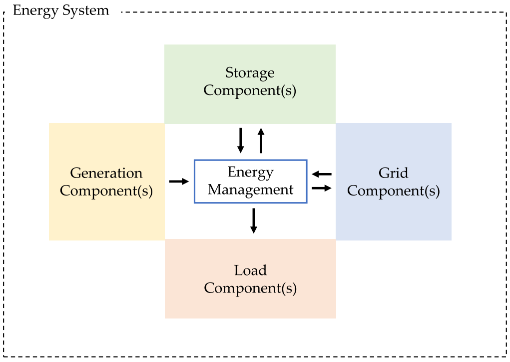

Fig. 1. Schematic representation of an *Energy System*, its constituent *Energy System Components*, and the Energy Management System (EMS) that regulates the power flows among them.

2.1. Energy system

An *Energy System* is a self-sufficient simulation unit representing a single node subjected to an energy balance. Each Energy System essentially represents a group of energy system components connected at the same node that directly satisfy the energy and power balance constraints at that node. Each energy system must consist of two or more *Energy System Components*, which belong to either of the four component classes:

1. Generation components
2. Grid components
3. Storage components
4. Load components

A grid component is a grid section that connects the node within the system boundaries to the larger energy system that lies beyond the boundaries. The operation and the energy flows among these components are regulated by algorithms in the Energy Management System (EMS), an instance of which is contained in each energy system. Fig. 1 depicts an energy system with its constituents.

The energy system components and their attributes are described in the following section. Models belonging to each component class emulate the central characteristics of each component class — generation, transmission, storage, or load. Each energy system component has a common structure: the physical model, time-series profiles, state, environmental data, and other additional component data. At the core of each component model lies the physical system of governing equations. This model enables the response of the component to be simulated. The components require user-defined or default profiles to model time-variant quantities such as generation, consumption, availability, and time-dependent carbon intensity. The environmental data pertains to its lifecycle emissions in all phases, including production, operation, power generation, and EOL processes. At each timestep, the EMS determines target powers for all components based on its algorithm. All quantities of interest are stored in the *State* of the EMS. Each energy system component receives the power target and runs it through the physical model to obtain the actual power. All parameters of interest are subsequently stored in the *State* of each component, which acts as a data logger. The contents of the state are analyzed and evaluated after each simulation run to obtain consolidated results for all components and the energy system.

The emissions calculation methodology for each component class is presented and discussed in the following sections. Documentation on installation, configuration, and exemplary simulations are found in the open-source code repository for the project. As this work focuses on the emissions modeling of localized energy systems, the following sections focus primarily on those aspects.

Table 1
Class attributes of energy system component classes.

	Energy system components			
	Generation	Grid	Storage	Load
Energy form applicable	x	x	x	x
Peak power	x	x	x	x
Energy capacity	–	–	x	–
State	x	x	x	x
Profile(s)	Generation	Carbon-Intensity	–	Load
Flag(s)	Must-run	Feed-in enabled		Must-fulfill
			–	Discrete load
Capacity factor	x	–	–	–
Production phase emissions	x	x	x	–
End-of-life emissions	x	x	x	–

2.2. Generation components

Generation components emulate the functioning of power generation systems. Each generation component exhibits class attributes tabulated in Table 1. Renewable energy sources such as PV solar and wind turbines are modeled using generation profiles for specified locations, whereas a diesel generator is modeled using an efficiency curve to model power output with respect to fuel consumption. For a generation component, the total emissions across its entire service life, ε^{gen}, are given by Eq. (1), where $\varepsilon^{gen,prod}$, $\varepsilon^{gen,op}$, and $\varepsilon^{gen,EOL}$ refer to the production phase, operation phase, and EOL phase emissions respectively. Export emissions, $\varepsilon^{gen,exp}$, are associated with the exported energy. This is discussed towards the end of this sub-section. Fig. 2 depicts the power flows and emissions associated with a generation component within the system boundaries.

$$\varepsilon^{gen} = \varepsilon^{gen,prod} + \varepsilon^{gen,op} + \varepsilon^{gen,EOL} - \varepsilon^{gen,exp} \tag{1}$$

The total operation phase emissions, $\varepsilon^{gen,op}$, can be calculated as shown in Eq. (2). Here, CI_t^{gen} refers to the carbon intensity of the generated energy before losses at time t and is equal to the combustion emissions per kW h of electricity for conventional generation components. For generation components such as the PV solar system and wind turbines, CI_t^{gen} is zero. $P_t^{gen,loss}$ is the loss power associated with an effective power generation P_t^{gen} at time t. P_t^{gen} does not include the exported power. Δt is the chosen simulation timestep. With this line of thought, the operation phase emissions for PV solar system and wind turbines are essentially zero.

$$\varepsilon^{gen,op} = \sum_{t=start}^{end} (CI_t^{gen} \cdot P_t^{gen,loss}) \cdot \Delta t \tag{2}$$

The power generation emissions, $\varepsilon^{gen,en}$, are allocated to all components either consuming or losing some of this generated energy during transmission or storage of this energy (Eq. (3)). For non-combusting generation components, $\varepsilon^{gen,en}$ equals zero.

$$\varepsilon^{gen,en} = \sum_{t=start}^{end} (CI_t^{gen} \cdot P_t^{gen}) \cdot \Delta t \tag{3}$$

The surplus energy produced by a generation component can also be exported to actors outside the system boundaries. The export emissions, $\varepsilon^{gen,exp}$, are then obtained as follows (Eq. (4)), where $P_t^{gen,exp}$ is the exported generation power at time t. Here, $CI^{gen,exp,fix}$ refers to the fixed component of the emissions per unit of energy generated. These emissions are deducted from the total emissions of the generation component.

$$\varepsilon^{gen,exp} = \sum_{t=start}^{end} \left(CI^{gen,exp,fix} \cdot P_t^{gen,exp}\right) \Delta t \tag{4}$$

$CI^{gen,exp,fix}$ is defined as in Eq. (5). CF^{gen} is the expected capacity factor for the generator at the specified location, $P^{gen,rated}$ is the rated

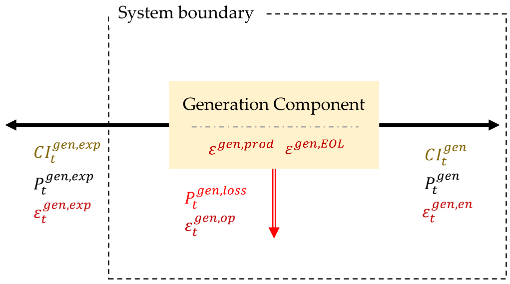

Fig. 2. Block diagram of a generation component depicting the power flows, emissions categories, and carbon intensities.

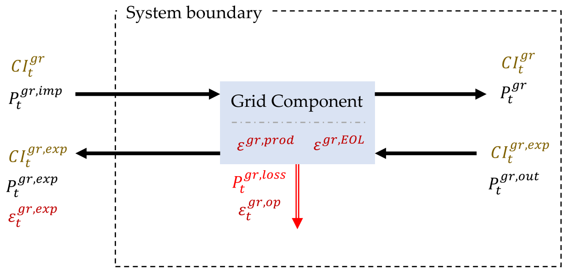

Fig. 3. Block diagram of a grid component depicting the power flows, emissions categories, and carbon intensities.

peak power, and l^{gen} is the expected service lifetime of the generation component.

$$CI^{gen,exp,fix} = \frac{\varepsilon^{gen,prod} + \varepsilon^{gen,EOL}}{CF^{gen} \cdot P^{gen,rated} \cdot l^{gen}} \tag{5}$$

The exported energy has a carbon intensity, $CI_t^{gen,exp}$, given by Eq. (6). The second term indicates the operation emissions associated with the generation of each unit of energy, where η_t^{gen} is the efficiency of the generation component at time t. These operation emissions are also reallocated to actors beyond the system boundaries. This second term is zero in the case of PV systems and wind turbines. Only the fixed component is considered.

$$CI_t^{gen,exp} = CI^{gen,exp,fix} + \frac{CI_t^{gen}}{\eta_t^{gen}} \tag{6}$$

ESN currently supports the calculation of export emissions for renewable generation components.

2.3. Grid components

Grid components emulate the functioning of grid connections or limited grid sections. Each grid component exhibits the attributes listed in Table 1. If the grid component is included in the system boundaries, the lifecycle emissions associated with it, ε^{gr}, are given by Eq. (7), where $\varepsilon^{gr,prod}$, $\varepsilon^{gr,op}$, and $\varepsilon^{gr,EOL}$, are the production, operation, and EOL phase emissions respectively. If a grid component is to be modeled purely as a grid connection, it is considered outside the system boundaries, with the connection itself enabling the import and export of power from the larger grid. In this case, no production and EOL emissions are associated with the grid component. If the grid component is excluded from the system boundary, ε^{gr} is merely equal to $\varepsilon^{gr,op}$. Export emissions, $\varepsilon^{gr,exp}$, are associated with the exported energy. This is discussed towards the end of this sub-section. Fig. 3 depicts the power flows and emissions associated with a grid component within and outside the system boundaries.

$$\varepsilon^{gr} = \varepsilon^{gr,prod} + \varepsilon^{gr,op} + \varepsilon^{gr,EOL} - \varepsilon^{gr,exp} \tag{7}$$

The total operation phase emissions, $\varepsilon^{gr,op}$, are calculated as follows, where CI_t^{gr} is the carbon intensity of the energy transported by the grid component. $P_t^{gr,loss}$ is the loss power associated with the effective imported grid power, P_t^{gr}, at time t.

$$\varepsilon^{gr,op} = \sum_{t=start}^{end} (CI_t^{gr} \cdot P_t^{gr,loss}) \cdot \Delta t \tag{8}$$

The grid energy import emissions, $\varepsilon^{gr,en}$, are allocated to all components either consuming or losing some of this imported energy during storage (Eq. (9)).

$$\varepsilon^{gr,en} = \sum_{t=start}^{end} (CI_t^{gr} \cdot P_t^{gr}) \cdot \Delta t \tag{9}$$

The export emissions to be deducted from the total emissions of the grid component are given by Eq. (10). $CI^{gr,exp,fix}$ is the fixed component of the export emissions, and $P_t^{gr,exp}$ represents the export power. A scheme to determine this fixed component, considering grid component production and EOL emissions, could also be devised, similar to the generation components. Given the high durability, correspondingly long service lifetimes, and ubiquitousness of grid components, this value is estimated to be negligible and is hence not considered further. Moreover, for grid components treated as mere grid connections, the value of $CI^{gr,exp,fix}$ would be zero, in any case, as the production and EOL phase emissions are also zero.

$$\varepsilon^{gr,exp} = \sum_{t=start}^{end} \left(CI^{gr,exp,fix} \cdot P_t^{gr,exp}\right) \Delta t \tag{10}$$

Depending on the sources of the exported energy, the carbon intensity of the exported energy, $CI_t^{ES,exp}$, is calculated below (Eq. (11)), where m is the number of generation components, and n is the number of storage components.

$$CI_t^{ES,exp} = \frac{\sum_{i=1}^{m} P_t^{gen,exp,i} \cdot CI_t^{gen,exp,i} + \sum_{j=1}^{n} P_t^{st,dch,exp,j} \cdot CI_t^{st,exp,j}}{\sum_{i=1}^{m} P_t^{gen,exp,i} + \sum_{j=1}^{n} P_t^{st,dch,exp,j}} \tag{11}$$

The carbon intensity of the exported energy through the grid component, $CI_t^{gr,exp}$, taking into account the additional emissions due to the operation losses in the grid section, is calculated as in Eq. (12), where η_t^{gr} is the efficiency of the grid component at time t.

$$CI_t^{gr,exp} = CI^{gr,exp,fix} + \frac{CI_t^{ES,exp}}{\eta_t^{gr}} \tag{12}$$

As it is cumbersome and infeasible to track the portion of exported energy first imported, Eq. (12) contains only a single efficiency term, corresponding to the losses in the export process, instead of two efficiency terms, as in the case of storage components. ESN does not currently support the calculation of export emissions for the grid components.

2.4. Storage components

Storage components model the characteristics of an energy storage system. The attributes of these components are listed in Table 1. The total emissions across the lifetime of a storage component, ε^{st}, consist of the production, operation, and EOL phases (Eq. (13)), represented by $\varepsilon^{st,prod}$, $\varepsilon^{st,op}$, and $\varepsilon^{st,EOL}$ respectively. If a portion of the discharged energy is exported outside the system boundaries, a corresponding amount of emissions $\varepsilon^{st,exp}$ is deducted from ε^{st}. This is discussed towards the end of this sub-section. Fig. 4 depicts the power flows and emissions associated with a storage component within the system boundaries.

$$\varepsilon^{st} = \varepsilon^{st,prod} + \varepsilon^{st,op} + \varepsilon^{st,EOL} - \varepsilon^{st,exp} \tag{13}$$

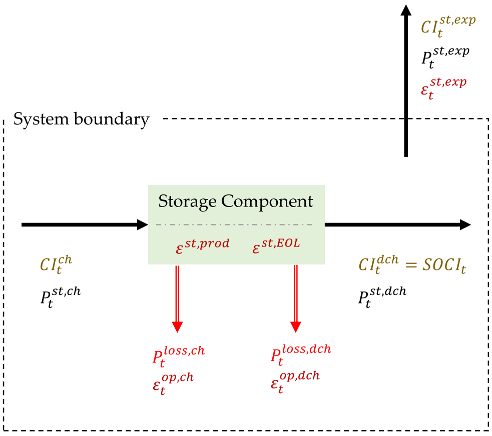

Fig. 4. Block diagram of a storage component, depicting the power flows, emissions categories, and carbon intensities.

The operations emissions of the charging process are proportional to the charging losses, $P_t^{ch,loss}$, of the storage component and the carbon intensity of the charging energy CI_t^{ch}. In the simplest case, CI_t^{ch} could be equal to the carbon intensity of the central energy system node CI_t^{ES} (Eq. (14)). In other cases, the storage might only be charged from energy sourced solely from one or more sources, in which case, CI_t^{ch} might need to be determined separately.

$$CI_t^{ES} = \frac{\sum_{i=1}^{m} P_t^{gen,i} \cdot CI_t^{gen,i} + CI_t^{gr} \cdot P_t^{gr}}{\sum_{i=1}^{m} P_t^{gen,i} + P_t^{gr}} \tag{14}$$

The operation phase emissions during discharge are proportional to discharge losses, $P_t^{dch,loss}$, and the SOCI, a new state variable, first introduced in a previous study [43]. The SOCI is defined as follows in Eq. (15), where $SOCI_t$ and SOC_t are the values of the SOCI and SOC variables at time t.

$$SOCI_{t+1} = \frac{SOCI_t \cdot SOC_t + \Delta SOC \cdot CI_t^{ch}}{SOC_{t+1}} \tag{15}$$

The total operation emissions $\varepsilon^{st,op}$ for the storage component consist of the operation emissions in the charging and the discharging processes. $\varepsilon^{st,op}$ is then obtained as the sum of emissions in the charging and discharging processes.

$$\varepsilon^{st,op} = \sum_{t=start}^{end} (CI_t^{ch} \cdot P_t^{ch,loss} + SOCI_t \cdot P_t^{dch,loss}) \cdot \Delta t \tag{16}$$

The export emissions to be deducted from the total emissions of the storage component are given by Eq. (17). The first term in the sum, $CI^{st,exp,fix}$, represents a reallocation of the fixed component of the storage component emissions, whereas the second term indicates the reallocation of the operation emissions associated with the charging and discharging of the exported energy. It is assumed that the discharged exported energy was charged with a carbon intensity equal to $SOCI_t$, with an efficiency equal to the average charging efficiency $\eta^{st,ch}$. $\eta_t^{st,dch}$ refers to the instantaneous discharging efficiency, and $P_t^{st,dch,exp}$ refers to the exported discharge power at time t.

$$\varepsilon^{st,exp} = \sum_{t=start}^{end} \left[\left(CI^{st,exp,fix} + SOCI_t \cdot \left(\frac{1}{\eta^{st,ch} \eta_t^{st,dch}} - 1 \right) \right) \cdot P_t^{st,dch,exp} \right] \Delta t \tag{17}$$

$CI^{st,exp,fix}$ is defined as in Eq. (18), where $E_l^{st,dch}$ is the total energy discharged by the storage technology over its service life. An estimate of this quantity can be obtained through prior simulations based on accurately parameterized battery degradation models or approximations based on values provided in datasheets. The carbon intensity of the exported energy, $CI_t^{st,exp}$, can then be simplified and written as follows (Eq. (19)).

$$CI^{st,exp,fix} = \frac{\varepsilon^{st,prod} + \varepsilon^{st,EOL}}{E_l^{st,dch}} \tag{18}$$

$$CI_t^{st,exp} = CI^{st,exp,fix} + \frac{SOCI_t}{\eta^{st,ch} \cdot \eta_t^{st,dch}} \tag{19}$$

ESN does not currently support the calculation of export emissions for the storage components.

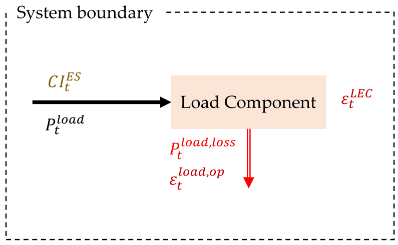

Fig. 5. Block diagram of a load component depicting the power flows, emissions categories, and carbon intensities.

2.5. Load components

Load components approximate the functioning of power consumers. Each load component exhibits the attributes listed in Table 1. The load power, P_t^{load}, supplied to the load can be divided into the actual power consumed by the end application, $P_t^{load,c}$, and the power lost to conversion processes, $P_t^{load,loss}$, for example in the charger of an EV (eq. (20)) (see Fig. 5).

$$P_t^{load} = P_t^{load,c} + P_t^{load,loss} \tag{20}$$

Over the simulated period, the total emissions allocated to a load component, ε^{load}, are given by Eq. (21), where ε^{LEC} are the Load Energy Consumption (LEC) emissions, and $\varepsilon^{load,op}$ are the operation emissions assigned to the load (if required). The carbon intensity of the energy at the central node, CI_t^{ES}, is calculated as in Eq. (14). The total operation phase emissions of the load component are calculated as the sum of the products of the load loss power $P_t^{load,loss}$ and the carbon intensity of the energy consumed by the load, CI_t^{ES} (Eq. (23)).

$$\varepsilon^{load} = \varepsilon^{LEC} + \varepsilon^{load,op} = \sum_{t=start}^{end} (P_t^{load} \cdot CI_t^{ES}) \cdot \Delta t \tag{21}$$

$$\varepsilon^{LEC} = \sum_{t=start}^{end} (P_t^{load,c} \cdot CI_t^{ES}) \cdot \Delta t \tag{22}$$

$$\varepsilon^{load,op} = \sum_{t=start}^{end} (P_t^{load,loss} \cdot CI_t^{ES}) \cdot \Delta t \tag{23}$$

The LEC emissions, ε^{LEC}, are obtained as a sum of the GENEC, the Grid Energy Consumption (GEC), and the DEC emissions (Eq. (24)). The Generation Energy Consumption (GENEC) emissions, ε^{GENEC}, are the sum of emissions on account of direct consumption of energy produced by the generators (Eq. (25)). The Grid Energy Consumption (GEC) emissions, ε^{GEC}, are the sum of emissions on account of direct consumption of energy imported from the grid (Eq. (26)). The Discharge Energy Consumption (DEC) emissions, ε^{DEC} are the sum of emissions on account of direct consumption of energy discharged from the storage components (Eq. (27)). $P_t^{gen,load,i}$ refers to the direct consumption of power from generation component i at time t. $P_t^{gr,load}$ represents the direct consumption of grid power at time t. Similarly, $P_t^{st,dch,load,i}$ signifies the direct consumption of power discharged by storage component i at time t. By definition, the GENEC emissions for power generated by PV solar systems and wind turbines are zero.

$$\varepsilon^{LEC} = \varepsilon^{GENEC} + \varepsilon^{GEC} + \varepsilon^{DEC} \tag{24}$$

$$\varepsilon^{GENEC} = \sum_{t=start}^{end} \sum_{i=1}^{m} (CI_t^{gen,i} \cdot P_t^{gen,load,i}) \cdot \Delta t \tag{25}$$

$$\varepsilon^{GEC} = \sum_{t=start}^{end} (CI_t^{gr} \cdot P_t^{gr,load}) \cdot \Delta t \tag{26}$$

$$\varepsilon^{DEC} = \sum_{t=start}^{end} \sum_{j=1}^{n} (SOCI_t^{j} \cdot P_t^{st,dch,load,j}) \cdot \Delta t \tag{27}$$

2.6. Emissions balance and general discussion

With the quantities introduced and defined in the previous sections, an emissions balance for the energy system within the specified system boundaries can be obtained. This balance excludes the exported energy and only considers the actual energy quantities consumed or lost within the system boundaries (Eq. (28)), where p is the number of load components in the energy system.

$$P_t^{gr,imp} \cdot CI_t^{gr} + \sum_{i=1}^{m} \frac{P_t^{gen,i}}{\eta_t^{gen,i}} CI_t^{gen,i}$$
$$= \varepsilon_t^{gr,op} + \sum_{i=1}^{m} \varepsilon_t^{gen,op,i} + \sum_{j=1}^{n} \varepsilon_t^{st,op,j} + \sum_{k=1}^{p} (\varepsilon_t^{LEC,k} + \varepsilon_t^{load,op,k}) \tag{28}$$

From the presented mathematical framework, from an allocation perspective, emissions during the operation phase can:

1. originate within the system boundaries (e.g., from a combustion-based generator)
2. enter the system boundaries from a source beyond the system boundaries (e.g., through a grid connection)
3. terminate at one or more components within the system boundaries (e.g., operation and energy consumption emissions)
4. exit the system boundaries and terminate at components outside the system boundaries (via exported energy)

Production phase and EOL phase emissions of all components within the system boundaries are allocated to the energy system. Some emissions are deducted from each component due to the exported energy. The choice of system boundaries depends on the purpose of a simulation. If the sole purpose of a simulation is to compare two competing system configurations, all common fixed elements may be disregarded, as these merely introduce a fixed offset in both analyses. In this case, the LEES values of the two competing configurations do not reflect absolute values but help determine the delta in this case. If some energy system components have a service lifetime longer than the simulated duration and are expected to still possess a so-called Remaining Useful Life (RUL), specific adjustments can be made to deduct a suitably determined quantity of emissions. The same applies to components that need to be replaced during the simulated duration and do not reach their EOL by the end of the simulated period. Table 2 lists the emissions categories applicable to each class of energy system components.

2.7. Energy management

Each energy system possesses an Energy Management System (EMS). The EMS regulates the energy flows among the various components in an energy system by generating reference powers for all components while considering the specified constraints. Each EMS consists of two blocks: an operation strategy, which defines the logic/algorithm to govern energy flows, and a *State*, where values of all parameters are logged at each time t. The state enables subsequent analyses to be conducted after each simulation run. Two types of strategies regulate the energy flows with the EMS: rule-based and optimization-based strategies. The modular nature of ESN allows for the incorporation of new tailor-made rule-based and optimization-based strategies to suit the specific requirement of the user and the use case to be simulated.

Table 2
Emissions categories applicable to each energy system component class.

	Emissions categories	Generation	Grid	Storage	Load
Static	Production	x	x	x	–
	End-of-life	x	x	x	–
Time-dependent	Operation	x	x	x	–
	Export	x	x	x	–
	Generation energy consumption	–	–	–	x
	Grid energy consumption	–	–	–	x
	Discharge energy consumption	–	–	–	x

2.7.1. Rule-based strategies

Rule-based strategies regulate the energy flows among components of the energy system based on a set of sequential commands or rules that depend on certain conditions being met. Three available rule-based strategies in ESN are discussed in the following sub-sections.

SimpleDeficitCoverage. The EMS strategy *SimpleDeficitCoverage* relies on a specified priority list of energy system components to meet the load power demand. The power generation of the must-run generation components (generation from PV solar and wind is also classified as such in many jurisdictions) is factored in first at every timestep (Eq. (29)). $P_t^{residual}$ refers to the residual power after factoring in the must-run generation, whereas $P_t^{gen,must-run}$ refers to the total generation power of all must-run generation components. Users can then specify which energy system component is to be used first, second, or third to meet the residual demand. The default priority list is as follows:

(I) Storage components
(II) Grid components
(III) Can-run generation components

With the default specification, the strategy attempts to meet the residual load first with discharged energy from the storage components. If available, the power is drawn from the grid components next. If further power is required, can-run generation components (such as the diesel generator) are run to deliver the demanded power (Eq. (30)). Here $P_t^{gen,can-run}$ refers to the total can-run generation power requested.

$$P_t^{residual} = P_t^{load} - P_t^{gen,must-run} \tag{29}$$

$$(P_t^{st,dch})^{I} + (P_t^{gr})^{II} + (P_t^{gen,can-run})^{III} = P_t^{residual} \tag{30}$$

The same priority is used to regulate the order of absorption of surplus generation from the must-run generation components. In the default setting, surplus generation is used to charge the storage components before being fed back into the grid. This strategy has been successfully demonstrated to control the energy system components operating in an island grid [44].

SimplePeakShaving. The EMS strategy *SimplePeakShaving* controls power flows in energy systems with constrained grid connections. Peak shaving is performed with a storage component that discharges additional power in parallel to meet the peak power demand. Must-run generation components can also be included. If the load power exceeds the rated power rating of the grid connection (and possibly power generated by the must-run components), the residual load is met by discharging energy from the storage component. The storage component is recharged at maximum available power as soon as the load power goes below the rated grid power, and grid capacity is available to recharge the storage component (Eq. (31)).

$$P_t^{residual} = P_t^{load} - P_t^{gr} \tag{31}$$

This strategy has been successfully demonstrated in the provision of peak shaving service for EV high-power charging stations [43].

SimSESExternalStrategy. The EMS strategy *SimSESExternalStrategy* is used to operate the BESS based on power targets directly generated by EMS strategies available in SimSES. This EMS strategy currently supports the SimSES strategy *FcrIdmRechargeStacked*, which has been presented in a previous publication [37]. This strategy generates power targets for the BESS that react to the frequency fluctuations, allowing participation in the grid frequency regulation market. Further information on this strategy can be found in the SimSES project git repository.

2.7.2. Optimization-based strategies

Optimization-based strategies rely on mathematical optimization, rather than a set of rules, to determine the power targets for all energy system components. A suitably chosen objective function governs the optimum power values at each timestep. All optimization-based strategies in ESN currently rely on linear and mixed integer linear optimization to obtain the optimal energy flows. Two such strategies are discussed in the following subsections.

RHOptimization. The strategy *RHOptimization* regulates energy flows by solving a Rolling Horizon (RH) optimization problem to generate power targets for all components. The users can set the time span of the optimization horizon (h) and the frequency of re-optimization based on their requirements. This is a general-purpose strategy designed to handle multiple components with the sole aim of meeting load demand with the available energy system components while minimizing the emissions over each optimization horizon. The objective function deployed in this strategy attempts to minimize the emissions in each optimization horizon (Eq. (32)).

$$\min \sum_{t=t}^{t+h} \left[P_t^{gr} \cdot CI_t^{gr} + \sum_{i=1}^{m} (P_t^{gen,i} \cdot CI_t^{gen,i}) \right] \tag{32}$$

The following peak power constraint applies to each generation and grid component in the energy system to formulate the optimization problem. $P_t^{gen,peak}$ and $P^{gr,peak}$ refer to the peak power generation capability of the generation component and the peak power capability of the grid component, respectively, at time t (Eq. (33),(34)).

$$P_t^{gen} \leq P_t^{gen,peak} \tag{33}$$

$$P_t^{gr} \leq P^{gr,peak} \tag{34}$$

The following set of constraints applies to each storage component in the energy system and during the optimization problem formulation. Where $P_t^{st,ch}$ and $P_t^{st,dch}$ refer to the charging and discharging powers, respectively, of the storage component at time t. $P^{st,peak}$ refers to the storage peak power, while b_t^{st} represents the binary variable used to prevent simultaneous charging and discharging of the storage component at time t. $\eta_t^{st,ch}$ refers to the charging efficiency of the storage component at time t. E_t^{st} represents the energy content of the storage component at time t.

$$P_t^{st,ch} - b_t^{st} \cdot P_{peak}^{st} \leq 0 \tag{35}$$

$$P_t^{st,dch} + (b_t^{st} - 1) \cdot P_{peak}^{st} \leq 0 \tag{36}$$

$$0 \leq SOC_t \leq 1 \tag{37}$$

$$SOC_{t-1} \cdot E_t^{st} + (P_t^{st,ch} \cdot \eta_t^{st,ch} - \frac{P_t^{st,dch}}{\eta_t^{st,dch}}) \cdot \Delta t = SOC_t \cdot E_t^{st} \tag{38}$$

$$P_t^{st,ch} \cdot \eta_t^{st,ch} \cdot \Delta t \leq \left(1 - SOC_{t-1}\right) \cdot E_t^{st} \tag{39}$$

$$\frac{P_t^{st,dch}}{\eta_t^{st,dch}} \cdot \Delta t \leq SOC_{t-1} \cdot E_t^{st} \tag{40}$$

The following energy balance constraint applies to the energy system, ensuring that the sum of all component powers and allocations equals zero (Eq. (41)).

$$P_t^{gr} + \sum P_t^{st,dch} + \sum P_t^{gen} = P_t^{load} + \sum P_t^{st,ch} \tag{41}$$

A previous study successfully demonstrated this strategy on battery-assisted high-power charging for EVs [43].

ArbitrageOptimization. The *ArbitrageOptimization* strategy determines the scheduling of a grid-connected storage component such as BESS participating in energy arbitrage to buy and sell power on the intraday market. The strategy has been designed to optimize one of two objective functions — one that maximizes monetary profit and another that maximizes the difference between the product of grid carbon intensity and storage power during charging and discharging. The second objective essentially directs the storage to charge at low grid carbon intensity values and discharge at times of high grid carbon intensity values. The objective functions used in the economic and emissions-drive optimization are given in Eqs. (42) and (43) respectively. c_t^{IDM} represents the energy price on the intraday market at time t.

$$\max \sum_{t=t}^{t+h} \left[(P_t^{st,ch} + P_t^{st,dch}) \cdot c_t^{IDM} \right] \cdot \Delta t \tag{42}$$

$$\max \sum_{t=t}^{t+h} \left[(P_t^{st,ch} + P_t^{st,dch}) \cdot CI_t^{gr} \right] \cdot \Delta t \tag{43}$$

The storage component constraints (Eq. (35) to (40)) described under RHOptimization are also applicable to the optimization problem in this strategy. Further documentation and simulation examples can be found on the project git repository.

3. Case studies with typical applications

Simulation results of selected case studies to demonstrate the quantification of the total emissions over the lifecycle of an energy system are presented and discussed in this section. As the leading energy storage technology, we focus on lithium-ion Battery Energy Storage System (BESS) technology. In Section 3.1, a typical grid-connected application for BESSs is simulated — Energy Arbitrage. In Section 3.2, four typical Home Energy System (HES) scenarios with electromobility, rooftop solar, and home storage systems are simulated and discussed from the emissions perspective. In addition to the case studies presented here, this framework has already been successfully applied to applications such as island grids and EV high-power charging [43,44].

3.1. Energy arbitrage

Several energy markets exist to ensure a balanced grid at all times. BESSs can participate in these markets and provide services conveniently owing to their attributes. In these applications, the BESS interacts solely with the grid, charging and discharging energy from and to the grid. Typical system boundaries, power flows, and emissions categories are depicted in Fig. 6A. As the BESS is charged solely with power imported from the grid, the carbon intensity of the charging energy (CI_t^{ch}) is equal to the carbon intensity of power imported from the grid (CI_t^{gr}). The total emissions of the BESS across all phases is given by ε^{BESS}.

$$\varepsilon^{BESS} = \varepsilon^{BESS,prod} + \varepsilon^{BESS,op} + \varepsilon^{BESS,EOL} \tag{44}$$

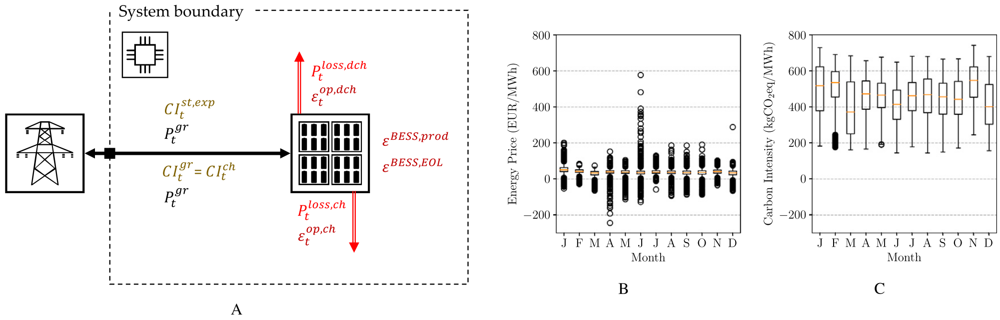

Fig. 6. C: Power flows and emissions categories for a typical grid-connected storage application. B: Depiction of the monthly energy price spreads on the Intraday Market over one year. C: Monthly variation in the Grid carbon intensity (CI_t^{gr}) over the selected year. Data for Germany for the year 2019.

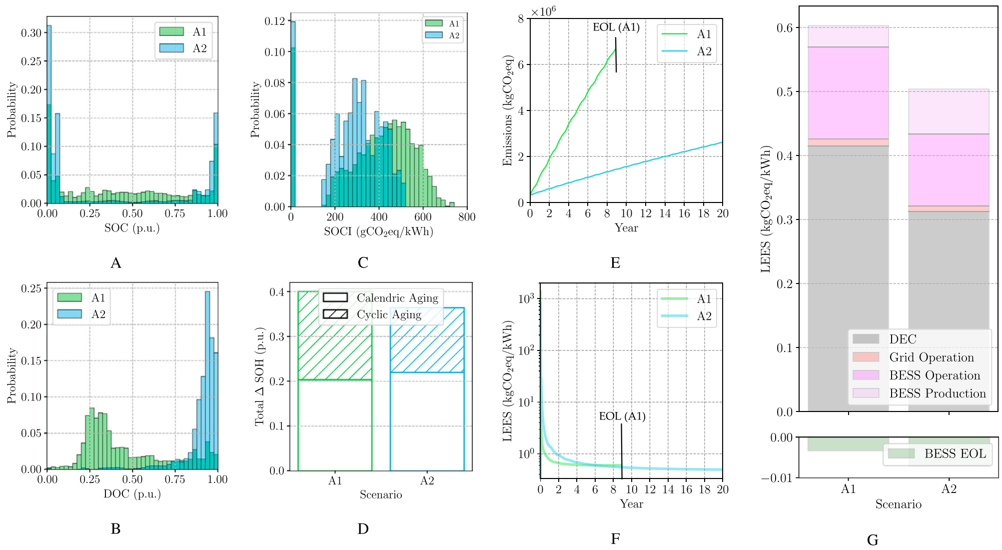

Fig. 7. A, B: Distributions of SOC and DOC values respectively in scenarios A1 and A2 over the simulated period. C: Distribution of the State of Carbon Intensity (SOCI) values in scenarios A1 and A2 over the simulated period. D: Change in the battery SOH over the simulated period and shares of calendric and cyclic aging in scenarios A1 and A2. E: Cumulative emissions for the two scenarios over the simulated period. F: Evolution of the Levelized Emissions of Energy Supply (LEES) value for the two scenarios over the simulated period. G: Breakdown of LEES values for the two scenarios into the constituent emissions categories at the end of the simulation period.

As a simplification, the grid can be considered a load, which consumes energy discharged by the BESS. The LEC emissions for this hypothetical load are solely made up of the DEC emissions (Eq. (45)). Levelized Emissions of Energy Supply (LEES) is a useful metric to obtain the carbon footprint of the energy supplied to a load [44]. The LEES value for the application enables us to look at the BESS as a grid-connected generator with a carbon intensity equal to LEES. This is akin to a retrospective calculation of the carbon intensity of the exported energy $CI_t^{st,exp}$ for the BESS (Eq. (46)).

$$\varepsilon^{DEC} = \sum_{t=start}^{end} SOCI_t \cdot P_t^{st,dch} \cdot \Delta t \tag{45}$$

$$LEES = \frac{\varepsilon^{BESS} + \varepsilon^{DEC}}{E^{dch}} \tag{46}$$

The price spreads on various energy markets, such as the Intraday and Day-Ahead markets, present energy arbitrage opportunities. Figs. 6B,C depict the spreads in the average 15-minute prices on the Intraday-Continuous (IDC) market and the spreads in the grid carbon intensity for the year 2019 in Germany. The price profile used has been generated from data obtained from the *energy-charts*[3] project [45]. The grid carbon intensity profile is also based on data from the same database combined with other data [43]. A conventional energy arbitrage scenario (A1) to maximize economic profit is simulated in this section alongside a novel emissions-arbitrage scenario (A2). The scenarios demonstrate the effect of the EMS strategy on the LEES values of the arbitrage application. The *ArbitrageOptimization* EMS strategy presented earlier (Section 2.7) is used in this application. An identical BESS system configuration is deployed in both scenarios to enable a fair comparison (see Table 3). Table 4 presents the streamlined LCA for the BESS system.

In scenario A1, the EMS strategy is set to generate the economically optimal BESS dispatch schedule. The SOC values are spread across the entire range from 0 to 1, with peaks around both 0 and 1 (depicted in Fig. 7A). As the spread in prices is relatively narrow, with a significant number of outliers, the BESS operates with a lot of shallow half-cycles with a DOC peak around 0.25 (depicted in Fig. 7B). Since the strategy responds to the spread in the energy prices, the distribution of the SOCI

3 https://energy-charts.info/

Table 3
Battery Energy Storage System (BESS) configuration for participating in energy arbitrage.

Energy arbitrage	
Parameter	Value
Cell type	Lithium Iron Phosphate (LFP)
Cell format	Cylindrical, 26650
Rated energy capacity (MWh)	1.6
Rated power (MW)	1.6
Initial State of Health (SOH)	100%
Battery model	R-int Equivalent Circuit Model (ECM) (based on [46,47])
Battery degradation model	Semi-empirical calendric and cyclic (based on [48,49])
Power electronics	AC/DC Converter, 8 units (based on [50–52])
Housing type	40 ft. standard shipping container
HVAC thermal power (kW)	50
Ambient conditions	Berlin
Grid section efficiency	95% (assumed)

Table 4
Streamlined LCA for a utility-scale grid-connected Battery Energy Storage System (BESS) (based on [44]).

Battery Energy Storage System (BESS) streamlined LCA			
Component	Production ($kgCO_2eq$)	End-of-Life (EOL) ($kgCO_2eq$)	Source
Cells	257592.79	−18719.48	[53,54]
Power Electronics	61535.83	−15124.78	[55–58]
Miscellaneous Electronics	25235.73	−3656.66	[55,58]
Housing	28810.92	0.00	[55]
HVAC	426.12	0.00	[59]
Sum	373601.39	−37500.91	
Total	**336100.48**		

Table 5
Simulation results for the two energy arbitrage scenarios.

Simulation results energy arbitrage			
	Scenario		
Parameter	A1	A2	Δ%
Application			
Energy bought (GWh)	14.91	7.11	−52.29
Energy sold (GWh)	11.11	5.29	−52.35
Energy costs (k€)	383.94	172.43	−55.09
Revenue (k€)	548.75	293.51	−46.51
Profit (k€)	164.81	121.08	−26.53
Cumulative emissions (tCO_2)	6664.47	2630.39	−60.53
System temporal utilization (%)	86.00	31.00	−63.95
Fulfillment ratio (%)	87.86	99.60	13.36
LEES ($kgCO_2eq/kWh$)	0.5997	0.4968	−17.15
BESS			
Lifetime (y)	9	20	122.22
Round-Trip Efficiency (%)	74.53	74.43	−0.13
Remaining Capacity (%)	60	63.6	6.00
$\overline{\text{SOC}}$ (%)	43.51	37.67	−13.42
$\overline{\text{DOC}}$ (%)	46.43	90.44	94.79
Equivalent Full Cycles (EFCs)	8506.6	4063	−52.24
Mean C-rate (ch) (1/h)	0.79	0.75	−5.06
Mean C-rate (dch) (1/h)	0.84	0.77	−8.33
$\overline{\text{SOCI}}$ (gCO_2eq/kWh)	388.27	284.73	−26.67

values (Fig. 7C) are observed to tend towards the distribution of the grid carbon intensity (Fig. 8A) without any preference. The BESS is subjected to over 8500 EFCs in this application, and the EOL criterion (SOH = 0.6) is reached in around nine years of operation. The BESS loses 40% of its initial energy storage capacity within the operation period, with over 49% of this capacity loss occurring due to cyclic degradation mechanisms (Fig. 7D). Fig. 8A depicts the grid carbon intensity, CI^{gr}_t during charging and discharging. As the strategy does not take CI^{gr}_t into account, no pattern is discernible in the two distributions during charging and discharging can be observed. Fig. 8C depicts the energy prices during charging and discharging. It can be seen that the EMS strategy charges and discharges the BESS at a wide range of prices. A round-trip efficiency value of 77% is considered in the optimization algorithm. Corresponding to this value, a minimum price difference of around 29% between the buy and sell prices is required for the BESS to enter into energy arbitrage.

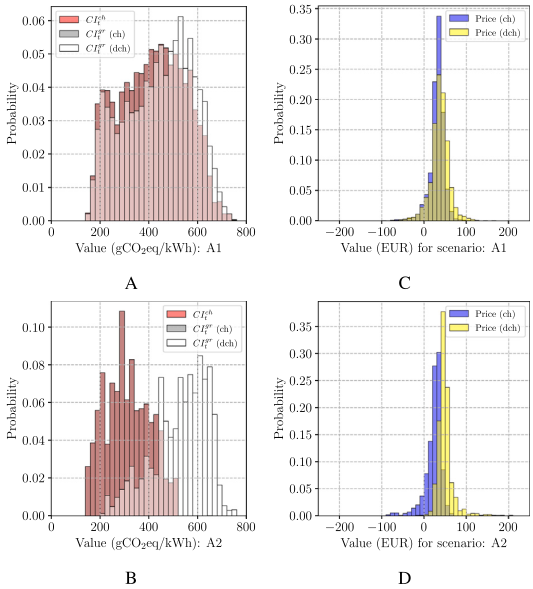

Fig. 8. A, B: Depictions of distributions of CI^{ch}_t, CI^{gr}_t during charging and CI^{gr}_t during discharging in scenarios A1 and A2, respectively. C and D: Distributions of energy price values during charging and discharging in scenarios A1 and A2, respectively.

In scenario A2, the EMS strategy is set to determine the optimal BESS dispatch schedule to shift energy from periods of low CI^{gr}_t to periods of high CI^{gr}_t. A BESS operating in this mode can essentially be considered as supporting the firming of renewable energy generation. The SOC values are skewed much stronger to the extremes with a sparser distribution over the intervening values (Fig. 7A). The BESS is cycled much less (over 4063 EFCs), albeit with higher DOC values (Fig. 7B). The distribution of the SOCI values is shifted leftwards, as the BESS specifically charges when CI^{gr}_t is low (Fig. 7C). The BESS is cycled gentler and reaches an SOH value of around 63% at the end of 20 years. The contribution of cyclic degradation to this capacity loss is over 39% (Fig. 7D). Fig. 8B depicts the distributions of the values of CI^{gr}_t during charging and discharging. A clear separation in the two distributions can be seen, with a preference to charge when CI^{gr}_t assumes relatively lower values and discharging at times that coincide with higher CI^{gr}_t values. A distinct separation in the distributions of the energy prices during charging and discharging can also be observed here (Fig. 8D). This can be explained by the observation that the energy prices positively correlate to the grid carbon intensity values with a correlation coefficient of 0.6132 for 2019. With a round-trip efficiency of around 77%, a minimum ΔCI^{gr}_t of around 29% is required for the BESS to enter into the energy arbitrage.

In Fig. 7E, the cumulative emissions in scenarios A1 and A2 are depicted. As the energy throughput in scenario A1 is higher than in scenario A2, the variable emissions categories (DEC emissions, BESS

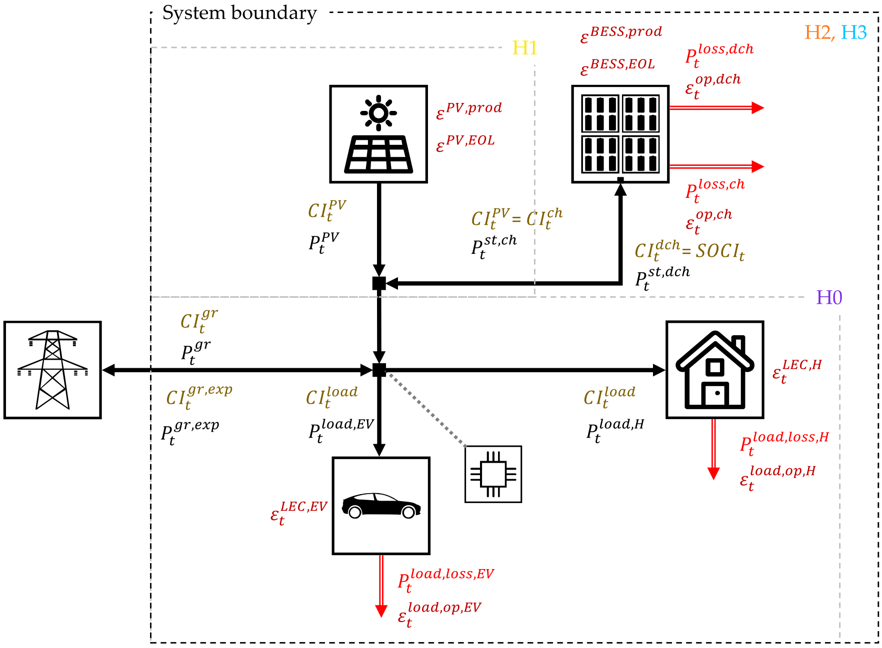

Fig. 9. Power flows and emissions categories for a typical Home Energy System (HES). The four scenarios H0, H1, H2, H3 are depicted here.

operation emissions, and the grid operation emissions) rise faster than in scenario A2. Fig. 7F depicts the evolution of the LEES values over the simulated period. Although a lower LEES value is exhibited in scenario A1 in the first five years, due to the higher energy throughput, from the fifth year onward, scenario A2 exhibits a consistently lower LEES value until the end of the simulation period. Fig. 7G depicts a snapshot of the emissions category-wise breakdown of the LEES value at the end of the simulated period in each scenario. Scenario A1 has a LEES value of 0.5997 $kgCO_2/kWh$, whereas A2 exhibits a LEES value of 0.4968 $kgCO_2/kWh$, which is over 17% lower than that of scenario A1. This trend is also supported by the movement in the mean SOCI values, which in scenario A2 is over 26% lower than in A1. Table 5 summarizes the salient numerical results of each scenario. Despite 52% lower volumes of energy sold, the profit in scenario A2 is only about 26% lower, whereas the cumulative emissions are over 60% lower. Figs. A.1 A,D in the appendix depict the grid carbon intensity and the energy prices during exemplary winter and summer weeks, respectively. Figs. A.1 and A.2 in the appendix also depict the evolution of other parameters of interest.

3.2. Home Energy System (HES)

HESs are gaining in popularity as the prices of PV installations and residential BESSs continue on their downward trend [63]. An additional factor underpinning the popularity of such systems is the rise of electromobility and potential synergies. Studies in the reviewed literature present some form of rules-based emissions-aware EMS strategies to operate a PV-coupled BESS to increase the emissions saving [64]. This section illustrates the modeling and simulation of four HES scenarios (H0, H1, H2, H3) to obtain their Global Warming Potential (GWP) footprints over an operation period of 20 years. A grid-connected household with an EV is considered in this case study (Fig. 9). The annual household load profile is based on a standard profile published by the authors in a previous work [65]. This standard profile is based on a published collection of 74 household load profiles [66]. The profile has an annual household energy consumption of around 4360 kWh. The EV charging load profile is based on simulated data for a Volkswagen ID.3, which is generated with data obtained from the *emobpy* tool and simulated separately with SimSES. This profile has an annual energy consumption of over 1927 kWh [67]. In general, the LEES values for these scenarios are calculated as in Eq. (47). $E^{s,H}$ and $E^{s,EV}$ represent the total energy supplied to the household and to the EV respectively. Table 7 presents the streamlined LCA for the BESS and the rooftop solar system.

Table 6
Battery Energy Storage System (BESS) configuration for the Home Energy System (HES).

Battery Energy Storage System (BESS) for HES	
Parameter	Value
Cell type	Lithium Iron Phosphate (LFP)
Cell format	Cylindrical, 26650
Rated energy capacity (kWh)	5
Rated power (kW)	5
Initial State of Health (SOH)	100%
Battery model	R-int Equivalent Circuit Model (ECM) (based on [46,47])
Battery degradation model	Semi-empirical calendric and cyclic (based on [48,49])
Power electronics	AC/DC Converter (based on [50])
Ambient conditions	Constant temperature, no solar irradiation
Grid section efficiency	95% (assumed)

$$LEES = \frac{\varepsilon^{LEC,H} + \varepsilon^{LEC,EV} + \varepsilon^{gr} + (\varepsilon^{PV}) + [\varepsilon^{BESS}]}{E^{s,H} + E^{s,EV}} \tag{47}$$

In the baseline scenario H0, we consider that the household electric loads and the EV charging load are met entirely with power drawn from the grid. In this case, the energy system consists of one grid component and two load components — the household load and the EV. The

Table 7
Streamlined LCA for the Battery Energy Storage System (BESS) and Photovoltaic Solar (PV) solar system in the Home Energy System (HES) (based on [43,44]).

Home Energy System (HES) Streamlined LCA			
Component	Production ($kgCO_2eq$)	End-of-Life (EOL) ($kgCO_2eq$)	Source
BESS			
Cells	803.71	−58.41	[53,54]
Power Electronics	399.43	−47.26	[55–58]
Miscellaneous Electronics	90.56	−13.12	[55,58]
Sum	1293.70	−118.79	
Total (BESS)	**1174.91**		
Photovoltaic Solar System			
Panels	5500.00	37.00	[60–62]
Power Electronics	489.80	−47.26	[55–58]
Sum	5989.80	−10.26	
Total (PV system)	**5979.54**		

Table 8
Simulation results for the four Home Energy System (HES) scenarios.

Simulation results home energy system				
	Scenario			
Parameter	H0	H1	H2	H3
Application				
Energy consumed (H) (MWh)	87.38	87.38	87.38	87.38
Energy consumed (EV) (MWh)	37.40	37.40	37.40	37.40
Energy import (grid) (MWh)	124.8	95.9	74.01	81.54
Δ% (rel. to H0)		−23.18	−40.69	−34.65
PV energy (MWh)	–	90.19	90.19	90.19
Energy discharged (MWh)	–	–	21.84	14.69
Δ% (rel. to H2)		–	–	−32.75
Energy export (grid) (MWh)	–	61.27	34.8	43.7
Δ% (rel. to H1)	–	–	−43.25	−28.67
Cumulative emissions (tCO_2)	58.91	48.59	40.96	36.87
Δ% (rel. to H0)	–	−17.52	−30.47	−37.41
LEES ($kgCO_2eq/kWh$)	0.4758	0.3930	0.3319	0.2991
Δ% (rel. to H0)	–	−17.39	−30.24	−37.13
BESS				
Lifetime (y)	–	–	20	20
Round-Trip Efficiency (%)	–	–	82.43	81.87
Remaining Capacity (%)	–	–	73.22	71.33
$\overline{\text{SOC}}$ (%)	–	–	24.82	49.41
$\overline{\text{DOC}}$ (%)	–	–	22.62	20.94
Equivalent Full Cycles (EFCs)	–	–	4952.53	3329.29
Mean C-rate (ch) (1/h)	–	–	0.16	0.12
Mean C-rate (dch) (1/h)	–	–	0.14	0.11
$\overline{\text{SOCI}}$ (gCO_2eq/kWh)	–	–	0	0

EV is treated as a load component; consequently, only unidirectional charging is permitted. Fig. 9 also depicts the baseline scenario. As there are no storage components in this configuration, the LEC emissions of both loads are composed solely of the GEC emissions. Another emissions category in this configuration is the grid operation emissions for the grid section within the system boundaries. This configuration is simulated for 20 years, and all emissions categories are tracked. In the numerator of Eq. (47), the bracketed quantities are not applicable to H0. The salient numerical results for this scenario are listed in Table 8. Cumulative emissions for H0 amount to around 59 t Carbon Dioxide Equivalent (CO_2eq), accompanied by a LEES value of 0.4758 kg CO_2eq/kW h at the end of 20 years. Fig. 10E depicts the cumulative emissions of the energy system over the simulated period. In Fig. 10F, the evolution of the LEES value over the simulation period is depicted. The LEES value remains largely constant over the simulation period in this scenario. The primary assumption of constant grid carbon intensity over the 20-year period may be considered as the worst-case scenario. The grid carbon intensity is expected to reduce year-over-year with increasing renewable generation capacity. Fig. 10G depicts the breakdown of this value and the contributions of the three emissions categories.

In scenario H1, the configuration from H0 is augmented by adding a rooftop PV solar system (Fig. 9). The installed PV solar system has a peak power rating of 5 kW_p. A standard annual PV solar power generation profile based on measured data for Munich, Germany, is used to obtain the generated power at each simulation timestep [65,68]. The EMS strategy *SimpleDeficitCoverage* regulates the power flows in this scenario. The energy system now consists of a generation component – the rooftop solar installation – and the components from H0. The lifetime emissions for such a system are described in Section 2.2. The energy generation emissions for a PV solar system are zero. Consequently, the GENEC emissions for both loads are also zero. The LEC emissions for both loads are still solely comprised of the GEC emissions. In the numerator of Eq. (47), the quantities in the square brackets do not apply to H1. Table 8 summarizes the important results for this scenario. The cumulative emissions drop to over 48 t. The LEES value drops to 0.3930 kg CO_2eq/kW h. The drop in cumulative emissions and the LEES value corresponds to over 17% as compared to scenario H0. Fig. 10E depicts the cumulative emissions of the energy system over the simulation period. Fig. 10F illustrates the trend of the LEES value over the simulation period. The LEES value starts from a high value and crosses the value for scenario H0 during the seventh year of operation and maintains this downward trend till the end of the simulated period, essentially implying that the system breaks even from an emissions perspective at this point. Fig. 10G presents the breakdown of the LEES value at the end of 20 years. The power generated by the rooftop solar system displaces some of the grid energy, causing the GEC emissions to be lower. The additional emissions due to the rooftop PV solar system are offset by the drop in GEC emissions,

Scenario H2 builds upon H1 by adding a residential BESS, i.e., a storage component is introduced in this scenario. Table 6 lists the relevant battery parameters. The lifetime emissions for the BESS are described in Section 2.4. For this scenario, we continue using the EMS strategy *SimpleDeficitCoverage* to control the energy flows. As the BESS is never charged with energy from the grid, the SOCI remains zero. As a result, no operation phase emissions are associated with the BESS, and no DEC emissions are associated with the two load components. At the end of 20 years, the cumulative emissions add up to around 41 t CO_2eq. In this case, all terms in Eq. (47) are applicable, and the LEES value is 0.3319 kg CO_2eq/kW h. These values represent a drop of over 30% vis-a-vis H0. From Fig. 10E, it can be seen that the emissions start at a higher value as compared to H1 due to the additional production and EOL emissions of the BESS. After the second year of operation, the cumulative emissions are already lower than in H1. During the fifth year, the cumulative emissions fall below those in H0 and remain lower till the end of the simulated period. Fig. 10F depicts the evolution of the LEES value, and the same trend is also observed here. From Fig. 10G, it can be seen that the additional emissions due to the production of the BESS are more than offset by a more substantial reduction in the GEC emissions. During the simulation period, the BESS is subjected to over 4950 EFCs with a mean DOC of over 22%. The mean SOC during this period is around 25%, and the SOH reaches a value of around 73% (Figs. 10A, B, D). Fig. 10C depicts the total energy supplied to the load and the total energy discharged from the BESS.

Scenario H3 is physically identical to H2 but is run with the *RHOptimization* EMS strategy. Although not explicitly prohibited, the strategy never chooses to charge the BESS with grid energy. Consequently, the SOCI remains zero, as in H2. The operation emissions for the BESS and

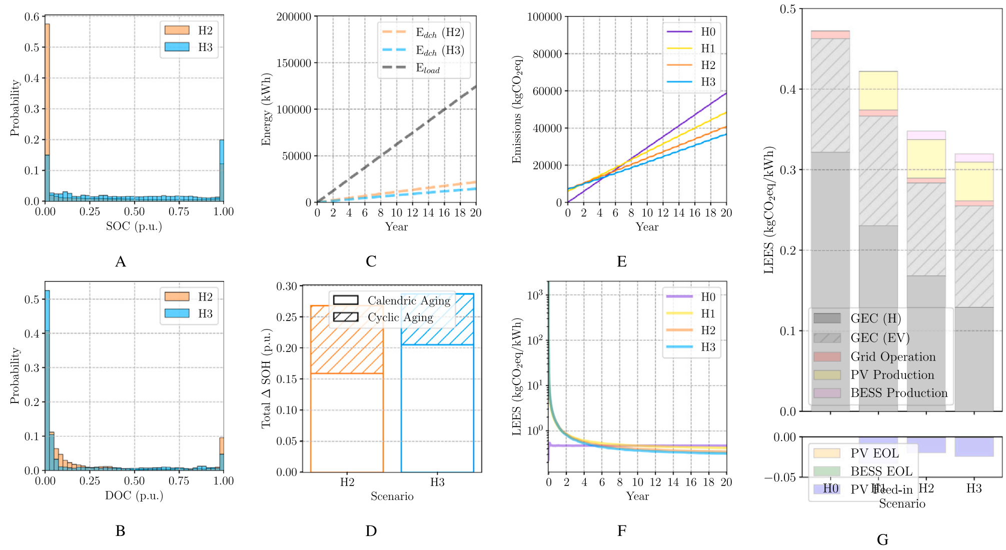

Fig. 10. A, B: Distributions of SOC and DOC values respectively in scenarios H2 and H3 over the simulated period. C: Depiction of the cumulative supplied energy for the four Home Energy System (HES) scenarios and energy discharged in scenarios H2 nd H3 over the simulated period. D: Change in the battery SOH over the simulated period and shares of calendric and cyclic aging in scenarios H2 and H3. E: Cumulative emissions for the four HES scenarios over the simulated period. F: Evolution of the Levelized Emissions of Energy Supply (LEES) value for the HES scenarios over the simulated period. G: Breakdown of LEES values for the HES scenarios into the constituent emissions categories at the end of the simulation period.

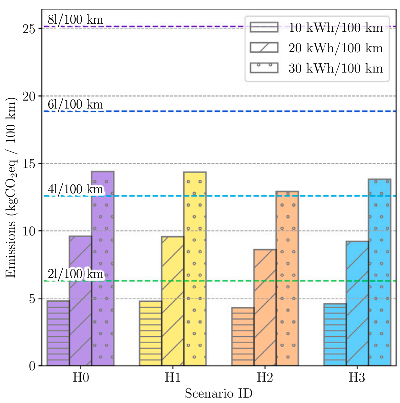

C

Fig. 11. Energy consumption emissions for EVs in the four HES configurations for the three energy economy levels considered relative to the four indicative fuel economy levels for internal combustion vehicles.

the DEC emissions for both loads are also zero. At the end of 20 years, the cumulative emissions, in this case, add up to over 36 t, and these are associated with a LEES of 0.2991 kg CO_2eq/kW h. This represents a drop of over 37% vis-a-vis H0. From Fig. 10E, it can be seen that the emissions start at the same value as H2 but remain lower from the get-go, reaching the lowest value among all scenarios by the end of the simulation. The LEES trend depicted in Fig. 10F exhibits the same behavior, with H3 attaining the lowest LEES among all scenarios. 10G depicts a snapshot of the emissions category-wise breakdown of the LEES value at the end of the simulated period. The lower LEES can be attributed to the optimal scheduling of the BESS to discharge energy at times with the highest grid carbon intensity values. This effectively reduces the GEC emissions of the household while marginally increasing the GEC emissions for the EV. The net reduction, however, manages to offset the production and EOL emissions of the PV solar system and the BESS. Figs. B.1–B.3 in the appendix depict the evolution of some more parameters of interest. In this scenario, the BESS is subjected to around 3330 EFCs with a mean DOC of around 21%. The mean SOC during this period is over 49%, and the SOH reaches a value of just over 71% (Figs. 10A, B, D). Despite the lower number of EFCs and the lower mean DOC than in H2, the total degradation is greater in H3, with a larger proportion of calendric degradation. This is attributed to the higher mean SOC, which leads to dominant calendric degradation for this cell type. Fig. 10C depicts the total energy supplied to the load and the total energy discharged from the BESS.

Fig. 11 depicts the energy consumption emissions of the EV for three energy economy scenarios with each of the four scenarios per 100 km driven. The three EV energy economy scenarios considered here are — 10 kW h/100 km, 20 kW h/100 km, and 30 kW h/100 km. The CO_2 emissions for four reference fuel-economy values for vehicles with petrol engines are also indicated on the plot — 2 l/100 km, 4 l/100 km, 6 l/100 km, and 8 l/100 km [69,70]. These values also reflect the fuel's well-to-wheel emissions without considering other emissions associated with the distribution infrastructure. It can be seen that there is barely any difference in the values for scenarios H0 and H1. This can be explained by the fact that the installed power of the PV system is much lower than the peak charging power, and a substantial number of charging events occur after sunset. There is a reduction in the EV emissions for scenario H2, as this strategy discharges the BESS right after it is charged, which possibly overlaps more frequently with the EV charging events. The higher EV emissions in scenario H3 imply that the EMS strategy optimizes for both loads taken together and is unable to selectively supply the EV with low carbon PV solar energy while reducing the combined footprint of both the loads. Significantly, this analysis indicates that the energy consumption emissions for a moderately efficient EV are much lower than those for a vehicle with a very efficient petrol engine (4 l/100 km).

4. Conclusion and outlook

This article introduces Energy System Network (ESN) — an open-source energy system simulation program written in Python. The supporting mathematical framework to enable a time-resolved, component-wise, bottom-up calculation of the various emissions categories is described comprehensively. Two case studies to demonstrate the usage of this program have also been presented. The first case study investigates a grid-connected BESS application — energy arbitrage. The second case study looks at a home energy system with an electric vehicle.

An unconventional energy arbitrage strategy to shift energy from periods of low grid carbon intensities to periods of high grid carbon intensities has been explored in addition to the conventional profit-driven variant. The emissions-reducing strategy attains a LEES value over 17% lower while sacrificing 26% of the profits as compared to the conventional energy arbitrage. This shows that while emissions-driven energy arbitrage differs from the profit-driven variant, it is not entirely contrary to it. These results also Future market design studies to develop compensation mechanisms and revenue streams to incentivize such energy arbitrage strategies monetarily, which could spark exciting developments in this area. The Home Energy System (HES) simulations show that solely drawing power from the grid entails a lower carbon footprint in the first few years of operation while resulting in the highest emissions over the 20-year period. Integrating a rooftop PV solar system alone leads to a LEES reduction of over 17% and lower emissions from the seventh year of operation. Integrating a rooftop PV solar system coupled with a BESS home storage results in a LEES reduction of over 30% compared to the base case and lower operation emissions from just before the sixth year of operation. An emissions-reducing optimal EMS strategy can unlock a further LEES reduction of 7% points vis-á-vis the base scenario, which results in lower emissions from the fifth year of operation. For the EV in the base scenario, the energy consumption emissions for a moderate energy economy of 20 kW h/100 km are slightly higher than the emissions attributable to an internal combustion vehicle with an unrealistically low fuel economy of 3 L/100 km. All other scenarios fare better than the base scenario, if not comparably. This indicates that for the energy consumed for mobility, the present grid energy mix already fares better than fossil fuel combustion. This analysis does not consider the carbon footprint of the production and EOL phases of the vehicles,

The results of the two presented case studies must be interpreted with their limitations in mind. For both studies, perfect foresight has been assumed for all forward-looking time series data. Real-world forward-looking time series data will inevitably suffer from forecasting and prediction errors. The grid carbon intensity time series profile is assumed to remain static over the entire duration of the simulation. As historical data reveals an enduring downward trend in the grid carbon intensity, our assumption represents a worst-case scenario. Modeling an evolving grid carbon intensity profile is not a trivial matter of scaling down the entire profile by an arbitrary amount, as future values for grid carbon intensities are highly dependent on the shares and scheduling of participating generation technologies and the prevalent market and policy mechanisms.

The code base of this program is open-source, enabling the scientific community to use it for their own studies and possibly even contribute to further development of features. Complementary features from other energy system tools could also be coupled with ESN to enhance the scope of studies possible. For instance, the grid carbon intensity calculation functionality available in the tool elmada is a valuable feature [35]. The focus of this article has been limited to single energy systems primarily centered around a single energy form — electricity. Future functionality to support interconnected networks comprising multi-vector energy systems can enable studies on multi-modal energy systems and sector coupling. Other future functionalities, including sizing calculations for energy system components and demand-side management, will enhance the program's ability to estimate the carbon footprint of energy systems. An economic evaluation suite is also conceivable for integration with the program to complement the carbon footprint analysis.

CRediT authorship contribution statement

Anupam Parlikar: Conceptualization, Data curation, Formal analysis, Investigation, Methodology, Software, Visualization, Writing – original draft, Writing – review & editing. **Benedikt Tepe:** Data curation, Formal analysis, Investigation, Visualization, Writing – original draft, Writing – review & editing. **Marc Möller:** Software, Writing – review & editing. **Holger Hesse:** Formal analysis, Funding acquisition, Supervision, Visualization, Writing – review & editing. **Andreas Jossen:** Funding acquisition, Resources, Supervision, Writing – review & editing.

Declaration of competing interest

The authors declare that they have no known competing financial interests or personal relationships that could have appeared to influence the work reported in this paper.

Data availability

Data will be made available on request.

Declaration of Generative AI and AI-assisted technologies in the writing process

During the preparation of this article, the authors used Grammarly in order to check the syntax and grammar of the text. After using these services, the authors reviewed and edited the content as needed; and take full responsibility for the content in the publication.

Acknowledgments

This research is funded by the German Federal Ministry of Education and Research (BMBF) via the research project greenBattNutzung (grant number 03XP0302D). The project is overseen by Project Management Juelich (PtJ). The authors express their gratitude to Houman Heidarabadi for his assistance in facilitating the open-source code release.

Appendix A. Additional plots (grid-connected applications)

See Figs. A.1 and A.2.

Appendix B. Additional plots (HES)

See Figs. B.1–B.3.

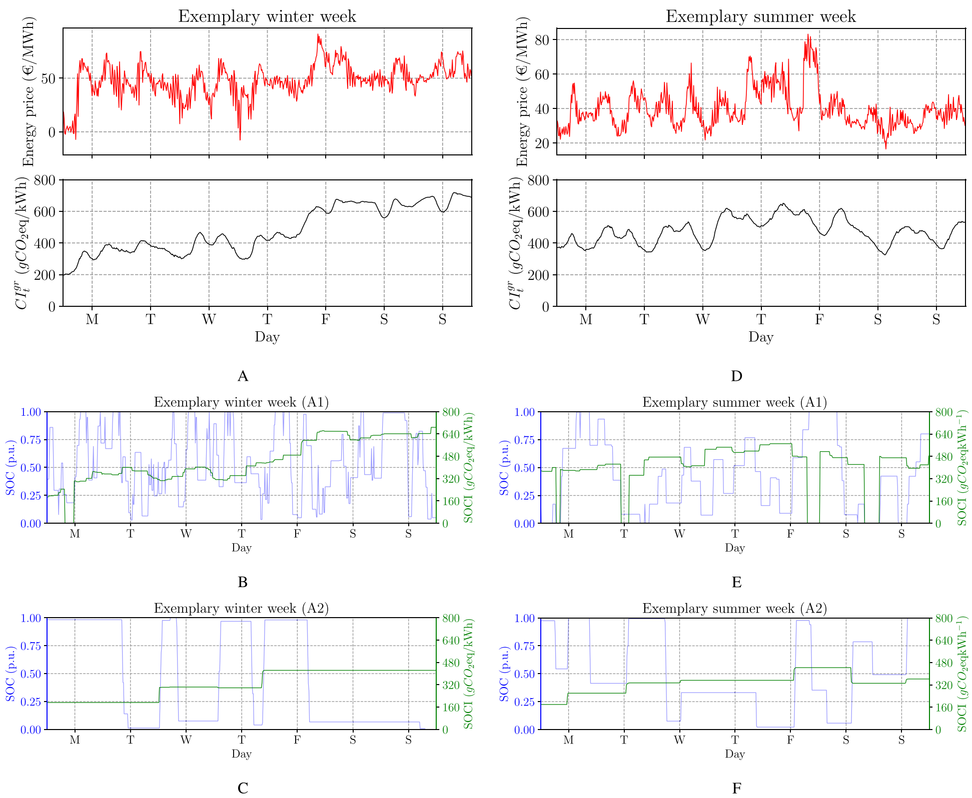

Fig. A.1. A, D: Energy prices and grid carbon intensity evolution with respect to time for an exemplary winter and summer week, respectively. B, C: State of Charge (SOC) and State of Carbon Intensity (SOCI) evolution with respect to time for an exemplary winter week for scenarios A1 and A2, respectively. E, F: State of Charge (SOC) and State of Carbon Intensity (SOCI) evolution with respect to time for an exemplary summer week for scenarios A1 and A2, respectively.

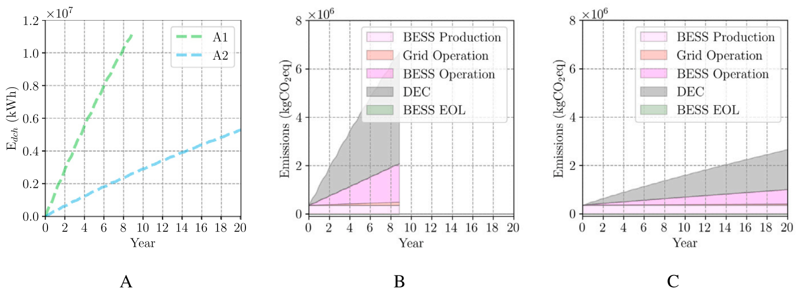

Fig. A.2. A: Energy discharged from the BESS in scenarios A1 and A2. B, C: Category-wise cumulative emissions in scenarios A1 and A2, respectively.

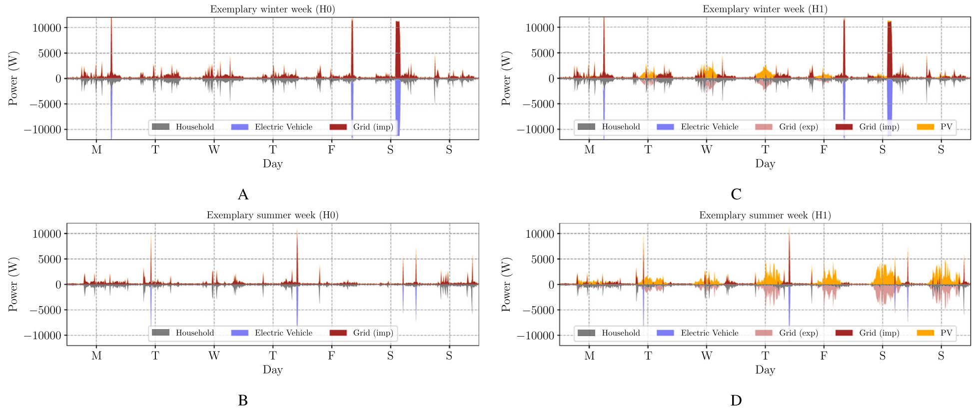

Fig. B.1. A, C: Power flows among energy system components for an exemplary winter week for scenarios H0 and H1, respectively. B, D: Power flows among energy system components for an exemplary summer week for scenarios H0 and H1, respectively.

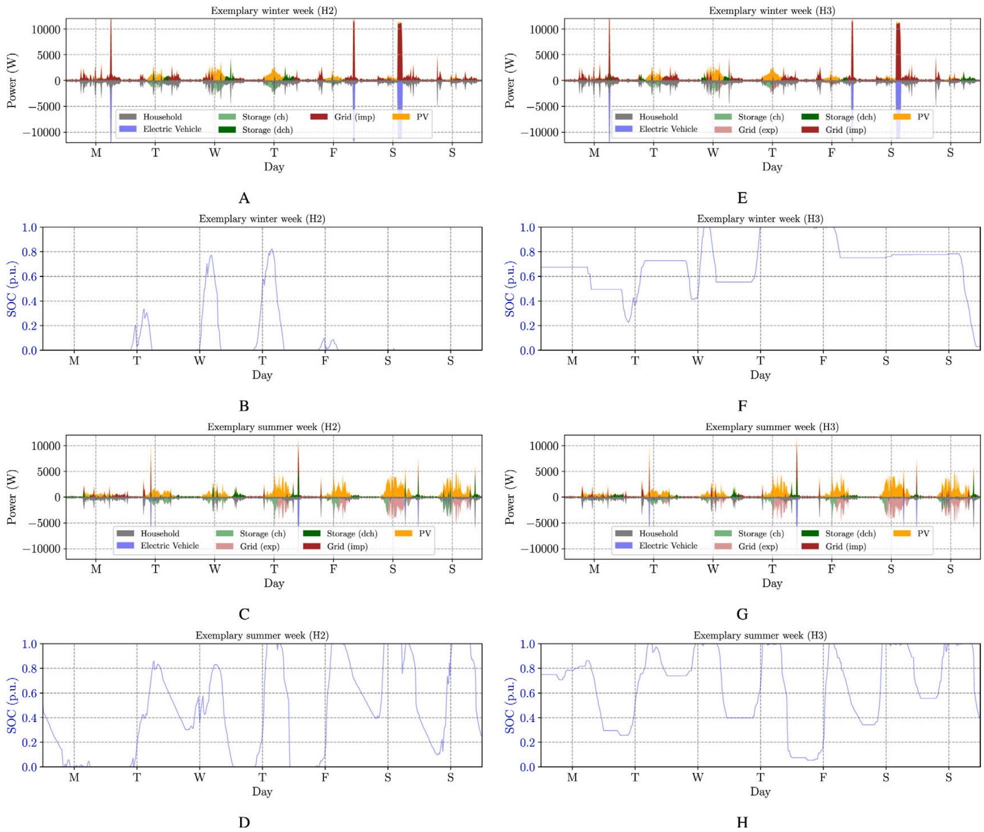

Fig. B.2. A, E: Power flows among energy system components for an exemplary winter week for scenarios H2 and H3, respectively. B, F: State of Charge (SOC) evolution with respect to time for the exemplary winter week for scenarios H2 and H3, respectively. C, G: Power flows among energy system components for an exemplary summer week for scenarios H2 and H3, respectively. D, H: State of Charge (SOC) evolution with respect to time for the exemplary summer week for scenarios H2 and H3, respectively.

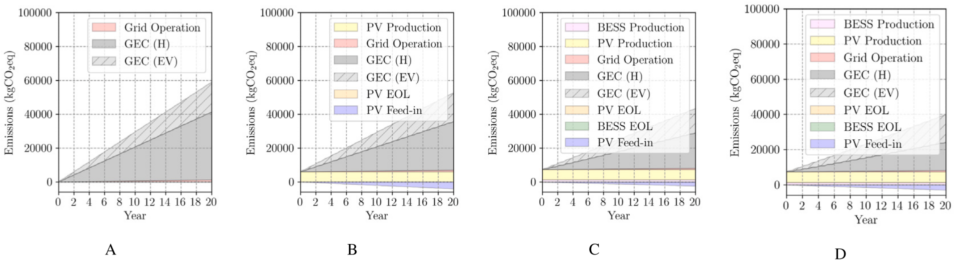

Fig. B.3. A, B, C, D: Category-wise cumulative emissions in scenarios H0, H1, H2, H3 respectively.

References

[1] International Renewable Energy Agency. Renewable capacity statistics 2023. Abu Dhabi: International Renewable Energy Agency; 2023, URL https://mc-cd8320d4-36a1-40ac-83cc-3389-cdn-endpoint.azureedge.net/-/media/Files/IRENA/Agency/Publication/2023/Mar/IRENA_RE_Capacity_Statistics_2023.pdf?rev=d2949151ee6a4625b65c82881403c2a7.

[2] DeCarolis J, Daly H, Dodds P, Keppo I, Li F, McDowall W, et al. Formalizing best practice for energy system optimization modelling. Appl Energy 2017;194:184–98.

[3] Hesse H, Schimpe M, Kucevic D, Jossen A. Lithium-ion battery storage for the grid—A review of stationary battery storage system design tailored for applications in modern power grids. Energies 2017;10(12):2107.

[4] Kebede AA, Coosemans T, Messagie M, Jemal T, Behabtu HA, van Mierlo J, et al. Techno-economic analysis of lithium-ion and lead-acid batteries in stationary energy storage application. J Energy Storage 2021;40:102748.

[5] International Energy Agency. Global EV outlook 2023. Paris: International Energy Agency; 2023, URL https://www.iea.org/reports/global-ev-outlook-2023.

[6] Figgener J, Hecht C, Haberschusz D, Bors J, Spreuer KG, Kairies K-P, et al. The development of battery storage systems in Germany: A market review (status 2023). 2023, URL http://arxiv.org/pdf/2203.06762v3.

[7] Gutsch M, Leker J. Global warming potential of lithium-ion battery energy storage systems: A review. J Energy Storage 2022;52:105030.

[8] Brown T, Hörsch J, Schlachtberger D. PyPSA: Python for power system analysis. J Open Res Softw 2018;6(1):4.

[9] Lund H, Thellufsen JZ, Østergaard PA, Sorknæs P, Skov IR, Mathiesen BV. EnergyPLAN – advanced analysis of smart energy systems. Smart Energy 2021;1:100007.

[10] Lund H, Thellufsen JZ. EnergyPLAN - advanced energy systems analysis computer model: documentation version 16.2. Aalborg: Zenodo, Sustainable Energy Planning Research Group, Aalborg University, Denmark; 2022, http://dx.doi.org/10.5281/zenodo.6602938, URL https://www.energyplan.eu/training/documentation/.

[11] Pfenninger S, Pickering B. Calliope: A multi-scale energy systems modelling framework. J Open Source Softw 2018;3(29):825.

[12] Calliope contributors listed in AUTHORS. Calliope: A multi-scale energy systems modelling framework: Documentation. 2024, URL https://calliope.readthedocs.io/en/stable/index.html.

[13] Eshraghi H, de Queiroz AR, DeCarolis JF. US energy-related greenhouse gas emissions in the absence of federal climate policy. Environ Sci Technol 2018;52(17):9595–604.

[14] TEMOA Developer Team. Temoa project documentation. 2024, URL https://temoacloud.com/temoaproject/Documentation.html.

[15] Dorfner J. Urbs: A linear optimisation model for distributed energy systems: Documentation. 2014, URL https://urbs.readthedocs.io/en/latest/index.html.

[16] Dorfner J. Open source modelling and optimisation of energy infrastructure at urban scale [Ph.D. thesis], Munich, Germany: Fakultät für Elektrotechnik und Informationstechnik, Technical University of Munich; 2016, URL https://mediatum.ub.tum.de/1285570.

[17] Krien U, Schönfeldt P, Launer J, Hilpert S, Kaldemeyer C, Pleßmann G. Oemof.solph—A model generator for linear and mixed-integer linear optimisation of energy systems. Softw Impacts 2020;6:100028.

[18] Hilpert S, Kaldemeyer C, Krien U, Günther S, Wingenbach C, Plessmann G. The open energy modelling framework (oemof) - a new approach to facilitate open science in energy system modelling. Energy Strategy Rev 2018;22:16–25.

[19] Welder L, Ryberg D, Kotzur L, Grube T, Robinius M, Stolten D. Spatio-temporal optimization of a future energy system for power-to-hydrogen applications in Germany. Energy 2018;158:1130–49.

[20] FINE Developer Team. FINE - a framework for integrated energy system assessment: Documentation. 2023, URL https://vsa-fine.readthedocs.io/en/latest/index.html.

[21] US Department of Energy. GridLAB-D: A unique tool to design the smart grid. 2023, URL https://www.gridlabd.org/index.stm.

[22] Schneider KP, Fuller J, Tuffner F, Chen Y. Modern grid strategy: Enhanced gridlab-d capabilities: Final report. 2009, https://www.pnnl.gov/main/publications/external/technical_reports/PNNL-18864.pdf.

[23] Bahramara S, Moghaddam MP, Haghifam MR. Optimal planning of hybrid renewable energy systems using HOMER: A review. Renew Sustain Energy Rev 2016;62:609–20.

[24] UL Solutions. HOMER software. 2023, URL https://www.homerenergy.com/index.html.

[25] UL Solutions. HOMER pro 3.15: Documentation. 2023, URL https://www.homerenergy.com/products/pro/docs/3.15/how_homer_calculates_emissions.html.

[26] Freeman J. Recent and planned improvements to the system advisor model (SAM). Albuquerque, New Mexico, USA: NREL; 2019, URL https://www.nrel.gov/docs/fy22osti/74214.pdf.

[27] Blair N, DiOrio N, Freeman J, Gilman P, Janzou S, Neises T, et al. System advisor model (sam) general description (version 2017.9.5). 2018, https://www.nrel.gov/docs/fy18osti/70414.pdf.

[28] Electric Power Research Institute. DER VET user guide. EPRI; 2022, URL https://storagewiki.epri.com/index.php/DER_VET_User_Guide.

[29] Langiu M. COMANDO documentation. 2020, URL https://comando.readthedocs.io/en/latest/index.html.

[30] Langiu M, Shu DY, Baader FJ, Hering D, Bau U, Xhonneux A, et al. COMANDO: A next-generation open-source framework for energy systems optimization. Comput Chem Eng 2021;152:107366.

[31] Weniger J, Tjaden T, Orth N, Maier S. Performance simulation model for PV-battery systems (PerMod): Documentation. Version 2.1. Research group Solar Storage Systems, University of Applied Sciences Berlin; 2020, URL https://solar.htw-berlin.de/wp-content/uploads/HTW-PerMod-Dokumentation.pdf.

[32] Atabay D. An open-source model for optimal design and operation of industrial energy systems. Energy 2017;121:803–21.

[33] Atabay D. Ficus: A (mixed integer) linear optimisation model for local energy systems: Documentation. 2015, URL https://ficus.readthedocs.io/en/latest/.

[34] Fleschutz M, Bohlayer M, Braun M, Murphy MD. Demand response analysis framework (DRAF): An open-source multi-objective decision support tool for decarbonizing local multi-energy systems. Sustainability 2022;14(13):8025.

[35] Fleschutz M, Murphy M. Elmada: Dynamic electricity carbon emission factors and prices for europe. J Open Source Softw 2021;6(66):3625.

[36] Smith K, Gasper P. BLAST: Battery lifetime analysis and simulation tool suite. NREL; 2023, URL https://www.nrel.gov/transportation/blast.html.

[37] Möller M, Kucevic D, Collath N, Parlikar A, Dotzauer P, Tepe B, et al. SimSES: A holistic simulation framework for modeling and analyzing stationary energy storage systems. J Energy Storage 2022;49:103743.

[38] Hall LM, Buckley AR. A review of energy systems models in the UK: Prevalent usage and categorisation. Appl Energy 2016;169:607–28.

[39] Lopion P, Markewitz P, Robinius M, Stolten D. A review of current challenges and trends in energy systems modeling. Renew Sustain Energy Rev 2018;96:156–66.

[40] Pfenninger S, Hawkes A, Keirstead J. Energy systems modeling for twenty-first century energy challenges. Renew Sustain Energy Rev 2014;33:74–86.

[41] Prina MG, Manzolini G, Moser D, Nastasi B, Sparber W. Classification and challenges of bottom-up energy system models - a review. Renew Sustain Energy Rev 2020;129:109917.

[42] Pellow MA, Ambrose H, Mulvaney D, Betita R, Shaw S. Research gaps in environmental life cycle assessments of lithium ion batteries for grid-scale stationary energy storage systems: End-of-life options and other issues. Sustain Mater Technol 2020;23:e00120, URL http://www.sciencedirect.com/science/article/pii/S2214993718302318.

[43] Parlikar A, Schott M, Godse K, Kucevic D, Jossen A, Hesse H. High-power electric vehicle charging: Low-carbon grid integration pathways with stationary lithium-ion battery systems and renewable generation. Appl Energy 2023;333:120541.

[44] Parlikar A, Truong CN, Jossen A, Hesse H. The carbon footprint of island grids with lithium-ion battery systems: An analysis based on levelized emissions of energy supply. Renew Sustain Energy Rev 2021;149:111353.

[45] Fraunhofer Institute for Solar Energy Systems ISE. In: Burger B, editor. Electricity generation in Germany 2019. Freiburg, Germany: Fraunhofer Institute for Solar Energy Systems ISE; 2019, URL https://energy-charts.info/charts/power/chart.htm?l=en&c=DE&stacking=stacked_absolute_area&year=2019&interval=year.
[46] Schimpe M, von Kuepach ME, Naumann M, Hesse HC, Smith K, Jossen A. Comprehensive modeling of temperature-dependent degradation mechanisms in lithium iron phosphate batteries. J Electrochem Soc 2018;165(2):A181–93.
[47] Schimpe M, Becker N, Lahlou T, Hesse HC, Herzog H-G, Jossen A. Energy efficiency evaluation of grid connection scenarios for stationary battery energy storage systems. Energy Procedia 2018;155:77–101.
[48] Naumann M, Schimpe M, Keil P, Hesse HC, Jossen A. Analysis and modeling of calendar aging of a commercial LiFePO4/graphite cell. J Energy Storage 2018;17:153–69.
[49] Naumann M, Spingler FB, Jossen A. Analysis and modeling of cycle aging of a commercial LiFePO4/graphite cell. J Power Sources 2020;451:227666.
[50] Notton G, Lazarov V, Stoyanov L. Optimal sizing of a grid-connected PV system for various PV module technologies and inclinations, inverter efficiency characteristics and locations. Renew Energy 2010;35(2):541–54.
[51] Schimpe M, Naumann M, Truong N, Hesse HC, Santhanagopalan S, Saxon A, et al. Energy efficiency evaluation of a stationary lithium-ion battery container storage system via electro-thermal modeling and detailed component analysis. Appl Energy 2018;210:211–29.
[52] Parlikar A, Hesse H, Jossen A. Topology and efficiency analysis of utility-scale battery energy storage systems. In: Proceedings of the 13th international renewable energy storage conference 2019. IRES 2019, 2019, URL https://www.atlantis-press.com/proceedings/ires-19/125923324.
[53] Baumann M, Peters JF, Weil M, Grunwald A. CO 2 footprint and life-cycle costs of electrochemical energy storage for stationary grid applications. Energy Technol 2017;5(7):1071–83.
[54] Mohr M, Peters JF, Baumann M, Weil M. Toward a cell–chemistry specific life cycle assessment of lithium–ion battery recycling processes. J Ind Ecol 2020;24(6):1310–22.
[55] Wernet G, Bauer C, Steubing B, Reinhard J, Moreno-Ruiz E, Weidema B. The ecoinvent database version 3 (part i): Overview and methodology. Int J Life Cycle Assess 2016;21(9):1218–30.
[56] Hu A, Huang L, Lou S, Kuo C-H, Huang C-Y, Chian K-J, et al. Assessment of the carbon footprint, social benefit of carbon reduction, and energy payback time of a high-concentration photovoltaic system. Sustainability 2017;9(1):27.
[57] de Simón Martín M, Díez-Mediavilla M, Alonso-Tristán C. Real energy payback time and carbon footprint of a GCPVS. AIMS Energy 2017;5(1):77–95.
[58] Bulach W, Schüler D, Sellin G, Elwert T, Schmid D, Goldmann D, et al. Electric vehicle recycling 2020: Key component power electronics. Waste Manag Res : J Int Solid Wastes Public Clean Assoc ISWA 2018;36(4):311–20.
[59] Ylmén P, Peñaloza D, Mjörnell K. Life cycle assessment of an office building based on site-specific data. Energies 2019;12(13):2588.
[60] Reich NH, Alsema EA, van Sark W, Turkenburg WC, Sinke WC. Greenhouse gas emissions associated with photovoltaic electricity from crystalline silicon modules under various energy supply options. Prog Photovolt, Res Appl 2011;19(5):603–13.
[61] Latunussa CE, Ardente F, Blengini GA, Mancini L. Life cycle assessment of an innovative recycling process for crystalline silicon photovoltaic panels. Sol Energy Mater Sol Cells 2016;156:101–11.
[62] Reese MO, Glynn S, Kempe MD, McGott DL, Dabney MS, Barnes TM, et al. Increasing markets and decreasing package weight for high-specific-power photovoltaics. Nat Energy 2018;3(11):1002–12.
[63] Figgener J, Hecht C, Haberschusz D, Bors J, Spreuer KG, Kairies K-P, et al. The development of battery storage systems in Germany: A market review (status 2023). 2022, arXiv.
[64] Sun S, Crossland A, Chipperfield A, Wills R. An emissions arbitrage algorithm to improve the environmental performance of domestic PV-battery systems. Energies 2019;12(3):560.
[65] Kucevic D, Tepe B, Englberger S, Parlikar A, Mühlbauer M, Bohlen O, et al. Standard battery energy storage system profiles: Analysis of various applications for stationary energy storage systems using a holistic simulation framework. J Energy Storage 2020;28:101077.
[66] Tjaden T, Bergner J, Weniger J, Quaschning V. Repräsentative elektrische Lastprofile für Wohngebäude in Deutschland auf 1-sekündiger Datenbasis. Berlin, Germany: HTW Berlin - University of Applied Sciences; 2015, URL https://solar.htw-berlin.de/wp-content/uploads/HTW-Repraesentative-elektrische-Lastprofile-fuer-Wohngebaeude.pdf.
[67] Gaete-Morales C, Kramer H, Schill W-P, Zerrahn A. An open tool for creating battery-electric vehicle time series from empirical data, emobpy. Sci Data 2021;8(1):152.
[68] Zeh A, Witzmann R. Operational strategies for battery storage systems in low-voltage distribution grids to limit the feed-in power of roof-mounted solar power systems. Energy Procedia 2014;46:114–23.
[69] The ERM International Group Limited. Bp target neutral: Global online travel calculator: Method for calculating greenhouse gas emissions. 2021, https://www.bp.com/bptargetneutralnavapp/consumer/bpTN_Online%20Travel%20GHG%20Emissions%20Calculator_Updated%20Methodology%20Statement_01July2021.961acd71.pdf.
[70] Prussi M, Yugo M, De Prada L, Padella M, Edwards R. JEC well-to-wheels report v5: Anticipation and foresight, technical guidance. In: KJ-NA-30284-EN-N (online). Luxembourg (Luxembourg): Publications Office of the European Union; 2020.

6 The carbon footprint of Li-ion BESSs operating in island grids

This study evaluates the carbon footprint of integrating lithium-ion BESSs within isolated island grid energy systems. This evaluation is particularly relevant to the current times, given the global transition towards renewable energy sources, which, while sustainable, introduce intermittency challenges that a BESS is particularly well-suited to address. This study makes use of both the SimSES and ESN modeling frameworks described in the earlier chapters to simulate the BESS and energy system, respectively. The core of the research introduces two innovative metrics: Levelized Emissions of Energy Supply (LEES) and the reduction in emissions per additional unit of energy storage capacity (R). These metrics serve as tools for quantifying the carbon footprint reduction achievable through the strategic deployment of BESS, offering a nuanced understanding of the environmental implications of such integrations.

The methodology of this study encompasses a simplified LCA of a utility-scale lithium-ion BESS, spanning production, operation, and end-of-life phases within the context of an island grid system. The island grid model simulated includes renewable energy sources (photovoltaic and wind turbines), a diesel generator for backup, and varied configurations of BESS. These simulations evaluate the impact of different BESS configurations on the system's carbon footprint, providing insights into the optimal setups for maximizing environmental benefits. The highlights of this study are:

- The carbon footprints for producing, operating, and decommissioning lithium-ion BESS in island grids
- Effectiveness of lithium-ion BESS at reducing the net GHG emissions of island grid energy systems
- A methodology to accurately ascertain the effect of BESS integration on the carbon footprint of island grids
- Energy storage capacities to be installed to maximize emissions reduction and justify the resources invested
- Identification of isolated energy systems to be prioritized for the incorporation of additional energy storage capacity based on their potential for emission reduction

The findings from the simulations underscore a consistent theme: integrating BESS into island grids invariably leads to a reduction in the GHG emissions, with certain configurations enabling nearly a 50% reduction compared to scenarios devoid of energy storage. The LEES and R metrics prove instrumental in this analysis, highlighting the variation in effectiveness across different BESS configurations. This approach not only facilitates a clearer understanding of the environmental impact of BESS but also aids in identifying configurations that offer the greatest emissions reduction for the resources invested. While energy storage generally leads to lower emissions, the extent of emission reduction depends significantly on the capacity and configuration of the storage system. The results suggest a diminishing return on emission reductions as the storage capacity increases beyond a certain threshold, indicating an optimal range for BESS capacity.

In conclusion, this work helps to establish a methodological framework for assessing the carbon footprint reduction afforded by BESS in island grid energy systems. The limitations of the current study include the scope of the life cycle analysis and the geographic and system-specific assumptions that may not generalize across all island grids. The authors suggest that future research could expand the environmental assessment to include more comprehensive life cycle analyses and explore the impact of other renewable and storage technologies. Future research could further refine these methodologies and build upon them.

Author contributions

Anupam Parlikar was the primary author leading the conceptualization, methodology development, data curation, formal analysis, and investigation. He also handled the software and visualization aspects and was responsible for writing both the original draft and subsequent editing. Cong Nam Truong contributed to developing the methodology, curated data, and participated in the review and editing of the manuscript. Andreas Jossen played an important role in acquiring funding and resources, supervised the project, and contributed to the manuscript's review and editing. Holger Hesse acquired funding, conducted formal analyses, assisted with visualization, supervised the research, and participated in the manuscript's review and editing.

The carbon footprint of island grids with lithium-ion battery systems: An analysis based on levelized emissions of energy supply

Anupam Parlikar, Cong Nam Truong, Andreas Jossen, and Holger Hesse

Renewable and Sustainable Energy Reviews (149), 111353, 2021

Permanent weblink:
https://doi.org/10.1016/j.rser.2021.111353

Renewable and Sustainable Energy Reviews 149 (2021) 111353

Contents lists available at ScienceDirect

Renewable and Sustainable Energy Reviews

journal homepage: www.elsevier.com/locate/rser

The carbon footprint of island grids with lithium-ion battery systems: An analysis based on levelized emissions of energy supply

Anupam Parlikar [a,*], Cong Nam Truong [b], Andreas Jossen [a], Holger Hesse [a]

[a] Institute of Electrical Energy Storage Technology (EES), Technical University of Munich (TUM), Arcisstr. 21, 80333 Munich, Germany
[b] STABL Energy GmbH, Rupert-Mayer-Str. 44, 81379 Munich, Germany

A R T I C L E I N F O

Keywords:
Energy storage
Island grid
Carbon dioxide emissions
Lithium-ion battery
Battery energy storage system
Levelized Emissions of Energy Supply (LEES)
Life Cycle Analysis (LCA)

A B S T R A C T

Electrical energy storage systems are key to the integration of intermittent renewable energy technologies such as photovoltaic solar systems and wind turbines. As installed battery energy storage system capacities rise, it is crucial that the environmental impacts of these systems are also positive. In this work, a methodology to ascertain the effect and effectiveness of integration of energy storage on the carbon footprint of isolated island grid energy systems and its reduction is presented. Two metrics are introduced — the Levelized Emissions of Energy Supply (LEES), and the reduction in emissions per additional unit of energy storage (R). The proposed methodology is applied to an island grid scenario to ascertain the variation in the LEES value with the peak power and energy storage capacity of the BESS. A simplified LCA of a utility-scale Lithium-ion BESS is also carried out for this purpose. It is found that for the considered scenarios, incorporation of battery systems is always effective in reducing emissions, with a maximum possible reduction of nearly 50% compared to no storage. With the help of the metric R, the proposed methodology is also useful in identifying isolated energy systems which should be prioritized for incorporation of additional energy storage capacity.

1. Introduction

The global shift from fossil-based energy sources toward clean energy produced by renewable energy sources is now well underway with installed renewable generation capacity worldwide, having more than doubled in the last decade of 2010–19, standing at an impressive 2, 532, 866 MW at the end of 2019 [1]. As the share of installed capacities of intermittent power generators such as PV and WTs in the global energy system rises, provisioning of measures to ensure quality and security of energy supply at a larger scale becomes inevitable. These measures include time-shifting of renewable energy generation — ensuring supply in times of generation shortfalls, mitigating excessive power flows in places with weak grid infrastructure, and containing the frequency and voltage fluctuations in the electricity grid to within the stipulated tolerances [2].

The energy sector, as a whole, is the single largest emitter of GHG in the world [3]. In isolated island grid energy systems, conventional power generation technologies, such as DGs and gas turbines are the major source of GHG emissions [4]. The environmental impact of techno-economically feasible energy storage technologies, which have the potential for large-scale adoption, should be diligently investigated. Electrochemical energy storage systems, such as Battery Energy Storage Systems (BESSs), are already the leading energy storage technology class in terms of the number of projects installed worldwide [5]. It is worth noting that there exists economic potential for the deployment of electrical energy storage systems to provide services in several applications [6]. A thorough analysis of these systems should hence be carried out in order to ensure that the base rationale behind the system installation — which is to enable the energy system to operate at lower emission levels, is not inadvertently defeated. Most prevalent performance assessment methodologies focus on techno-economic evaluation of energy storage systems, and the environmental aspects thereof do not play a central role in the decision process. This observation is corroborated by Pellow et al. [7]. The probable factors which explain this tendency have been identified — the complexity associated with the meticulous tracing of material, energy, and emissions streams while carrying out a Life Cycle Analysis (LCA), and the availability of reliable and sufficiently detailed Life Cycle Analysis (LCA) data (particularly primary data) in the public domain. Few et al. report that experts themselves express low confidence in carrying out environmental and energetic analyses of the processes for battery production and decommissioning. They also identify this area as one in need of greater focus within the scientific community [8].

* Corresponding author.
E-mail addresses: anupam.parlikar@tum.de (A. Parlikar), nam.truong@stabl.com (C.N. Truong), andreas.jossen@tum.de (A. Jossen), holger.hesse@tum.de (H. Hesse).

https://doi.org/10.1016/j.rser.2021.111353
Received 20 October 2020; Received in revised form 14 May 2021; Accepted 10 June 2021
Available online 23 June 2021

Abbreviations

BESS	Battery Energy Storage System.
CO_2eq	Carbon Dioxide equivalent.
DG	Diesel Generator.
DOD	Depth of Discharge.
ECM	Equivalent Circuit Model.
EFC	Equivalent Full Cycles.
EMS	Energy Management System.
EOL	End-of-Life.
EPR	Energy-to-Power Ratio.
ESN	Energy System Network (Simulation Tool).
FU	Functional Unit.
GHG	Greenhouse Gases.
GWP	Global Warming Potential.
HVAC	Heating, Ventilation, Air Conditioning.
LCA	Life Cycle Analysis.
LEES	Levelized Emissions of Energy Supply.
LFP	Lithium Iron Phosphate.
OCV	Open Circuit Voltage.
PV	Photovoltaic Solar.
SimSES	Simulation of Stationary Energy Storage Systems (Simulation Tool).
SOC	State of Charge.
SOH	State of Health.
VRFB	Vanadium Redox Flow Batteries.
WT	Wind Turbine.

Parameters

C_n	Installed Energy Storage Capacity in Energy System Configuration *n*.
E_{BESS}	Rated BESS Energy Capacity.
$E_{load\ center,a}$	Total Useful Energy at Load Center *a* years.
P_{PV}	Photovoltaic Solar Power Generation.
P_{WT}	Wind Turbine Power Generation.
P_{BESS}	Rated BESS Peak Power.
P_{load}	Load Power.
$P_{residual}$	Residual Power.
$R^{unit\ storage}_{n,n-1}$	Reduction in System Emissions per Additional Unit of Energy Storage Capacity.
ϵ_{EOL}	End-of-Life Phase Emissions.
$\epsilon_{op,a}$	Operation Phase Emissions *a* years
ϵ_{prod}	Production Phase Emissions.

A review of existing literature in this area has been conducted to examine the existing metrics and environmental performance evaluation methodologies in the context of decarbonization. Some of the findings are discussed in the following paragraphs.

The *time to ecological amortization* of an energy storage technology is the time required for a cumulative energy equal to its embodied energy footprint to be discharged from it [9]. The *Energy Stored on Energy Invested (ESOI)* is defined as the ratio of the amount of energy stored over the lifetime of an energy storage technology and the energy required to produce it [10]. The *Energy Return on Energy Invested (EROI)* metric from the *Net Energy Analysis* concept can also be modified to incorporate the analysis of energy storage [11]. The *Life Cycle Greenhouse Gas Emissions*, which is the emissions analog of the Levelized Cost of Energy Storage (LCOS), can be used to quantify the GHG emissions per kWh of energy stored by the system, calculated over its entire lifetime [12]. These metrics are applicable to the energy storage system level, and are ideal to compare two competing technologies, but do not capture the effect of the energy storage technology on the net energy system emissions. Metrics and evaluation methodologies applicable at the energy system level are required to study decarbonization of energy systems.

Energy storage technologies such as BESSs, when deployed to provide grid-services in grids with large conventional generation capacities (i.e. high carbon intensities), lead to higher energy input and net energy systems emissions as compared to existing solutions due to the energetic losses [13]. Energy storage technologies, when used to replace conventional generation technologies for the provision of a grid-related service, may in some cases lower the net energy system emissions [14], especially if the grid carbon intensity is low, indicating high shares of renewable generation capacities and curtailment [15,16]. These outcomes are also highly dependent on the round-trip efficiency of the energy storage technology and its lifetime in addition to the factors mentioned earlier [17]. The boundaries for analysis also ostensibly influence this inference. Charging the energy storage directly instead of feeding-back the energy into the grid is detrimental to the reduction in net energy system emissions, as a greater amount of energy is lost due to losses. Charging on energy which could otherwise be curtailed is the most beneficial [18,19].

This work restricts itself to the evaluation of the environmental performance of lithium-ion BESSs providing renewable time-shifting services in isolated island grid energy systems. Time-shifting of renewable energy generation in large grids with energy storage is subject to the inferences discussed above. Renewable time-shifting is particularly crucial in isolated island grid energy systems. Incorporation of energy storage in isolated island grid with high shares of renewable generation capacities and conventional backup power generation always results in a reduction in the net energy system emissions by partially displacing the conventional power generation from the energy mix. This finding holds true for Vanadium Redox Flow Batteries (VRFB) [20], as well as for lithium-ion BESSs [4]. The present work builds upon existing literature in this area by presenting a holistic evaluation methodology, which enables the comparison of the effectiveness of various energy storage configurations in reducing the net emissions in island grid energy systems. This work is also able to confirm results presented in the reviewed literature sources.

The prominent questions which arise in the context of carrying out such evaluations are:

1. How large are the GHG emission footprints for the production, operation, and decommissioning of lithium-ion BESSs?
2. How effective are lithium-ion BESSs at reducing the net GHG emissions of the island grid energy system?
3. What energy storage capacities ought to be installed to maximize the reduction in emissions, and to justify the resources invested?

Addressing the first question is an indispensable step, and is specific to the scenario and energy storage technology under consideration. presents a simplified LCA for a utility-scale lithium-ion BESS. The impact category Global Warming Potential (GWP) is used throughout this work to quantify the carbon footprint of technologies and the entire energy system. The results from this analysis are used in the simulative analyses carried out in the subsequent sections. To answer the second question, a performance evaluation methodology is presented in Section 2.1. The proposed methodology introduces two metrics — the first metric *Levelized Emissions of Energy Supply (LEES)* fixes an emissions value for every unit of useful energy supplied by the energy system to its load center. The second metric $R^{unit\ storage}_{n,n-1}$ denotes the reduction in energy system emissions per additional unit of energy storage capacity. These metrics enable the third question to be addressed in a quantifiable manner. As the research questions raised are relevant to a wide range of scenarios and energy storage technologies, the methodology is also correspondingly general enough. The methodology is demonstrated through simulative analyses in the context of provision of renewable energy time-shifting services in isolated island grid energy systems with lithium-ion BESSs. The simulation results are discussed in Section 3. The emissions of the island grid energy system, the energetic behavior of the energy system, the effect on the BESS, and the influence of other parameters on the LEES are examined. Section 4 summarizes the major conclusions and achievements of this work. The limitations and the future outlook of this work are also touched upon.

2. Methods

Section 2.1 describes the proposed methodology and the two metrics, which are key features of this performance evaluation methodology. Section 2.2 discusses the modeling procedure for the island grid, the Lithium-ion BESS, and the power generation components. The calculation procedure for the indirect and direct GHG emissions for the components in the island grid energy system is presented in Section 2.3.

2.1. Proposed methodology for evaluation of impact of energy storage on system emissions

BESSs, like PV panels and WTs, belong to a class of technologies which cause almost no direct emissions during operation, but whose production and decommissioning at the end of life can cause substantial emissions. The GWP footprint of generated energy consists of two components, one – a fixed component dependent on the production and decommissioning processes for the components in the energy system, and the other – an operation-dependent component. A carbon intensity calculation based solely on the operation-dependent emissions, as is currently the case [21], risks completely overlooking the emissions impact of PV and WT installations on power generation, as the operation-dependent component is negligible in this case. Incorporation of a BESS into the system leads to a further uncertainty in accounting of emissions, as this is neither a power generation technology, nor is it directly responsible for emissions during operation. In cases wherein the input energy to a BESS has an operation-dependent component in its footprint, additional emissions can be attributed to the BESS on account of energy lost in the conversion processes. For an island grid system without a conventional grid connection, once the production and decommissioning emissions for PV panels, WTs, and BESS, which is charged by surplus renewable energy, is taken into account, the operation-dependent emissions emanate from the DG alone, that steps in every now and then to cover load which the renewable generators and the BESS are unable to cover.

For energy systems with predominantly renewable power generation, such as solar PV and WTs with fluctuating power generation, not all power produced can be put to use at all instants of time. The generators can also not be relied upon to be able to supply sufficient power at all instants. This leads us to the concept of *useful energy* which is actually supplied to the load centers. This section outlines a modified methodology to obtain the resultant carbon intensity for the energy supplied by an energy system with a high share of renewable energy generators, energy storage and some conventional generation as backup. Production of PV panels, WTs, and BESS components is highly energy-intensive, resulting in substantial emissions, which makes the inclusion of this phase highly relevant. The process for determination of electrical energy storage system capacity ranges with the highest impact on emissions reduction is also explained briefly. The steps outlined in this methodology can be applied to any energy storage technology providing a similar service in a comparable use-case.

2.1.1. Levelized Emissions of Energy Supply (LEES) : A modified carbon intensity measure for energy systems

The *Levelized Emissions of Energy Supply (LEES)* is formulated and defined in this section for use in the proposed methodology. The *LEES* metric takes into account direct and indirect emissions within an energy supply system. Additionally, this metric is based on the *useful energy* supplied by the power generators plus supporting components such as energy storage (if present) to the load centers rather than the energy generated (see Fig. 1). In an isolated energy system with predominantly renewable generators, the losses due to energy conversion in the BESS do not result in any additional emissions in the operations phase, as the BESS is charged with renewable energy sources exclusively, and the emissions in the production and decommissioning phase for the renewable generators are explicitly factored in. This metric, *LEES*, fixes an emission value (in kg CO_2eq) to each unit (kW h) of useful energy supplied by the energy system to its load center over a pre-defined period of time. It is mathematically defined in Eq. (1).

$$LEES = \frac{\Sigma\varepsilon_{prod} + \Sigma\varepsilon_{op,a} + \Sigma\varepsilon_{EOL}}{E_{load\ center,a}} \tag{1}$$

where:

$\Sigma\epsilon_{\mathrm{prod}}$ denotes the sum total of the emissions entailed on account of production of all components included in the energy system

$\Sigma\epsilon_{\mathrm{op,a}}$ denotes the emissions entailed on account of operating all the components making up the energy system during the considered simulation period of *a* years

$\Sigma\epsilon_{\mathrm{EOL}}$ denotes the sum total of the emissions entailed on account of EOL treatments for all the components making up the energy system

$E_{\mathrm{load\ center,a}}$ denotes the total useful energy supplied by the system to the load center over the simulation period of *a* years

The values of ε_{prod} and ε_{EOL} for each component are a fraction of the total production and EOL emissions if the component does not reach the end of its estimated/projected service life at the end of the simulation period. The value of the fraction is obtained from aging/degradation models or from lifetime estimates, and is equal to the ratio of the utilized service capacity/metric to the estimated/projected service capacity/metric. In the case of lithium-ion BESSs, this fraction can be conveniently based on the State of Health (SOH) metric. Other ways of assigning emissions to the simulation period may also be possible.

Some key features of the Levelized Emissions of Energy Supply (LEES) metric:

- *Zero load-shedding condition:* The metric is calculated under the constraint of zero load-shedding — i.e. power supplied by the generation and storage equipment together must, at least, be equal to the demand at all instants of time
- *Internalization of losses:* All energetic losses in the energy system, such as curtailment, generation and transmission losses, and losses on account of energy storage operation are lumped together and internalized in the metric. The useful energy, which is considered for the calculation is directly affected by any changes in these loss mechanisms. These losses are directly reflected in the LEES value, with higher losses reflecting in a higher value of LEES, and vice-versa
- *Identification of sub-optimal sizing:* Sub-optimally sized systems can also be identified, if a change in system sizing is found to fulfill the zero load-shedding condition at a lower LEES value

Once the value of LEES for a particular system configuration is obtained, the manner of its variation with system configuration can be examined. We are primarily interested in the impact of energy storage capacities on our stated goal of emissions reduction. The steps involved in such an analysis are depicted in Fig. 2. In the backdrop of limited resources, a method to be able to quantify this impact for every unit of monetary and material investment made is an absolute necessity.

2.1.2. Reduction in system emissions per additional unit of energy storage capacity

The *Reduction in system emissions per additional unit of energy storage capacity* $\mathrm{R}_{\mathrm{n,n-1}}^{\mathrm{unit\ storage}}$ is defined as the ratio of reduction in the LEES value

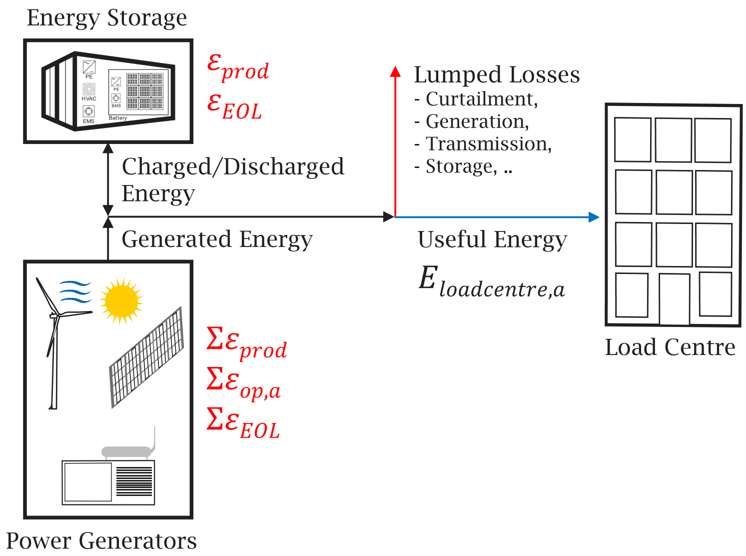

Fig. 1. Depiction of the lumped losses, and the useful energy supplied to the load center.

per additional unit of energy storage with respect to that of a previous configuration. It is mathematically defined as:

$$R^{unit\ storage}_{n,n-1} = \frac{\Delta LEES_{n,n-1}}{(C_n - C_{n-1})} \quad (2)$$

where:

$\Delta LEES_{n,n-1}$ denotes difference in LEES values of system configurations n and n-1, wherein configuration n has a larger energy storage capacity.

C_n denotes the energy storage capacity for system configuration n, $C_n > C_{n-1}$.

The reciprocal of $R^{\text{unit storage}}_{n,n-1}$ is the *Energy Storage Capacity per Unit Reduction in System Emissions*, which is defined as the ratio of the additional energy storage capacity required to bring about a unit reduction in the LEES value with respect to that of a previous configuration.

Identification of capacity ranges exhibiting the highest environmental benefits is possible using the metric $R^{\text{unit storage}}_{n,n-1}$. Large negative values signify high emissions reduction potential, whereas positive values indicate a worse configuration with respect to the previous configuration. This metric is thus, a complementary metric to the LEES in analyses of total emissions in island grid energy systems, and can aid in obtaining the best return in terms of emissions reduction for the invested resources.

2.2. Modeling: island grid energy system and components

The modeling and simulation of the system is carried out with two python-based simulation tools - *Energy System Network (Simulation Tool) (ESN)*, and *Simulation of Stationary Energy Storage Systems (Simulation Tool) (SimSES)*[1] [22]. Both the tools have been developed in-house. The tool Energy System Network (Simulation Tool) (ESN) is capable of modeling and simulating several user-defined energy system configurations and scenarios. In scenarios which include energy storage systems, ESN operates in conjunction with the tool Simulation of Stationary Energy Storage Systems (Simulation Tool) (SimSES), which can model and simulate the electro-thermal behavior of BESSs in a very detailed fashion. The degradation of the Lithium-ion cells under operation in the given load scenario is also considered.

[1] SimSES open-source code repository: https://gitlab.lrz.de/open-ees-ses/simses

Table 1
Island grid system simulation parameters.

	Parameter	Value
Simulation	Sample time (s)	900
	Duration of simulation (years)	20
Load	Annual load (MWh)	10 000
	Peak load (MW)	1.59
	Minimum load (MW)	0.72
	Mean load (MW)	1.14
	Peak residual load (MW)	1.59
Wind	Installed capacity Wind Turbines (WTs) (MW_p)	3.25
	Capacity factor (%)	26.62
Photovoltaic Solar (PV)	Installed capacity Photovoltaic Solar (PV) (MW_p)	2.00
	Capacity factor (%)	22.65
Diesel Generator (DG)	Rated power (MW)	1.60

The energy system considered consists of Wind Turbine (WT) and Photovoltaic Solar (PV) generators as the sources of primary energy. A Diesel Generator (DG) picks up the slack when renewable generation is inadequate. Excess generation from the renewable power generators is simply curtailed. This configuration represents the base case. The load and renewable energy generation curves are based on those of Tenerife, the largest of the Canary islands, situated off the northwest coast of Africa in the Atlantic ocean. The annual load and renewable energy generation time series have been normalized and used for this study. The profiles are available on the website of the utility company serving these areas [23]. Values for the year 2016 are used in this study. The hypothetical island system differs from the original energy supply system of Tenerife in several respects. Firstly, the system is largely down-scaled, and secondly, the proportions and types of various generators in the system have been altered. The configuration of this hypothetical energy system is presented in Table 1.

The influence of integration of a BESS into this hypothetical island grid is then investigated. The island grid can be understood to consist of the components depicted in Fig. 1. The methodology for the calculation of the LEES metric, which was presented earlier in Section 2.1.1, is applied to a hypothetical island grid system in this section.

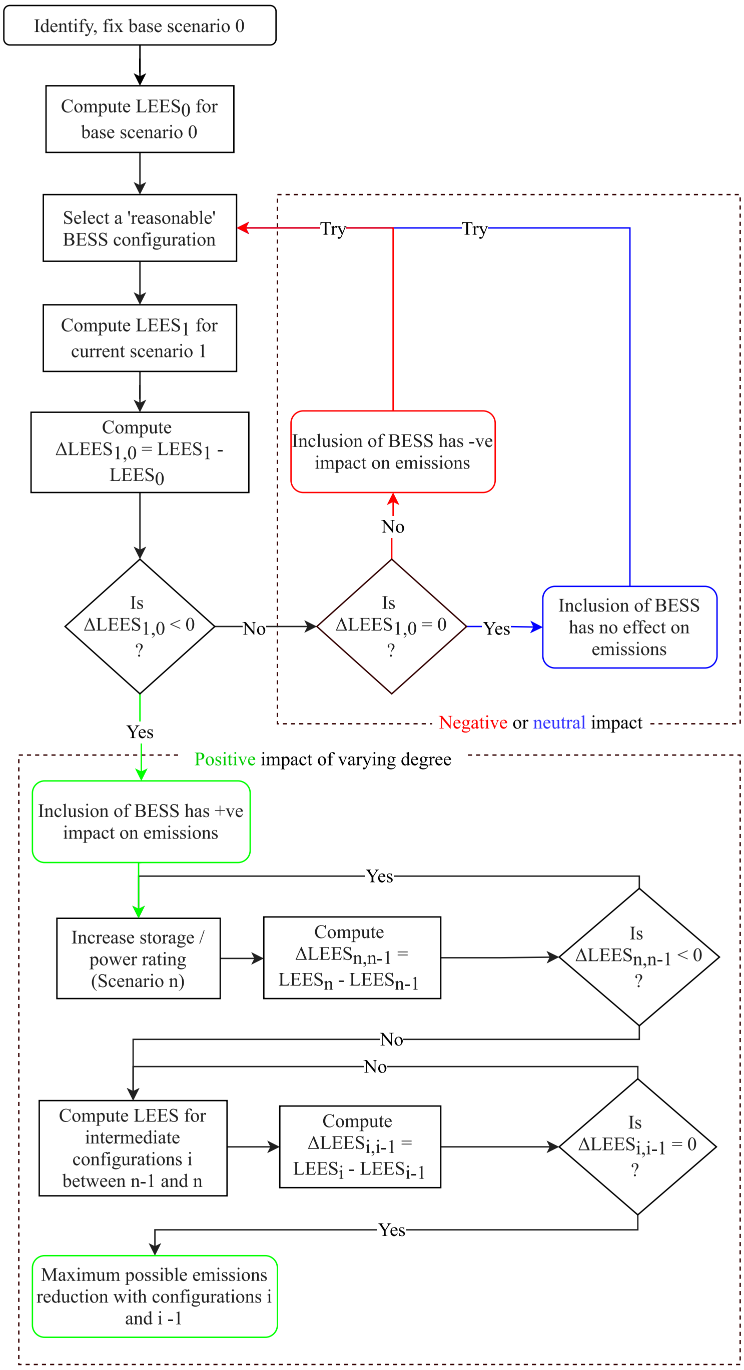

Fig. 2. Process flowchart outlining the steps involved in conducting a Levelized Emissions of Energy Supply (LEES) analysis for an isolated energy system. *+ve* stands for positive, and *-ve* stands for negative. The choice of a 'reasonable' Battery Energy Storage System (BESS) configuration is arrived at by conducting a sizing exercise based on the application requirements for performance indicators, such as the fulfillment ratio.

2.2.1. Energy management

A simple rule-based operating strategy implemented in ESN, termed 'Simple Deficit Coverage', is utilized to simulate the interplay between the operations of the BESS and the DG. The residual load at each instant of time is defined as the difference between the sum of power generation from the renewable generators and the load. The residual load at each time-step is then represented as:

$$P_{residual} = (P_{PV} + P_{WT}) - P_{load} \quad (3)$$

where:

$P_{residual}$ denotes the residual power, at each time-step
P_{PV} denotes the generation from the PV installation

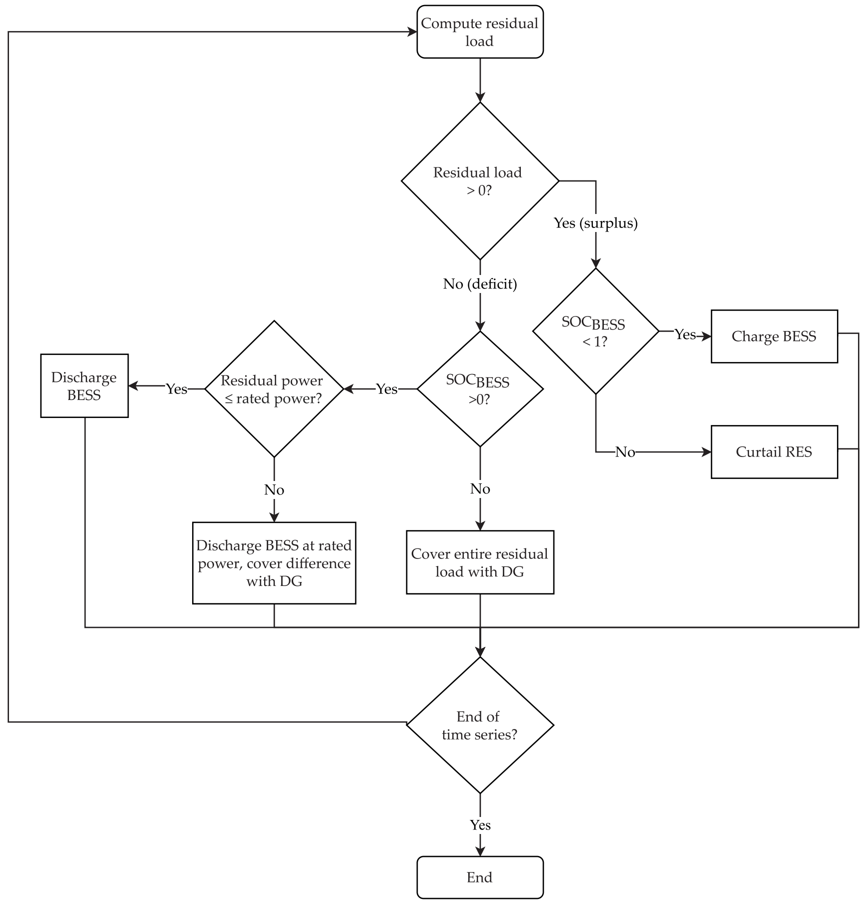

Fig. 3. Rule-based operating strategy for the Battery Energy Storage System (BESS) and the Diesel Generator (DG) operating in tandem to cover the load in the absence of sufficient renewable power generation.

P_{WT} denotes the generation from the WT installation
P_{load} denotes the load power

This rule-based Energy Management System (EMS) deploys the BESS as frequently as possible to cover the residual load (Eq. (3)), which the PV and WT generators are unable to cover. In the event that the BESS is incapable of covering the residual load, owing to power or energy constraints, the DG is brought online to cover the deficit. The BESS is charged exclusively with surplus generation from the PV and WT installations. This rule-based decision-making algorithm is depicted in Fig. 3.

2.2.2. Component models

The power generation, storage, and load components present in the energy system are simulated based on models found in literature. The models for the PV and WT generators are relatively simple, and the values of power generation are directly based on their generation profiles. Similarly, the load is also modeled as a demand profile. The models for the BESS and the DG are modeled to a much greater level of detail. These are described in the following subsections.

Battery Energy Storage System (BESS)

The BESS model is based on a 'R-int', or internal resistance Equivalent Circuit Model (ECM), which consists of a voltage source in series with an ohmic resistance. The values of both the voltage of the source and the ohmic resistance at any instant of time are dependent on the State of Charge (SOC) at any particular instant. The model has been parameterized based on experimental data from a commercial 'new' Lithium Iron Phosphate (LFP) cylindrical 26650 cell (see Fig. 4) [24, 25]. The State of Health (SOH) is defined as the ratio of the cell's charge capacity in 'new' condition to its charge capacity at any later point in time. At an SOH value of 80%, the cell is said to have reached its End-of-Life (EOL). As the sample time and simulation duration of the time series analysis simulations is 15 min and 20 years respectively, the R-int ECM representation of the battery is adequate in light of simulation speed and desired detail of simulation results. The degradation model for the Lithium Iron Phosphate (LFP) cells is semi-empirical in nature, and is based on extensive aging tests for calendric and cyclic degradation carried out in-house [26,27]. The models for the BESS subcomponents, such as for the battery, power electronics, are all modeled in *SimSES*. The model for the AC/DC converter efficiency is based on a model found in literature [28]. The BESS is assumed to operate under a constant ambient temperature of 298.15 K, and the thermal behavior thereof is not considered in this paper (see Table 2).

Diesel Generator (DG)

The model of the DG is based on a model found in published literature [29]. This model estimates part-load DG efficiencies for a range of power values below its rated peak power. Based on the electricity generated, this model permits the calculation of fuel consumption and the corresponding emissions on account of fuel combustion for

Table 2
Battery Energy Storage System (BESS) parameters for the R-int Equivalent Circuit Model (ECM) model used.

	Parameter	Value
BESS	Battery type	Lithium Iron Phosphate (LFP)
	Battery format	Cylindrical, 26 650
	Rated energy capacity (MWh)	0.1 - 192
	Rated power (MW)	0.1 - 1.6
	Initial State of Charge (SOC)	0%
	Initial State of Health (SOH)	100%
	End-of-Life (EOL) SOH criterion	80%
	Battery model	R-int ECM (based on [24,25])
	Aging model	Semi-empirical calendric and cyclic (based on [26,27])

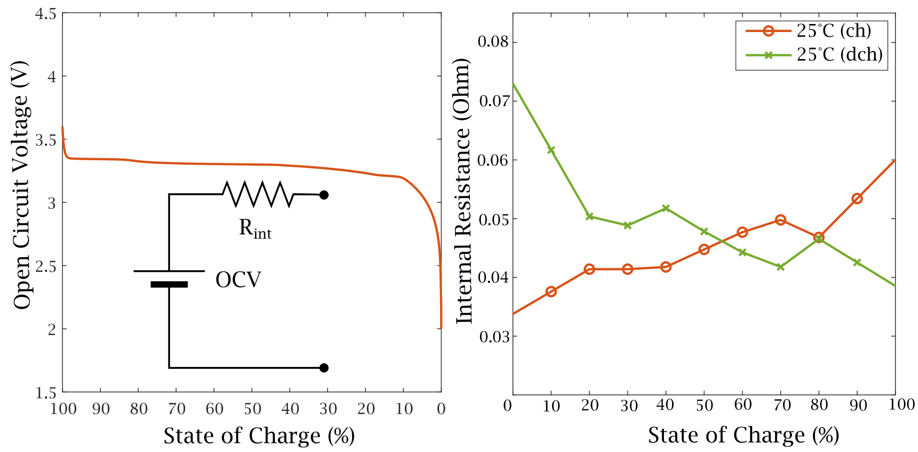

Fig. 4. Open Circuit Voltage (OCV) curve vs. State of Charge (SOC) for the considered Lithium Iron Phosphate (LFP) cell (left), and the R-int Equivalent Circuit Model (ECM) (inset, left). Values of the charging (ch) and discharging (dch) internal resistance versus the SOC for the considered cell type (right).

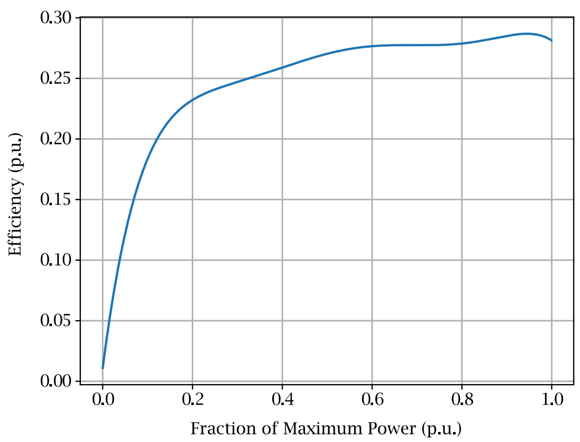

Fig. 5. Efficiency curve with respect to the normalized power for the Diesel Generator (DG) model .
Source: Based on [29].

each time step. The efficiency curve for the DG with respect to the normalized power is depicted in Fig. 5.

2.3. Modeling of Greenhouse Gases (GHG) emissions

Indirect emissions associated with the major components relevant for this study — the BESS and its sub-components, the PV and WT installations, and the DG, have been determined from various literature sources , which were reviewed during the course of this study. The only source of direct emissions is the DG, which emits GHGs as a by-product of the combustion process. Except for the PV panels, whose production emissions can be scaled up linearly with power owing to the visibly modular nature of the technology, the values for WTs and the DG are non-linear. A more rigorous treatment with regards to this feature of the data is beyond the scope of this work, and the values taken here are representative, and are not applicable to WTs and DGs of all sizes, as the specific production emissions (in kg CO_2eq/kW) for large systems are not identical to those for small systems. The reader is requested to bear in mind that the presented analysis can be thought of as a simplified LCA at best, as it is neither based on primary data, nor is it as comprehensive as a full-fledged LCA can be expected to be as per the ISO standards 14040, 14041, 14042, and 14043. But, it is deemed to be sufficient for the purpose of this work, wherein the focus lies on the *LEES* methodology presented, and not on the LCA itself.

Battery Energy Storage System (BESS)

An in-house experimental container BESS is studied, and a simplified LCA has been carried out based on this system as a reference point [30]. The production and EOL phase emissions for its components have been obtained from published literature sources. An overview of the lifecycle phases for a utility-scale container BESS is depicted in Fig. 6.

For the considered LFP cell technology, the GHG emissions in the production phase for the Functional Unit (FU) kWh of energy storage capacity, amount to around 161 kg CO_2eq/kWh on average [31]. The GWP impact of the EOL phase for the processing of each kWh

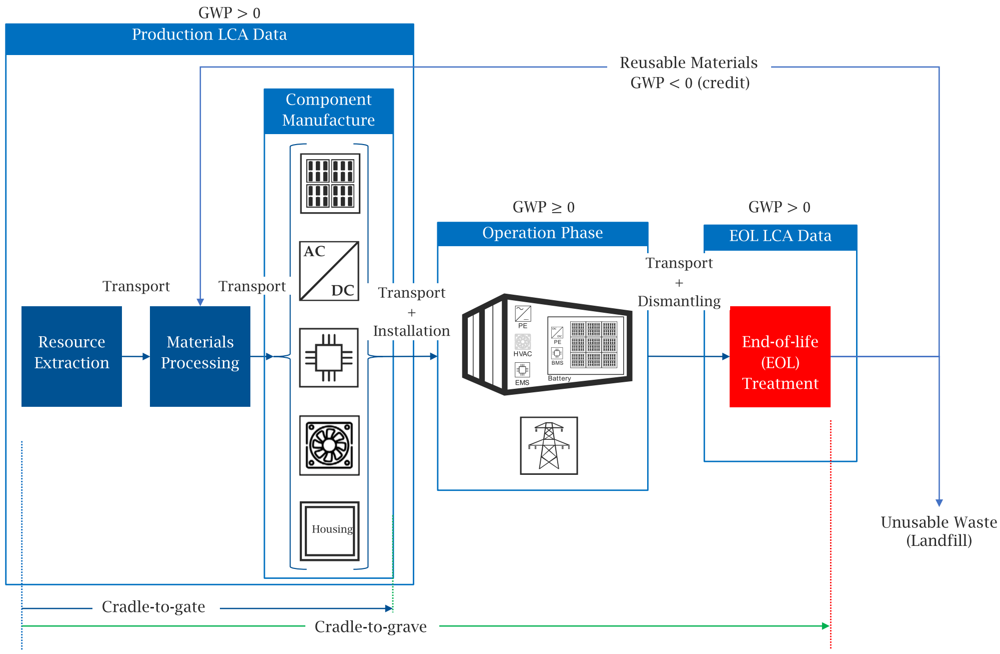

Fig. 6. Overview of lifecycle phases of a container utility-scale Battery Energy Storage System (BESS). The impact factor category Global Warming Potential (GWP) is considered.

of LFP cells varies from 0.45 kg of additional emissions for the pyrometallurgical process to −11.70 kg of reduction in emissions for the advanced hydrometallurgical process [32]. We consider the advanced hydrometallurgical process in the current analysis , which represents an optimistic scenario.

The carbon footprint of the production phase for each Functional Unit (FU) (kW of power conversion capability) of the power electronics is non-linearly dependent on the power rating, as the power density of these devices increases non-linearly with the power. Based on multiple literature sources, including the *Ecoinvent* database, a function to determine the GWP footprint for a functional unit of 1 kW has been obtained [33–35]. The EOL phase for electronics components, for optimal recycling, results in a reduction in the overall emissions to the tune of −9.45 kg CO_2eq/kW assuming an average power density of 1000 W/kg for the power electronics [36].

For the peripheral electronic components such as circuit breakers, relays, monitoring equipment, and other circuitry in the considered experimental BESS, based on values from the *Ecoinvent* database,it can be expected that these components make up around 7% of total production emissions [33]. The EOL phase is understood to result in reduced emissions overall on account of effective recycling. The resultant emissions reductions, for lack of better data, are assumed to be comparable to those for the power electronics at around −14.49% of production emissions [36].

For utility-scale BESSs, a standard shipping container is generally used to house all the components. Production of a 20 ft steel container with a mass of around 2400 kg is estimated to emit around 15 720 kg CO_2eq [33]. With the understanding that shipping containers are constructed from abundant materials such as steel, and other metals, which are already largely recycled, no additional emissions or emissions reductions are allocated to the EOL phase. With a preliminary estimate that 20% of a container's volume may be occupied by the cells, around 1600 kW h of LFP cells with a specific volumetric density of 278 kWh/m^3 may be installed in one such container [2].

The production of the
Heating, Ventilation, Air Conditioning (HVAC) system is estimated to cause around 426.16 kg CO_2eq of emissions for the floor area of the

Table 3
Production and End-of-Life (EOL) phase emissions for a container Battery Energy Storage System (BESS) with a rating of 1 MW/1 MW h in kg CO_2eq.

Component	Production	EOL	Net
Cells	161 000	−11 700	149 300
Power Electronics	28 170	−9450	18 720
Housing (20 ft. Container)	15 720	0	15 720
Misc. Electronics	15 454	−2239	13 215
Heating, Ventilation, Air Conditioning (HVAC)	426	0	426
Total (kg CO_2eq)	220 770	−23 389	**197 381**

20 ft standard shipping container [37]. Similar to the Housing, the EOL phase for the HVAC components is assumed to cause no additional emissions, due to the ubiquitous materials used therein.

Based on the values presented in this section, the net emissions of a BESS for any given rating for the two lifecycle phases of production and EOL may be roughly estimated. As an example, the emissions of a system with a power/energy rating of 1 MW/1 MW h is presented in Table 3. One 20 ft container is used to house all the components, including the LFP cells. The power electronics consist of two inverters of 500 kW each.

Photovoltaic Solar (PV)

For the production of PV panels, assuming an average grid carbon intensity of 500 g CO_2eq/kWh for each kW h of electrical energy consumed in the production processes, an average emissions value of 1100 g CO_2eq per Functional Unit (FU) (kW$_p$ (peak power)) of PV generation capacity is obtained for crystalline Silicon modules, averaged over multiple energy efficiencies [38]. The EOL treatment of PV panels is understood to cause net emissions of 7.40 kg CO_2eq/kW$_p$. This value is calculated by combining the GWP value for the recycling process from a published research article [39] with the value of power density for PV panels obtained from another literature source [40]. This analysis, for the sake of simplicity, solely considers the PV panels themselves, and not other auxiliary components such as the power electronics.

Table 4
Indirect and direct emissions for other island grid energy system components for the production and EOL lifecycle phases.

	Parameter	Value
Photovoltaic Solar (PV) Panels	Production emissions (kg CO_2eq/kW_p) EOL emissions (kg CO_2eq/kW_p)	1100.00 [38] 7.40 [39]
Wind Turbine (WT)	Production emissions (kg CO_2eq/kW) EOL emissions (kg CO_2eq/kW)	683.70 [41] −227.90 [41]
Diesel Generator (DG)	Production emissions (kg CO_2eq/kW) Diesel combustion emissions (kg CO2/liter) Diesel upstream emissions (kg CO_2eq/liter) EOL emissions (kg CO_2eq/kW)	47.84 [42] 2.63 [43] 0.53 [43] 0

Wind Turbine (WT)

Owing to the non-linear behavior of the power scaling with respect to the materials used in a WT, the production emissions per FU (kW of power generation capacity) are strictly valid only in the neighborhood of the original data point. For the considered WT power rating of 3.25 MW, this value is determined from a publicly available LCA report for a WT of a comparable power rating [41]. The production GWP footprint for the WT in the current analysis is estimated to be around 683.70 kg CO_2eq/kW. The recycling and EOL treatments cause a reduction of 227.90 kg CO_2eq/kW, thereby improving the lifetime GWP of the technology.

Diesel Generator (DG)

The production emissions for an exemplary DG are obtained from the Ecoinvent database, and similar to the WT, are not as readily scalable [33]. A value of 47.84 kg CO_2eq per FU (kW of power generation capacity) is determined and used in this study. The GWP impact of the EOL process for the DG, which largely contains abundant metals such as Iron and Aluminum, is assumed to be negligibly low, and is subsequently not considered. The direct emissions due to combustion of diesel are obtained for each time step with the help of theDG model explained in .

The values of the indirect and direct emissions for all components used in the simulations are tabulated in Table 4.

3. Simulation and discussion of results

The island grid energy system is simulated for a variety of scenarios with variations in the BESS parameters. A parameter sweep is carried out by varying the rated energy capacity and peak power of the BESS to investigate the influence of the integration of energy storage into the energy system. The system operation and the energy flows are governed by the operating strategy discussed earlier (Fig. 3). Transmission losses and energy conversion losses in the PV and WT installations, which are not modeled in the current work, are disregarded. If modeled, however, additional loss mechanisms could easily be incorporated within the analysis, and will be reflected in a higher value of the LEES metric. The power generation components such as the PV panels, the WT, and the DG are considered to have a service lifetime of 20 years, after which they are decommissioned [44,45]. The base case does not include a BESS. The LEES value of the base case (without energy storage) over a period of 20 years is 0.5450 kg CO_2eq/kWh. The energy flows in the base case are depicted in Fig. 7.

To concisely capture the information contained in the parameter variation, we make use of the term *Energy-to-Power Ratio (EPR)*. The EPR is defined as the ratio of the rated energy capacity (E_{BESS} to the rated peak power (P_{BESS}).

$$EPR = \frac{E_{BESS}}{P_{BESS}} \tag{4}$$

Table 5 lists the peak power–energy capacity ratings of the BESS in the simulated scenarios. The scenarios can be grouped into six categories - *the base case* (with EPR = 0, i.e. no storage), EPR = 0.5, EPR = 1.0, EPR = 2.0, EPR > 2.0, and *the extreme case (with EPR = 120)*. The peak power rating of the BESS in all the simulations is varied from 0.1 MW - 1.6 MW. The rated peak power is not increased beyond 1.6 MW, as this is the value of the maximum power deficit that either the DG or the BESS are expected to cover (even in the case of zero renewable generation) at any given point in time. Between EPR = 4 to 100, the energy capacity of the BESS is increased in steps of 6.4 MW h, with the peak power remaining constant. The extreme case of EPR = 120 (E_{BESS} = 192 MW h) is simulated to see if any of the parameters change in unexpected ways. Each system configuration is simulated for 20 years. The results are grouped into the aforementioned six categories, and each of the categories are represented as a separate series in the graphical results.

Table 5
Simulation matrix: Variation in parameters of the BESS, grouping of the 52 simulated scenarios into six categories based on the EPR of the BESS.

EPR	Parameter	Value	# Simulations
0 (base case)	Power (MW) Energy capacity (MWh)	0 0	1
0.5	Power (MW) Energy capacity (MWh)	0.2 - 1.6 0.1 - 0.8	5
1.0	Power (MW) Energy capacity (MWh)	0.1 - 1.6 0.1 - 1.6	9
2.0	Power (MW) Energy capacity (MWh)	0.2 - 1.6 0.4 - 3.2	10
4.0 - 100.0	Power (MW) Energy capacity (MWh)	1.6 6.4 - 160	25
120 (extreme case)	Power (MW) Energy capacity (MWh)	1.6 192	1

3.1. Effect on the emissions of the island grid energy system

The LEES parameter is calculated for the entire island grid energy system over the simulation period for each scenario from Table 5. Fig. 9 plots the LEES values versus the corresponding BESS energy storage capacity (E_{BESS}) for each of the scenarios. For each of the simulated scenarios, excluding the base case, it can be seen that $\Delta LEES_{n,0} < 0$ - where n varies from 1 to 50. This implies that the incorporation of energy storage capacity in the energy system results in a reduction of the total energy system emissions with respect to the base case (without energy storage). The value of LEES decreases monotonically as the peak power (P_{BESS}) and energy capacity (E_{BESS}) of the BESS increase.

It is also worth noting that the values of reduction in system emissions per additional unit of energy storage capacity ($R^{\text{unit storage}}_{n,n-1}$) decrease monotonically when evaluated for any two scenarios as the energy storage capacity rises. The value of its reciprocal ($1/R^{\text{unit storage}}_{n,n-1}$), the energy storage capacity per unit reduction in system emissions increases monotonically. Alternatively, the magnitude of the slope of the LEES vs. E_{BESS} curve, which represents the quantity $R^{\text{unit storage}}_{n,n-1}$,

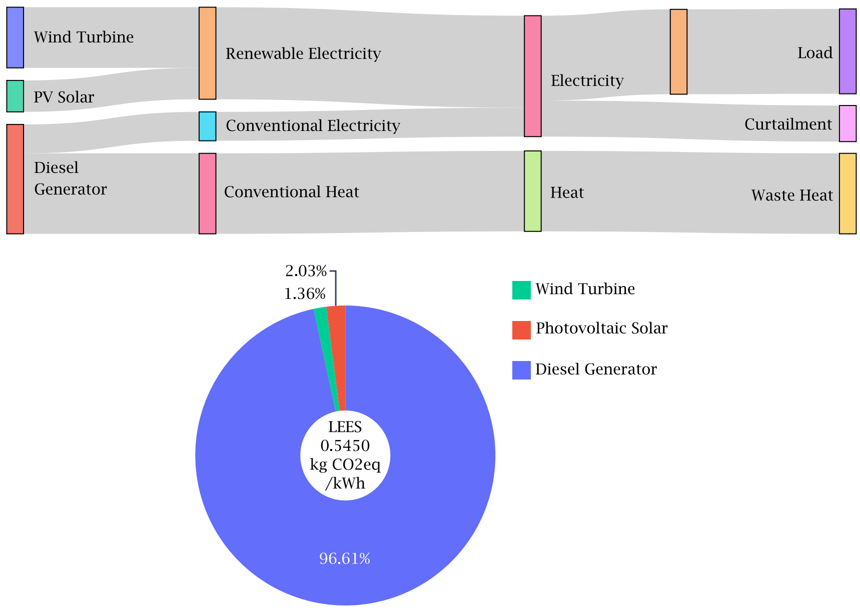

Fig. 7. Energy flows among the various energy system components in the **base case** without energy storage (top). Component-wise distribution of net emissions for the island grid energy system in the **base case** with its calculated Levelized Emissions of Energy Supply (LEES) value (bottom).

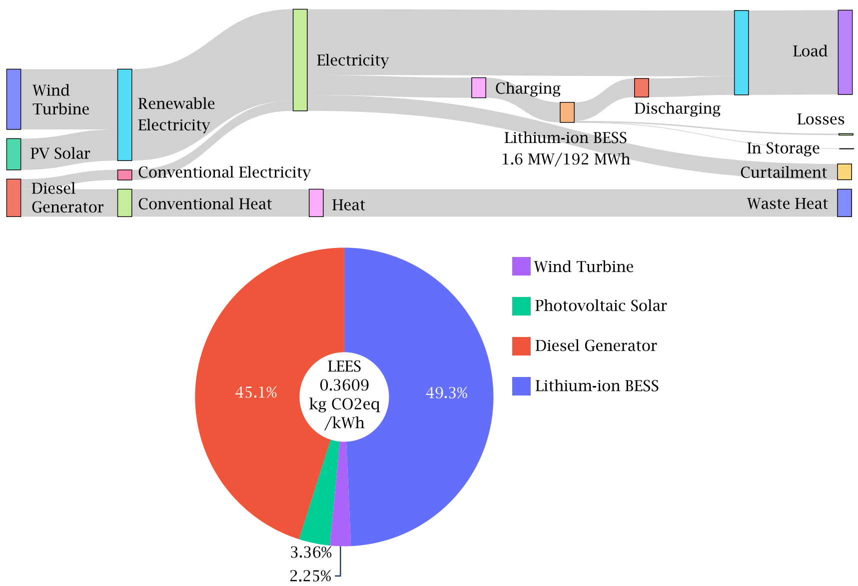

Fig. 8. Energy flows among the various energy system components in the island grid energy system for the **extreme case** with a 1.6 MW/192 MWh Lithium-ion Battery Energy Storage System (BESS) (top). Component-wise distribution of net emissions attributable to the island grid energy system in the **extreme case** with its calculated Levelized Emissions of Energy Supply (LEES) value (bottom).

decreases monotonically. The highest values of $R^{\text{unit storage}}_{n,n-1}$ are observed in the energy capacity range of 0.1 MW h - 1 MW h. As the energy capacity is further increased, values of $R^{\text{unit storage}}_{n,n-1}$ are modest up to roughly 10 MW h of energy storage capacity, after which the slope of the curve becomes increasingly gentle. The slope of the LEES vs. E_{BESS} curve, $R^{\text{unit storage}}_{n,n-1}$, eventually touches zero at a capacity of 51.2 MW h and a power rating of 1.6 MW (EPR = 32). This implies that it takes impractically large amounts of additional energy storage capacity to achieve a further 1 kg reduction in system emissions. Any further increase in the energy storage capacity slowly results in a reversal of the sign of the slope from negative to positive - i.e. a further installation of energy storage capacity in the energy system results in a rise in the LEES value with respect to the lowest possible value attained at EPR = 32. As a consequence, beyond this lowest attainable LEES value, every additional unit of energy storage capacity increases the LEES value of the system, and is sub-optimal. The diminishing energetic benefit of additional energy storage capacity is overshadowed by its increasing GWP footprint.

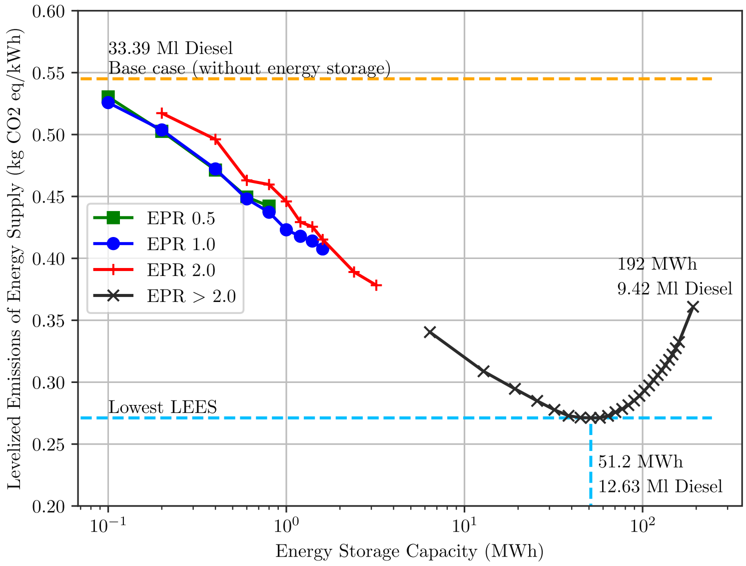

Fig. 9. Evolution of the value of Levelized Emissions of Energy Supply (LEES) for the island grid energy system with varying energy storage capacities. The magnitude of the slope of the curve $R^{unit\ storage}_{n,n-1}$ gradually decreases, underlining the falling effectiveness of each additional unit of energy storage capacity in reducing emissions. The slope is eventually zero at the minimum LEES, then changes sign and rises again, leading to a counter-productive increase in the LEES. The annotations for the three highlighted scenarios also depict the quantity of diesel consumed in each case (in Megalitres).

3.2. Effect on the energetic behavior of the island grid energy system

The energy flows in the extreme case (E_{BESS} = 192 MW h, EPR = 120) are graphically depicted in Fig. 8. It can be observed that despite the presence of an extremely high energy storage capacity within the energy system, curtailment cannot be avoided completely, and that the DG must run for some periods. This finding is particularly significant when considered in conjunction with Figs. 10A and 10B. The extent of curtailment in the system reduces incessantly with each additional MW h of energy storage system capacity, albeit at an increasingly gentler rate. An identical trend is also observed in the case of energy supplied by the DG. Within the range of values assumed by E_{BESS} (0 - 192 MW h), which are covered by the simulated scenarios, the curtailed energy, as well as the energy supplied by the DG both continue to drop.

This observation can be explained by the fact that more of the energy which would have otherwise been curtailed, is absorbed by the BESS in times of surplus generation, and is discharged to the load center in times of generation deficits. This results in more such instances wherein the BESS is able to supply the required energy, and the system's reliance on the DG drops correspondingly, while maintaining the no load-shedding condition. In the absence of Fig. 9, an isolated assessment of Fig. 10A could be misinterpreted to mean that increasing E_{BESS} in an unbounded fashion is environmentally beneficial, given that the curtailed energy and the operating hours of the DG keep reducing. A quick glance at Fig. 9 shows that the LEES value is nearly equal for systems with E_{BESS} = 25.6 MW h and 89.6 MW h. The only difference in the two scenarios is the lower curtailment and diesel generation values in the latter. The additional 64 MW h of energy storage capacity is then difficult to justify from the perspective of resource and material utilization, in the absence of any tangible benefit in terms of reduction in emissions.

Fig. 10B highlights the diminishing efficacy of the BESS as a tool to reduce curtailment. The energy throughput of the BESS gradually stagnates despite the larger E_{BESS} value and the prevalence of energy curtailment. This finding agrees well with the findings of Palmer et al. [11].

3.3. Effect on the Battery Energy Storage System (BESS)

Fig. 11A depicts the number of Equivalent Full Cycles (EFC) witnessed by the BESS at the given average Depth of Discharge (DOD) in each of the simulated scenarios. Evidently, for scenarios with higher values of E_{BESS}, the number of Equivalent Full Cycless (EFCs) over the 20 year period decreases at a diminishing rate. With the falling number of EFCs witnessed by the BESS, the stress induced by these cycles (represented by the mean depth of discharge, $\overline{DOD}$), also drops simultaneously. The share of cyclic aging in the total aging witnessed falls, and calendric aging becomes the dominant aging category. The total shares of the two dominant aging categories — calendric and cyclic, are depicted in Fig. 11B. Calendric aging, which in the scenario with the lowest E_{BESS} = 100 kW h, contributes just less than 50% to the total aging, is observed to be the dominant aging category for energy system scenarios with large energy storage capacities. The aging model used in this work superimposes calendric and cyclic aging to obtain the total aging. Among the simulated scenarios, the shortest lifespan observed for the LFP battery is for the scenario with E_{BESS} = 100 kW h and P_{BESS} = 200 kW (EPR = 0.5). In this scenario, the cells last for about 7.75 years, during which they endure 3046 EFCs at $\overline{DOD}$ = 63.84%. the share of calendric aging in the total aging at EOL is 41.78%. The longest lifespan of 19.5 years is observed in the scenario with E_{BESS} = 153.6 MW h and P_{BESS} = 1.6 MW (EPR > 2). During this period, the cells endure 283 EFCs with $\overline{DOD}$ = 2.5%. The share of calendric aging at the EOL = 99.47%. Given that at least one, or more replacements of the batteries are necessary during the simulated period of 20 years, there remains some residual useful service life at the end of each simulation. The GWP footprint of the BESS is adjusted to account for this remaining capacity, so that the LEES metric only reflects the capacity that has been lost to degradation. This adjustment is necessary to ensure comparability of the scenarios. As all the other components are considered to have reached the end of their service lives after 20 years, no adjustments have to be made to their values of production and EOL phase GWP footprints.

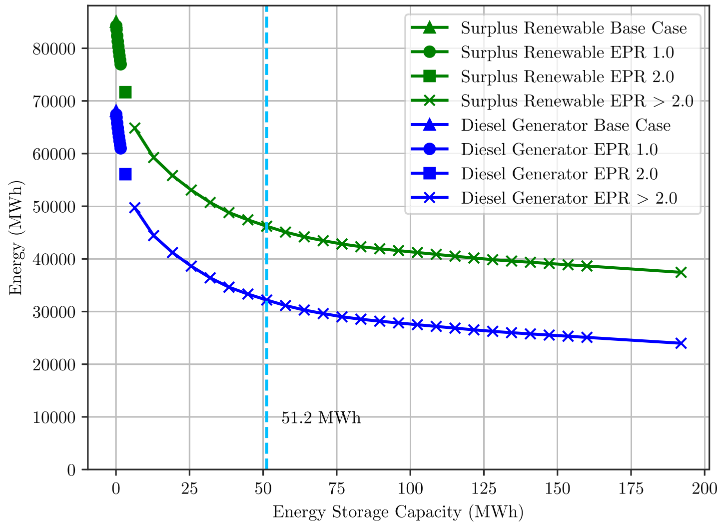

A

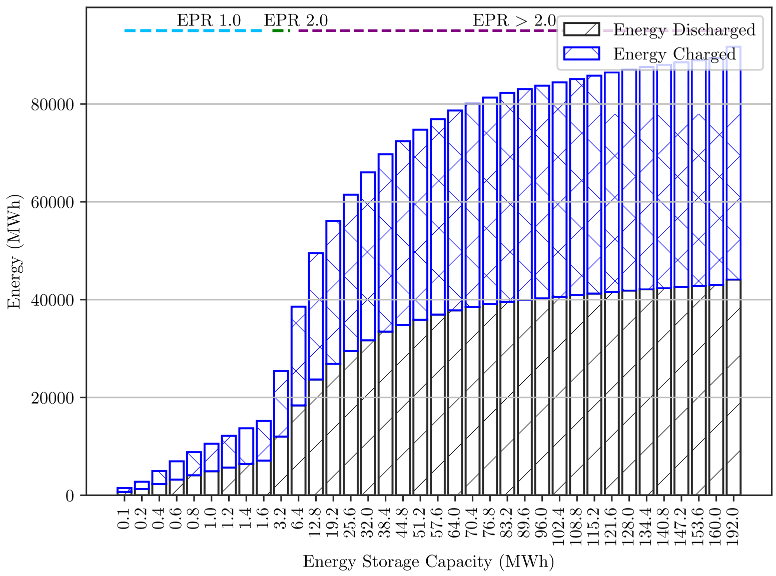

B

Fig. 10. Surplus renewable energy generation and energy generation from the Diesel Generator (DG) drop continuously with respect to energy storage capacity (A). Limited effectiveness of energy storage at completely eliminating curtailment, despite extremely large energy storage capacities, stagnating BESS energy throughput (B).

3.4. Effect of variation in other parameters: a short discussion

The present work introduces the metric LEES, and investigates the effect of BESS peak power and energy storage capacity on the value of LEES for the island grid energy system. Incorporation of energy storage is clearly not the only path to attaining a lower value of LEES vis-a-vis the base case. As an example, an alternative energy system with twice the renewable generation capacity as the base case and the same diesel generation capacity is also simulated - i.e. 6.5 MW of WT capacity, and 4 MW_p of PV generation capacity. The values of LEES for this energy system with E_{BESS} = 200 kW h and P_{BESS} = 200 kW is 0.4558 kg CO_2eq/kWh, as compared to 0.5037 kg CO_2eq/kWh for the original energy system. The LEES value with a BESS of 1.6 MW / 1.6 MW h rating is 0.3101 kg CO_2eq/kWh, as compared to 0.4076 kg CO_2eq/kWh for the same E_{BESS} in the original energy system. This oversized system has much higher levels of curtailment, but the curtailed energy, as already discussed, should not be the sole yardstick of comparison. This finding agrees well with results obtained by Arbabzadeh et al. who suggest that over-building WT capacity is a more effective method of reducing net energy system emissions [20]. Some other possible ways to achieve a reduction in the LEES value may be deduced directly from the expression for the LEES metric, and are not simulated in the current work. These are: higher lifetimes for all components, higher component efficiencies, cleaner production processes with lower carbon footprints, a greater degree of recycling, right-sizing of the installed capacities of renewable energy generators and the BESS. These remarks are comparable to those presented by Jones et al. [17].

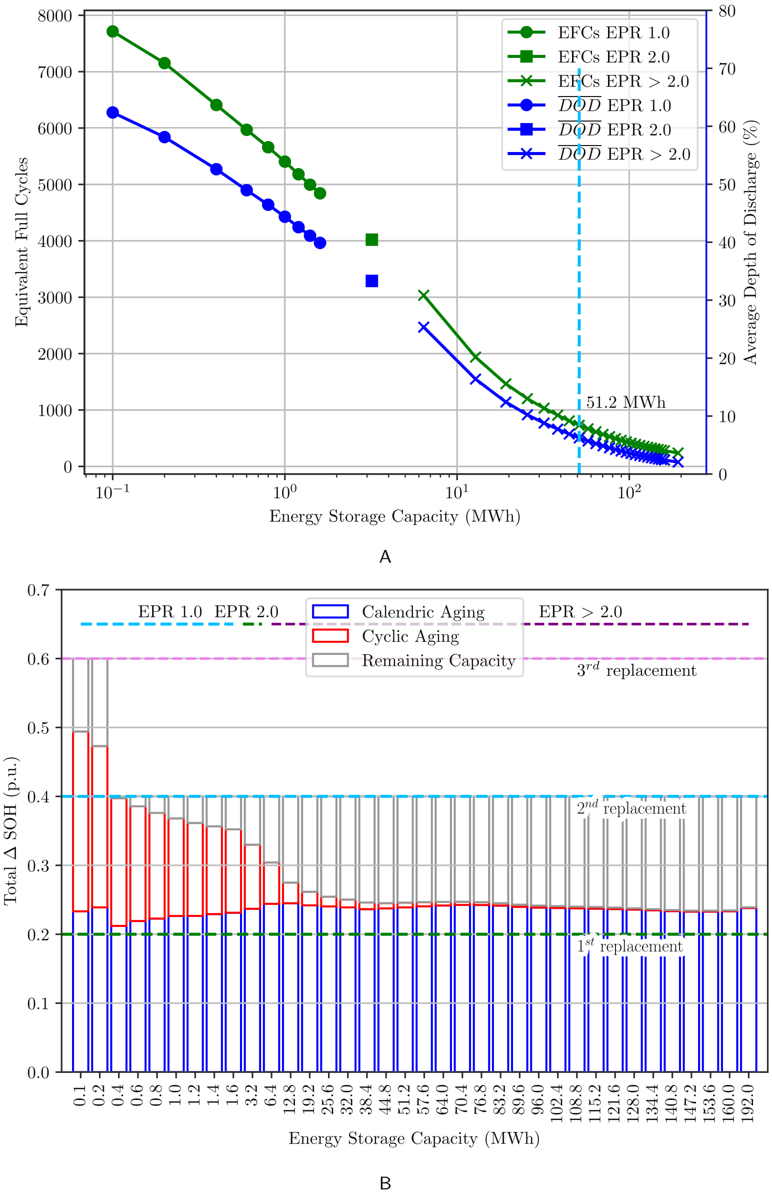

Fig. 11. Equivalent Full Cycles (EFC) and average Depth of Discharge (DOD) seen by each BESS configuration over the simulation period (A). Total calendric and cyclic aging experienced by the BESS with replacements (B).

The stochastic variations in the power outputs of the renewable energy sources could also add to the uncertainty and variability in the calculations. This work assumes perfect foresight for the calculation of the LEES for an energy system. The accuracy of forecasts may, however, affect the planned operation patterns of the various energy system components, and further aggravate the problem of mismatch between generation and demand [46]. In the worst case, curtailment and the operation hours of the DG may increase, and the energy throughput of the BESS may decrease. Occurrence of these effects together can lead to a higher value of LEES. Low response times and large permissible ramp-rates of the DGs can also counteract negative impacts of inaccurate renewable generation forecasts.

The LEES metric can prove to be useful when used in conjunction with other metrics for performance comparisons. A more detailed investigation into the variation of other parameters is not presented in the current work, but will be addressed in subsequent works. This concluding section serves to prove the utility of the LEES metric as a holistic evaluation parameter for island grid energy systems.

4. Conclusion and outlook

This work presents an environmental performance evaluation methodology to assess the reduction in the total GHG emissions of an island grid energy system. Two metrics — the LEES and $R^{\text{unit storage}}_{\text{n,n}-1}$ are introduced to better describe and discuss the incorporation of energy storage in such island grid energy systems. A simplified LCA of a Lithium-ion BESS is carried out to demonstrate the methodology. The methodology and the results from the simplified LCA are applied to an island grid energy system.

It was shown that for the considered conditions, the inclusion of a BESS in an isolated island grid energy system always leads to lower overall emissions than in the base case. It is found that the maximum achievable reduction in total emissions through the incorporation of energy storage capacity in an island grid energy system is bounded by a value which is a function of the characteristics of the energy system and all its components. Focusing solely on minimizing the curtailed energy, or the power generation from the DG through incorporation of energy storage capacity does not necessarily lead to lower total emissions.

The prudent selection of nameplate energy storage capacities can be achieved by considering the value and sign of $R^{\text{unit storage}}_{n,n-1}$ - large negative values indicate higher reductions in emissions, positive values indicate a sub-optimal configuration. From a global perspective, for a given amount of material and monetary investment, a higher total global reduction in emissions can be expected if energy storage capacities are installed in energy systems exhibiting a high $R^{\text{unit storage}}_{n,n-1}$ value, rather than building-up large energy storage capacities in energy systems with substantial pre-existing energy storage capacities, and which exhibit a low $R^{\text{unit storage}}_{n,n-1}$ value.

There exists scope for future works to build upon and further refine the results of this work. Improving the level of detail of the LCA could help enhance the accuracy of the calculation. The current work uses simple energy flow models for the island grid energy system and its components, which do not consider the variations in voltages and frequencies. Transmission losses are entirely disregarded, and the loss mechanisms in the PV, WT, and DG are not modeled. The challenge of obtaining a minimum possible LEES value by varying all possible energy system parameters to yield an optimal system configuration could be formulated as an optimization problem. Uncertainties stemming from the forecasts of renewable energy generation could also potentially be incorporated in future works, and confidence-bounds for the LEES value may be obtained.

CRediT authorship contribution statement

Anupam Parlikar: Conceptualization, Methodology, Data curation, Formal analysis, Investigation, Software, Visualization, Writing - original draft and editing. **Cong Nam Truong:** Methodology, Data curation, Writing - review & editing. **Andreas Jossen:** Funding acquisition, Resources, Supervision, Writing - review & editing. **Holger Hesse:** Funding acquisition, Formal analysis, Visualization, Supervision, Writing - review & editing.

Declaration of competing interest

The authors declare that they have no known competing financial interests or personal relationships that could have appeared to influence the work reported in this paper.

Acknowledgment

This research is funded by the German Federal Ministry of Education and Research (BMBF) and the German Federal Ministry for Economic Affairs and Energy (BMWi) via the research projects greenBattNutzung (grant number 03XP0302D) and EffSkalBatt (grant number 03ET6148A) respectively. Both the projects are overseen by Project Management Juelich (PtJ).

References

[1] IRENA. Renewable energy statistics 2020. Abu Dhabi: International Renewable Energy Agency; 2020, URL: https://www.irena.org/publications/2020/Jul/Renewable-energy-statistics-2020.
[2] Hesse H, Schimpe M, Kucevic D, Jossen A. Lithium-ion battery storage for the grid—A review of stationary battery storage system design tailored for applications in modern power grids. Energies 2017;10(12):2107.
[3] Ritchie H, Roser M. CO_2 and greenhouse gas emissions. Our World Data 2017. https://ourworldindata.org/co2-and-other-greenhouse-gas-emissions.
[4] Stenzel P, Schreiber A, Marx J, Wulf C, Schreieder M, Stephan L. Environmental impacts of electricity generation for Graciosa Island, Azores. J Energy Storage 2018;15:292–303.
[5] Sandia National Laboratories. DOE OE global energy storage database. 2020, URL: https://www.sandia.gov/ess-ssl/global-energy-storage-database-home/.
[6] Diouf B, Pode R. Potential of lithium-ion batteries in renewable energy. Renew Energy 2015;76:375–80.
[7] Pellow MA, Ambrose H, Mulvaney D, Betita R, Shaw S. Research gaps in environmental life cycle assessments of lithium ion batteries for grid-scale stationary energy storage systems: End-of-life options and other issues. Sustain Mater Technol 2020;23:e00120.
[8] Few S, Schmidt O, Offer GJ, Brandon N, Nelson J, Gambhir A. Prospective improvements in cost and cycle life of off-grid lithium-ion battery packs: An analysis informed by expert elicitations. Energy Policy 2018;114:578–90.
[9] Pettinger K-H, Dong W. When does the operation of a battery become environmentally positive? J Electrochem Soc 2017;164(1):A6274–7.
[10] Barnhart CJ, Benson SM. On the importance of reducing the energetic and material demands of electrical energy storage. Energy Environ Sci 2013;6(4):1083.
[11] Palmer G. A framework for incorporating EROI into electrical storage. BioPhys Econ Resour Qual 2017;2(2):1701.
[12] Abdon A, Zhang X, Parra D, Patel MK, Bauer C, Worlitschek J. Techno-economic and environmental assessment of stationary electricity storage technologies for different time scales. Energy 2017;139:1173–87.
[13] Denholm P, Kulcinski GL. Life cycle energy requirements and greenhouse gas emissions from large scale energy storage systems. Energy Convers Manage 2004;45(13–14):2153–72.
[14] Stenzel P, Koj JC, Schreiber A, Hennings W, Zapp P. Primary control provided by large-scale battery energy storage systems or fossil power plants in Germany and related environmental impacts. J Energy Storage 2016;8:300–10.
[15] Lin Y, Johnson JX, Mathieu JL. Emissions impacts of using energy storage for power system reserves. Appl Energy 2016;168:444–56.
[16] Chowdhury JI, Balta-Ozkan N, Goglio P, Hu Y, Varga L, McCabe L. Techno-environmental analysis of battery storage for grid level energy services. Renew Sustain Energy Rev 2020;131:110018.
[17] Jones C, Gilbert PJ, Stamford L. Assessing the climate change mitigation potential of stationary energy storage for electricity grid services. Environ Sci Technol 2019.
[18] McKenna E, McManus M, Cooper S, Thomson M. Economic and environmental impact of lead-acid batteries in grid-connected domestic PV systems. Appl Energy 2013;104:239–49.
[19] Truong CN, Viernstein L, Schimpe M, Witzmann R, Jossen A, Hesse HC. Maximizing solar home battery systems' contribution to the energy transition of the power system. URL: https://ieeexplore.ieee.org/abstract/document/8421821.
[20] Arbabzadeh M, Johnson JX, de Kleine R, Keoleian GA. Vanadium redox flow batteries to reach greenhouse gas emissions targets in an off-grid configuration. Appl Energy 2015;146:397–408.
[21] Emission factors 2018: database documentation. International Energy Agency; 2018.
[22] Naumann M, Truong CN, Schimpe M, Kucevic D, Jossen A, Hesse HC. SimSES: Software for techno-economic simulation of stationary energy storage systems. 2017, URL: https://ieeexplore.ieee.org/document/8278770.
[23] Red Eléctrica de Espana. Canary electricity demand in real-time. 2016, URL: https://www.ree.es/en/activities/canary-islands-electricity-system/canary-electricity-demand-in-real-time.
[24] Schimpe M, von Kuepach ME, Naumann M, Hesse HC, Smith K, Jossen A. Comprehensive modeling of temperature-dependent degradation mechanisms in lithium iron phosphate batteries. J Electrochem Soc 2018;165(2):A181–93.
[25] Schimpe M, Naumann M, Truong N, Hesse HC, Santhanagopalan S, Saxon A, et al. Energy efficiency evaluation of a stationary lithium-ion battery container storage system via electro-thermal modeling and detailed component analysis. Appl Energy 2018;210:211–29.
[26] Naumann M, Schimpe M, Keil P, Hesse HC, Jossen A. Analysis and modeling of calendar aging of a commercial $LiFePO_4$/graphite cell. J Energy Storage 2018;17:153–69.
[27] Naumann M, Spingler FB, Jossen A. Analysis and modeling of cycle aging of a commercial $LiFePO_4$/graphite cell. J Power Sources 2020;451:227666.
[28] Notton G, Lazarov V, Stoyanov L. Optimal sizing of a grid-connected PV system for various PV module technologies and inclinations, inverter efficiency characteristics and locations. Renew Energy 2010;35(2):541–54.

[29] Guinot B, Champel B, Montignac F, Lemaire E, Vannucci D, Sailler S, et al. Techno-economic study of a PV-hydrogen-battery hybrid system for off-grid power supply: Impact of performances' ageing on optimal system sizing and competitiveness. Int J Hydrogen Energy 2015;40(1):623–32.
[30] Truong CN, Schimpe M, Naumann M, Jossen A, Hesse HC. Impact of sub-components on the overall performance of stationary battery systems: Insights on the prototype energy neighbor: 28–29 nov. 2017. 2017.
[31] Peters JF, Baumann M, Zimmermann B, Braun J, Weil M. The environmental impact of li-ion batteries and the role of key parameters–A review. Renew Sustain Energy Rev 2017;67:491–506.
[32] Mohr M, Peters JF, Baumann M, Weil M. Toward a cell–chemistry specific life cycle assessment of lithium–ion battery recycling processes. J Ind Ecol 2020.
[33] Wernet G, Bauer C, Steubing B, Reinhard J, Moreno-Ruiz E, Weidema B. The ecoinvent database version 3 (part I): overview and methodology. Int. J. Life Cycle Assess. 2016;21(9):1218–30.
[34] Hu AH, Huang LH, Lou S, Kuo C-H, Huang C-Y, Chian K-J, et al. Assessment of the carbon footprint, social benefit of carbon reduction, and energy payback time of a high-concentration photovoltaic system. Sustainability 2016;9(1):27.
[35] Simón Martín Md, Diez Mediavilla M, Alonso Tristán C, et al. Real energy payback time and carbon footprint of a GCPVS. AIMS Energy 2017;5(1):77–95.
[36] Bulach W, Schüler D, Sellin G, Elwert T, Schmid D, Goldmann D, et al. Electric vehicle recycling 2020: Key component power electronics. Waste Manag Res: J Int Solid Wastes Public Cleansing Assoc ISWA 2018;36(4):311–20.
[37] Ylmén P, Peñaloza D, Mjörnell K. Life cycle assessment of an office building based on site-specific data. Energies 2019;12(13):2588.
[38] Reich NH, Alsema EA, van Sark W, Turkenburg WC, Sinke WC. Greenhouse gas emissions associated with photovoltaic electricity from crystalline silicon modules under various energy supply options. Prog Photovolt, Res Appl 2011;19(5):603–13.
[39] Latunussa CE, Ardente F, Blengini GA, Mancini L. Life cycle assessment of an innovative recycling process for crystalline silicon photovoltaic panels. Sol Energy Mater Sol Cells 2016;156:101–11.
[40] Reese MO, Glynn S, Kempe MD, McGott DL, Dabney MS, Barnes TM, Booth S, Feldman D, Haegel NM. Increasing markets and decreasing package weight for high-specific-power photovoltaics. Nat Energy 2018;3(11):1002–12.
[41] Razdan P, Garrett P. Life cycle assessment of electricity production from an onshore V112-3.45 MW wind plant. Vestas Wind Systems A/S; 2017.
[42] Wernet G, Bauer C, Steubing B, Reinhard J, Moreno-Ruiz E, Weidema B. The ecoinvent database version 3 (part I): overview and methodology. Int J Life Cycle Assess 2016;21(9):1218–30.
[43] Edwards R, Mahieu V, Griesemann J-C, Larivé J-F, Rickeard DJ. Well-to-wheels analysis of future automotive fuels and powertrains in the European context. In: SAE technical paper series. Warrendale, PA, United States: SAE International400 Commonwealth Drive; 2004, http://dx.doi.org/10.4271/2004-01-1924.
[44] Liu P, Barlow CY. Wind turbine blade waste in 2050. Waste Manage (New York, N.Y.) 2017;62:229–40.
[45] Flowers ME, Smith MK, Parsekian AW, Boyuk DS, McGrath JK, Yates L. Climate impacts on the cost of solar energy. Energy Policy 2016;94:264–73.
[46] Notton G, Nivet M-L, Voyant C, Paoli C, Darras C, Motte F, Fouilloy A. Intermittent and stochastic character of renewable energy sources: Consequences, cost of intermittence and benefit of forecasting. Renew Sustain Energy Rev 2018;87:96–105.

7 Low carbon pathways for high-power EV charging with Li-ion BESSs

The transition to EVs is rapidly increasing the demand for electricity, causing a shift in the energy demand from the oil and gas sector to the electricity grid. This shift is leading to increased demand for High-Power Charging (HPC) stations, which could cause bottlenecks and overloading in vulnerable sections of the electricity grid. This article explores Battery-Assisted (BA)-HPC as a competing measure to Grid Reinforcement (GR) strategies for integration of HPC stations into the grid. This involves using stationary BESSs to provide additional peak power in parallel to grid power. A significant aspect of the study is the calculation and comparison of the carbon footprints for HPC stations with BA and GR. The study develops a comprehensive mathematical framework for this analysis, including the extension of the LEES methodology introduced in the previous chapters and the introduction of the State of Carbon Intensity (SOCI) to calculate the operation phase carbon footprint of the BESS.

The study further presents case studies consisting of various scenarios that investigate the LEES values for both BA-HPC and GR. The effect of integrating local PV generation into energy flows is investigated. The study also explores how the choice of EMS strategy affects BESS performance and examines the impact of on-site renewable energy generation on carbon footprints. The highlights of this article include:

- The quantification of the carbon footprint for BA-HPC
- The influence of the choice of the EMS strategy on the performance of the BESS operating at BA-HPC stations
- The role of the integration of on-site renewable energy generation on the carbon footprints of the scenarios
- The carbon footprint of a comparable configuration with GR

The study finds that the integration of on-site PV generation consistently lowers the LEES in all scenarios compared to similar scenarios without local PV generation. The decarbonization potential of local PV generation is higher in locations with greater annual sunshine hours and solar irradiation. The choice of the EMS strategy significantly affects the LEES values. Both the baseline rule-based greedy charging strategy and the optimizer-based strategy can meet the requirements of peak-shaving service for BA-HPC, but the optimal strategy can further reduce the LEES, especially when combined with local PV generation. These values are compared with the carbon footprint of configurations with GR. In scenarios combining BA with on-site PV generation, a reduction of 24% in LEES values was achieved compared to the baseline strategy. The study also indicates that with an optimized EMS strategy to minimize emissions and integrate local PV generation, BA can potentially charge EVs with a lower carbon footprint compared to GR. The study compares various grid integration pathways and concludes that deploying a BESS at HPC stations can significantly reduce emissions if an optimal EMS strategy is used. BA-HPC combined with local renewable power generation can achieve significantly high emissions savings while charging EVs. The study notes that these findings are subject to the specific location, its electricity grid, and the charging load profile. Future studies should consider location-specific data, and the potential reduction in LEES with enabling feed-in of curtailed power generation should be further explored. As the grid penetration of renewable generation and grid-connected energy storage increases, the carbon intensity of the grid is expected to decrease, potentially reducing the local LEES reduction achievable using BA-HPC.

Author contributions

Anupam Parlikar was the main author, handling the conceptualization, methodology, data curation, software development, formal analysis, investigation, and visualization, along with writing the original draft and its subsequent editing. Maximilian Schott contributed to the methodology, data curation, software development, and manuscript review. Ketaki Godse was involved in developing the methodology and software, also assisting in the manuscript review. Daniel Kucevic supported the methodology development, was responsible for data curation, and reviewed the manuscript. Andreas Jossen was instrumental in acquiring funding and resources for the project, provided supervision, and contributed to manuscript reviews. Holger Hesse secured funding, conducted formal analyses, assisted with visualization, supervised the research project, and played a significant role in both reviewing and editing the manuscript.

High-power electric vehicle charging: Low-carbon grid integration pathways with stationary lithium-ion battery systems and renewable generation

Anupam Parlikar, Maximilian Schott, Ketaki Godse, Daniel Kucevic, Andreas Jossen, and Holger Hesse

Applied Energy (333), 120541, 2023

Permanent weblink:
https://doi.org/10.1016/j.apenergy.2022.120541

Applied Energy 333 (2023) 120541

Contents lists available at ScienceDirect

Applied Energy

journal homepage: www.elsevier.com/locate/apenergy

High-power electric vehicle charging: Low-carbon grid integration pathways with stationary lithium-ion battery systems and renewable generation

Anupam Parlikar [a,*], Maximilian Schott [a], Ketaki Godse [a], Daniel Kucevic [a], Andreas Jossen [a], Holger Hesse [a,b]

[a] Technical University of Munich (TUM), School of Engineering and Design, Department of Energy and Process Engineering, Chair for Electrical Energy Storage Technology (EES), Arcisstr. 21, 80333 Munich, Germany
[b] Kempten University of Applied Sciences, Faculty of Mechanical Engineering, Bahnhofstr. 61, 87435 Kempten, Germany

GRAPHICAL ABSTRACT

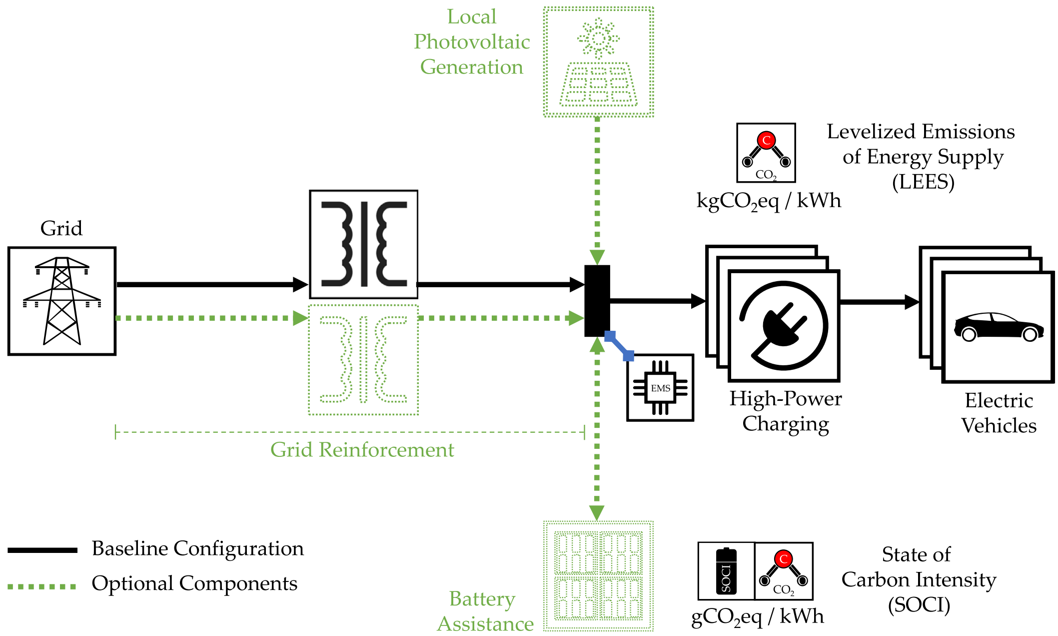

ARTICLE INFO

Keywords:
Energy storage
High-power charging
Electric vehicles

ABSTRACT

The energy transition in the mobility sector is well underway. The electrification of road transport is resulting in a shift of the energy demand from the oil and gas sector to the electricity grid. Increasingly aggressive targets for low charging times for Electric Vehicles (EVs) are slated to raise the demand for High-Power

* Corresponding author.
E-mail addresses: anupam.parlikar@tum.de (A. Parlikar), maxi.schott@tum.de (M. Schott), ketaki.godse@tum.de (K. Godse), daniel.kucevic@tum.de (D. Kucevic), andreas.jossen@tum.de (A. Jossen), holger.hesse@tum.de (H. Hesse).

https://doi.org/10.1016/j.apenergy.2022.120541
Received 22 August 2022; Received in revised form 14 December 2022; Accepted 18 December 2022
Available online 30 December 2022

Charging station
Carbon dioxide emissions
Lithium-ion battery
Battery energy storage system
Energy management
Operation strategy
Levelized Emissions of Energy Supply
State of Carbon Intensity
LEES
SOCI

Charging (HPC). This is likely to lead to bottlenecks and overloading in vulnerable sections of the electricity grid. Battery Assistance (BA) is a promising grid integration measure for High-Power Charging (HPC) to mitigate these problems. As decarbonization is the primary objective of the energy transition, the determination and comparison of the Global Warming Potential (GWP) footprints for HPC stations with BA is crucial. A comprehensive mathematical framework for the modelling and quantification of GWP footprints for HPC has been developed. The Levelized Emissions of Energy Supply (LEES) methodology has been extended and generalized to handle energy from the grid. A new state variable for the Battery Energy Storage System (BESS) — the State of Carbon Intensity (SOCI) has been introduced to calculate the operation phase GWP footprint of the BESS. The energy consumption GWP footprint for the load is also described by a new quantity — the Load Energy Consumption (LEC) emissions. The effect of incorporation of local Photovoltaic Solar (PV) generation in the energy flows is also investigated. An optimized Energy Management System (EMS) strategy with rolling horizon optimization to minimize emissions has been implemented to regulate energy flows in scenarios with BA and local PV generation. The Levelized Emissions of Energy Supply (LEES) values are obtained for all simulated scenarios and compared against a baseline rule-based EMS strategy. In combination with on-site PV generation, BA could achieve a reduction of 24% in the LEES vis-á-vis the baseline strategy. For reference, two scenarios with Grid Reinforcement (GR) for the grid section with and without local PV generation have also been simulated. With Grid Reinforcement (GR), a reduction of over 2% can be achieved with respect to the baseline EMS strategy for BA. Grid Reinforcement (GR) in conjunction with local PV generation can bring about a further reduction of about 6% with respect to the baseline EMS strategy for BA.

1. Introduction

Decarbonization is the central objective driving the energy transition in the mobility sector. A wide range of vehicle segments, such as two-wheelers, passenger cars, and electric buses, are being electrified. During the period 2015–2020, EV sales volumes rose by 600% over 2015 levels. Sales volumes in the current decade are projected to rise between twelve and twenty times as compared to 2020. Cumulative installed charging power is expected to sharply rise by 1600% compared to 2020 values in some scenarios [1]. Direct Current (DC) charging can attain higher power values as compared to Alternating Current (AC) charging owing to the external on-site installation of the bulky power electronics [2,3]. Drastically reduced charging times can be achieved as a result, provided the automotive battery pack can handle the large currents [4]. The scope of the current work is restricted to DC High-Power Charging (HPC).

CSs are comprised of multiple DC high-power chargers — each of which can charge an EV at a time. The automaker *Tesla* for instance has an average of ten chargers per CS in its *Supercharger Charging Network* [5]. These high-power DC chargers usually operate at an AC voltage rating of around 400 V and are linked to the Medium Voltage (MV) grid via a step-up transformer. Chargers can now attain peak power ratings of around 350 kW [6,7]. DC HPC is expected to introduce an additional large and variable power demand on electricity grids worldwide, which are grappling with the variability of renewable generation. The demand for DC HPC is predicted to increase, especially in dense urban areas without access to home-charging. Instances of grid overloading and bottlenecks may become frequent in such areas, and Grid Reinforcement (GR) may become necessary to augment the power transmission capacity of the affected grid sections [8]. Effective grid integration of EV HPC is key to the success of electromobility.

Lithium-ion BESS technology is well-suited to the provision of a wide array of grid-related services [9,10]. Battery Assistance (BA) can be used to improve grid integration of HPC stations, by reducing the peak power demand [11,12]. The stationary BESS provides additional peak power in parallel to the grid power. BA lowers the instantaneous power demand, while increasing the utilization factor of the grid. This allows the grid to operate within the bounds of the existing infrastructure at low peak power values, without requiring any additional GR. A wide range of system architectures and topologies are available in the implementation of this concept at CSs [13]. The sizing of the various hardware components is a widely studied topic in the technical community, and the subject of several publications [14]. This solution is also appealing as the installation is relatively non-disruptive.

The study of the combination of BA with renewable generation such as PV solar and wind turbines is also of significant interest in the energy community [15,16]. The determination of optimal sizing parameters is a keenly studied aspect of these systems [17,18]. Optimal operation of the stationary BESS is a topic of intense research. A common criterion to determine the optimal operation is the economic performance over the project lifetime [19]. Several studies include the time-of-use (TOU) effect on the prices of electricity in the optimization [16,20]. Some studies also investigate the economic performance of BA with the provision of additional grid-related services, such as energy arbitrage [21]. BA is also seen as a resilience measure to ensure energy security for EVs during grid outages. An optimal charging strategy for the BA-HPC stations to ensure resilience while providing the core peak shaving functionality has also been found in the reviewed literature [22]. Incorporation of the carbon (GWP) footprint as a criterion to determine optimal operation is relatively rare. Studies incorporating the GWP footprint in their analyses, often treat it as a secondary aspect and do not consider the temporal variation of the carbon intensity of the energy drawn from the grid [16]. One detailed study was found, which considered the time-variant grid carbon intensity for the Netherlands [23].

The state-of-the-art in the analysis of energy storage systems operating in various energy systems was found lacking in its resolution of the GWP footprint at a component level and over its various lifecycle phases. In most studies, the operation phase of the energy storage system, in particular, is analysed using lumped parameters, and the temporal variations in the operating conditions, such as the carbon intensity of the electricity grid, and the variations in efficiency are often not considered. The calculation of the GWP footprint attributable to the energy storage system is often not precise. There is a dearth of quantities and metrics to describe and capture all relevant information, thereby preventing its inclusion in the analysis. As decarbonization is the stated goal for the transition to electromobility, any decision-making process concerning EV HPC infrastructure should incorporate the GWP footprint of the solution into the analysis. This work endeavours to bridge some of this gap by first introducing some useful quantities, which enhance the informational content of an emissions analysis. A detailed analytical and mathematical framework for the calculation of the GWP footprints of all components of a CS across all lifecycle phases, with a detailed breakdown of the emissions into several emissions categories.

Scope and outline

The contents of this paper are structured as follows. In Section 2 a detailed techno-environmental model of the grid integration measure BA (and GR) has been developed. A comprehensive mathematical framework for the quantification and analysis of the GWP footprint of

Abbreviations

AC	Alternating Current
BA	Battery Assistance
BESS	Battery Energy Storage System
CO_2eq	Carbon Dioxide Equivalent
CS	Charging Station
DC	Direct Current
DEC	Discharge Energy Consumption
DOC	Depth of Cycle
EFC	Equivalent Full Cycle
EMS	Energy Management System
EOL	End-of-Life
ESN	Energy System Network (Simulation Tool)
EV	Electric Vehicle
GCS	Greedy Charging Strategy
GEC	Grid Energy Consumption
GR	Grid Reinforcement
GWP	Global Warming Potential
HPC	High-Power Charging
HVAC	Heating, Ventilation, Air Conditioning
LCA	Life Cycle Analysis
LEC	Load Energy Consumption
LEES	Levelized Emissions of Energy Supply
LV	Low Voltage
MV	Medium Voltage
OCS	Optimal Charging Strategy
PE	Power Electronics
PV	Photovoltaic Solar
SimSES	Simulation of Stationary Energy Storage Systems (Simulation Tool)
SOC	State of Charge
SOCI	State of Carbon Intensity
SOH	State of Health

Parameters

CI_t^{ch}	Carbon intensity of charging power for BESS at time t
CI_t^{PV}	Carbon intensity of the on-site PV system at time t
$CI_t^{gen,gr,j}$	Carbon intensity of the grid-connected generation technology j in the grid mix at time t
CI_t^{gr}	Effective carbon intensity of the grid mix at time t
CI_t^{mix}	Carbon intensity of the energy in the grid mix at time t
E_s	Energy supplied to the load over simulation period in kW h
$P_t^{ch,loss}$	Charging loss power for BESS
$P_t^{ch,st}$	Stored charging power for BESS
$P_t^{dch,loss}$	Discharging loss power for BESS
P_{peak}^{gr}	Peak grid power
$P_{t,peak}^{PV}$	Peak generation power of on-site PV system at time t
$P_t^{PV,ch}$	Power from on-site PV system used to charge the BESS at time t
$P_t^{PV,load}$	Power from on-site generation technology j directly supplied to the load at time t
P_t^{PV}	Generation power of on-site PV system at time t
P_t^{ch}	Charging power of the BESS at time t
$P_t^{dch,load}$	BESS discharge power supplied to the load at time t
P_t^{dch}	Discharging power of the BESS at time t
$P_t^{gen,gr,j}$	Generation power of grid-connected generation technology j in the grid-mix at time t
$P_t^{gr,ch}$	Grid power directly supplied to the BESS for charging at time t
$P_t^{gr,load}$	Grid power directly supplied to the load at time t
$P_t^{gr,loss}$	Power lost in the grid section during transmission at time t
P_t^{gr}	Total grid power entering the system boundaries at time t
P_t^{load}	Load demand power at time t
$SOCI_t$	SOCI at time t
SOC_t	SOC at time t
Δt	Simulation time t
η_{gr}	Average grid transmission energy efficiency
$\overline{DOC}$	Mean DOC over simulation period
$\overline{SOCI}$	Mean SOCI over simulation period
$\overline{SOC}$	Mean SOC over simulation period
$\varepsilon^{BESS,EOL}$	EOL phase emissions for BESS
$\varepsilon^{BESS,op}$	Total operation phase emissions for BESS
$\varepsilon^{BESS,prod}$	Production phase emissions for BESS
ε^{BESS}	Total emissions of the BESS over simulation period
ε^{DEC}	Total Discharge Energy Consumption (DEC) emissions for the load over simulation period
ε^{GEC}	Total Grid Energy Consumption (GEC) emissions for the load over simulation period
$\varepsilon^{HVAC,EOL}$	EOL phase emissions for Heating, Ventilation, Air Conditioning (HVAC) system
$\varepsilon^{HVAC,prod}$	Production phase emissions for HVAC system
ε^{LEC_t}	LEC emissions for the load at time t
ε^{LEC}	Total LEC emissions over simulation period
$\varepsilon^{PE,EOL}$	EOL phase emissions for Power Electronics (PE)
$\varepsilon^{PE,prod}$	Production phase emissions for PE
$\varepsilon^{PV,EOL}$	EOL phase emissions of on-site generation technology
$\varepsilon^{PV,prod}$	Production phase emissions of on-site generation technology
ε^{PV}	Total emissions on-site PV system over simulation period
$\varepsilon^{c,EOL}$	EOL phase emissions for the cables in the grid section
$\varepsilon^{c,prod}$	Production phase emissions for the cables in the grid section
$\varepsilon^{cell,EOL}$	EOL phase emissions for cells
$\varepsilon^{cell,prod}$	Production phase emissions for cells
$\varepsilon^{ch,op}$	Total operation phase emissions charging for BESS
$\varepsilon^{dch,op}$	Total operation phase emissions discharging for BESS

$\varepsilon^{\mathrm{el,EOL}}$	EOL phase emissions for miscellaneous electronics
$\varepsilon^{\mathrm{el,prod}}$	Production phase emissions for miscellaneous electronics
$\varepsilon^{\mathrm{gr,EOL}}$	EOL phase emissions for the grid section
$\varepsilon^{\mathrm{gr,op}}$	Operation phase emissions for the grid section over simulation period
$\varepsilon^{\mathrm{gr,prod}}$	Production phase emissions for the grid section
$\varepsilon^{\mathrm{gr}}$	Total attributable emissions for the grid section over simulation period
$\varepsilon^{\mathrm{hsg,EOL}}$	EOL phase emissions for the housing
$\varepsilon^{\mathrm{hsg,prod}}$	Production phase emissions for the housing
$\varepsilon^{\mathrm{load}}$	Total emissions attributable to the load over the entire simulation period
$\varepsilon^{\mathrm{panel,EOL}}$	EOL phase emissions of PV panels
$\varepsilon^{\mathrm{panel,prod}}$	Production phase emissions of PV panels
$\varepsilon^{\mathrm{tr,EOL}}$	EOL phase emissions for the transformers in the grid section
$\varepsilon^{\mathrm{tr,prod}}$	Production phase emissions for the transformers in the grid section
$\varepsilon_{t\mathrm{DEC}}$	DEC emissions for the load at time *t*
$\varepsilon_{t\mathrm{GEC}}$	GEC emissions for the load at time *t*
$\varepsilon_{t\mathrm{ch,op}}$	Operation phase emissions charging for BESS
$\varepsilon_{t\mathrm{dch,op}}$	Operation phase emissions discharging for BESS
$\varepsilon_{t\mathrm{gr,op}}$	Operation phase emissions for the grid section at time *t*
$\mathrm{b}_t^{\mathrm{BESS}}$	Binary variable *b* to preclude simultaneous BESS charging and discharging at time t
h	Optimization time horizon *h*
t	Time *t*

this measure with a streamlined Life Cycle Analysis (LCA) is presented. The existing LEES methodology is extended and generalized to include grid energy [24]. To this end, a new state variable for energy storage — the SOCI is introduced, along with emission categories Discharge Energy Consumption (DEC), Grid Energy Consumption (GEC), and the Load Energy Consumption (LEC) emissions. In Section 3, long-term simulations over a period of 20 years are run with the developed models to obtain the GWP footprints of the scenarios, enabling the following research questions to be addressed:

1. How can the GWP footprint for HPC with BA be quantified?
2. To what extent does the choice of the EMS strategy alter the performance of the BESS providing BA to HPC stations?
3. How does the integration of on-site renewable energy generation influence the GWP footprints of the scenarios?
4. What is the GWP footprint of a comparable configuration with GR?

The 'carbon-quality' of the energy dispensed by the CS in the considered scenarios is quantified with the LEES metric [24]. The implications of the value of LEES of the dispensed energy on the emissions per 100 km driven with an EV with three different energy economy values is also estimated. This GWP footprint of the energy consumption of EVs is compared with typical values for well-to-wheel emissions per 100 km for gasoline-powered internal combustion engine vehicles. In Section 4 a brief summary of the key findings is presented, with some potential topics for future follow-up studies.

2. Methods

The modelling and subsequent analyses in this study are carried out with the help of python-based simulation programs. These programs offer specialized capabilities to model and simulate the components of an energy system. The central program used to model and simulate the site of the CS is Energy System Network (Simulation Tool) (ESN). This program has been developed by the authors of the present work. Simulation programs for specific components are embedded within ESN. The program SimSES is used to model the BESS [25]. Techno-environmental time-series simulations spanning over a duration of 20 years are run for the CS with several system configurations.

Table 1
Charging station parameters in the baseline configuration.

Charging station baseline configuration parameters	
Parameter	Value
Location	Berlin
Location type	Urban
Grid coupling	Medium Voltage (MV) 10 kV
Grid section installation	Underground (UG)
Grid section effective peak power (MW)	2.5
Charger connection	Low Voltage (LV) 0.4 kV
Max. charger power (MW)	0.35
Number of chargers	10

2.1. Modelling: EV HPC station

This work considers CSs at urban locations. Each charger is modelled with AC/DC and DC/DC converters. Efficiency curves are used to model the losses in the AC/DC and DC/DC converters. Additional losses due to the cooling system for the charger are not modelled in this analysis, as their inclusion does not fundamentally alter the results. The chosen parameters for such an exemplary setup are described in Table 1. At any time t, the power demand of the chargers (load), $\mathrm{P}_t^{\mathrm{load}}$, is met by power from the grid, $\mathrm{P}_t^{\mathrm{gr,load}}$, power discharged by the BESS, $\mathrm{P}_t^{\mathrm{dch,load}}$, and power generation by the PV system (if present), $\mathrm{P}_t^{\mathrm{PV,load}}$ (Eq. (1)). Augmentation of the power capacity is necessary to enable parallel operation of all chargers at rated power.

$$P_t^{load} = P_t^{gr,load} + P_t^{dch,load} + (P_t^{PV,load}) \tag{1}$$

A synthetic load profile for the CS has been generated using published data from a CS in Italy. Based on log data of over three years, a representative day capturing hourly charge events, and a representative week capturing daily charge events have been prepared by Soldan et al. [26]. Based on this data, a synthetic load profile has been created for the representative week. This procedure has been explained in appendix Appendix A. This representative profile is concatenated back-to-back to obtain the load profile for an entire year. The annual energy demand with this load profile is around 3.29 GW h. Seasonal variations are assumed to not lead to major changes in consumer behaviour. This assumption can be justified, as the analysis presented in the current work is exemplary in nature and serves to demonstrate the application of the developed analytical framework. The authors also note that irrespective of the load profile chosen, sufficient generality can seldom be attained, and the finer results of any analysis are inevitably specific to that analysis.

2.2. Modelling: Battery Energy Storage System (BESS)

The BESS is modelled as a utility-scale system. An in-depth description of the modelling and simulation procedure in SimSES can be found in a previous publication [25]. The parameters used to model the BESS are listed in Table 2. A BESS rating of 1.5 MW / 1.5 MW h is chosen to ensure a maximum energy-rate (E-rate) of under 1 for the discharge power demand. Ambient environmental conditions for Berlin, Germany are used for the simulations. Under these conditions, system simulations for the BESS are run. These simulations also compute the cell degradation over the simulation period.

Table 2
Model parameters and values for the BESS simulation in SimSES.

Battery Energy Storage System (BESS)	
Parameter	Value
Cell type	Lithium Iron Phosphate (LFP)
Cell format	Cylindrical, 26650
Rated energy capacity (MWh)	1.5
Rated power (MW)	1.5
Initial state of health (SOH)	100%
Battery model	R-int Equivalent Circuit Model (ECM) (based on [27,28])
Battery degradation model	Semi-empirical calendric and cyclic (based on [29,30])
Power electronics	AC/DC Converter, 300 kW X 5 units (based on [31–33])
Housing type	20 ft. standard shipping container
HVAC power (kW)	30

Table 3
Grid section parameters in the baseline configuration.

Grid section baseline configuration parameters	
Parameter	Value
MV section voltage	10 kV
Installation	Underground
Line length	1.6 km
Conductor cross-section	70 mm^2
Transformer MV/LV	0.63 MVA 10 kV/0.4 kV
# Parallel units	6
LV section voltage	0.4 kV
Installation	Underground
Line length scenarios	B: 0.05 km
Conductor cross-section	10800 mm^2

2.3. Modelling: Local Photovoltaic Solar (PV)generation

The PV system is modelled with power generation curves for the PV panels and efficiency curves for the power electronics. Power generation curves for Berlin, Germany with a capacity factor of 0.1142 are used. The power generation curves for Berlin are generated using the tool *greenius* [34]. A peak power rating of 1 MW$_p$ is chosen. Such an installation corresponds to a surface-area footprint of around 10 000 m^2, and can either be present on-site, or on neighbouring rooftops [35]. The power generation, P_t^{PV}, at time t by the on-site PV system is split into the power supplied to the load, $P_t^{PV,load}$, the power used to charge the BESS, $P_t^{PV,ch}$, and the curtailment (Eq. (2)).

$$P_t^{PV} = P_t^{PV,load} + P_t^{PV,ch} + P_t^{PV,curt} \tag{2}$$

2.4. Modelling: Grid components and Grid Reinforcement (GR)

The grid section is modelled with an MV section, a bank of step-down transformers, and an Low Voltage (LV) section. The python package *Pandapower* is used to run the power flow calculations within the simulation framework [36]. Bus voltages, component loadings, energy losses, and the power delivery of the considered grid section can be obtained from power flow calculations [37]. The CS is connected to the nearest MV substation with an underground grid section as described in Table 3. For the 10 kV MV grid in Germany, most lines are around 1.6 km in length [38].

2.5. Streamlined Life Cycle Analysis (LCA)

In the following subsections, the emissions attributable to each component are described.

2.5.1. German grid carbon intensity

The power transmitted by the electricity grid is sourced from a wide variety of power generation technologies. At time t, the effective carbon intensity of the grid energy, CI_t^{gr}, can be computed from the power, $P_t^{gen,gr,j}$, and the carbon intensities of the participating power generation technologies, $CI_t^{gen,gr,j}$. Values for $CI_t^{gen,gr,j}$ have been obtained from literature sources and from the *Ecoinvent* database [39,40]. Technology-wise power generation data for the German grid for the year 2019 has been obtained from the *Energy-Charts*[1] platform [41]. This data represents pre-pandemic power generation. The combination of this data with the carbon intensities of the power generation technologies yields a time-dependent carbon intensity profile for the grid mix with a 15-minutes resolution (Fig. 1). The carbon intensity of the grid mix CI_t^{mix} is given by Eq. (3).

$$CI_t^{mix} = \frac{\sum_{j=1}^{n}\left(CI_t^{gen,gr,j} \times P_t^{gen,gr,j}\right)}{\sum_{j=1}^{n} P_t^{gen,gr,j}} \tag{3}$$

where *n* refers to the number of technologies participating in the energy mix. With a lumped transmission efficiency (including transmission and distribution grid) value of η_{gr} = 95% for the German grid [42], CI_t^{gr} is obtained as:

$$CI_t^{gr} = \frac{CI_t^{mix}}{\eta_{gr}} \tag{4}$$

2.5.2. Grid section components

The GWP footprints for the production and EOL phases $\varepsilon^{gr,prod}$ and $\varepsilon^{gr,EOL}$ for the grid section are a sum of the emissions in the respective phases for the transformers and cables. The production phase emissions for the cables, $\varepsilon^{c,prod}$, include emissions caused by the production itself, the creation of supporting infrastructure such as ditches, and the installation. The production emissions for the transformers, $\varepsilon^{tr,prod}$, include the emissions of the production process and the creation of supporting infrastructure. For the EOL phase emissions, negative values were found in the reviewed literature sources for $\varepsilon^{tr,EOL}$ and $\varepsilon^{c,EOL}$. Negative values indicate offsetting of emissions in subsequent production phases on the reintroduction of the recovered materials after recycling [43].

$$\varepsilon^{gr,prod} = \varepsilon^{tr,prod} + \varepsilon^{c,prod} \tag{5}$$

$$\varepsilon^{gr,EOL} = \varepsilon^{tr,EOL} + \varepsilon^{c,EOL} \tag{6}$$

The grid power entering the system boundaries at time t, P_t^{gr}, is split into the actual power supplied to the load, $P_t^{gr,load}$, the power used to charge the BESS, $P_t^{gr,ch}$, and the power lost in transmission, $P_t^{gr,loss}$. This lost energy must be generated in addition to the energy that is transported by the grid section for consumption at the load. The emissions attributable to the generation of this lost energy at time t are allocated to the grid section as the operation phase emissions, $\varepsilon_{t^{gr,op}}$.

$$P_t^{gr} = P_t^{gr,load} + P_t^{gr,ch} + P_t^{gr,loss} \tag{7}$$

$\varepsilon_{t^{gr,op}}$ is calculated using Eq. (8), where Δt is the length of a single timestep. The total emissions attributable to the operation phase of the grid section, $\varepsilon^{gr,op}$, are obtained by integrating Eq. (8) with respect to time over the entire simulation period.

$$\varepsilon_t^{gr,op} = CI_t^{gr} \times P_t^{gr,loss} \times \Delta t \tag{8}$$

The total emissions, ε^{gr}, attributable to the grid section within the system boundaries over the simulation period is then given by Eq. (9). The total emissions for the grid section include the production emissions, $\varepsilon^{gr,prod}$, the operation emissions, $\varepsilon^{gr,op}$, and the EOL emissions, $\varepsilon^{gr,EOL}$.

$$\varepsilon^{gr} = \varepsilon^{gr,prod} + \varepsilon^{gr,op} + \varepsilon^{gr,EOL} \tag{9}$$

[1] Energy Charts (https://energy-charts.info/) — online energy and power data platform for Germany created and maintained by the Fraunhofer Institute of Solar Energy (ISE), Freiburg, Germany.

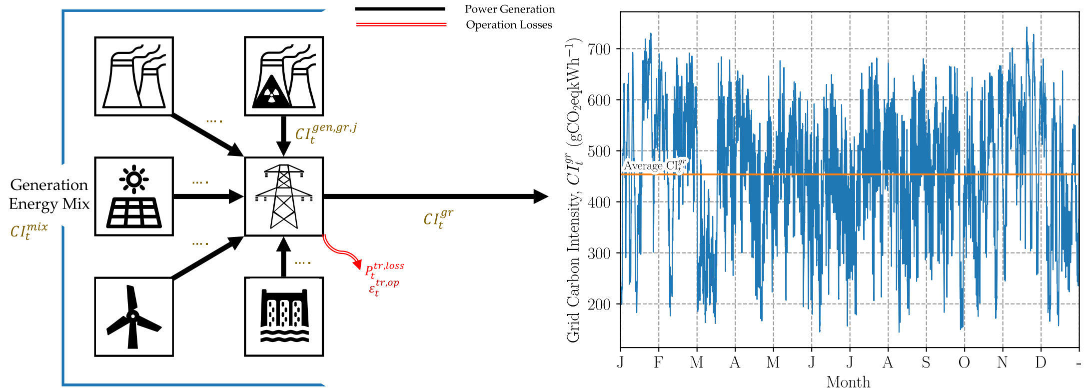

Fig. 1. Calculation procedure to obtain the annual grid carbon intensity (CI_t^{gr}) time-series profile. Depicted here is the carbon intensity profile for the German electricity grid, based on data for the last pre-pandemic year 2019.

Table 4
Streamlined Life Cycle Analysis (LCA) of the Battery Energy Storage System (BESS) (power/energy rating of 1.5 MW/1.5 MW h.

Battery Energy Storage System (BESS) streamlined LCA			
Component	Production (kgCO2eq)	End-of-Life (EOL) (kgCO2eq)	Source
Cells	241500.00	−17550.00	[44,45]
Power electronics	50859.78	−14179.48	[39,46–48]
Miscellaneous electronics	23220.87	−3364.70	[39,48]
Housing	31440.00	0.00	[39]
HVAC	426.12	0.00	[49]
Sum	347446.78	−35094.18	
Total	**312352.60**		

2.5.3. Charging Station (CS)

The production and EOL phase emissions for the chargers are excluded from the system boundaries as these remain invariable across scenarios. For the CS, the total lifecycle emissions within the system boundaries are equal to the total Load Energy Consumption (LEC) emissions described in Section 2.6 (Eq. (10)).

$$\varepsilon^{load} = \varepsilon^{LEC} \tag{10}$$

2.5.4. Battery Energy Storage System (BESS)

A streamlined LCA for a utility-scale BESS with Lithium Iron Phosphate (LFP) cell technology has already been conducted and described in a previous publication [24].

Production and End-of-Life (EOL) phase. The total emissions of the production and EOL phases of the BESS, $\varepsilon^{\mathrm{BESS,prod}}$ and $\varepsilon^{\mathrm{BESS,EOL}}$, can be calculated as the sum of production and EOL phase emissions of its components. These include the GWP footprints of the batteries ($\varepsilon^{\mathrm{cell,prod}}$, $\varepsilon^{\mathrm{cell,EOL}}$) the GWP footprints of the other components: Power Electronics (PE) ($\varepsilon^{\mathrm{PE,prod}}$, $\varepsilon^{\mathrm{PE,EOL}}$), the housing ($\varepsilon^{\mathrm{hsg,prod}}$, $\varepsilon^{\mathrm{hsg,EOL}}$), the miscellaneous electronics components ($\varepsilon^{\mathrm{el,prod}}$, $\varepsilon^{\mathrm{el,EOL}}$), and the HVAC system ($\varepsilon^{\mathrm{HVAC,prod}}$, $\varepsilon^{\mathrm{HVAC,EOL}}$).

$$\varepsilon^{BESS,prod} = \varepsilon^{cell,prod} + \varepsilon^{PE,prod} + \varepsilon^{hsg,prod} + \varepsilon^{el,prod} + \varepsilon^{HVAC,prod} \tag{11}$$

$$\varepsilon^{BESS,EOL} = \varepsilon^{cell,EOL} + \varepsilon^{PE,EOL} + \varepsilon^{hsg,EOL} + \varepsilon^{el,EOL} + \varepsilon^{HVAC,EOL} \tag{12}$$

In the present study, the streamlined LCA is adapted to the BESS configuration presented in Table 2. The GWP footprint of the BESS is calculated to be around 312 352.60 kg Carbon Dioxide Equivalent (CO_2eq) (Table 4).

Operation phase. The operation emissions, $\varepsilon^{\mathrm{BESS,op}}$, for a BESS are a direct function of the carbon intensity of the energy used for charging, $\mathrm{CI}_t^{\mathrm{ch}}$. The direct emissions of generation of the energy lost in the charging and discharging processes are allocated to the BESS. The charging power at time t, $\mathrm{P}_t^{\mathrm{ch}}$, is the sum of charging powers from the grid, $\mathrm{P}_t^{\mathrm{gr,ch}}$, and from the local PV generation, $\mathrm{P}_t^{\mathrm{PV,ch}}$, if present. Charging loss power, $\mathrm{P}_t^{\mathrm{ch,loss}}$, is lost, while the rest, $\mathrm{P}_t^{\mathrm{ch,st}}$, is stored. With the values of $\mathrm{P}_t^{\mathrm{ch,loss}}$ and $\mathrm{CI}_t^{\mathrm{ch}}$, the emissions due to the charging losses, $\varepsilon_{t\mathrm{ch,op}}$, are obtained (Eq. (15), (16)). The total emissions attributable to the charging phase, $\varepsilon^{\mathrm{ch,op}}$, are the sum of all $\varepsilon_{t\mathrm{ch,op}}$ values over the simulation period.

$$P_t^{ch} = (P_t^{PV,ch}) + P_t^{gr,ch} \tag{13}$$

$$P_t^{ch} = P_t^{ch,st} + P_t^{ch,loss} \tag{14}$$

$$CI_t^{ch} = \frac{\left[(CI_t^{PV} \times P_t^{PV,ch}) + CI_t^{gr} \times P_t^{gr,ch}\right]}{P_t^{ch}} \tag{15}$$

$$\varepsilon_t^{ch,op} = CI_t^{ch} \times P_t^{ch,loss} \times \Delta t \tag{16}$$

A new state variable — the State of Carbon Intensity (SOCI) is introduced to quantify the emissions of the discharge phase. The SOCI at time t is defined as the carbon intensity of the energy stored within the BESS. When SOC = 0, the SOCI = 0. On charging, the values of $\mathrm{CI}_t^{\mathrm{ch}}$ lead to a change in the value of SOCI (Eq. (17)). The SOCI does not change on partially discharging the BESS. The units for SOCI are $\mathrm{gCO_2}eq\mathrm{kW\,h^{-1}}$. SOC_t is the SOC of the BESS (see Fig. 2).

$$SOCI_{t+1} = \frac{SOCI_t \times SOC_t + \Delta SOC \times CI_t^{ch}}{SOC_{t+1}} \tag{17}$$

A portion of the discharging power, $\mathrm{P}_t^{\mathrm{dch,loss}}$, is lost to the energy conversion processes in the BESS. The remaining power, $\mathrm{P}_t^{\mathrm{dch,load}}$, is supplied to the load (see Eq. (18)). The operation emissions in the discharge phase, $\varepsilon_{t\mathrm{dch,op}}$, are dependent on the discharge loss power, $\mathrm{P}_t^{\mathrm{dch,loss}}$, and the SOCI_t (Eq. (19)). The total emissions attributable to the discharging phase, $\varepsilon^{\mathrm{dch,op}}$, is obtained by integrating Eq. (19) with respect to time over the entire simulation period. $\varepsilon^{\mathrm{BESS,op}}$ is the sum of $\varepsilon^{\mathrm{ch,op}}$ and $\varepsilon^{\mathrm{dch,op}}$ (Eq. (20)).

$$P_t^{dch} = P_t^{dch,load} + P_t^{dch,loss} \tag{18}$$

$$\varepsilon_t^{dch,op} = SOCI_t \times P_t^{dch,loss} \times \Delta t \tag{19}$$

$$\varepsilon^{BESS,op} = \varepsilon^{ch,op} + \varepsilon^{dch,op} \tag{20}$$

The total emissions, $\varepsilon^{\mathrm{BESS}}$, attributable to the BESS over the simulation period are then given by Eq. (21).

$$\varepsilon^{BESS} = \varepsilon^{BESS,prod} + \varepsilon^{BESS,op} + \varepsilon^{BESS,EOL} \tag{21}$$

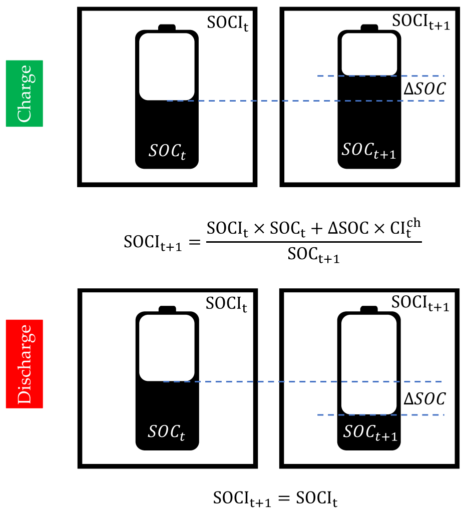

Fig. 2. The BESS state variable State of Carbon Intensity (SOCI) changes after each charging operation, but remains constant after discharging.

Table 5
Streamlined LCA for the PV system.

Photovoltaic (PV) system streamlined LCA			
Component	Production (kgCO2eq)	End-of-Life (EOL) (kgCO2eq)	Source
Panels	1100000.00	7400.00	[50–52]
Power electronics	38459.90	−9452.99	[39,46–48]
Sum	1138459.90	−2052.99	
Total	**1136406.91**		

2.5.5. On-site PV system

The GWP footprints of the production $\varepsilon^{\mathrm{PV,prod}}$ and EOL $\varepsilon^{\mathrm{PV,EOL}}$ phases of the PV system are considered to be equal to the sums of the production and EOL footprints of just the functional energetic components — the panels ($\varepsilon^{\mathrm{panel,prod}}$ and $\varepsilon^{\mathrm{panel,EOL}}$) and power electronics ($\varepsilon^{\mathrm{PE,prod}}$ and $\varepsilon^{\mathrm{PE,EOL}}$). A streamlined LCA for the 1 $\mathrm{MW_p}$ PV system is presented in Table 5. Other components are not considered in this analysis.

$$\varepsilon^{PV,prod} = \varepsilon^{panel,prod} + \varepsilon^{PE,prod} \tag{22}$$

$$\varepsilon^{PV,EOL} = \varepsilon^{panel,EOL} + \varepsilon^{PE,EOL} \tag{23}$$

There are no direct emissions attributable to the PV system during its operation phase, thus $\varepsilon^{PV,op} = 0$. The total emissions $\varepsilon^{\mathrm{PV}}$ attributable to the PV system over the simulation period are then given by Eq. (24).

$$\varepsilon^{PV} = \varepsilon^{PV,prod} + \varepsilon^{PV,EOL} \tag{24}$$

2.6. Levelized Emissions of Energy Supply (LEES): Extension and generalization

The quantity LEES is defined as the ratio of the sum of all attributable lifecycle emissions of components contained within the system boundaries to the amount of energy supplied to the load, $\mathrm{E_s}$, over the same period [24]. This metric enables a comparison of GWP footprints of the energy supplied from differing system configurations. To apply this methodology to a CS, a generalization of this methodology is carried out, which includes the grid connection. Some useful intermediate quantities are introduced to capture the additional complexity of a time-variant carbon intensity of the grid energy.

Grid Energy Consumption (GEC) emissions. The Grid Energy Consumption (GEC) emissions are defined as the emissions attributable to the load for the end-use consumption of grid energy. The GEC emissions at time t, $\varepsilon_{t\mathrm{GEC}}$, are calculated as the product of $\mathrm{CI_t^{gr}}$, $\mathrm{P_t^{gr,load}}$, and Δt (Eq. (25)). The total GEC emissions, $\varepsilon^{\mathrm{GEC}}$, are obtained by integrating Eq. (25) with respect to time over the entire simulation period.

$$\varepsilon_t^{GEC} = CI_t^{gr} \times P_t^{gr,load} \times \Delta t \tag{25}$$

Discharge Energy Consumption (DEC) emissions. The DEC emissions are defined as the emissions attributable to the load for the end-use consumption of energy discharged from the BESS. The DEC emissions at time t, $\varepsilon_{t\mathrm{DEC}}$, are calculated as the product of the SOCI, $\mathrm{P_t^{dch}}$, and Δt (Eq. (26)). The total DEC emissions, $\varepsilon^{\mathrm{DEC}}$, are obtained by integrating Eq. (26) with respect to time over the entire simulation period.

$$\varepsilon_t^{DEC} = SOCI_t \times P_t^{dch,load} \times \Delta t \tag{26}$$

Load Energy Consumption (LEC) emissions. The Load Energy Consumption (LEC) emissions for the load at time t, $\varepsilon^{\mathrm{LEC_t}}$, are defined as the sum of the emissions attributable to the end-use consumption of energy originating from the grid section, the BESS, and other local generators (see Eq. (27)). $\mathrm{CI_t^{PV}}$ is zero at all times, as the production and EOL phase emissions are fully included in the system boundaries. The total LEC emissions for the load over the entire simulation period, $\varepsilon^{\mathrm{LEC}}$, are the sum of the total GEC and the DEC emissions.

$$\varepsilon_t^{LEC} = \varepsilon_t^{GEC} + \varepsilon_t^{DEC} \tag{27}$$

With the help of the above quantities, $\varepsilon^{\mathrm{load}}$, can be obtained. The quantity LEES is calculated as follows (Eq. (28)).

$$LEES = \frac{\varepsilon^{load} + \varepsilon^{BESS} + \varepsilon^{PV} + \varepsilon^{gr}}{E_s} \tag{28}$$

2.7. Emissions balance within system boundaries

At time t, an emissions balance for the CS is formulated (Eq. (29)). The left-hand side represents the physical emissions attributable to energy drawn from the grid. The emissions listed on the right-hand side are the grid section and BESS operation phase emissions and the LEC emissions. This emissions balance is depicted in Fig. 3.

$$P_t^{gr} CI_t^{gr} \Delta t = \varepsilon_t^{gr,op} + \varepsilon_t^{ch,op} + \varepsilon_t^{dch,op} + \varepsilon_t^{GEC} + \varepsilon_t^{DEC} \tag{29}$$

2.8. Energy management

The Energy Management System (EMS) regulates the energy flows among all the components present at the CS site by continuously calculating power targets for each component. The energy flows at the CS location are simulated with two EMS strategies. A baseline rule-based strategy is compared with an advanced strategy deploying rolling-horizon optimization to minimize operation phase emissions. These strategies are discussed in this section.

GCS. This rule-based operation strategy draws power from the grid to meet the power demand of the load. On reaching grid capacity, residual load, if any, is met by power discharged from the BESS (Eq. (30)). The BESS is charged with its maximum rated power as soon as grid capacity is available (Eq. (31)). The strategy attempts to maintain the BESS in a fully-charged state (SOC = 1). No other factors are taken into account in the decision to charge or discharge. The GCS strategy can also prioritize direct consumption of local PV power generation in scenarios with local PV generation. Surplus PV power generation is used to charge the BESS, while the rest is curtailed. Power is discharged from the BESS to meet demand when grid capacity is reached.

$$(P_t^{PV,load}) + P_t^{gr,load} + P_t^{dch,load} = P_t^{load} \tag{30}$$

$$P_t^{ch} = (P_t^{PV,ch}) + P_t^{gr,ch} \tag{31}$$

The power flows among the CS, the grid, and the BESS with the GCS strategy for an exemplary summer week without and with local PV generation are depicted in Fig. 4.

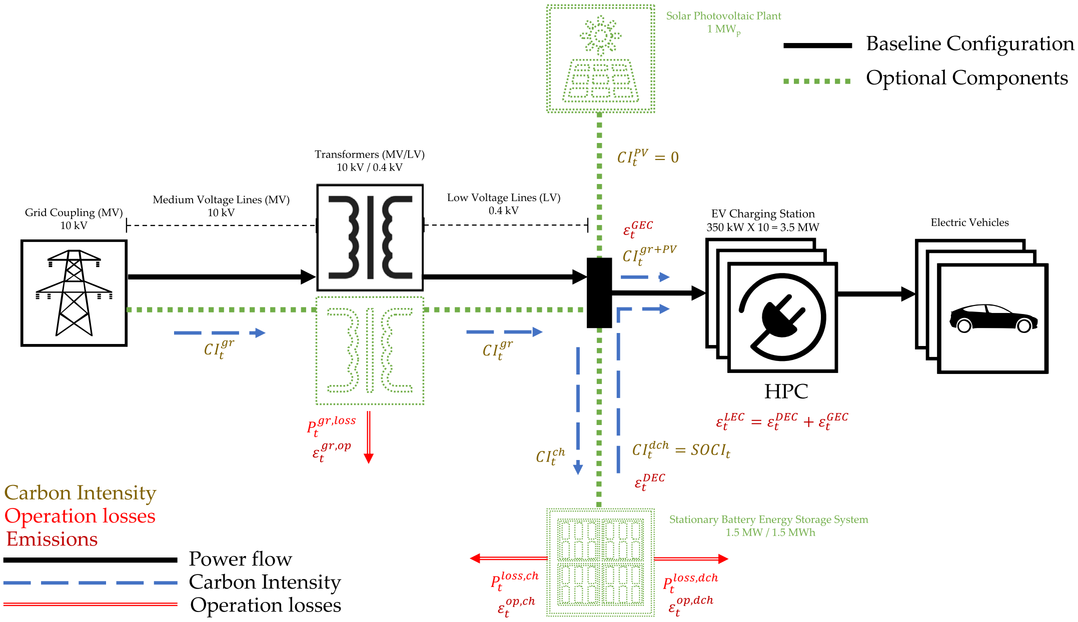

Fig. 3. Emissions balance across the system boundaries for the charging station in the most general case.

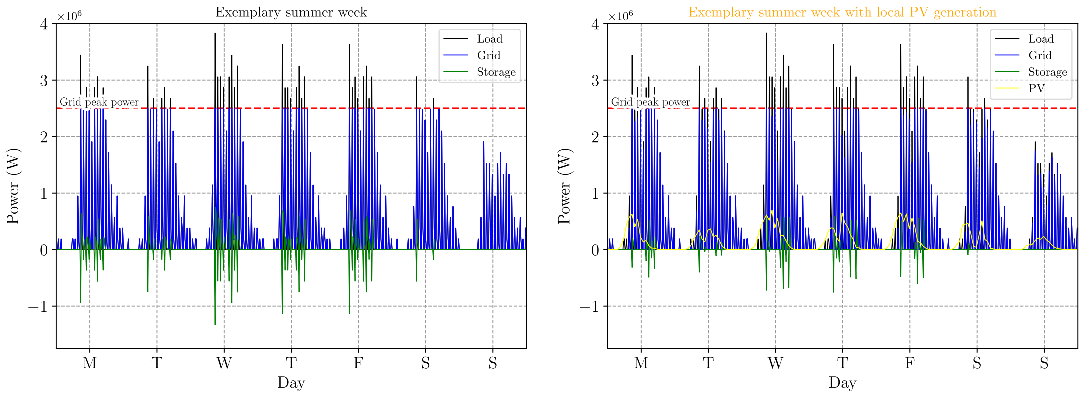

Fig. 4. Regulation of power flow among the Charging Station (CS), grid, and the BESS with the Greedy Charging Strategy (GCS) operation strategy without (left), and with local PV generation (right) for an exemplary summer week. (-) power for the BESS represents discharging, and vice-versa.

Optimal Charging Strategy (OCS). This operation strategy implements a rolling horizon linear optimization approach to minimize the operation emissions of the system setup over each optimization horizon. This optimization approach to achieve energy management has been effectively used in previous studies in this area [53]. A necessary constraint is the mandatory zero load-loss condition — i.e. the power demand at the CS must be met at all instants of time. With forecasts for CI_t^{gr}, P_t^{load}, and P_t^{PV} (if available) over each optimization horizon, the strategy generates a series of power targets for each of the components. For each horizon h, a linear programming optimization problem with an objective function to minimize the left-hand side of the emissions balance is solved (Eq. (32)). The optimal power targets are passed to the detailed component models, and the state variables such as the SOC, SOH from the previous run are updated in the optimizer. The optimization is then rerun for the next horizon, until the end of the simulation period is reached.

$$\min \sum_{t=t}^{t+h} [P_t^{gr} CI_t^{gr}] \tag{32}$$

The optimization is subject to the following constraints in each h. The power drawn from the grid (P_t^{gr}) and the power supplied by the local PV generation, P_t^{PV}, may not exceed their peak power (P_{peak}^{gr}) and present peak generation ($P_{t,peak}^{PV}$) respectively.

$$P_t^{gr} \le P_{peak}^{gr} \tag{33}$$

$$(P_t^{PV} \le P_{t,peak}^{PV}) \tag{34}$$

$$P_t^{gr} + P_t^{dch} + (P_t^{PV}) = P_t^{load} + P_t^{ch} \tag{35}$$

Owing to its relative simplicity and low computational effort, a so-called *bucket model* or the *Energy Reservoir Model* is used to model the BESS and its constraints [54]. b_t^{BESS} is a binary variable used to permit

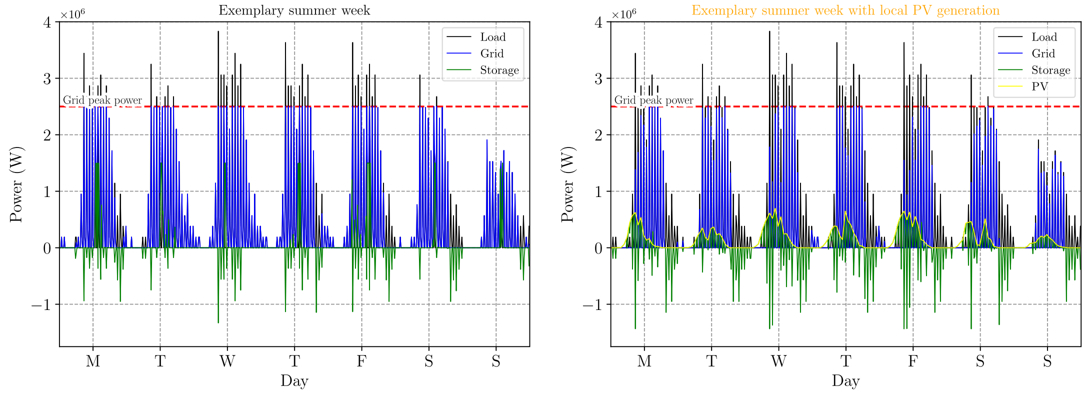

Fig. 5. Regulation of power flow among the Charging Station (CS), grid, and the BESS with the Optimal Charging Strategy (OCS) operation strategy without (left), and with local PV generation (right) for the exemplary summer week. (-) power for the BESS represents discharging, and vice-versa.

either charging (= 1), or discharging (= 0) at time t, and not both simultaneously.

$$P_t^{ch} - b_t^{BESS} \times P_{peak}^{BESS} \leq 0 \tag{36}$$

$$P_t^{dch} + (b_t^{BESS} - 1) \times P_{peak}^{BESS} \leq 0 \tag{37}$$

$$0 \leq SOC_t \leq 1 \tag{38}$$

$$SOC_{t-1} \times E_t^{BESS} + (P_t^{ch} \times \eta_{ch} - \frac{P_t^{dch}}{\eta_{dch}}) \times \Delta t = SOC_t \times E_t^{BESS} \tag{39}$$

$$P_t^{ch} \times \eta_{ch} \times \Delta t \leq \left(1 - SOC_{t-1}\right) \times E_t^{BESS} \tag{40}$$

$$\frac{P_t^{dch}}{\eta_{dch}} \times \Delta t \leq SOC_{t-1} \times E_t^{BESS} \tag{41}$$

Power flows among the CS, the grid, and the BESS with the OCS strategy for an exemplary summer week without and with local PV generation are depicted in Fig. 5.

3. Simulation setup and discussion of results

The operation of the CS is simulated over a period of 20 years in four scenarios with BA. The energy flows and the emissions attributable to all components over the simulation period are calculated. The LEES value for the energy supplied by the energy system to the load in each scenario is obtained from the simulation results. For reference, two scenarios with GR are also simulated, and are discussed towards the end of this section. The summarized results for all scenarios have been tabulated in Table 10.

3.1. Battery Assistance (BA) and local renewable generation

Four system scenarios with BA have been simulated, corresponding to the two EMS strategies, each simulated with and without local PV generation (Table 6). The choice of the EMS strategy influences the LEES of the energy supplied by the energy system to the chargers. The results are summarized in Table 7 and graphically depicted in Fig. 10 A.

Table 6
Simulation matrix and list of scenarios for the BA concept.

Simulation matrix BA			
Scenario ID	Operation strategy	On-site PV generation	Scenario name
1	GCS	No	BA GCS
2	OCS	No	BA OCS
3	GCS	Yes	BA GCS PV
4	OCS	Yes	BA OCS PV

In scenario 1, the solution BA is simulated at the CS location with the GCS strategy. The evolution of the values of the SOC, the SOCI, and the CI_t^{gr} for an exemplary winter and summer week each are depicted in Fig. 6 A and B. Energy is supplied to the chargers with a LEES of $0.4702\,kgCO_2eq\,kWh^{-1}$. The most significant contributor to this value is ε^{GEC}. The second largest contribution is ε^{DEC}. The operation phase emissions of the grid section, $\varepsilon^{gr,op}$, contribute the third largest share. While the BESS operation phase emissions, $\varepsilon^{BESS,op}$, account for the second lowest contribution, the BESS production phase emissions, $\varepsilon^{BESS,prod}$, are responsible for the smallest contribution to the LEES. The BESS is cycled for over 3635 EFCs with $\overline{DOC} = 0.11$ and $\overline{SOC} = 0.99$. Over the simulation period, this leads predominantly to calendric aging of the cells, with a small share of cyclic aging. The cells are estimated to still possess over 69% of the original capacity (Fig. 8).

In scenario 3, local PV generation is combined with scenario 1. Values of SOC, SOCI, and CI_t^{gr} for the exemplary winter and summer weeks are depicted in Fig. 6 C and D. Incorporation of PV generation leads to a lower LEES of $0.4336\,kgCO_2eq\,kWh^{-1}$. ε^{GEC} makes up the largest portion of the LEES value. There is a marked reduction in ε^{GEC} due to the direct consumption of PV power generation. $\varepsilon^{gr,op}$ is the second largest contributing category. These emissions are higher than those in scenario 1 despite the lower amount of energy drawn from the grid. This can be attributed to the shift in the time of charging of the BESS. The production phase emissions of the PV system come in at third, followed by ε^{DEC} in the fourth place. The BESS production phase emissions make up the fifth largest contribution to the LEES, with $\varepsilon^{BESS,op}$ making the least impact. The drastic drop in both ε^{DEC} and $\varepsilon^{BESS,op}$ is anticipated as PV power is also used to charge the BESS. The $\overline{SOCI}$ decreases from 422.59 g $CO_2eq\,kWh^{-1}$ in scenario 1 to 328.46 g CO_2eq/kWh^{-1} in scenario 3, which corroborates this finding. Despite the additional production phase emissions of the PV system, and the increase in $\varepsilon^{gr,op}$, lower values of ε^{GEC}, ε^{DEC}, and $\varepsilon^{BESS,op}$ drive a net reduction in the LEES value. If grid feed-in of the curtailed PV generation were to be permitted, 11.99 GW h of energy can be exported to the grid over the simulation period of 20 years. Based on the capacity factor for the location, and an estimated lifetime of 20 years for the PV system, PV power generation has a carbon intensity of $56.81\,gCO_2eq\,kWh^{-1}$ based on the calculated production and EOL phase footprints. The feed-in of surplus power can result in a further reduction of emissions to the tune of $681.18\,tCO_2eq$. These emissions can potentially be excluded from the system boundaries and be allocated to grid consumers elsewhere. This can reduce the value of LEES by a further $0.0104\,kgCO_2eq\,kWh^{-1}$.

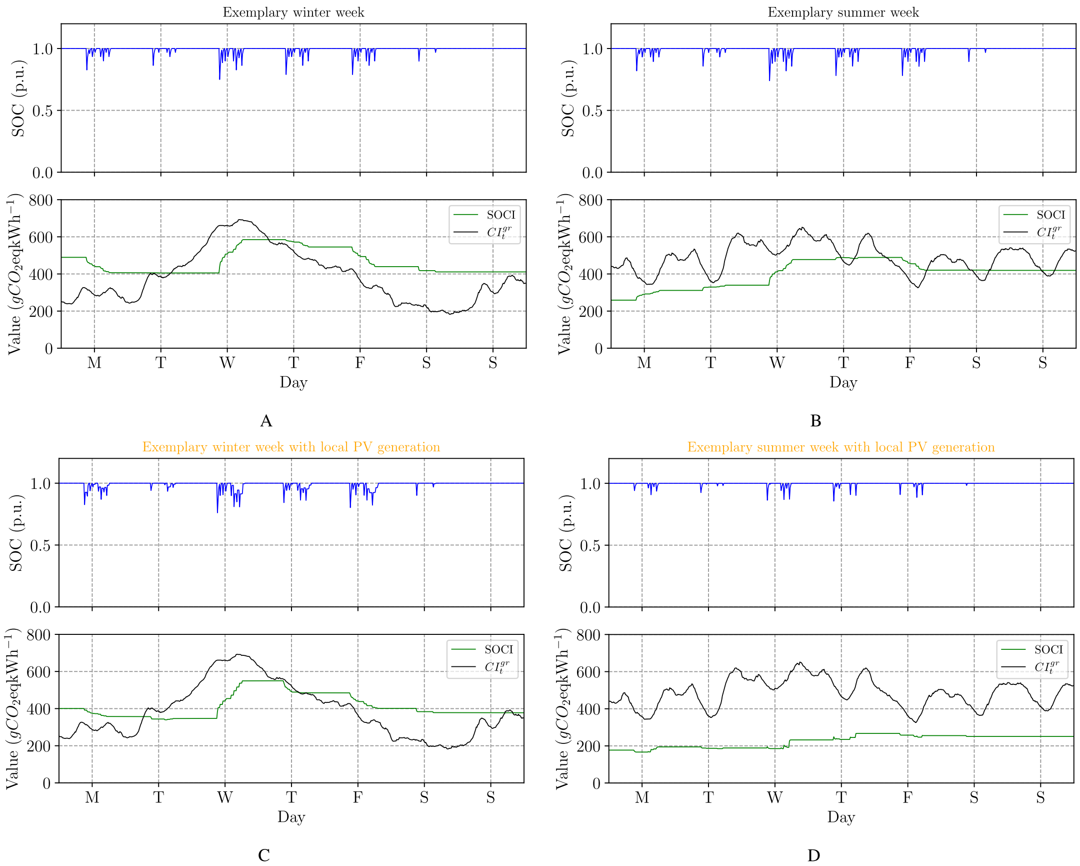

Fig. 6. A, B: State of Charge (SOC) and State of Carbon Intensity (SOCI) evolution with respect to time for the Greedy Charging Strategy (GCS) operation strategy (scenario 1) for an exemplary winter and summer week respectively. C, D: State of Charge (SOC) and State of Carbon Intensity (SOCI) evolution with respect to time for the GCS strategy with local PV generation (scenario 3) for an exemplary winter and summer week respectively.

Due to the availability of the additional PV power generation, the instances of grid capacity being reached are fewer, and consequently, the number of EFCs experienced by the BESS are also lower at 2310, as compared to 3635 in scenario 1. The degradation of the BESS in this scenario is primarily calendric in nature. A high $\overline{SOC} = 0.99$ with gentler cyclization ($\overline{DOC} = 0.03$) and a lower number of cycles explains a comparably high calendric aging as scenario 1, coupled with lower cyclic aging (Fig. 8).

In scenario 2, the BA solution is simulated with the OCS strategy. Fig. 7 A and B present the values of SOC, SOCI, and CI_t^{gr} over exemplary winter and summer weeks respectively. The LEES of the supplied energy in this case is 0.4581 kg CO_2eqkWh^{-1}, which is over 2.5% lower than that of scenario 1. The value of ε^{GEC}, while still being the largest contributing category, is lower than in scenario 1, as the OCS strategy actively charges the BESS with low-CI_t^{gr} grid energy, and avoids drawing energy from the grid when CI_t^{gr} is high. This is in contrast to the GCS strategy, which focuses solely on function fulfilment (see Fig. 9 A, B). Consequently, a greater amount of grid energy is routed to the load over the BESS, and leads to a larger ε^{DEC} value, which is the second biggest contributor. The larger BESS energy throughput of nearly 51% does not cause a correspondingly large increase in ε^{DEC} as $\overline{SOCI}$ is lowered from 422.59 g CO_2eqkWh^{-1} to 345.81 g CO_2eqkWh^{-1} (Fig. 9 E, G). The raised energy throughput of the BESS leads to a slightly higher value of $\varepsilon^{gr,op}$ and $\varepsilon^{BESS,op}$, which contribute the third and fourth largest shares respectively. $\varepsilon^{BESS,prod}$ is the category with the least impact. Higher values of ε^{DEC}, $\varepsilon^{gr,op}$, and $\varepsilon^{BESS,op}$ are offset by a lower ε^{GEC}. The BESS cyclization is higher in scenario 2 with nearly 5642 EFCs as compared to over 3635 EFCs in scenario 1. Higher cyclization leads to stronger cyclic aging in scenario 2, but to a milder calendric aging, as the lower $\overline{SOC}$ value of 0.46, as compared to nearly 0.99 in scenario, 1 decelerates the rate of calendric degradation (Fig. 8).

In scenario 4, scenario 2 is augmented with local PV generation. Fig. 7 C and D illustrate the values of SOC, SOCI, and CI_t^{gr} over the exemplary winter and summer week respectively. With this configuration, a low value of LEES = 0.3571 kgCO_2eqkWh^{-1} is achieved, corresponding to a reduction of over 22% with respect to scenario 2. The biggest contributing category is ε^{GEC}, which is lower than in scenarios 1, 2, and 3. This is attributed to over 93% lower curtailment of PV generation than in scenario 3. The energy discharged by the BESS is over 141% higher than in scenario 1. The second largest emissions category is $\varepsilon^{PV,prod}$. $\varepsilon^{gr,op}$ makes up for the third largest emissions category. ε^{DEC}, $\varepsilon^{BESS,prod}$, and $\varepsilon^{BESS,op}$ make for the three lowest contributions to the LEES. As the BESS is charged optimally with both low-CI_t^{gr} grid energy and PV power generation, a reduction in ε^{DEC} is observed with respect to scenarios 1, 2, 3. The drop in ε^{DEC} and $\varepsilon^{BESS,op}$ can also be discussed in relation to the value of $\overline{SOCI}$, which decreases to a low value of 80.64 gCO_2eqkWh^{-1} (see Figs. 9 D and 9 F, H). In case of feed-in of the curtailed PV generation, 0.77 GW h of energy can be exported to the grid, resulting in an emissions reduction of 43.75 tCO_2eq, which corresponds to a LEES reduction of 0.0006 kgCO_2eqkWh^{-1}. The BESS cyclization is much more intense as compared to all other scenarios. With over 9020 EFCs at $\overline{DOC}$= 12.58%, the amount of capacity lost

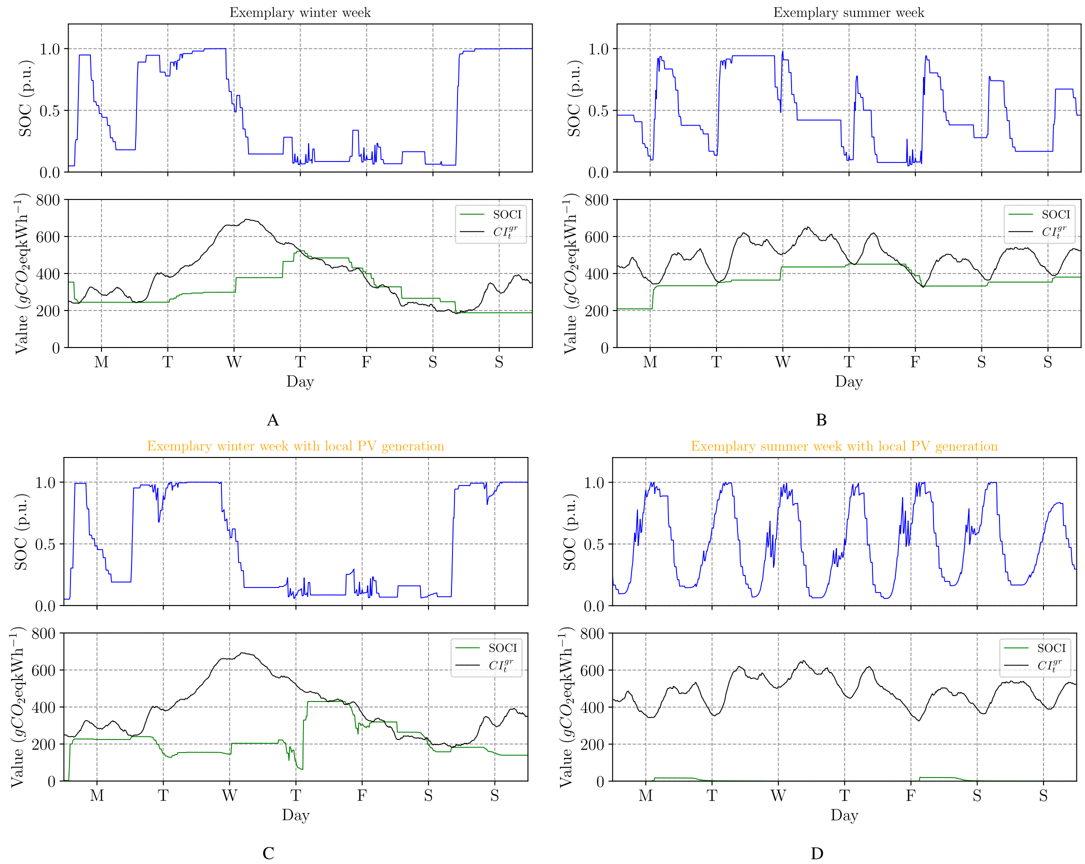

Fig. 7. A, B: State of Charge (SOC) and State of Carbon Intensity (SOCI) evolution with respect to time for the Optimal Charging Strategy (OCS) operation strategy (scenario 2) for an exemplary winter and summer week respectively. C, D: State of Charge (SOC) and State of Carbon Intensity (SOCI) evolution with respect to time for the OCS strategy with local PV generation (scenario 4) for an exemplary winter and summer week respectively.

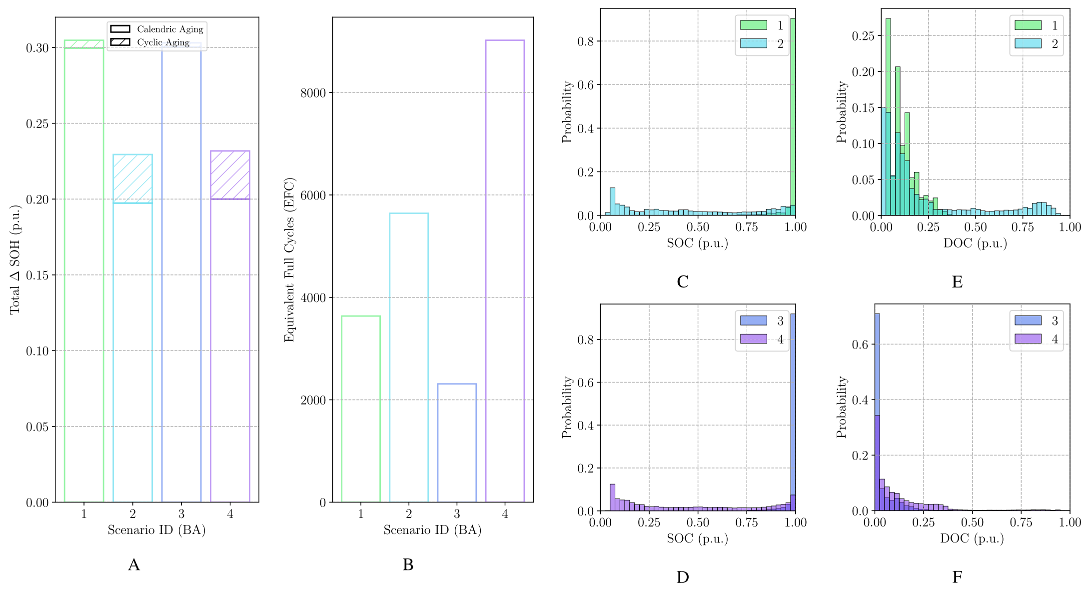

Fig. 8. A: Change in SOH and shares of calendric and cyclic aging in the four BA scenarios. B: EFCs faced by the BESS in each BA scenario. C and D: Distributions of SOC in scenarios 1,2 and 3,4 respectively. E and F: Distributions of DOC in scenarios 1,2 and 3,4 respectively.

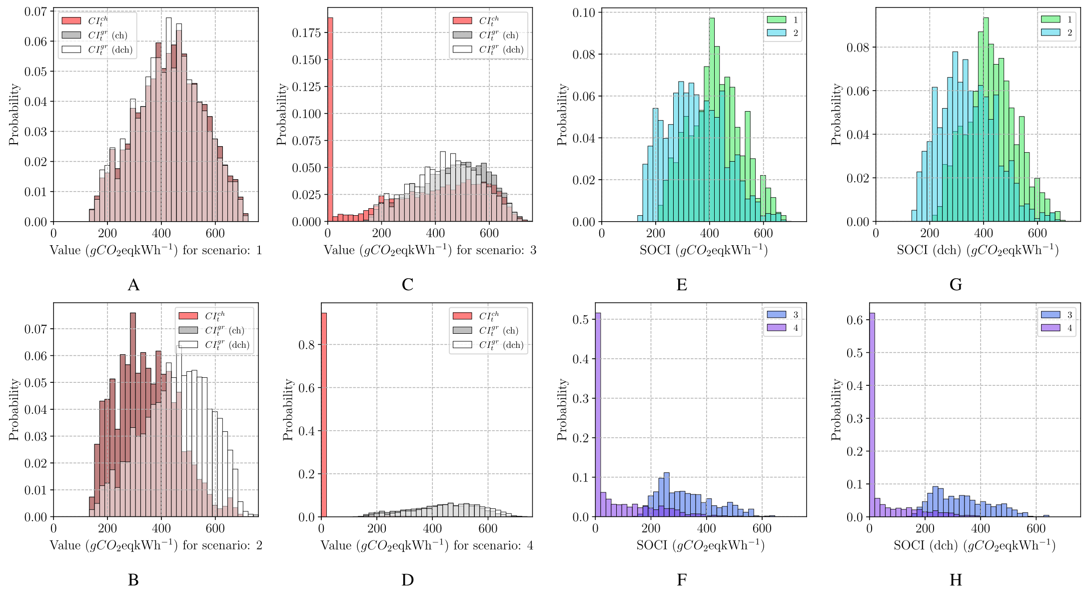

Fig. 9. A, B, C, D: Depictions of distributions of $\mathrm{CI}_t^{\mathrm{ch}}$, $\mathrm{CI}_t^{\mathrm{gr}}$ during charging and $\mathrm{CI}_t^{\mathrm{gr}}$ during discharging in each of the BA scenarios 1, 2, 3, and 4 respectively. E, F: Distributions of State of Carbon Intensity (SOCI) in scenarios 1, 2, and in scenarios 3, 4 respectively. G and H: Distributions of SOCI during discharging in scenarios 1, 2, and in scenarios 3, 4 respectively.

to cyclic aging is higher than in scenarios 1 and 2. However as $\overline{\mathrm{SOC}}$ remains low at over 0.46, calendric aging is much milder than in scenarios 1 and 3, leading to a lower total capacity loss (Fig. 8).

To investigate the sensitivity of the effect of energy storage capacity of the BESS, a variant of scenario 2 with 2.5 MW h of storage capacity is simulated. The LEES reduces marginally vis-á-vis scenario 2 by over 1% to $0.4529\,\mathrm{kgCO_2}eq\mathrm{kWh}^{-1}$. Two variants (i and ii) of scenario 4 are also simulated to determine the sensitivity of energy storage capacity and peak PV power respectively. Scenario 4i is simulated with 2.5 MW h of storage capacity, everything else remaining constant, whereas scenario 4ii is simulated with $2\,\mathrm{MW}_p$ of peak PV power, with all other parameters remaining unchanged. The LEES values for these additional scenarios are $0.3476\,\mathrm{kgCO_2}eq\mathrm{kWh}^{-1}$ and $0.3103\,\mathrm{kgCO_2}eq\mathrm{kWh}^{-1}$ respectively. Relative to scenario 2, this corresponds to a further reduction of over 2% and 10% respectively on top of the reduction observed in scenario 4. If feed-in of the surplus power generation were to be considered, further reductions of $0.0003\,\mathrm{kgCO_2}eq\mathrm{kWh}^{-1}$ and $0.0085\,\mathrm{kgCO_2}eq\mathrm{kWh}^{-1}$ in the respective LEES values can be expected. These results point to a diminishing ability of additional capacities of both the BESS and the PV system at reducing the LEES.

3.2. Comparison with Grid Reinforcement (GR)

For context, two scenarios with GR have been simulated (see Table 8). The values for LEES for each of the simulated scenarios are summarized in Table 9 and visually depicted in Fig. 10 B. Additional lines and transformers are installed in parallel to augment power transmission capacity [55,56]. The original power transmission capability of the grid section is 2.5 MW at the CS location, excluding losses. Additional line capacities are installed in the MV and LV sections, doubling the cross-section in the MV section, and increasing the LV cross-section by 50%. Two additional transformers are also installed to handle the increased power demand. Maximum line and transformer loadings of 80% and line voltage drops of 5% are permitted for determining additional capacities for GR. Values for $\varepsilon^{\mathrm{gr,prod}}$ and $\varepsilon^{\mathrm{gr,EOL}}$ for the reinforced grid section are listed in the appendix (Tables 11 and 12). As $\varepsilon^{\mathrm{gr,prod}}$ and $\varepsilon^{\mathrm{gr,op}}$ are functions of the grid section length, these can generally be expected to rise with the length of the grid section.

Table 7
Simulation results for Battery Assistance (BA) scenarios.

Simulation results BA				
Parameter	Scenario			
	1	2	3	4
Charging station				
Grid energy (GWh)	69.58	70.29	61.07	51.51
Δ% (rel. to 1)	–	1.0	−12.2	−26.0
Discharged energy (GWh)	4.98	7.51	3.18	12.02
Δ% (rel. to 1)	–	50.8	−36.2	141.4
PV Energy (GWh)	–	–	20.00	20.00
Curtailment (GWh)	–	–	11.99	0.77
Δ% (rel. to 3)	–	–	–	−93.6
LEES ($\mathrm{kgCO_2eq/kWh}$)	0.4702	0.4581	0.4338	0.3571
Δ% (rel. to 1)	–	−2.6	−7.7	−24.1
BESS				
Round-trip efficiency (%)	85.33	82.85	85.56	83.15
Remaining capacity (%)	69.52	77.06	69.69	76.82
$\overline{\mathrm{SOC}}$	0.99	0.46	0.99	0.46
$\overline{\mathrm{DOC}}$	0.11	0.22	0.03	0.13
EFCs	3635	5642	2310	9020
$\overline{\mathrm{SOCI}}$ ($\mathrm{gCO_2eq/kWh}$)	422.59	345.81	328.46	80.65

Table 8
Simulation matrix and list of scenarios for the Grid Reinforcement (GR) concept.

Simulation matrix GR			
Scenario ID	Operation strategy	On-site PV generation	Scenario name
I	None	No	GR
II	PV priority	Yes	GR PV

In scenario I, the CS is augmented with GR on the grid section connecting to the nearest point of sufficient power transmission capacity. $\varepsilon^{\mathrm{GEC}}$ is the largest contributing category to the LEES value of $0.4615\,\mathrm{kgCO_2}eq\mathrm{kWh}^{-1}$. The second largest contributor is $\varepsilon^{\mathrm{gr,op}}$. $\varepsilon^{\mathrm{gr,prod}}$ contributes the smallest share.

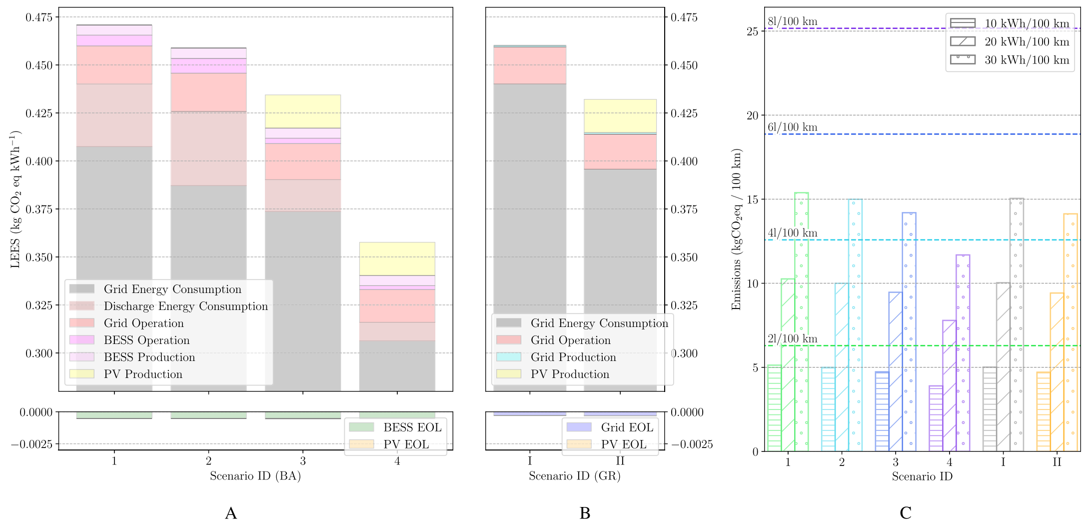

Fig. 10. A: Breakdown of Levelized Emissions of Energy Supply (LEES) values for Battery Assistance (BA) scenarios 1–4 into the constituent emissions categories. B: Breakdown of Levelized Emissions of Energy Supply (LEES) values for Grid Reinforcement (GR) scenarios I and II into the constituent emissions categories. C: Energy consumption emissions for EVs for energy from the six CS configurations with respect to three energy-consumption levels.

Table 9
Simulation results for Grid Reinforcement (GR) scenarios.

Simulation results GR		
Parameter	Scenario	
	I	II
Charging station		
Grid energy (GWh)	68.62	61.11
Δ% (rel. to I)	–	−10.95
PV Energy (GWh)	–	20.00
Curtailment (GWh)	–	12.67
LEES ($kgCO_2eq/kWh$)	0.4599	0.4317
Δ% (rel. to I)	–	−6.13

In scenario II, local PV power generation is combined with scenario I. The EMS prioritizes the consumption of PV power generation and the residual load is covered with grid power. The LEES in this case reduces to 0.4317 $kgCO_2eq kWh^{-1}$ (reduction of over 6.4%). ε^{GEC} retains its position as the largest contributor to the LEES value. ε^{GEC} is lower than in scenario I, as the PV power generation is able to offset some of the energy drawn from the grid. The energy drawn from the grid is around 11% lower. The second largest contributor is $\varepsilon^{gr,op}$. $\varepsilon^{PV,prod}$ makes up the third largest category. $\varepsilon^{gr,prod}$ has the lowest impact on the LEES. The introduction of $\varepsilon^{PV,prod}$ is offset by a lower ε^{GEC}, leading to a net reduction in the LEES. If grid feed-in of the curtailed PV generation were to be permitted, 12.67 GW h of energy can be exported to the grid. This can result in a further reduction of 719.66 tCO_2eq of emissions, leading to a potential LEES reduction of 0.0109 $kgCO_2eq kWh^{-1}$.

To investigate the sensitivity of the peak PV power on the LEES, a variant of scenario II with 2 MW_p is simulated. The LEES reduces to 0.4170 $kgCO_2eq kWh^{-1}$ (further reduction of nearly 1.5% on top of that achieved in scenario II). A further reduction of 0.0237 $kgCO_2eq kWh^{-1}$ can be achieved if the surplus energy were to be fed into the grid.

3.3. Effect on EV energy consumption emissions

The results presented so far can be translated into real terms by associating them to the energy consumption emissions of EVs. A portion of the energy supplied to the high-power chargers is lost in the power electronics and other auxiliary systems. For the sake of simplicity, only the losses in the power electronics units of the chargers have been estimated. These losses amount to over 8% of the total energy supplied to the chargers. The LEES value of the energy flowing to the EV battery packs from the chargers can be further adjusted to internalize these losses. We define three EV energy economy scenarios:

1. High: 10 kW h/100 km
2. Moderate: 20 kW h/100 km
3. Low: 30 kW h/100 km

With energy from each of the six simulated CS configurations, the emissions per 100 km for each of the three EV scenarios have been calculated. These eighteen values are depicted in Fig. 10 C. For reference, well-to-wheel emissions per 100 km for petrol/gasoline-powered internal combustion engine vehicles are also calculated [57,58]. These values are calculated for fuel economy values of 2–8 l/100 km. An EV with Low energy economy, and charged with energy from scenario 1, would cause the highest emissions among these eighteen cases. This value is nevertheless lower than the emissions per 100 km for a 'fuel-efficient' petrol-powered vehicle with a fuel economy of 6 l/100 km. In contrast, the emissions per 100 km for the same EV, charged with energy from scenario 4, are less than those caused by an ultra-efficient petrol-powered vehicle with a fuel economy of 4 l/100 km.

These analyses do not consider the entire life cycle of the EV and of the internal combustion engine vehicle, and pertain solely to the GWP footprints of the energy consumed per 100 km driven. These values are only indicative, as they do not include the GWP footprints of the chargers and the existing grid infrastructure. The well-to-wheel values also do not include the entire distribution infrastructure and equipment.

4. Conclusion and outlook

A mathematical model to compute the GWP footprint for Electric Vehicle (EV) High-Power Charging (HPC) with Battery Assistance (BA) has been presented in this work. A necessary expansion and generalization of the LEES methodology has been undertaken to include the grid connection. Some useful quantities have been defined to aid this extended methodology. These quantities are the Grid Energy Consumption (GEC), Discharge Energy Consumption (DEC), and the Load Energy Consumption (LEC) emissions. A new state variable for the BESS — the

Table 10
Category-wise breakdown of Levelized Emissions of Energy Supply (LEES) values for energy from Charging Station (CS) configurations in the six considered scenarios.

Levelized Emissions of Energy Supply (LEES)						
	Scenario					
	1	2	3	4	I	II
LEES ($kgCO_2eq kWh^{-1}$)	0.4702	0.4581	0.4338	0.3571	0.4599	0.4317
Emissions (tCO_2eq)	30931	30135	28536	23487	30253	28400
Emissions category	Category-wise Breakdown (%)					
Grid Energy Consumption	86.65	84.51	86.13	85.78	95.69	91.65
Discharge Energy Consumption	6.94	8.45	3.83	2.71	0.00	0.00
Grid Operation	4.21	4.33	4.33	4.77	4.19	4.22
BESS Operation	1.19	1.68	0.64	0.57	0.00	0.00
BESS Production	1.12	1.15	1.22	1.48	0.00	0.00
Grid Production	0	0	0	0	0.19	0.20
PV Production	0	0	3.99	4.85	0.00	4.01
BESS EOL	−0.11	−0.12	−0.12	−0.15	0.00	0.00
Grid EOL	0	0	0	0	−0.06	−0.07
PV EOL	0	0	−0.01	−0.01	0.00	−0.01
Total	100	100	100	100	100	100

State of Carbon Intensity (SOCI), has been introduced. This metric acts as an indicator of the carbon intensity of the charging energy since the last fully-discharged state. A lower value of the SOCI translates to lower $\varepsilon^{\mathrm{BESS,op}}$ and $\varepsilon^{\mathrm{DEC}}$ values. It can be loosely construed as representing the 'carbon-quality' of the charging energy — the lower the value, the higher the 'carbon-quality'.

Integration of on-site PV generation lowers the LEES of the supplied energy in all cases with respect to a comparable scenario without local PV generation. The decarbonization potential of local PV generation will be greater in locations with a higher number of hours of sunshine and solar irradiation, as compared to Berlin, Germany. The choice of the EMS strategy strongly influences the LEES. While it is possible to successfully meet the requirements of the peak-shaving service in BA with the baseline rule-based GCS strategy, the optimizer-based OCS strategy can drive down the LEES, both with and without local PV generation. BA offers several apparent advantages, such as speedy and non-disruptive installation.

This study further indicates that with an optimized EMS strategy to minimize emissions and integrate local PV generation, BA can potentially charge EVs with a lower GWP footprint, as compared to GR. A comparison of BA with GR has also been carried out. Under the stated assumptions of this study, over the simulation period of 20 years, the grid integration pathways can be ordered as follows (increasing LEES):

1. BA with OCS and on-site PV generation
2. BA with GCS and on-site PV generation
3. GR with on-site PV generation
4. BA with OCS
5. GR
6. BA with GCS

Thus, deploying a BESS to provide BA for EV HPC can provide some significant benefit in terms of emissions reduction, if and only if an optimal EMS strategy is used. Effective energy management can fully leverage the flexibility offered by energy storage in the form of temporal offsetting of the consumption of low-carbon energy. BA coupled with local renewable power generation can unlock significantly higher savings in emissions while charging EVs. An important caveat pertaining to this order of grid pathways is that it is subject to the chosen location, its electricity grid, and the charging load profile. To conduct future studies, the steps laid out in the present work must be carried out with location-specific data. With increasing grid penetration of renewable generation and grid-connected energy storage, the carbon intensity of the grid is expected to sink further. The potential to bring about a local reduction in LEES of the CS site using BA will reduce, as this role will increasingly be filled-in by grid-connected storage systems. As demonstrated in a previous work, the decarbonization potentials of energy storage and renewable generation diminish with each additional unit of installed capacity [33].

Follow-up studies in this area could build upon the methods and findings of the present study. The $\mathrm{CI}_t^{\mathrm{gr}}$ profile is assumed to be invariable over the simulation period of 20 years. Scenarios with projections for installed capacities of participating technologies in the German energy mix could be developed to update this profile. Carbon intensity profiles for electricity grids of other nations and regions with their own generation technology mixes can also be developed and used to conduct further analyses. Enabling feed-in of curtailed power can potentially further reduce the LEES values, the extent of this reduction has been discussed in Section 3. Reinforcement of grid sections with overhead cables has lower production and installation footprints. But, as $\varepsilon^{\mathrm{gr,prod}}$ makes up for a small portion of the LEES value for each scenario, no substantial movement in the results is anticipated. The simulation duration of 20 years is assumed to be equal to the lifetimes of all components. A proportionate reduction in the production and EOL phase footprints for the components might be a valid solution to account for longer lifetimes, but these actions do not change the nature of the results, and will lead to a slight adjustment in the LEES values.

CRediT authorship contribution statement

Anupam Parlikar: Conceptualization, Methodology, Data curation, Software, Formal analysis, Investigation, Visualization, Writing – original draft, Editing. **Maximilian Schott:** Methodology, Data curation, Software, Writing – review. **Ketaki Godse:** Methodology, Software, Writing – review. **Daniel Kucevic:** Methodology, Data curation, Writing – review. **Andreas Jossen:** Funding acquisition, Resources, Supervision, Writing – review. **Holger Hesse:** Funding acquisition, Formal analysis, Visualization, Supervision, Writing – review & editing.

Declaration of competing interest

The authors declare that they have no known competing financial interests or personal relationships that could have appeared to influence the work reported in this paper.

Data availability

Data will be made available on request.

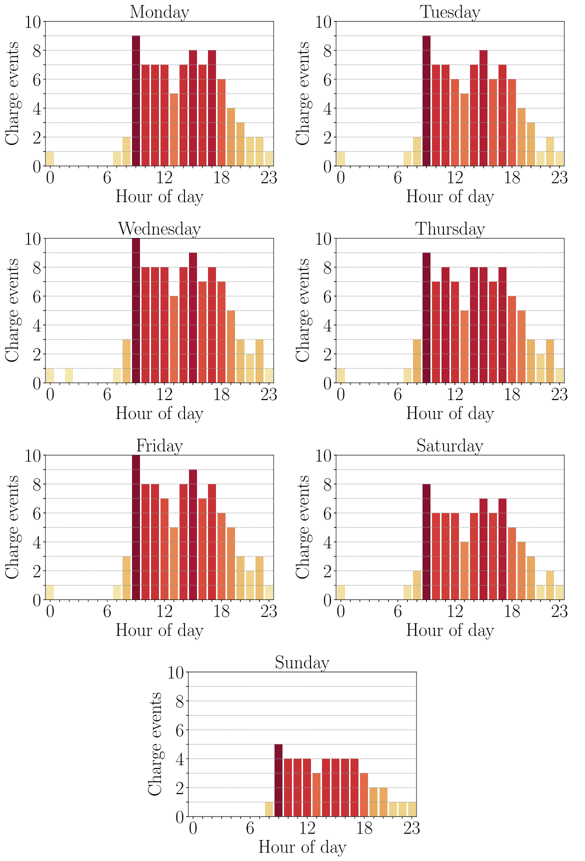

Fig. 11. Hourly charging events on each day at the charging station over the representative week.

Acknowledgements

This research is funded by the German Federal Ministry of Education and Research (BMBF) and the German Federal Ministry for Economic Affairs and Climate Action (BMWK) via the research projects greenBattNutzung (grant number 03XP0302D) and EffSkalBatt (grant number 03ET6148A) respectively. Both the projects are overseen by Project Management Juelich (PtJ).

Appendix A. Charging station synthetic load profile

A synthetic load profile for the charging station has been created based on published data for an EV charging station in Italy [26]. Based on log data spanning over three years, the distributions of hourly charge events for a representative day and total daily charge events for each day of a representative week are presented in this work. By superposing the distribution of charge events from the representative day to each day of the representative week, an hourly charger occupancy profile spanning over a week has been developed. This occupancy has then been adapted to the charging station configuration considered in the present work. Each day of this superposed profile is depicted in Fig. 11.

For each charging event, in order to obtain the power drawn from the chargers by the batteries, two quantities are required — the energy capacity of the incoming EV battery, and the battery SOC on arrival. The battery energy capacity is selected from a normal distribution, whereas the SOC value on arrival is selected from a Weibull distribution. The distribution of EV battery energy capacities is depicted in Fig. 12 (left), while the distribution of battery SOCs on arrival is depicted in Fig. 12 (right). The values for the battery energy capacity lie between 50 kWh and 97 kWh. The SOC values are in the range of 0.05–0.89. Based on these two values, the duration of each charging event is determined. Each charging event is assumed to have been completed when the SOC of the battery reaches 1.0. The power drawn by each charger is summed up at each timestep to yield a cumulative load profile. The resultant synthetic load profile for a week is depicted in Fig. 13.

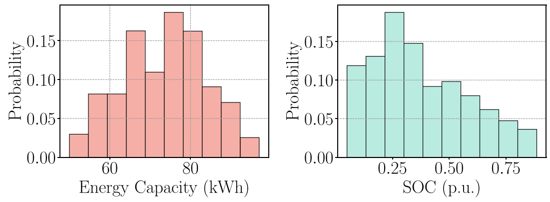

Fig. 12. Left: Distribution of incoming EV battery energy capacities. Right: Distribution of incoming EV battery SOCs on arrival.

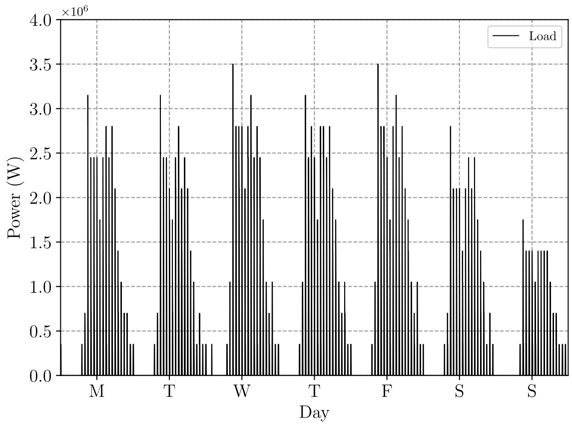

Fig. 13. Cumulative charging station load profile for the representative week considering individual charger occupancies.

Table 11
Streamlined Life Cycle Analysis (LCA) of grid section components. Based on data from [43,59,60].

Grid components streamlined LCA		
Component	Production (kgCO2eq)	End-of-Life (EOL) (kgCO2eq)
Cables MV (per km)	9902.07	−906.81
Transformer MV/LV (per kVA)	22.70	−9.42
Cables LV (per km)	28761.70	−14015.88

Appendix B. Grid components streamlined Life Cycle Analysis (LCA): production and EOL phases

The following tables present a streamlined LCA for the grid components. Table 11 presents the GWP footprints of several grid components corresponding to their production and end-of-life phases. Based on the values presented in Table 11, component-wise GWP footprints corresponding to the production and end-of-life phases of the reinforced grid section can be obtained. These values are tabulated in Table 12.

Table 12
Component-wise streamlined Life Cycle Analysis (LCA) for Grid Reinforcement (GR) configuration.

Grid Reinforcement streamlined LCA					
Component	Parallel units #	Quantity Reinforcement	Unit	Production (kgCO2eq)	End-of-Life (EOL) (kgCO2eq)
Grid coupling power (MW) Baseline: 2.60 Reinforced: 3.98					
Cables MV	1	1.6	km	15843.31	−1450.90
Transformer MV/LV 0.63 kVA	2	1260	kVA	28607.47	−11875.45
Cables LV	9	0.45	km	12942.77	−6307.14
Sum				57393.55	−19633.49
Total				**37760.06**	

References

[1] International Energy Agency. Global EV outlook 2021. 2021, International Energy Agency, Paris, France, URL: https://www.iea.org/reports/global-ev-outlook-2021.

[2] Das HS, Rahman MM, Li S, Tan CW. Electric vehicles standards, charging infrastructure, and impact on grid integration: A technological review. Renew Sustain Energy Rev 2020;120:109618.

[3] Brenna M, Foiadelli F, Leone C, Longo M. Electric vehicles charging technology review and optimal size estimation. J Electr Eng Technol 2020;15(6):2539–52.

[4] F. Rodrigues MT, Son S-B, Colclasure AM, Shkrob IA, Trask SE, et al. How fast can a Li-ion battery be charged? Determination of limiting fast charging conditions. ACS Appl Energy Mater 2021;4(2):1063–8.

[5] Lambert F. Tesla supercharger network reaches new milestone: 30,000 chargers worldwide. 2021, URL: https://electrek.co/2021/11/11/tesla-supercharger-network-new-milestone-30000-chargers-worldwide/.

[6] ABB EV Infrastructure. Specifications ABB terra high power - GEN III. 2021, URL: https://search.abb.com/library/Download.aspx?DocumentID=9AKK107991A9632&LanguageCode=en&DocumentPartId=&Action=Launch.

[7] Siemens AG. Specifications Siemens Sicharge D. 2021, Siemens AG URL: https://assets.new.siemens.com/siemens/assets/api/uuid:10128ff2-4bc0-440b-9cda-a153c2172658/sicharge-d-brochure-en.pdf.

[8] Mathieu L. In: Todts W, editor. Recharge EU: How many charge points will Europe and its member states need in the 2020s. Brussels, Belgium: Transport & Environment; 2020.

[9] Hesse H, Schimpe M, Kucevic D, Jossen A. Lithium-ion battery storage for the grid—A review of stationary battery storage system design tailored for applications in modern power grids. Energies 2017;10(12):2107.

[10] Kucevic D, Tepe B, Englberger S, Parlikar A, Mühlbauer M, Bohlen O, et al. Standard battery energy storage system profiles: Analysis of various applications for stationary energy storage systems using a holistic simulation framework. J Energy Storage 2020;28:101077.

[11] Kucevic D, Englberger S, Sharma A, Trivedi A, Tepe B, Schachler B, et al. Reducing grid peak load through the coordinated control of battery energy storage systems located at electric vehicle charging parks. Appl Energy 2021;295:116936.

[12] Shao C, Qian T, Wang Y, Wang X. Coordinated planning of extreme fast charging stations and power distribution networks considering on-site storage. IEEE Trans Intell Transp Syst 2021;22(1):493–504.

[13] Rafi MAH, Bauman J. A comprehensive review of DC fast-charging stations with energy storage: Architectures, power converters, and analysis. IEEE Trans Transp Electr 2021;7(2):345–68.

[14] Held L, Kramer H, Zimmerlin M, Suriyah MR, Leibfried T, Ratajczak L, et al. Dimensioning of battery storage as temporary equipment during grid reinforcement caused by electric vehicles. In: 2018 53rd international universities power engineering conference. IEEE; 2018, p. 1–6.

[15] Rautiainen A, Rauma K, Rohde L, Supponen A, Raulf F, Rehtanz C, et al. Anatomy of electric vehicle fast charging: Peak shaving through a battery energy storage—A case study from Oslo. IET Electr Syst Transport 2021;11(1):69–80.

[16] Sun B. A multi-objective optimization model for fast electric vehicle charging stations with wind, PV power and energy storage. J Clean Prod 2021;288:125564.

[17] Vermeer W, Chandra Mouli GR, Bauer P. A multi-objective design approach for PV-battery assisted fast charging stations based on real data. In: 2022 IEEE transportation electrification conference & expo. IEEE; 2022, p. 114–8.

[18] Liu G, Xue Y, Chinthavali MS, Tomsovic K. Optimal sizing of PV and energy storage in an electric vehicle extreme fast charging station. In: 2020 IEEE power & energy society innovative smart grid technologies conference. [Piscataway, NJ]: IEEE; 2020, p. 1–5.

[19] Moradzadeh M, Abdelaziz MMA. A new MILP formulation for renewables and energy storage integration in fast charging stations. IEEE Trans Transport Electrification 2020;6(1):181–98.

[20] Yang M, Zhang L, Zhao Z, Wang L. Comprehensive benefits analysis of electric vehicle charging station integrated photovoltaic and energy storage. J Clean Prod 2021;302:126967.

[21] Rehman Wu, Bo R, Mehdipourpicha H, Kimball J. Sizing energy storage system for energy arbitrage in extreme fast charging station. In: 2021 IEEE power & energy society general meeting. IEEE; 2021, p. 01–5.

[22] Ali AY, Hussain A, Baek J-W, Kim H-M. Optimal operation of static energy storage in fast-charging stations considering the trade-off between resilience and peak shaving. J Energy Storage 2022;53:105197.

[23] Brinkel N, Schram WL, AlSkaif TA, Lampropoulos I, van Sark W. Should we reinforce the grid? Cost and emission optimization of electric vehicle charging under different transformer limits. Appl Energy 2020;276:115285.

[24] Parlikar A, Truong CN, Jossen A, Hesse H. The carbon footprint of island grids with lithium-ion battery systems: An analysis based on levelized emissions of energy supply. Renew Sustain Energy Rev 2021;149:111353.

[25] Möller M, Kucevic D, Collath N, Parlikar A, Dotzauer P, Tepe B, et al. SimSES: A holistic simulation framework for modeling and analyzing stationary energy storage systems. J Energy Storage 2022;49:103743.

[26] Soldan F, Bionda E, Mauri G, Celaschi S. Short-term forecast of EV charging stations occupancy probability using big data streaming analysis. 2021, URL: https://arxiv.org/abs/2104.12503.

[27] Schimpe M, Naumann M, Truong N, Hesse HC, Santhanagopalan S, Saxon A, et al. Energy efficiency evaluation of a stationary lithium-ion battery container storage system via electro-thermal modeling and detailed component analysis. Appl Energy 2018;210:211–29.

[28] Schimpe M, Becker N, Lahlou T, Hesse HC, Herzog H-G, Jossen A. Energy efficiency evaluation of grid connection scenarios for stationary battery energy storage systems. Energy Procedia 2018;155:77–101.

[29] Naumann M, Schimpe M, Keil P, Hesse HC, Jossen A. Analysis and modeling of calendar aging of a commercial LiFePO4/graphite cell. J Energy Storage 2018;17:153–69.

[30] Naumann M, Spingler FB, Jossen A. Analysis and modeling of cycle aging of a commercial LiFePO4/graphite cell. J Power Sources 2020;451:227666.

[31] Notton G, Lazarov V, Stoyanov L. Optimal sizing of a grid-connected PV system for various PV module technologies and inclinations, inverter efficiency characteristics and locations. Renew Energy 2010;35(2):541–54.

[32] Schimpe M, von Kuepach ME, Naumann M, Hesse HC, Smith K, Jossen A. Comprehensive modeling of temperature-dependent degradation mechanisms in lithium iron phosphate batteries. J Electrochem Soc 2018;165(2):A181–93.

[33] Parlikar A, Hesse H, Jossen A. Topology and efficiency analysis of utility-scale battery energy storage systems. In: Proceedings of the 13th international renewable energy storage conference 2019. 2019, URL: https://www.atlantis-press.com/proceedings/ires-19/125923324.

[34] Deutsches Zentrum fuer Luft- und Raumfahrt (DLR), Institute of Solar Research. Greenius: The green energy system analysis tool. 2022, Deutsches Zentrum fuer Luft- und Raumfahrt e.V. (DLR, German Aerospace Centre)), URL: https://www.dlr.de/sf/en/desktopdefault.aspx/tabid-11688/20442_read-44865/.

[35] Wirth H. Recent facts about photovoltaics in Germany. 2021, Fraunhofer Institute for Solar Energy Systems ISE, Freiburg, Germany, URL: https://www.ise.fraunhofer.de/content/dam/ise/en/documents/publications/studies/recent-facts-about-photovoltaics-in-germany.pdf.

[36] Thurner L, Scheidler A, Schafer F, Menke J-H, Dollichon J, Meier F, et al. Pandapower—An open-source Python tool for convenient modeling, analysis, and optimization of electric power systems. IEEE Trans Power Syst 2018;33(6):6510–21.

[37] Chatterjee S, Mandal S. A novel comparison of Gauss-Seidel and Newton-Raphson methods for load flow analysis. In: 2017 international conference on power and embedded drive control. IEEE; 2017, p. 1–7.

[38] VDE - Verband der Elektrotechnik Elektronik Informationstechnik eV. Batteriespeicher in der nieder- und mittelspannungsebene: Anwendungen und wirtschaftlichkeit sowie auswirkungen auf die elektrischen netze. 2015, Verband der Elektrotechnik Elektronik Informationstechnik e.V., Frankfurt am Main, Germany, URL: https://shop.vde.com/de/vde-studie-batteriespeicher-in-der-nieder-und-mittelspannungsebene-3.

[39] Wernet G, Bauer C, Steubing B, Reinhard J, Moreno-Ruiz E, Weidema B. The ecoinvent database version 3 (part I): Overview and methodology. Int J Life Cycle Assess 2016;21(9):1218–30.
[40] Intergovernmental Panel on Climate Change. In: Edenhofer O, Pichs-Madruga R, Sokona Y, Minx JC, Farahani E, Kadner S, Seyboth K, Adler A, Baum I, Brunner S, Eickemeier P, Kriemann B, Savolainen J, Schlömer S, von Stechow C, Zwickel T, editors. Climate change 2014: Mitigation of climate change: Working group III contribution to the fifth assessment report of the intergovernmental panel on climate change. Cambridge, United Kingdom and New York, NY, USA: Intergovernmental Panel on Climate Change; 2014, URL: https://www.ipcc.ch/report/ar5/wg3/.
[41] Fraunhofer Institute for Solar Energy Systems ISE. In: Burger B, editor. Electricity generation in Germany 2019. Freiburg, Germany: Fraunhofer Institute for Solar Energy Systems ISE; 2019, URL: https://energy-charts.info/charts/power/chart.htm?l=en&c=DE&stacking=stacked_absolute_area&year=2019&interval=year.
[42] Bundesnetzagentur, Bundeskartellamt. Monitoring report 2020. Bonn, Germany: Bundesnetzagentur für Elektrizität, Gas and Bundeskartellamt; 2021, URL: https://www.bundesnetzagentur.de/EN/Areas/Energy/Companies/DataCollection_Monitoring/start.html;jsessionid=AC48537DA50D535DC4B2BF7A3512A244.
[43] Turconi R, Simonsen CG, Byriel IP, Astrup T. Life cycle assessment of the Danish electricity distribution network. Int J Life Cycle Assess 2014;19(1):100–8.
[44] Baumann M, Peters JF, Weil M, Grunwald A. CO 2 footprint and life-cycle costs of electrochemical energy storage for stationary grid applications. Energy Technol 2017;5(7):1071–83.
[45] Mohr M, Peters JF, Baumann M, Weil M. Toward a cell–chemistry specific life cycle assessment of lithium–ion battery recycling processes. J Ind Ecol 2020;24(6):1310–22.
[46] Hu A, Huang L, Lou S, Kuo C-H, Huang C-Y, Chian K-J, et al. Assessment of the carbon footprint, social benefit of carbon reduction, and energy payback time of a high-concentration photovoltaic system. Sustainability 2017;9(1):27.
[47] de Simón-Martín M, Díez-Mediavilla M, Alonso-Tristán C. Real energy payback time and carbon footprint of a GCPVS. AIMS Energy 2017;5(1):77–95.
[48] Bulach W, Schüler D, Sellin G, Elwert T, Schmid D, Goldmann D, et al. Electric vehicle recycling 2020: Key component power electronics. Waste Manag Res : J Int Solid Wastes Public Clean Assoc, ISWA 2018;36(4):311–20.
[49] Ylmén P, Peñaloza D, Mjörnell K. Life cycle assessment of an office building based on site-specific data. Energies 2019;12(13):2588.
[50] Reich NH, Alsema EA, van Sark W, Turkenburg WC, Sinke WC. Greenhouse gas emissions associated with photovoltaic electricity from crystalline silicon modules under various energy supply options. Prog Photovolt, Res Appl 2011;19(5):603–13.
[51] Latunussa CE, Ardente F, Blengini GA, Mancini L. Life cycle assessment of an innovative recycling process for crystalline silicon photovoltaic panels. Sol Energy Mater Sol Cells 2016;156:101–11.
[52] Reese MO, Glynn S, Kempe MD, McGott DL, Dabney MS, Barnes TM, et al. Increasing markets and decreasing package weight for high-specific-power photovoltaics. Nature Energy 2018;3(11):1002–12.
[53] Englberger S, Abo Gamra K, Tepe B, Schreiber M, Jossen A, Hesse H. Electric vehicle multi-use: Optimizing multiple value streams using mobile storage systems in a vehicle-to-grid context. Appl Energy 2021;304:117862.
[54] Rosewater D, Ferreira S, Schoenwald D, Hawkins J, Santoso S. Battery energy storage state-of-charge forecasting: Models, optimization, and accuracy. IEEE Trans Smart Grid 2019;10(3):2453–62.
[55] Deutsche Energie-Agentur GmbH. dena-verteilnetzstudie: Ausbau- und innovationsbedarf der stromverteilnetze in Deutschland bis 2030. Berlin, Germany: Deutsche Energie-Agentur GmbH; 2012, URL: https://www.dena.de/fileadmin/dena/Dokumente/Pdf/9100_dena-Verteilnetzstudie_Abschlussbericht.pdf.
[56] Resch M, Bühler J, Klausen M, Sumper A. Impact of operation strategies of large scale battery systems on distribution grid planning in Germany. Renew Sustain Energy Rev 2017;74:1042–63.
[57] The ERM International Group Limited. Bp target neutral: Global online travel calculator: Method for calculating greenhouse gas emissions. 2021, URL: https://www.bp.com/bptargetneutralnavapp/consumer/bpTN_Online%20Travel%20GHG%20Emissions%20Calculator_Updated%20Methodology%20Statement_01July2021.961acd71.pdf.
[58] Prussi M, Yugo M, De Prada L, Padella M, Edwards R. JEC well-to-wheels report v5: Anticipation and foresight, Technical guidance. KJ-NA-30284-EN-N (online), Luxembourg (Luxembourg): Publications Office of the European Union; 2020.
[59] NKT GmbH & Co KG. Specifications NAYY 0.6/1 kV power cable. 2022, URL: https://nkt.widen.net/content/kylr51gsli/pdf/NAYY-0.6_1-kV_DSDEENAPP_LV_DS_DE-EN.pdf?u=gj0n1y.
[60] NKT GmbH & Co KG. Specifications NA2XS2Y 6/10 kV medium voltage cables. 2022, URL: https://nkt.widen.net/content/uvhp2rr9wk/pdf/NA2XS2Y-6_10_DSDEENMV_MV_DS_DE-EN.pdf?u=gj0n1y.

8 Evaluating the carbon footprint of Li-ion battery lifecycle pathways

Lithium-ion battery technology is central to both EVs and stationary BESSs. While lithium-ion batteries themselves do not generate direct emissions, their carbon footprint encompasses indirect emissions from production, operation, repurposing, and EOL phases. This article explores the environmental impact of lithium-ion batteries across different stages of their lifecycle. The study analyzes the carbon footprint of lithium-ion batteries in three distinct pathways: in automotive applications (A), in stationary applications (S), and in a sequential use (second-life) first in automotive, then in stationary storage applications (AS), following the initial automotive use phase.

The open-source simulation programs — ESN and SimSES — are used to simulate these pathways to quantitatively assess their carbon footprints. Using LEES as a comparative metric, the study seeks to investigate the impact of each pathway, providing insights into the lifecycle emissions of lithium-ion battery systems. The study examines the impact of battery second life through repurposing decommissioned automotive batteries for stationary applications on the overall carbon footprint. The article evaluates the carbon footprints of lithium-ion batteries across different lifecycle pathways. The highlights of this article include:

- The lifetime carbon footprints of lithium-ion batteries operating in three distinct pathways
- Evaluation of the LEES for these pathways under the considered assumptions and simulation conditions
- Impact of repurposing decommissioned automotive batteries for 'second-life' stationary applications on the overall carbon footprint of these batteries compared to their use solely in automotive or stationary applications

The carbon footprint of lithium-ion batteries in an exemplary automotive application (pathway A) is determined using a specific drive-power profile. Pathway S is demonstrated with a lithium-ion BESS operating in a typical stationary application - the provision of Frequency Control Reserve (FCR). Pathway AS combines both automotive and stationary applications, with batteries repurposed for stationary use after reaching a certain SOH in the automotive phase. The study aims to determine the most environmentally efficient lifecycle pathways for lithium-ion battery systems, contributing valuable insights towards optimizing battery usage for decarbonization and resource efficiency in the energy sector.

The investigation reveals that the stationary application pathway (S) is the most environmentally favorable option, exhibiting the lowest LEES value among the considered pathways, while the automotive pathway (A) has the highest. This finding is attributable to the higher BESS utilization in the stationary application, leading to better resource efficiency. The combined pathway (AS) shows that repurposing batteries for second-life applications can improve the carbon footprint compared to the automotive pathway. From a carbon footprint perspective, deploying batteries in stationary applications, with or without a prior automotive phase, is more desirable than solely automotive applications.

The results suggest that the choice of EOL criterion can significantly affect the LEES value. Follow-on analyses with better primary data and further investigations into different applications are required to improve the accuracy and comprehensiveness of these analyses. The degradation model used in this study may not perfectly capture the real-world degradation patterns, especially the rapid capacity loss after the onset of the knee point. Future studies could explore alternative degradation models and their impact on the LEES values.

Author contributions

Anupam Parlikar was the lead author, tasked with conceptualizing, methodology, data curation, software development, formal analysis, investigation, visualization, and preparing the original draft and its subsequent editing. Nils Collath contributed to the data curation, software development, and investigations. Benedikt Tepe contributed to the methodology, data curation, software development, and manuscript review. Holger Hesse assisted with visualization, supervised the research project, and played a significant role in reviewing the manuscript. Andreas Jossen was instrumental in acquiring funding and resources for the project, provided supervision, and contributed to manuscript reviews.

The Lifetime Carbon Footprint of Lithium-Ion Battery Systems in Exemplary Applications

Anupam Parlikar, Nils Collath, Benedikt Tepe, Holger Hesse, and Andreas Jossen

Energy Proceedings (Volume 38), 2024

Permanent weblink:
https://doi.org/10.46855/energy-proceedings-10893

Energy Proceedings
Vol 38, 2024
ISSN 2004-2965

The Lifetime Carbon Footprint of Lithium-Ion Battery Systems in Exemplary Applications

Anupam Parlikar[1],*, Nils Collath[1], Benedikt Tepe[1], Holger Hesse[2], Andreas Jossen[1]

1 Technical University of Munich (TUM), School of Engineering and Design, Department of Energy and Process Engineering, Chair of Electrical Energy Storage Technology (EES), Arcisstr. 21, 80333 Munich, Germany

2 Kempten University of Applied Sciences, Faculty of Mechanical Engineering, Institute for Energy and Propulsion Technologies, Bahnhofstr. 61, 87435 Kempten, Germany

* Corresponding Author: anupam.parlikar@tum.de

ABSTRACT

Energy storage plays a crucial role in the energy transition. Lithium-ion cell technology is the leading energy storage technology today across both the major pillars of the energy sector: mobility and electricity. Lithium-ion batteries are deployed in electric vehicles spanning all segments, and in stationary battery energy storage systems to provide a variety of both grid-connected and off-grid services. While there are no direct emissions due to the use of this technology, the carbon footprint of a Lithium-ion battery comprises of indirect emissions in its production, its operation, and recycling phases. Repurposing of decommissioned automotive batteries in 'second-life' stationary applications is a widely discussed concept to meaningfully extend the battery lifecycle before recycling. In this work, the lifecycle carbon footprint of Lithium-ion batteries operating in three overarching pathways is quantified simulatively with open-source python-based energy system and battery system simulation programs. These pathways are – i) automotive application (A), ii) stationary application (S), and iii) automotive application followed by a second-life stationary application (AS). From the dual perspective of decarbonization and resource efficiency, it is essential to identify the most effective lifecycle pathways for battery system applications. The metric 'Levelized Emissions of Energy Supply', LEES, is used to compare the scenarios. It is found that under the considered assumptions and simulation conditions, the S pathway performs the best, followed by the cascaded AS pathway. The automotive pathway A has the highest LEES value.

Keywords: Battery Electric Vehicle, Second-Life Battery System, Battery Energy Storage System, Electric Vehicle Battery, Levelized Emissions of Energy Supply (LEES), Carbon Footprint

NOMENCLATURE

Abbreviations	
BESS	Battery Energy Storage System
BOL	Beginning-of-Life
CI	Carbon Intensity
EOL	End-of-Life
EV	Electric Vehicle
EVB	Electric Vehicle Battery
GWP	Global Warming Potential
LCA	Lifecycle Analysis
LEC	Load Energy Consumption
LEES	Levelized Emissions of Energy Supply
LFP	Lithium Iron Phosphate
NMC	Nickel Manganese Cobalt Oxide
SOC	State of Charge
SOCI	State of Carbon Intensity
SOH	State of Health
Symbols	
ε	Emissions
E	Energy
P	Power
Subscripts	
A	Automotive application
S	Stationary application
t	At time t
Superscripts	
ch	Charge
dch	Discharge
el	Electronics
gr	Grid section
hsg	Housing
op	Operation phase
prod	Production phase

This is a paper for 15th International Conference on Applied Energy (ICAE2023), Dec. 3-7, 2023, Doha, Qatar.

repurp	Repurposing
trans	Transport

1. INTRODUCTION

Lithium-ion battery technology is the primary enabler of the recent advances in electromobility and the driving force behind its adoption globally. The global Electric Vehicle (EV) stock was 26 million in 2022, which is five times the number of EVs on the road in 2018 [1]. EV volumes are only expected to rise in all major global regions due to favorable policy incentives and technology improvements. Lithium-ion Battery Energy Storage Systems (BESSs) are also now a mature energy storage technology for the provision of grid-related services [2]. The demand for BESSs in grid applications has risen manifold over the recent past and is also expected to rise further [3]. Typical stationary BESS applications include residential self-consumption increase, provision of Frequency Containment Reserve (FCR), and peak load shaving [4].

Due to a multitude of cell-internal aging mechanisms, lithium-ion batteries are subject to degradation, which among others leads to a decrease in cell capacity and an increase of the cell's internal resistance [5]. In the case of automotive battery packs, these gradually become unfit for service due to capacity and power fade. This leads to reduced range and acceleration/regenerative braking capabilities. The extent of degradation depends on the operating conditions (state-of-charge, charge/discharge-rate, etc.), and multiple modelling approaches exist to quantify battery degradation as a functions of a battery's operating conditions, which can be classified into empirical, semi-empirical and physicochemical models [6]. A common assumption is that after a certain extent of aging, for example at a remaining capacity, or State of Health (SOH) of 70 % or 80 %, the battery reaches its end-of-life upon which it can no further be used, since battery cells often show significantly accelerated aging behavior past this point [7,8]. Furthermore, the reduced capacity and increased resistance negatively affect the economic [9] benefit gained from operating a BESS in the respective application.

Decommissioned automotive battery packs can be redeployed in stationary applications where the reduced energy and power densities are not as critical. The battery packs are collected at vehicle dealerships and other locations and are sent to battery repurposing centers for testing and integration in stationary BESSs [10]. Fig. 1 depicts the typical lifecycle of a Lithium-ion battery. Three possible lifecycle pathways for Lithium-ion batteries are discussed in this work. The first pathway, A, considers the use of batteries in an automotive application, followed by recycling on reaching the End-of-Life (EOL) criterion. The second pathway, S, consists of the use of these batteries in an exemplary stationary application (such as the provision of frequency Containment Reserve (FCR)), followed by recycling on reaching the EOL criterion. The third pathway, AS, is the so-called cascaded lifecycle pathway, which consists of a first-use phase in the automotive application, repurposing for use in the chosen second-life stationary application, and finally recycling. The present work investigates these three pathways from a carbon footprint/emissions perspective. The three pathways are simulated to obtain and compare their lifetime carbon footprints. Section 2 describes the simulation programs and the modeling procedure to compute the lifetime emissions. Section 3 describes the simulation setup, scenarios, and discusses the results. Section 4 briefly concludes with a summary of the results and provides a short outlook.

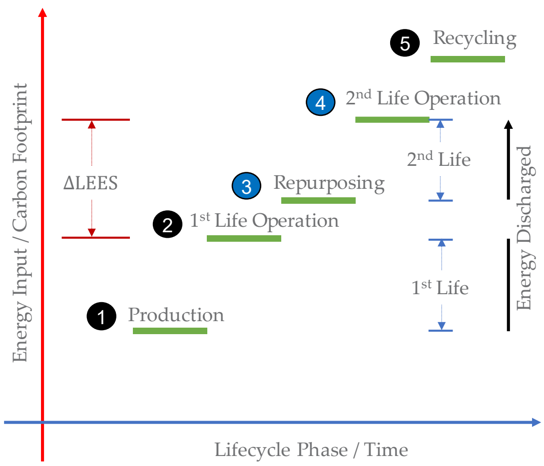

Figure 1: Qualitative depiction of the lifecycle of Lithium-ion battery systems, and the associated carbon footprint.

2. METHODS

This section describes the simulation tools used to model the localized energy system and the battery system in both automotive and stationary applications. The calculation methodology for the emissions in each lifecycle phase is also briefly described here.

2.1 Simulation Tool: Energy System Network (ESN)

The energy system simulation program *Energy System Network (ESN)* is used to model the scenarios considered in this work. ESN is capable of modelling localized energy systems, consisting of generation, storage, grid, and load components. The program captures the energy flows and lifetime emissions associated with each component included within the specified system boundaries. This program is used to model energy system scenarios within which the battery lifecycle pathways are embedded. ESN [1] is already available to the wider scientific community as an open-source program, while the associated publication is currently under review [11].

2.2 Simulation Tool: Simulation of Stationary Energy Storage Systems (SimSES)

Battery system modelling in ESN is achieved through seamless coupling with the open-source python program, *Simulation of Stationary Energy Storage Systems (SimSES)* [2]. SimSES is capable of modelling a battery system from the cell-level up to the ambient environment in which it is placed. [12]

2.3 Modelling an automotive application

The modeling procedure of an automotive battery application is presented in this section. Fig. 2 depicts the automotive battery system installed in an EV. The chosen system boundaries include the EV battery (EVB) system itself, but not the external power electronics in the charging infrastructure.

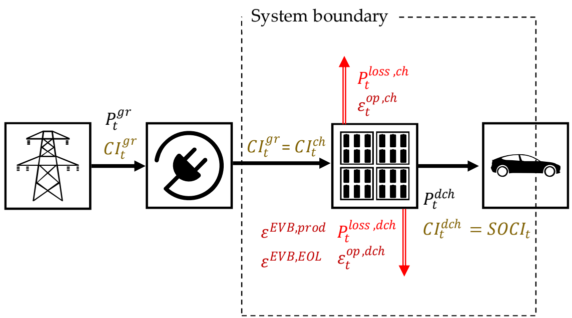

Figure 2: Modelling an automotive application and its system boundaries. The EVB includes power electronics and other peripheral components.

The GWP footprint of the automotive application, i.e., of the system contained within the system boundaries, as depicted in fig. 2 comprises of the production phase, the operation phase, and the EOL phase emissions of all included components. In addition, the Load Energy Consumption (LEC) emissions associated with the consumption of energy are also considered [13]. We use a versatile metric, the Levelized Emissions of Energy Supply (LEES) to capture the effect of all these quantities on the carbon footprint of the energy system contained within the system boundaries (eq. 1) [14].

$$LEES_A = \frac{\varepsilon_A^{EVB,prod} + \varepsilon_A^{EVB,op} + \varepsilon_A^{EVB,EOL} + \varepsilon_A^{LEC}}{E_A^{dch}} \quad (1)$$

2.4 Modelling a stationary application

In this section, the modeling procedure for a stationary battery application is presented. Fig. 3 depicts the battery installed in a grid-connected stationary application. The chosen system boundaries include the BESS itself, but not its coupling with the grid, which may also include a transformer. Analogous to the automotive application discussed earlier, the GWP footprint of the system contained within the system boundaries includes the production phase, operation phase, and EOL phase emissions of all components. Additionally, the LEC emissions on account of energy consumption are also calculated.

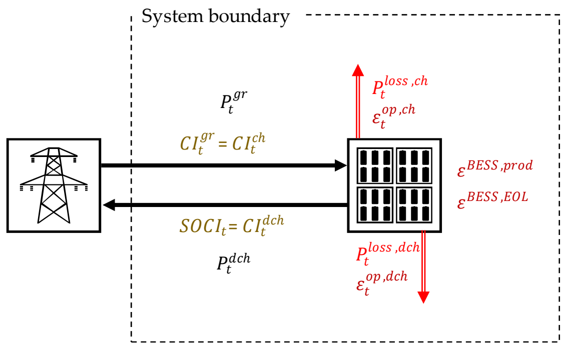

Figure 3: Modelling a stationary application and its system boundaries. The BESS includes the power electronics and other peripheral components, except the grid coupling.

These quantities can be captured in the LEES metric (eq. 2). As there is no explicit energy consuming load in a purely grid-connected battery application, the energy discharged back to the grid is treated as the consumed energy.

$$LEES_S = \frac{\varepsilon_S^{BESS,prod} + \varepsilon_S^{BESS,op} + \varepsilon_S^{BESS,EOL} + \varepsilon_S^{LEC}}{E_S^{dch}} \quad (2)$$

[1] ESN code repository: https://gitlab.lrz.de/open-ees-ses/energy_system_network

[2] SimSES code repository: https://gitlab.lrz.de/open-ees-ses/simses

2.5 Production phase

The production phase of a Lithium-ion BESS is energy intensive and is responsible for GHG emissions. These emissions are due to the production of Lithium-ion cells, power electronics modules, and other components. These emissions are assigned to the lifecycle of the BESS. The exact BESS configuration and the energy mix available at the production location both play an important role in the determination of these emissions. A literature-based streamlined LCA study of a BESS with cells of the Lithium Irion Phosphate (LFP) chemistry has been compiled in a previous study, and is deemed sufficient for the purpose of this work [14]. The production phase footprint for each of the chosen configurations in this study is discussed in section 3.

2.6 Operation phase

The operation phase emissions of battery systems are calculated from the energy conversion losses during the charge and discharge processes. These emissions are indirect emissions, which occur during the generation of the lost energy. As these emissions are caused due to the presence of the battery system in the energy system, they are allocated to the operation phase of the battery. The operation emissions in the charge process at each instant are given by the product of the carbon intensity of the charging energy, the charging loss power, $P_t^{ch,loss}$, and the simulation timestep, Δt. The carbon intensity of the charging energy is equal to the grid carbon intensity, CI_t^{gr}, in the current study, as no other power generation sources are present in the chosen configurations. The operation emissions at each instant during the discharge process are equal to the product of the State of Carbon Intensity (SOCI) at time t, $SOCI_t$, the discharge loss power, $P_t^{dch,loss}$, and the simulation timestep, Δt. The state variable SOCI has been introduced and extensively discussed in a previous work [13]. The emissions over the entire simulation period are obtained by summing up the emissions over all timesteps (eq. 3). The operation phase emissions are a function of the carbon intensity of the grid energy, and the energy losses during charging and discharging.

$$\varepsilon^{batt,op} = \Sigma\left(CI_t^{gr} \cdot P_t^{ch,loss} + SOCI_t \cdot P_t^{dch,loss}\right)\Delta t \qquad (3)$$

2.7 End-of-Life (EOL) phase

The battery reaches End-of-Life (EOL) due to either having reached a preset EOL criterion, such as a set value of the remaining capacity, beyond which a battery is not expected to perform reliably or safely, or if the required performance is not being met. Such batteries are sent to recycling facilities to recover metals and to suitably process other materials. Representative EOL phase emissions values have also been determined in a previous study as part of the literature-based streamlined LCA [14]. The EOL phase emissions are negative if materials are recovered and can be reused in the production process. This leads to emissions savings, which are 'credited' as negative emissions values. The EOL phase emissions for the configurations chosen in this study are discussed in section 3.

2.8 Repurposing of automotive batteries

In automotive applications, the battery witnesses a gradual fading of the capacity and power capability due to degradation processes occurring in the cells, as discussed in section 1. These batteries can be repurposed for operation in stationary applications. Additional components are installed to create a stationary BESS. Based on the studied literature, the carbon footprint of the repurposing process, excluding any disassembly and reassembly is found to be around 7.72 kgCO2eq/kWh of nominal battery energy capacity [15]. Two additional transport phases to and from the repurposing are also to be considered in the carbon footprint of the repurposing phase. For the LFP batteries, this amounts to an additional 0.2 kgCO2eq/kWh of nominal battery capacity assuming two transport phases of 200 km in each direction to and from the battery repurposing center [16,17].

3. SIMULATION RESULTS AND DISCUSSION

In this section, the three possible overarching lifecycle pathways for Lithium-ion batteries discussed in section 1 are presented. Exemplary simulations for these three pathways are run using ESN and SimSES. The results of these simulations are presented and discussed in this section.

The three overarching lifecycle pathways for Lithium-Ion batteries are (also depicted in Fig. 4):

1. **A:** Deployment in automotive application followed by recycling on reaching of EOL criterion corresponding to SOH = 60%
2. **S:** Deployment in stationary application followed by recycling on reaching EOL criterion of SOH = 60%
3. **AS:** Deployment in automotive application until SOH = 80% is reached followed by repurposing for deployment in a stationary application, and recycling on reaching SOH = 60%

In the following subsections, the simulation setup and the influencing factors in each of the pathways are discussed.

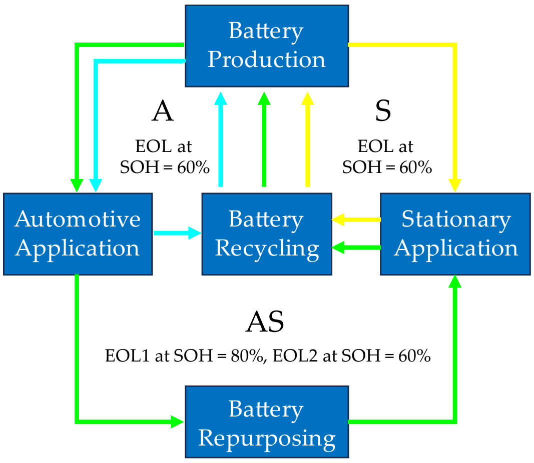

Figure 4: The three possible battery lifecycle pathways: A (Automotive), S (Stationary), and AS (Automotive application followed by a stationary second-life application).

3.1 Pathway A

In pathway A, the carbon footprint of a Lithium-ion battery pack deployed in an automotive application over its entire lifetime is determined. The metric LEES is obtained for the application within the system boundaries as described in section 2. The automotive application is modeled using an EV drive-power profile. This profile has been generated based on driver vehicle utilization behavior using the tool *emobpy* [18]. The application is simulated with a timestep of 900 seconds. This dataset and its attributes have been extensively described in a previous study. The profile and EV battery pack configuration used in this work is based on the drive profile expected for an EV from a leading vehicle manufacturer. [19]

The battery pack configuration is described in Table 1. Table 2 presents the calculated production and EOL phase emissions for the specified battery configuration. The Lithium Iron Phosphate (LFP) cell chemistry is used for the simulations. A parametrized cell model for this chemistry is available in SimSES. In this pathway, cells with SOH = 100% at the Beginning-of-Life (BOL), i.e. new cells, are considered. The EOL criterion signifies the SOH value at which the end of service life is assumed. This criterion is set at SOH = 60% in this pathway. The Lithium-ion cells are recycled at the end of the assumed operation period of 20 years, or on reaching the EOL criterion, whichever is earlier.

Table 1: Automotive application battery pack configuration.

Parameter	Value
Cell type	Lithium Iron Phosphate (LFP)
Cell format	Cylindrical, 26650
Rated energy capacity (kWh)	45
Rated power (kW)	100
Initial State of Health (SOH)	100%
Battery model	R-int Equivalent Circuit Model (ECM) (based on [20,21])
Battery degradation model	Semi-empirical calendric and cyclic (based on [22,23])
Power electronics	AC/DC converter, 5 units (based on [24–26])
Housing type	No Housing assumed
Cooling system	Passive cooling in constant temperature
Ambient conditions	Constant temperature

Table 2: Production and EOL emissions (in kgCO2eq) for the automotive battery pack described in Table 1.

Component	Production	End-of-Life	Source
Cells	7,245	-527	[27,28]
Power Electronics	980	-104	[29,30]
Electronics	619	-90	[29,30]
Total	8,844	-720	

The simulation results and emissions categories in each phase of the battery lifecycle are determined (Table 6). The value of LEES is obtained from the values of the emissions categories presented in the simulation results. The LEES value for the automotive application comes out to 0.7457 kgCO_2eq/kWh. The largest contributor to this value are the DEC emissions, followed by the BESS production phase emissions. The BESS operation phase emissions and the grid section operation phase emissions are the third and fourth largest emissions categories. The EOL phase emissions for the BESS are negative due to the carbon credits on account of material recovered from the recycling process. If the EVB were to be decommissioned on reaching SOH = 80%, the LEES value rises to 1.1124 kgCO_2eq/kWh. In this case, it takes around 7 years for the EVB to reach the EOL criterion operating with the simulated load profile. 50% of the production and EOL phase emissions associated with the power electronics are associated with the battery. This is under the assumption that the power electronics can be used in the EV with a battery replacement. The choice of the EOL criterion also affects the LEES value for the pathway.

3.2 Pathway S

In pathway S, the carbon footprint of a Lithium-ion BESS deployed in the chosen stationary grid-connected application – provision of Frequency Control Reserve (FCR) is determined over its entire lifecycle.

Table 3: Stationary application BESS configuration.

Parameter	Value
Cell chemistry	Lithium Iron Phosphate (LFP)
Cell format	Cylindrical, 26650
Rated energy capacity (MWh)	1.62
Rated power (MW)	1.6
Initial State of Health (SOH)	100%
Battery model	R-int Equivalent Circuit Model (ECM) (based on [20,21])
Battery degradation model	Semi-empirical calendric and cyclic (based on [22,23])
Power electronics	AC/DC Converter, 8 units (based on [24–26])
Housing type	20 ft. standard shipping container
HVAC thermal power (kW)	30
Ambient conditions	Berlin

Table 4: Production and End-of-Life emissions (in kgCO2eq) for the stationary BESS described in Table 3.

Component	Production	End-of-Life	Source
Cells	260,805	-18,953	[27,28]
Power Electronics	61,536	-15,125	[29,30]
Electronics	25,477	-3692	[29,30]
Housing	15,720	0	[30]
HVAC	426	0	[31]
Total	363,964	-37,769	

In this application, grid frequency data is used to generate the power target for the BESS based on the grid frequency at the current timestep. This energy management strategy is explained in greater detail in previous publications [4,12]. Grid frequency data of the German grid for the year 2019 is used in this analysis. This data has been obtained from information made available in the public domain by the transmission system operator, TransNetBW [32]. Any potential deviations from the stipulated BESS SOC limits required to provide symmetrical reserves in both the positive and negative directions are corrected by buying/selling energy on the intraday energy markets. The BESS configuration is described in Table 3. Table 4 presents the calculated production and EOL phase emissions for the specified battery configuration.

This application is simulated for a period of 20 years with a downsampled time resolution of 15 minutes (900 seconds), which reduces the number of data points to 35,040 per year, instead of over 31.5 million per year with a time resolution of 1 second [33]. Although this is less accurate than simulating the operation with a time resolution of 1 second, a significant reduction in both the simulation time and the data volumes is achieved.

The LEES value for the application is obtained from the calculated emissions categories in Table 6. The LEES value for the application is 0.5938 $kgCO_2eq/kWh$. The largest contributing category to this value are the DEC emissions, followed by the BESS operation phase emissions, and the BESS production emissions. The grid operation phase emissions constitute the smallest emissions category. The BESS EOL phase emissions are again negative, reflecting the emissions credits on recycling recovered materials.

3.3 Pathway AS

In pathway AS, the carbon footprint of the Lithium-ion battery pack over its lifetime with an automotive 'first-life' application, and a stationary 'second-life' application is calculated. The battery pack is first deployed in an automotive application. After attaining an SOH value of 80%, the battery pack is repurposed for use in a stationary application. The battery is operated in the stationary application until it either reaches the second EOL criterion of 60%, or until a total service duration of 20 years is reached. It is then sent to the recycling facility to recover the metals and other materials used in its construction.

The simulated automotive application is identical to pathway A, with the exception of the EOL criterion, which is set to 80%, and not 60%. Repurposing is carried out between the automotive and stationary applications. It is assumed that the power electronics of the EV remain fit for service with a battery pack replacement, until the vehicle is scrapped. As the EV could potentially operate two battery packs during its lifetime, 50% of the production and EOL emissions for the power electronics are then allocated to the first life battery application. The stationary application is identical to pathway S, and is simulated until an SOH value of 60% is reached, or when the battery completes a total 20 year operation period. Additional components such as the power electronics, container housing, and air conditioning systems are installed with the repurposed battery packs. In the stationary application, 45 repurposed automotive packs are installed. These 45 packs together possess an effective energy capacity of 1.62 MWh (at SOH = 80%) with an original nominal energy capacity of 2.025 MWh.

Table 5: Battery parameters (simulation results)

Quantity	A	S	A|S	
Start SOH	100%	100%	100%	80%
Mean SOC	97.61%	47.58%	97.87%	47.28%
Mean DOC	18.95%	4.22%	16.85%	3.72%
Total EFCs	945.43	3,953.27	327.53	2,489
Mean SOCI (gCO_2eq/kWh)	458.36	444.94	459.20	442.19
End SOH	65%	76%	80%	72%
Resistance increase	17.44%	46.23%	6.02%	28.81%
Operation duration (years)	20	20	7	13

The LEES value for this cascaded lifecycle pathway is calculated as in eq. 6. Eqs. 4 and 5 present the emissions associated with the battery in automotive and stationary applications. f_A and f_S are factors to determine the share of the production and EOL phase emissions for the peripheral components which are allocated to the automotive and stationary applications respectively. This includes the power electronics (PE), the container housing, and the Heating, Ventilation, Air Conditioning (HVAC) system. In this case, f_A is set to 0.5, as discussed earlier in this section. As the repurposed BESS can be operated in the stationary application for 13 years, f_S is set to 0.65. These factors control the allocation of the emissions for the peripheral components.

$$\varepsilon_A^{EVB} = \varepsilon^{cells,prod} + \varepsilon_A^{el} + f_A \cdot (\varepsilon_A^{PE}) + \varepsilon_A^{EVB,op} + \varepsilon_A^{LEC} \quad (4)$$

$$\varepsilon_S^{BESS} = f_S \cdot (\varepsilon_S^{PE} + \varepsilon_S^{el} + \varepsilon_S^{hsg} + \varepsilon_S^{HVAC}) + \varepsilon_S^{BESS,op} + \varepsilon_S^{LEC} + \varepsilon^{cells,EOL} \quad (5)$$

$$LEES = \frac{\varepsilon_A^{EVB} + \varepsilon^{trans} + \varepsilon^{repurp} + \varepsilon_S^{BESS}}{E_A^{dch} + E_S^{dch}} \quad (6)$$

The LEES value for this pathway is calculated to be 0.6285 $kgCO_2/kWh$. The category-wise emissions results are tabulated in Table 6. In the automotive application, it takes 7 years under the simulated load conditions to reach the EOL criterion of SOH = 80%. In the stationary application, the battery system is in operation for 13 years, and loses a further 8% of capacity. The EOL criterion of SOH = 60% is not reached within this time period.

From the simulated scenarios, it is observed that the LEES value for pathway A is the highest. This is due to the low utilization of the BESS in the automotive application, which sees just over 945 EFCs over the 20-year simulation period (Table 5). The SOH of the battery gradually drops to 65% in this period. In contrast, the LEES value for pathway S is the lowest over the 20-year period. This is attributable to the higher utilization (3953 EFCs) of the BESS over the 20-year simulated duration, despite which the battery reaches SOH = 76%. The evaluation of the pathway AS is more nuanced. The LEES value is lower than that of pathway A, but higher than that of pathway S. In the first phase, i.e., the A phase of the pathway, the BESS is subjected to over 327 EFCs, while in the second phase (S), the BESS is subjected to a further 2489 EFCs. At the end of the second-use phase, the SOH of the battery is 72%.

Table 6: Simulation results with each emissions category (in kgCO2eq), the discharged energy, and LEES values.

Emissions Category	A	S	A|S	
Production phase (BESS)	8,844.26	363,963.98	8,354.18 (x 45)	54,905.71
Operation phase (BESS)	2,865.12	418,102.75	982.44 (x 45)	255,708.11
Operation phase (grid section)	409.42	63,995.52	142.24 (x 45)	40,157.15
Repurposing	0	0	0	15,633
Transport	0	0	0	406.22
DEC emissions	17,180.82	2,717,493.62	5,964.88 (x 45)	1,711,802.73
EOL phase (BESS)	-720.19	-37,769.34	-668.20 (x 45)	-10,470.47
Energy discharged (kWh)	**38,324.60**	**593,7712.52**	**13,282.33 (x 45)**	**3,751,143.71**
LEES ($kgCO_2eq/kWh$)	**0.7457**	**0.5938**	**0.6285**	

In comparison to pathway A, the SOH drop in the pathways S and AS is lower, due to the degradation characteristics of cell, and the load characteristics of the application. The considered LFP cell is especially susceptible to high calendric degradation at higher SOC values. In pathway A, the EVB remains at high SOC values to maintain drive-readiness. In the pathways S and AS, the chosen stationary application – provision of FCR is peculiar as it maintains the BESS in a mid-SOC range, deviating around SOC = 50% as it provides power to counter the grid frequency deviations. As the chosen cell is also especially stable under intense cyclization, the S and AS pathways do not lead to a correspondingly high cyclic degradation, despite the high EFCs it is subjected to. Despite the high total number of EFCs (over 2816) in the automotive and stationary applications, the LEES for the AS pathway remains higher than that for the S pathway. Fig. 5 depicts the LEES values for the three pathways and the contributions of each emissions category to the value.

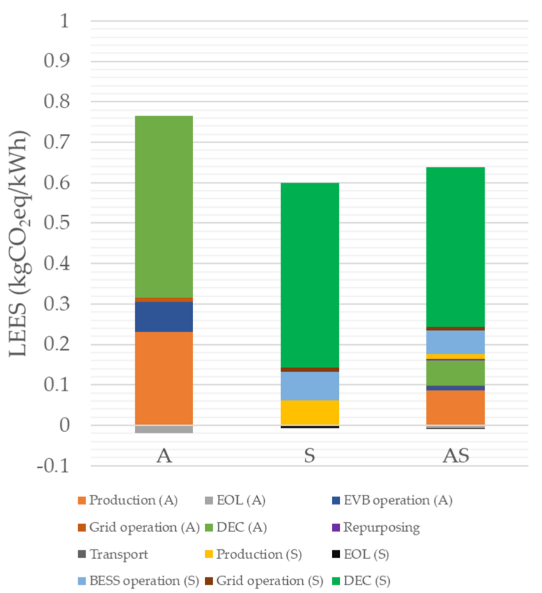

Figure 5: LEES values for the three pathways: A, S, AS. Also depicted are the relative contributions of each emissions category to the LEES value.

4. CONCLUSION AND OUTLOOK

This study investigates the emissions footprint of three possible Lithium-ion battery lifecycle pathways. It is found that for the chosen automotive drive profile and stationary application, the S pathway exhibits the lowest LEES value. The AS cascaded lifecycle pathway fares better than the A pathway. This implies that a cascaded lifecycle pathway (AS) is desirable from the carbon footprint perspective, as compared to the automotive (A) pathway. This also implies that dedicated BESS installations for stationary applications are indispensable, but stationary energy storage can be augmented with repurposed batteries from automotive applications, as the batteries have already been produced, and may as well be deployed in stationary applications to improve their lifetime LEES values. The choice of the EOL criterion in the automotive application is also found to influence the LEES value for the pathway.

The goal of this study is to illustrate the analytical methodology to compare the three possible Lithium-ion battery lifecycle pathways. This study relies on a streamlined LCA based on data published in scientific literature. Primary data is difficult to obtain and remains the biggest hurdle to conducting extremely detailed and precise LCA studies. Access to better data would ensure that this analysis can be updated at a later time. Although the LFP cell model used in this study is known to be especially durable, the cell degradation model used has a square root dependency on time and charge throughput. Consequently, it exhibits slowing degradation with time and charge throughput. The cell can be expected to suffer stronger degradation towards the end of its service life under real-world conditions, which would affect the LEES values. Follow-on analyses to check the sensitivity of cell degradation, the effect of the chosen stationary application on the LEES values are planned. An investigation into the LEES values of a Vehicle-to-Home, or Vehicle-to-X configuration wherein the automotive and stationary applications are serviced within the same timeframe, rather than sequentially as in pathway AS would also be of particular interest. The carbon intensity profile for the German grid in 2019 is used to represent each year in the simulation. This can be thought of as the worst-case scenario since the grid carbon intensity is expected to go down with time as the penetration of renewable energy sources in the energy mix rises.

ACKNOWLEDGEMENT

This research is funded by the German Federal Ministry of Education and Research (BMBF) via the research project *greenBattNutzung* (grant number 03XP0302D). The project is overseen by Project Management Juelich (PtJ). The authors thank Amey Kulkarni for contributing to some aspects of the literature review.

DECLARATION OF INTEREST STATEMENT

The authors declare that they have no known competing financial interests or personal relationships that could have appeared to influence the work reported in this paper. All authors read and approved the final manuscript.

REFERENCES

[1] International Energy Agency (IEA). Global EV Outlook 2023, Paris, France; 2023.

[2] Hesse H, Schimpe M, Kucevic D, Jossen A. Lithium-Ion Battery Storage for the Grid—A Review of Stationary Battery Storage System Design Tailored for Applications in Modern Power Grids: Energies 2017;10(12):2107.

[3] Figgener J, Hecht C, Haberschusz D, Bors J, Spreuer KG, Kairies K-P, Stenzel P, Sauer DU. The development of battery storage systems in Germany: A market review (status 2023). arXiv; 2022.

[4] Kucevic D, Tepe B, Englberger S, Parlikar A, Mühlbauer M, Bohlen O, Jossen A, Hesse H. Standard battery energy storage system profiles: Analysis of various applications for stationary energy storage systems using a holistic simulation framework: Journal of Energy Storage 2020;28:101077.

[5] Vetter J, Novák P, Wagner MR, Veit C, Möller K-C, Besenhard JO, Winter M, Wohlfahrt-Mehrens M, Vogler C, Hammouche A. Ageing mechanisms in lithium-ion batteries: Journal of Power Sources 2005;147:269–81.

[6] Collath N, Tepe B, Englberger S, Jossen A, Hesse H. Aging aware operation of lithium-ion battery energy storage systems: A review: Journal of Energy Storage 2022;55(11):105634.

[7] Collath N, Cornejo M, Engwerth V, Hesse H, Jossen A. Increasing the lifetime profitability of battery energy storage systems through aging aware operation: Applied Energy 2023;348(14):121531.

[8] Attia PM, Bills A, Brosa Planella F, Dechent P, dos Reis G, Dubarry M, Gasper P, Gilchrist R, Greenbank S, Howey D, Liu O, Khoo E, Preger Y, Soni A, Sripad S, Stefanopoulou AG, Sulzer V. Review—“Knees” in Lithium-Ion Battery Aging Trajectories: J. Electrochem. Soc. 2022;169(6):60517.

[9] Uddin K, Gough R, Radcliffe J, Marco J, Jennings P. Techno-economic analysis of the viability of residential photovoltaic systems using lithium-ion batteries for energy storage in the United Kingdom: Applied Energy 2017;206(10):12–21.

[10] Martinez-Laserna E, Gandiaga I, Sarasketa-Zabala E, Badeda J, Stroe D-I, Swierczynski M, Goikoetxea A. Battery second life: Hype, hope or reality? A critical review of the state of the art: Renewable and Sustainable Energy Reviews 2018;93:701–18.

[11] Parlikar A, Tepe B, Möller M, Hesse H, Jossen A. Quantifying the carbon footprint of energy storage applications with an energy system simulation framework - Energy System Network(under review).

[12] Möller M, Kucevic D, Collath N, Parlikar A, Dotzauer P, Tepe B, Englberger S, Jossen A, Hesse H. SimSES: A holistic simulation framework for modeling and analyzing stationary energy storage systems: Journal of Energy Storage 2022;49:103743.

[13] Parlikar A, Schott M, Godse K, Kucevic D, Jossen A, Hesse H. High-power electric vehicle charging: Low-carbon grid integration pathways with stationary lithium-ion battery systems and renewable generation: Applied Energy 2023;333:120541.

[14] Parlikar A, Truong CN, Jossen A, Hesse H. The carbon footprint of island grids with lithium-ion battery systems: An analysis based on levelized emissions of energy supply: Renewable and Sustainable Energy Reviews 2021;149:111353.

[15] Bobba S, Podias A, Di Persio F, Messagie M, Tecchio P, Cusenza MA, Eynard U, Mathieux F, Pfrang A. Sustainability Assessment of Second Life Application of Automotive Batteries (SASLAB): JRC Exploratory Research (2016-2017). Final technical report: August 2018 2018.

[16] Argonne National Laboratory, U.S. Department of Energy. GREET® Model: The Greenhouse gases, Regulated Emissions, and Energy use in Technologies Model. Argonne National Laboratory; 2022.

[17] Ragon P-L, Rodríguez F. CO2 emissions from trucks in the EU: An analysis of the heavy-duty CO2 standards baseline data; 2021.

[18] Gaete-Morales C, Kramer H, Schill W-P, Zerrahn A. An open tool for creating battery-electric vehicle time series from empirical data, emobpy: Scientific data 2021;8(1):152.

[19] Tepe B, Jablonski S, Hesse H, Jossen A. Lithium-ion battery utilization in various modes of e-transportation: eTransportation 2023;18:100274.

[20] Schimpe M, Kuepach ME von, Naumann M, Hesse HC, Smith K, Jossen A. Comprehensive Modeling of Temperature-Dependent Degradation Mechanisms

in Lithium Iron Phosphate Batteries: J. Electrochem. Soc. 2018;165(2):A181-A193.
[21] Schimpe M, Naumann M, Truong N, Hesse HC, Santhanagopalan S, Saxon A, Jossen A. Energy efficiency evaluation of a stationary lithium-ion battery container storage system via electro-thermal modeling and detailed component analysis: Applied Energy 2018;210:211–29.
[22] Naumann M, Schimpe M, Keil P, Hesse HC, Jossen A. Analysis and modeling of calendar aging of a commercial LiFePO4/graphite cell: Journal of Energy Storage 2018;17:153–69.
[23] Naumann M, Spingler FB, Jossen A. Analysis and modeling of cycle aging of a commercial LiFePO4/graphite cell: Journal of Power Sources 2020;451:227666.
[24] Notton G, Lazarov V, Stoyanov L. Optimal sizing of a grid-connected PV system for various PV module technologies and inclinations, inverter efficiency characteristics and locations: Renewable Energy 2010;35(2):541–54.
[25] Schimpe M, Becker N, Lahlou T, Hesse HC, Herzog H-G, Jossen A. Energy efficiency evaluation of grid connection scenarios for stationary battery energy storage systems: Energy Procedia 2018;155:77–101.
[26] Parlikar A, Hesse H, Jossen A. Topology and Efficiency Analysis of Utility-Scale Battery Energy Storage Systems, In: Proceedings of the 13th International Renewable Energy Storage Conference 2019 (IRES 2019).
[27] Baumann M, Peters JF, Weil M, Grunwald A. CO 2 Footprint and Life-Cycle Costs of Electrochemical Energy Storage for Stationary Grid Applications: Energy Technol. 2017;5(7):1071–83.
[28] Mohr M, Peters JF, Baumann M, Weil M. Toward a cell-chemistry specific life cycle assessment of lithium-ion battery recycling processes: J of Industrial Ecology 2020;24(6):1310–22.
[29] Bulach W, Schüler D, Sellin G, Elwert T, Schmid D, Goldmann D, Buchert M, Kammer U. Electric vehicle recycling 2020: Key component power electronics: Waste management & research the journal of the International Solid Wastes and Public Cleansing Association, ISWA 2018;36(4):311–20.
[30] Wernet G, Bauer C, Steubing B, Reinhard J, Moreno-Ruiz E, Weidema B. The ecoinvent database version 3 (part I): overview and methodology: Int J Life Cycle Assess 2016;21(9):1218–30.
[31] Ylmén P, Peñaloza D, Mjörnell K. Life Cycle Assessment of an Office Building Based on Site-Specific Data: Energies 2019;12(13):2588.
[32] TransnetBW. Systemdienstleistungen: Regel-energie Bedarf und Abruf, 2023, https://www.transnetbw.de/de/strommarkt/systemdienstleistungen/regelenergie-bedarf-und-abruf, accessed 1 March 2023.
[33] Hoffmann M, Kotzur L, Stolten D, Robinius M. A Review on Time Series Aggregation Methods for Energy System Models: Energies 2020;13(3):641.

9 Conclusion and Outlook

9.1 Conclusion

The decarbonization of the energy system is the project of the century; it represents an inflection point in the history of human civilization, capping a period of centuries and even millennia of reliance on carbonaceous fuels. Future generations will look back at the 21^{st} century through the lens of the energy transition that we bear witness to and contribute to today. Energy storage enables the energy transition to go the last mile in the effective integration of renewable power generation. This being said, integrating energy storage systems in the energy system is not automatically beneficial to the overarching goal of decarbonization. This thesis presents a comprehensive mathematical framework to quantify the carbon footprint of energy storage systems operating in a wide variety of applications, with a focus on the leading technology of today - lithium-ion Battery Energy Storage Systems (BESSs). The application of the developed methodology to some widespread energy storage applications is illustrated through case studies.

The lifetime carbon footprint of a BESS is the sum of the individual carbon footprints of each phase lifecycle phase. The carbon footprints of the production and EOL phases are largely determined by the sizing, the material composition, the efficiency and energy intensity of the manufacturing and recycling processes, and the carbon intensity of the energy mix at the production and recycling locations. Additionally, the carbon footprint of the EOL phase depends on the material recovery rate or recycling efficiency. There is often little that can be done from the perspective of energy engineering to influence the magnitude of the carbon footprints of these lifecycle phases. The carbon footprint of the operation phase falls within the ambit of energy engineering, which can be influenced by sizing and operating energy storage systems in an efficient manner. Chapter 4 discusses the factors that play a role in the efficient operation of BESSs. The characteristics of the application influence the efficiency of a BESS, i.e., the layout and topology of a BESS must be customized to match the characteristics of the load profile. Furthermore, the system efficiency depends on battery parameters such as the capacity, internal resistance, and operating voltage range. The topology and power distribution strategies of the power electronics and other auxiliary components also influence the efficiency.

With the insights gained in chapter 4 on the centrality of the system efficiency to the analysis of the operation phase, an effort to formalize the methodology for the quantification of the carbon footprint of the operation phase is made in chapter 5. A systematic and coherent mathematical framework is presented to obtain the carbon footprint of energy storage systems operating in localized energy systems. This simulation program, christened Energy System Network (ESN), has been created in the open-source scientific programming language Python. Two case studies dealing with the popular BESS applications energy arbitrage and home energy systems are presented. An unconventional energy arbitrage strategy designed to exploit spreads in the grid carbon intensity, rather than the energy price spreads on the spot markets, is presented and explored here. Similarly, an optimization-based EMS strategy for the home energy system manages to achieve the lowest carbon footprint in combination with rooftop solar generation and a residential BESS. ESN is the common thread running through all the subsequent chapters from chapter 5 onwards and has been employed to create and simulate the case studies presented therein.

Chapter 6 investigates the carbon footprint of isolated island grid energy systems. This chapter introduces two new quantities - the Levelized Emissions of Energy Supply (LEES) and the reduction in emissions per additional unit of energy storage, R. It is found that the incorporation of energy storage always results in a reduction in the carbon footprint for all reasonable values of energy storage capacity, but the value of the maximum reduction possible is a characteristic of the system configuration, and does not incessantly correlate positively with increasing energy storage capacity. The reduction in the carbon footprint correlates negatively with the energy capacity for higher values beyond the characteristic value. The metric R aids decision-makers with efficiently allocating resources by identifying isolated energy systems that should be prioritized for incorporating additional energy storage capacity.

Chapter 7 investigates the carbon footprint of battery-assisted high-power charging stations for EVs, while comparing it to the alternative of grid reinforcement at the charging station locations. The chapter also introduces a novel state variable for BESSs - the State of Carbon Intensity (SOCI). The SOCI is an attempt to usher in transparency in the carbon footprint of the BESSs operation. This is also important for the operators of BESSs, who would be able to see the effects of their EMS strategies on the SOCI of the stored energy. This chapter also looks at the optimal operation of the charging station in tandem with the BESS and the on-site PV generation to reduce the LEES of the energy used to charge the EVs. An implication of this technology is that the carbon footprint of EVs being charged with energy from an optimally operated charging station would also be lower than a comparable charging station, which does not consider this aspect of the charging energy.

Chapter 8 investigates the carbon footprints of three lithium-ion battery lifecycle pathways, which are automotive (A), stationary (S), and a cascaded pathway (AS) consisting of an automotive application followed by a second-life stationary application. The evaluation of these three pathways reveals that for the considered application load profiles, the S pathway exhibited the lowest LEES value. This was followed by the AS pathway, which had a lower LEES than the A pathway. The findings suggest that the LEES values of a battery improve with higher utilization factors. The installation of stationary BESSs is indispensable if we are to accelerate the energy transition. However, the finding that used automotive batteries can be installed in second-life stationary applications to improve the LEES of an already manufactured automotive battery is particularly interesting.

9.2 Outlook on future research directions

The work presented in this thesis is multi-faceted and multi-pronged, enabling future research that builds on top of this work to branch out in several directions.

The availability of reliable and detailed primary LCA data is one of the biggest challenges in this area of research. This work attempts to establish a systematic and comprehensive foundation for the quantification of the carbon footprint of BESSs and other energy storage systems. This methodology can be used in conjunction with better data to evaluate the techno-environmental performance of existing and upcoming technologies with greater consistency and comparability.

The EMS strategies employed in this thesis rely on the principle of perfect foresight to obtain power targets for the various components in an energy system. The incorporation of forecast uncertainty into the EMS could bring the simulation results closer to real-world operation. Confidence intervals for the evaluations attributed to the uncertainties in the most significant input quantities could also be calculated. Operating the BESS in a degradation-aware manner while minimizing the overall carbon footprint is an interesting avenue for future works. The optimization-based EMS strategies illustrated in this thesis work with Mixed-Inter Linear Programming (MILP). This includes linearizing the battery degradation functions. This necessitates a linearization of all possible non-linear equations in the original problem formulation, including the degradation functions. Non-linear optimization approaches and meta-heuristics could also be used to extend the problem formulation to include the SOCI. The investigation of the carbon footprint of BESSs operating with multi-use EMS strategies, wherein multiple energy storage applications are serviced within the same timeframe, is an interesting topic for follow-up studies.

This work investigates the carbon footprints of the battery system in stationary, automotive, and a cascaded lifecycle pathway with sequential automotive and stationary use phases. The evaluation of the carbon footprint of vehicle-to-X scenarios with bidirectional charging can yield interesting insights, especially considering that the stationary and automotive use phases are serviced during the same period. Vehicle-to-X coupled with residential BESSs represents a multi-storage setup wherein more than one storage system can be operated in an optimal fashion to service the selected applications. A multi-storage setup also includes the concept of battery swapping stations. Battery swapping stations can also be used to service various stationary applications in addition to their primary function of charging and keeping swappable EV batteries in a ready state to be swapped.

References

[1] International Energy Agency: *World Energy Outlook 2023*. 2023. URL: https://www.iea.org/reports/world-energy-outlook-2023 (visited on 05/18/2024) (see p. 1).

[2] Stanners, D. and Bourdeau, P.: *Europe's Environment - The Dobris Assessment*. 1995. URL: https://www.eea.europa.eu/publications/92-826-5409-5 (visited on 05/07/2024) (see p. 1).

[3] United Nations Framework Convention on Climate Change: *The Paris Agreement*. Paris, France, 2015. URL: https://unfccc.int/process-and-meetings/the-paris-agreement (see p. 1).

[4] Friedlingstein, P. et al.: *Global Carbon Budget 2023*. In: *Earth System Science Data* 15.12 (2023), pp. 5301–5369. DOI: 10.5194/essd-15-5301-2023 (see p. 1).

[5] International Energy Agency: *Renewables 2023*. 2024. URL: https://www.iea.org/reports/renewables-2023 (visited on 05/11/2024) (see pp. 1, 2).

[6] United Nations Framework Convention on Climate Change: *UN Climate Change Conference - United Arab Emirates*. Dubai, united Arab Emirates, 2023. URL: https://unfccc.int/cop28 (see p. 1).

[7] Wirth, H.: *Recent Facts about Photovoltaic in Germany*. Freiburg, Germany, 2024. URL: https://www.ise.fraunhofer.de/en/publications/studies/recent-facts-about-pv-in-germany.html (visited on 07/05/2024) (see p. 1).

[8] Jones–Albertus, R., Feldman, D., Fu, R., Horowitz, K., and Woodhouse, M.: *Technology advances needed for photovoltaics to achieve widespread grid price parity*. In: *Progress in Photovoltaics: Research and Applications* 24.9 (2016), pp. 1272–1283. ISSN: 1062-7995. DOI: 10.1002/pip.2755 (see p. 1).

[9] Deshmukh, R., Wu, G. C., Callaway, D. S., and Phadke, A.: *Geospatial and techno-economic analysis of wind and solar resources in India*. In: *Renewable Energy* 134 (2019), pp. 947–960. ISSN: 09601481. DOI: 10.1016/j.renene.2018.11.073 (see p. 1).

[10] International Energy Agency: *Electricity 2024*. 2024. URL: https://www.iea.org/reports/electricity-2024 (visited on 05/12/2024) (see pp. 1, 2).

[11] Sajadi, A., Strezoski, L., Strezoski, V., Prica, M., and Loparo, K. A.: *Integration of renewable energy systems and challenges for dynamics, control, and automation of electrical power systems*. In: *WIREs Energy and Environment* 8.1 (2019). ISSN: 2041-8396. DOI: 10.1002/wene.321 (see p. 1).

[12] Zappa, W., Junginger, M., and van den Broek, M.: *Is a 100% renewable European power system feasible by 2050?* In: *Applied Energy* 233-234 (2019), pp. 1027–1050. ISSN: 03062619. DOI: 10.1016/j.apenergy.2018.08.109 (see p. 1).

[13] Cochran, J. et al.: *Flexibility in 21st Century Power Systems*. 2014. DOI: 10.2172/1130630 (see p. 2).

[14] Child, M., Kemfert, C., Bogdanov, D., and Breyer, C.: *Flexible electricity generation, grid exchange and storage for the transition to a 100% renewable energy system in Europe*. In: *Renewable Energy* 139 (2019), pp. 80–101. ISSN: 09601481. DOI: 10.1016/j.renene.2019.02.077 (see p. 2).

[15] Huggins, R.: *Energy Storage*. Cham: Springer International Publishing, 2016. ISBN: 978-3-319-21238-8. DOI: 10.1007/978-3-319-21239-5 (see p. 2).

[16] Nadeem, F., Hussain, S. M. S., Tiwari, P. K., Goswami, A. K., and Ustun, T. S.: *Comparative Review of Energy Storage Systems, Their Roles, and Impacts on Future Power Systems*. In: *IEEE Access* 7 (2019), pp. 4555–4585. DOI: 10.1109/ACCESS.2018.2888497 (see p. 2).

[17] Chen, M., Ma, X., Chen, B., Arsenault, R., Karlson, P., Simon, N., and Wang, Y.: *Recycling End-of-Life Electric Vehicle Lithium-Ion Batteries*. In: *Joule* 3.11 (2019), pp. 2622–2646. ISSN: 25424351. DOI: 10.1016/j.joule.2019.09.014 (see pp. 2, 17).

[18] Moseley, P. T., Garche, J., and Adelmann, P., eds.: *Electrochemical energy storage for renewable sources and grid balancing*. Amsterdam: Elsevier, 2015. ISBN: 9780444626103 (see p. 2).

[19] Scrosati, B. and Garche, J.: *Lithium batteries: Status, prospects and future*. In: *Journal of Power Sources* 195.9 (2010), pp. 2419–2430. ISSN: 03787753. DOI: 10.1016/j.jpowsour.2009.11.048 (see p. 2).

[20] Hesse, H., Martins, R., Musilek, P., Naumann, M., Truong, C., and Jossen, A.: *Economic Optimization of Component Sizing for Residential Battery Storage Systems*. In: *Energies* 10.7 (2017), p. 835. DOI: 10.3390/en10070835 (see p. 2).

[21] Hidalgo-Leon, R., Siguenza, D., Sanchez, C., Leon, J., Jacome-Ruiz, P., Wu, J., and Ortiz, D.: "A survey of battery energy storage system (BESS), applications and environmental impacts in power systems." In: *2017 IEEE Second Ecuador Technical Chapters Meeting (ETCM)*. IEEE, 2017, pp. 1–6. ISBN: 978-1-5386-3894-1. DOI: 10.1109/ETCM.2017.8247485 (see p. 2).

[22] International Energy Agency: *Batteries and Secure Energy Transitions*. 2024. URL: https://www.iea.org/reports/batteries-and-secure-energy-transitions (visited on 05/05/2024) (see p. 2).

[23] International Energy Agency: *Global EV Outlook 2024*. Paris, 2024. URL: https://www.iea.org/reports/global-ev-outlook-2024 (visited on 07/05/2024) (see p. 2).

[24] Letha, S. S. et al.: *Power Quality Issues of Electro-Mobility on Distribution Network—An Overview*. In: *Energies* 16.13 (2023), p. 4850. DOI: 10.3390/en16134850 (see p. 2).

[25] Elwert, T., Goldmann, D., Römer, F., Buchert, M., Merz, C., Schueler, D., and Sutter, J.: *Current Developments and Challenges in the Recycling of Key Components of (Hybrid) Electric Vehicles*. In: *Recycling* 1.1 (2016), pp. 25–60. DOI: 10.3390/recycling1010025 (see p. 2).

[26] Birkl, C. R., Roberts, M. R., McTurk, E., Bruce, P. G., and Howey, D. A.: *Degradation diagnostics for lithium ion cells*. In: *Journal of Power Sources* 341 (2017), pp. 373–386. ISSN: 03787753. DOI: 10.1016/j.jpowsour.2016.12.011 (see pp. 3, 8).

[27] Martinez-Laserna, E., Gandiaga, I., Sarasketa-Zabala, E., Badeda, J., Stroe, D.-I., Swierczynski, M., and Goikoetxea, A.: *Battery second life: Hype, hope or reality? A critical review of the state of the art*. In: *Renewable and Sustainable Energy Reviews* 93 (2018), pp. 701–718. ISSN: 13640321. DOI: 10.1016/j.rser.2018.04.035 (see pp. 3, 18).

[28] Gu, X., Bai, H., Cui, X., Zhu, J., Zhuang, W., Li, Z., Hu, X., and Song, Z.: *Challenges and Opportunities for Second-life Batteries: A Review of Key Technologies and Economy*. 08/13/2023. URL: http://arxiv.org/pdf/2308.06786v1 (see p. 3).

[29] Wali, S. B., Hannan, M. A., Ker, P. J., Rahman, M. A., Mansor, M., Muttaqi, K. M., Mahlia, T., and Begum, R. A.: *Grid-connected lithium-ion battery energy storage system: A bibliometric analysis for emerging future directions*. In: *Journal of Cleaner Production* 334 (2022), p. 130272. ISSN: 09596526. DOI: 10.1016/j.jclepro.2021.130272 (see p. 3).

[30] Da Deng: *Li–ion batteries: basics, progress, and challenges*. In: *Energy Science & Engineering* 3.5 (2015), pp. 385–418. ISSN: 2050-0505. DOI: 10.1002/ese3.95 (see p. 5).

[31] Pistoia, G.: *Lithium-ion batteries: Advances and applications / [editor] Gianfranco Pistoia*. First edition. Amsterdam: Elsevier, 2014. ISBN: 9780444595133 (see p. 5).

[32] Zubi, G., Dufo-López, R., Carvalho, M., and Pasaoglu, G.: *The lithium-ion battery: State of the art and future perspectives*. In: *Renewable and Sustainable Energy Reviews* 89 (2018), pp. 292–308. ISSN: 13640321. DOI: 10.1016/j.rser.2018.03.002 (see p. 5).

[33] Zimmerman, A. H.: *Self-discharge losses in lithium-ion cells*. In: *IEEE Aerospace and Electronic Systems Magazine* 19.2 (2004), pp. 19–24. ISSN: 0885-8985. DOI: 10.1109/MAES.2004.1269687 (see pp. 5, 12).

[34] Goodenough, J. B. and Park, K.-S.: *The Li-ion rechargeable battery: a perspective*. In: *Journal of the American Chemical Society* 135.4 (2013), pp. 1167–1176. DOI: 10.1021/ja3091438 (see p. 5).

[35] Eftekhari, A.: *Lithium-Ion Batteries with High Rate Capabilities*. In: *ACS Sustainable Chemistry & Engineering* 5.4 (2017), pp. 2799–2816. ISSN: 2168-0485. DOI: 10.1021/acssuschemeng.7b00046 (see pp. 5, 10).

[36] Korthauer, R.: *Lithium-Ion Batteries: Basics and Applications*. Berlin, Heidelberg: Springer Berlin Heidelberg, 2018. ISBN: 978-3-662-53069-6. DOI: 10.1007/978-3-662-53071-9 (see p. 5).

[37] Zhang, Z. and Zhang, S. S.: *Rechargeable Batteries*. Cham: Springer International Publishing, 2015. ISBN: 978-3-319-15457-2. DOI: 10.1007/978-3-319-15458-9 (see p. 5).

[38] Sterner, M. and Stadler, I.: *Handbook of Energy Storage*. Berlin, Heidelberg: Springer Berlin Heidelberg, 2019. ISBN: 978-3-662-55503-3. DOI: 10.1007/978-3-662-55504-0 (see p. 5).

[39] Brodd, R. J.: *Batteries for Sustainability*. New York, NY: Springer New York, 2013. ISBN: 978-1-4614-5790-9. DOI: 10.1007/978-1-4614-5791-6 (see p. 5).

[40] Reddy, T. B. and Linden, D.: *Linden's handbook of batteries*. 4th ed. New York: McGraw-Hill, 2011. ISBN: 9780071624190 (see pp. 5, 6).

[41] Julien, C., Mauger, A., Vijh, A., and Zaghib, K.: *Lithium Batteries*. Cham: Springer International Publishing, 2016. ISBN: 978-3-319-19107-2. DOI: 10.1007/978-3-319-19108-9 (see p. 6).

[42] Link, S. et al.: *Development perspectives for lithium-ion battery cell formats*. 2022. URL: https://www.isi.fraunhofer.de/en/blog/themen/batterie-update/lithium-ionen-batteriezellen-entwicklung-batteriezellformate.html (visited on 05/26/2024) (see p. 6).

[43] Li, M., Lu, J., Chen, Z., and Amine, K.: *30 Years of Lithium-Ion Batteries*. In: *Advanced materials (Deerfield Beach, Fla.)* (2018), e1800561. DOI: 10.1002/adma.201800561 (see p. 6).

[44] Manthiram, A.: *An Outlook on Lithium Ion Battery Technology*. In: *ACS central science* 3.10 (2017), pp. 1063–1069. ISSN: 2374-7943. DOI: 10.1021/acscentsci.7b00288 (see p. 6).

[45] Casals, L. C., Amante García, B., and Canal, C.: *Second life batteries lifespan: Rest of useful life and environmental analysis*. In: *Journal of environmental management* 232 (2019), pp. 354–363. DOI: 10.1016/j.jenvman.2018.11.046 (see pp. 6, 17, 18).

[46] Saldarini, A., Longo, M., Brenna, M., and Zaninelli, D.: *Battery Electric Storage Systems: Advances, Challenges, and Market Trends*. In: *Energies* 16.22 (2023), p. 7566. DOI: 10.3390/en16227566 (see p. 6).

[47] Truong, C. N., Schimpe, M., Naumann, M., Jossen, A., and Hesse, H. C.: *Impact of sub-components on the overall performance of stationary battery systems: Insights on the prototype Energy Neighbor*. In: *International ETG Congress 2017, Bonn, Germany*. 2017, pp. 1–6. URL: https://ieeexplore.ieee.org/abstract/document/8278767 (visited on 12/26/2023) (see pp. 7, 8).

[48] Koller, M., Borsche, T., Ulbig, A., and Andersson, G.: *Review of grid applications with the Zurich 1MW battery energy storage system*. In: *Electric Power Systems Research* 120 (2015), pp. 128–135. ISSN: 03787796. DOI: 10.1016/j.epsr.2014.06.023 (see p. 7).

[49] Baumann, M., Wildfeuer, L., Rohr, S., and Lienkamp, M.: *Parameter variations within Li-Ion battery packs – Theoretical investigations and experimental quantification*. In: *Journal of Energy Storage* 18 (2018), pp. 295–307. ISSN: 2352152X. DOI: 10.1016/j.est.2018.04.031 (see p. 7).

[50] Rumpf, K., Naumann, M., and Jossen, A.: *Experimental investigation of parametric cell-to-cell variation and correlation based on 1100 commercial lithium-ion cells*. In: *Journal of Energy Storage* 14 (2017), pp. 224–243. ISSN: 2352152X. DOI: 10.1016/j.est.2017.09.010 (see p. 7).

[51] Baumhöfer, T., Brühl, M., Rothgang, S., and Sauer, D. U.: *Production caused variation in capacity aging trend and correlation to initial cell performance*. In: *Journal of Power Sources* 247 (2014), pp. 332–338. ISSN: 03787753. DOI: 10.1016/j.jpowsour.2013.08.108 (see p. 7).

[52] Rumpf, K., Rheinfeld, A., Schindler, M., Keil, J., Schua, T., and Jossen, A.: *Influence of Cell-to-Cell Variations on the Inhomogeneity of Lithium-Ion Battery Modules*. In: *Journal of The Electrochemical Society* 165.11 (2018), A2587–A2607. ISSN: 0013-4651. DOI: 10.1149/2.0111811jes (see p. 7).

[53] Atcitty, S., Neely, J., Ingersoll, D., Akhil, A., and Waldrip, K.: *Battery Energy Storage System*. In: *Power Electronics for Renewable and Distributed Energy Systems*. Ed. by S. Chakraborty, M. G. Simões, and W. E. Kramer. Green Energy and Technology. London: Springer London, 2013, pp. 333–366. ISBN: 978-1-4471-5103-6. DOI: 10.1007/978-1-4471-5104-3{\textunderscore}9 (see p. 7).

[54] Fernão Pires, V., Romero-Cadaval, E., Vinnikov, D., Roasto, I., and Martins, J. F.: *Power converter interfaces for electrochemical energy storage systems – A review*. In: *Energy Conversion and Management* 86 (2014), pp. 453–475. ISSN: 01968904. DOI: 10.1016/j.enconman.2014.05.003 (see p. 7).

[55] Zhang, C., Wei, Y.-L., Cao, P.-F., and Lin, M.-C.: *Energy storage system: Current studies on batteries and power condition system*. In: *Renewable and Sustainable Energy Reviews* 82 (2018), pp. 3091–3106. ISSN: 13640321. DOI: 10.1016/j.rser.2017.10.030 (see p. 7).

[56] Hannan, M. A., Wali, S. B., Ker, P. J., Rahman, M. A., Mansor, M., Ramachandaramurthy, V. K., Muttaqi, K. M., Mahlia, T., and Dong, Z. Y.: *Battery energy-storage system: A review of technologies, optimization objectives, constraints, approaches, and outstanding issues*. In: *Journal of Energy Storage* 42 (2021), p. 103023. ISSN: 2352152X. DOI: 10.1016/j.est.2021.103023 (see p. 7).

[57] Yang, Y., Bremner, S., Menictas, C., and Kay, M.: *Modelling and optimal energy management for battery energy storage systems in renewable energy systems: A review*. In: *Renewable and Sustainable Energy Reviews* 167 (2022), p. 112671. ISSN: 13640321. DOI: 10.1016/j.rser.2022.112671 (see p. 7).

[58] Lawder, M. T., Suthar, B., Northrop, P. W. C., De, S., Hoff, C. M., Leitermann, O., Crow, M. L., Santhanagopalan, S., and Subramanian, V. R.: *Battery Energy Storage System (BESS) and Battery Management System (BMS) for Grid-Scale Applications*. In: *Proceedings of the IEEE* 102.6 (2014), pp. 1014–1030. ISSN: 0018-9219. DOI: 10.1109/JPROC.2014.2317451 (see p. 7).

[59] Wang, Y., Tian, J., Sun, Z., Wang, L., Xu, R., Li, M., and Chen, Z.: *A comprehensive review of battery modeling and state estimation approaches for advanced battery management systems*. In: *Renewable and Sustainable Energy Reviews* 131 (2020), p. 110015. ISSN: 13640321. DOI: 10.1016/j.rser.2020.110015 (see p. 7).

[60] Hannan, M. A., Lipu, M., Hussain, A., and Mohamed, A.: *A review of lithium-ion battery state of charge estimation and management system in electric vehicle applications: Challenges and recommendations*. In: *Renewable and Sustainable Energy Reviews* 78 (2017), pp. 834–854. ISSN: 13640321. DOI: 10.1016/j.rser.2017.05.001 (see p. 7).

[61] Olabi, A. G., Maghrabie, H. M., Adhari, O. H. K., Sayed, E. T., Yousef, B. A., Salameh, T., Kamil, M., and Abdelkareem, M. A.: *Battery thermal management systems: Recent progress and challenges*. In: *International Journal of Thermofluids* 15 (2022), p. 100171. ISSN: 26662027. DOI: 10.1016/j.ijft.2022.100171 (see p. 8).

[62] Liu, H., Wei, Z., He, W., and Zhao, J.: *Thermal issues about Li-ion batteries and recent progress in battery thermal management systems: A review*. In: *Energy Conversion and Management* 150 (2017), pp. 304–330. ISSN: 01968904. DOI: 10.1016/j.enconman.2017.08.016 (see p. 8).

[63] Henke, M. and Hailu, G.: *Thermal Management of Stationary Battery Systems: A Literature Review*. In: *Energies* 13.16 (2020), p. 4194. DOI: 10.3390/en13164194 (see p. 8).

[64] Hannan, M. A., Al-Shetwi, A., Begum, R. A., Young, S. E., Hoque, M. M., Ker, P., Mansur, M., and Alzaareer, K.: *The value of thermal management control strategies for battery energy storage in grid decarbonization: Issues and recommendations*. In: *Journal of Cleaner Production* 276 (2020), p. 124223. ISSN: 09596526. DOI: 10.1016/j.jclepro.2020.124223 (see p. 8).

[65] Kwon, H., Choi, J., Chul Sung, S., Min Kim, H., Kyum Lee, S., and Park, H.: *Conceptual thermal design for 40 ft container type 3.8 MW energy storage system by using computational simulation*. In: *Sustainable Energy Technologies and Assessments* 56 (2023), p. 103075. ISSN: 22131388. DOI: 10.1016/j.seta.2023.103075 (see p. 8).

[66] Rancilio, G., Merlo, M., Lucas, A., Kotsakis, E., and Delfanti, M.: "BESS modeling: investigating the role of auxiliary system consumption in efficiency derating." In: *2020 International Symposium on Power Electronics, Electrical Drives, Automation and Motion (SPEEDAM)*. IEEE, 2020, pp. 189–194. ISBN: 978-1-7281-7019-0. DOI: 10.1109/SPEEDAM48782.2020.9161875 (see p. 8).

[67] Conzen, J., Lakshmipathy, S., Kapahi, A., Kraft, S., and DiDomizio, M.: *Lithium ion battery energy storage systems (BESS) hazards*. In: *Journal of Loss Prevention in the Process Industries* 81 (2023), p. 104932. ISSN: 09504230. DOI: 10.1016/j.jlp.2022.104932 (see p. 8).

[68] Edge, J. S. et al.: *Lithium ion battery degradation: what you need to know*. In: *Physical chemistry chemical physics : PCCP* 23.14 (2021), pp. 8200–8221. DOI: 10.1039/d1cp00359c (see pp. 8, 9).

[69] Jafari, M., Khan, K., and Gauchia, L.: *Deterministic models of Li-ion battery aging: It is a matter of scale*. In: *Journal of Energy Storage* 20 (2018), pp. 67–77. ISSN: 2352152X. DOI: 10.1016/j.est.2018.09.002 (see p. 9).

[70] Reniers, J. M., Mulder, G., and Howey, D. A.: *Review and Performance Comparison of Mechanical-Chemical Degradation Models for Lithium-Ion Batteries*. In: *Journal of The Electrochemical Society* 166.14 (2019), A3189–A3200. ISSN: 0013-4651. DOI: 10.1149/2.0281914jes (see p. 9).

[71] Hoog, J. de, Timmermans, J.-M., Ioan-Stroe, D., Swierczynski, M., Jaguemont, J., Goutam, S., Omar, N., van Mierlo, J., and van den Bossche, P.: *Combined cycling and calendar capacity fade modeling of a Nickel-Manganese-Cobalt Oxide Cell with real-life profile validation*. In: *Applied Energy* 200 (2017), pp. 47–61. ISSN: 03062619. DOI: 10.1016/j.apenergy.2017.05.018 (see p. 9).

[72] Naumann, M., Schimpe, M., Keil, P., Hesse, H. C., and Jossen, A.: *Analysis and modeling of calendar aging of a commercial LiFePO4/graphite cell*. In: *Journal of Energy Storage* 17 (2018), pp. 153–169. ISSN: 2352152X. DOI: 10.1016/j.est.2018.01.019 (see p. 9).

[73] Naumann, M., Spingler, F. B., and Jossen, A.: *Analysis and modeling of cycle aging of a commercial LiFePO4/graphite cell*. In: *Journal of Power Sources* 451 (2020), p. 227666. ISSN: 03787753. DOI: 10.1016/j.jpowsour.2019.227666 (see p. 9).

[74] Schmalstieg, J., Käbitz, S., Ecker, M., and Sauer, D. U.: *A holistic aging model for Li(NiMnCo)O2 based 18650 lithium-ion batteries*. In: *Journal of Power Sources* 257 (2014), pp. 325–334. ISSN: 03787753. DOI: 10.1016/j.jpowsour.2014.02.012 (see p. 9).

[75] Sarasketa-Zabala, E., Martinez-Laserna, E., Berecibar, M., Gandiaga, I., Rodriguez-Martinez, L. M., and Villarreal, I.: *Realistic lifetime prediction approach for Li-ion batteries*. In: *Applied Energy* 162 (2016), pp. 839–852. ISSN: 03062619. DOI: 10.1016/j.apenergy.2015.10.115 (see p. 9).

[76] Raj, T., Wang, A. A., Monroe, C. W., and Howey, D. A.: *Investigation of Path–Dependent Degradation in Lithium–Ion Batteries***. In: *Batteries & Supercaps* 3.12 (2020), pp. 1377–1385. ISSN: 2566-6223. DOI: 10.1002/batt.202000160 (see p. 9).

[77] Rogge, M. and Jossen, A.: *Path–Dependent Ageing of Lithium–ion Batteries and Implications on the Ageing Assessment of Accelerated Ageing Tests*. In: *Batteries & Supercaps* (2023). ISSN: 2566-6223. DOI: 10.1002/batt.202300313 (see p. 9).

[78] Rubenbauer, H. and Henninger, S.: *Definitions and reference values for battery systems in electrical power grids*. In: *Journal of Energy Storage* 12 (2017), pp. 87–107. ISSN: 2352152X. DOI: 10.1016/j.est.2017.04.004 (see p. 10).

[79] Leadbetter, J. and Swan, L. G.: *Selection of battery technology to support grid-integrated renewable electricity*. In: *Journal of Power Sources* 216 (2012), pp. 376–386. ISSN: 03787753. DOI: 10.1016/j.jpowsour.2012.05.081 (see p. 10).

[80] Pellow, M. A., Emmott, C. J. M., Barnhart, C. J., and Benson, S. M.: *Hydrogen or batteries for grid storage? A net energy analysis*. In: *Energy & Environmental Science* 8.7 (2015), pp. 1938–1952. ISSN: 1754-5692. DOI: 10.1039/C4EE04041D (see p. 10).

[81] Koohi-Fayegh, S. and Rosen, M. A.: *A review of energy storage types, applications and recent developments*. In: *Journal of Energy Storage* 27 (2020), p. 101047. ISSN: 2352152X. DOI: 10.1016/j.est.2019.101047 (see p. 10).

[82] Kucevic, D., Tepe, B., Englberger, S., Parlikar, A., Mühlbauer, M., Bohlen, O., Jossen, A., and Hesse, H.: *Standard battery energy storage system profiles: Analysis of various applications for stationary energy storage systems using a holistic simulation framework*. In: *Journal of Energy Storage* 28 (2020), p. 101077. ISSN: 2352152X. DOI: 10.1016/j.est.2019.101077 (see pp. 10–12).

[83] Keil, P. and Jossen, A.: *Charging protocols for lithium-ion batteries and their impact on cycle life—An experimental study with different 18650 high-power cells*. In: *Journal of Energy Storage* 6 (2016), pp. 125–141. ISSN: 2352152X. DOI: 10.1016/j.est.2016.02.005 (see pp. 11, 12).

[84] Farhad, S. and Nazari, A.: *Introducing the energy efficiency map of lithium-ion batteries*. In: *International Journal of Energy Research* 43.2 (2019), pp. 931–944. ISSN: 0363907X. DOI: 10.1002/er.4332 (see p. 11).

[85] Bašić, H., Bobanac, V., and Pandžić, H.: *Determination of Lithium-Ion Battery Capacity for Practical Applications*. In: *Batteries* 9.9 (2023), p. 459. DOI: 10.3390/batteries9090459 (see p. 11).

[86] Yazami, R. and Reynier, Y.: *Mechanism of self-discharge in graphite–lithium anode*. In: *Electrochimica Acta* 47.8 (2002), pp. 1217–1223. ISSN: 00134686. DOI: 10.1016/S0013-4686(01)00827-1 (see p. 12).

[87] Tornheim, A. and O'Hanlon, D. C.: *What do Coulombic Efficiency and Capacity Retention Truly Measure? A Deep Dive into Cyclable Lithium Inventory, Limitation Type, and Redox Side Reactions*. In: *Journal of The Electrochemical Society* 167.11 (2020), p. 110520. ISSN: 0013-4651. DOI: 10.1149/1945-7111/ab9ee8 (see p. 12).

[88] Redondo-Iglesias, E., Venet, P., and Pelissier, S.: *Global Model for Self-Discharge and Capacity Fade in Lithium-Ion Batteries Based on the Generalized Eyring Relationship*. In: *IEEE Transactions on Vehicular Technology* 67.1 (2018), pp. 104–113. ISSN: 0018-9545. DOI: 10.1109/TVT.2017.2751218 (see p. 12).

[89] Smith, A. J., Burns, J. C., and Dahn, J. R.: *A High Precision Study of the Coulombic Efficiency of Li-Ion Batteries*. In: *Electrochemical and Solid-State Letters* 13.12 (2010), A177. ISSN: 10990062. DOI: 10.1149/1.3487637 (see p. 12).

[90] Roth, T., Streck, L., Mujanovic, N., Winter, M., Niehoff, P., and Jossen, A.: *Transient Self-Discharge after Formation in Lithium-Ion Cells: Impact of State-of-Charge and Anode Overhang*. In: *Journal of The Electrochemical Society* 170.8 (2023), p. 080524. ISSN: 0013-4651. DOI: 10.1149/1945-7111/acf164 (see p. 12).

[91] Hu, X., Feng, F., Liu, K., Zhang, L., Xie, J., and Liu, B.: *State estimation for advanced battery management: Key challenges and future trends*. In: *Renewable and Sustainable Energy Reviews* 114 (2019), p. 109334. ISSN: 13640321. DOI: 10.1016/j.rser.2019.109334 (see pp. 12, 13).

[92] Park, S., Ahn, J., Kang, T., Park, S., Kim, Y., Cho, I., and Kim, J.: *Review of state-of-the-art battery state estimation technologies for battery management systems of stationary energy storage systems*. In: *Journal of Power Electronics* 20.6 (2020), pp. 1526–1540. ISSN: 1598-2092. DOI: 10.1007/s43236-020-00122-7 (see p. 12).

[93] Ning, G. and Popov, B. N.: *Cycle Life Modeling of Lithium-Ion Batteries*. In: *Journal of The Electrochemical Society* 151.10 (2004), A1584. ISSN: 0013-4651. DOI: 10.1149/1.1787631 (see p. 12).

[94] Balagopal, B. and Chow, M.-Y.: "The state of the art approaches to estimate the state of health (SOH) and state of function (SOF) of lithium Ion batteries." In: *2015 IEEE 13th International Conference on Industrial Informatics (INDIN)*. IEEE, 2015, pp. 1302–1307. ISBN: 978-1-4799-6649-3. DOI: 10.1109/INDIN.2015.7281923 (see p. 13).

[95] Cabrera-Castillo, E., Niedermeier, F., and Jossen, A.: *Calculation of the state of safety (SOS) for lithium ion batteries*. In: *Journal of Power Sources* 324 (2016), pp. 509–520. ISSN: 03787753. DOI: 10.1016/j.jpowsour.2016.05.068 (see p. 13).

[96] Mancarella, P.: *MES (multi-energy systems): An overview of concepts and evaluation models*. In: *Energy* 65 (2014), pp. 1–17. ISSN: 03605442. DOI: 10.1016/j.energy.2013.10.041 (see p. 13).

[97] Günter, N. and Marinopoulos, A.: *Energy storage for grid services and applications: Classification, market review, metrics, and methodology for evaluation of deployment cases*. In: *Journal of Energy Storage* 8 (2016), pp. 226–234. ISSN: 2352152X. DOI: 10.1016/j.est.2016.08.011 (see p. 13).

[98] Rotella Junior, P., Rocha, L. C. S., Morioka, S. N., Bolis, I., Chicco, G., Mazza, A., and Janda, K.: *Economic Analysis of the Investments in Battery Energy Storage Systems: Review and Current Perspectives*. In: *Energies* 14.9 (2021), p. 2503. DOI: 10.3390/en14092503 (see p. 14).

[99] Naumann, M., Karl, R. C., Truong, C. N., Jossen, A., and Hesse, H. C.: *Lithium-ion Battery Cost Analysis in PV-household Application*. In: *Energy Procedia* 73 (2015), pp. 37–47. ISSN: 18766102. DOI: 10.1016/j.egypro.2015.07.555 (see p. 14).

[100] Jülch, V.: *Comparison of electricity storage options using levelized cost of storage (LCOS) method*. In: *Applied Energy* 183 (2016), pp. 1594–1606. ISSN: 03062619. DOI: 10.1016/j.apenergy.2016.08.165 (see p. 14).

[101] Belderbos, A., Delarue, E., Kessels, K., and D'haeseleer, W.: *Levelized cost of storage — Introducing novel metrics*. In: *Energy Economics* 67 (2017), pp. 287–299. ISSN: 01409883. DOI: 10.1016/j.eneco.2017.08.022 (see p. 14).

[102] Pawel, I.: *The Cost of Storage – How to Calculate the Levelized Cost of Stored Energy (LCOE) and Applications to Renewable Energy Generation*. In: *Energy Procedia* 46 (2014), pp. 68–77. ISSN: 18766102. DOI: 10.1016/j.egypro.2014.01.159 (see p. 14).

[103] Lai, C. S. and McCulloch, M. D.: *Levelized cost of electricity for solar photovoltaic and electrical energy storage*. In: *Applied Energy* 190 (2017), pp. 191–203. ISSN: 03062619. DOI: 10.1016/j.apenergy.2016.12.153 (see p. 14).

[104] Larcher, D. and Tarascon, J.-M.: *Towards greener and more sustainable batteries for electrical energy storage*. In: *Nature chemistry* 7.1 (2015), pp. 19–29. DOI: 10.1038/NCHEM.2085 (see p. 14).

[105] Peiseler, L., Wood, V., and Schmidt, T. S.: *Reducing the carbon footprint of lithium-ion batteries, what's next?* In: *Next Energy* 1.2 (2023), p. 100017. ISSN: 2949821X. DOI: 10.1016/j.nxener.2023.100017 (see p. 14).

[106] Oliveira, L., Messagie, M., Mertens, J., Laget, H., Coosemans, T., and van Mierlo, J.: *Environmental performance of electricity storage systems for grid applications, a life cycle approach.* In: *Energy Conversion and Management* 101 (2015), pp. 326–335. ISSN: 01968904. DOI: 10.1016/j.enconman.2015.05.063 (see pp. 14, 16).

[107] Schmidt, T. S., Beuse, M., Zhang, X., Steffen, B., Schneider, S. F., Pena-Bello, A., Bauer, C., and Parra, D.: *Additional Emissions and Cost from Storing Electricity in Stationary Battery Systems.* In: *Environmental science & technology* 53.7 (2019), pp. 3379–3390. DOI: 10.1021/acs.est.8b05313 (see pp. 14, 16, 17).

[108] Pellow, M. A., Ambrose, H., Mulvaney, D., Betita, R., and Shaw, S.: *Research gaps in environmental life cycle assessments of lithium ion batteries for grid-scale stationary energy storage systems: End-of-life options and other issues.* In: *Sustainable Materials and Technologies* 23 (2020), e00120. ISSN: 2214-9937. DOI: 10.1016/j.susmat.2019.e00120. URL: http://www.sciencedirect.com/science/article/pii/S2214993718302318 (see p. 15).

[109] Gutsch, M. and Leker, J.: *Costs, carbon footprint, and environmental impacts of lithium-ion batteries – From cathode active material synthesis to cell manufacturing and recycling.* In: *Applied Energy* 353 (2024), p. 122132. ISSN: 03062619. DOI: 10.1016/j.apenergy.2023.122132 (see pp. 15, 16).

[110] Peters, J. F., Baumann, M., Zimmermann, B., Braun, J., and Weil, M.: *The environmental impact of Li-Ion batteries and the role of key parameters – A review.* In: *Renewable and Sustainable Energy Reviews* 67 (2017), pp. 491–506. ISSN: 13640321. DOI: 10.1016/j.rser.2016.08.039 (see pp. 15, 16).

[111] Jones, C., Gilbert, P. J., and Stamford, L.: *Assessing the Climate Change Mitigation Potential of Stationary Energy Storage for Electricity Grid Services.* In: *Environmental science & technology* (2019). URL: http://dx.doi.org/10.1021/acs.est.9b06231 (see pp. 15, 16).

[112] Le Varlet, T., Schmidt, O., Gambhir, A., Few, S., and Staffell, I.: *Comparative life cycle assessment of lithium-ion battery chemistries for residential storage.* In: *Journal of Energy Storage* 28 (2020), p. 101230. ISSN: 2352152X. DOI: 10.1016/j.est.2020.101230 (see pp. 15, 16).

[113] Kloepffer, W. and Grahl, B.: *Life cycle assessment: A guide to best practice.* 1st ed. Somerset and Weinheim an der Bergstrasse, Germany: Wiley and Wiley-VCH, 2014. ISBN: 978-3-527-65565-6 (see p. 16).

[114] McDonough, W. and Braungart, M.: *Cradle to cradle: Remaking the way we make things.* First edition. New York: North Point Press, 2002. ISBN: 1429973846 (see p. 16).

[115] Stenzel, P., Koj, J. C., Schreiber, A., Hennings, W., and Zapp, P.: *Primary control provided by large-scale battery energy storage systems or fossil power plants in Germany and related environmental impacts.* In: *Journal of Energy Storage* 8 (2016), pp. 300–310. ISSN: 2352152X. DOI: 10.1016/j.est.2015.12.006 (see p. 16).

[116] Matheys, J., van Autenboer, W., Timmermans, J.-M., van Mierlo, J., van den Bossche, P., and Maggetto, G.: *Influence of functional unit on the life cycle assessment of traction batteries.* In: *The International Journal of Life Cycle Assessment* 12.3 (2007), pp. 191–196. ISSN: 0948-3349. DOI: 10.1065/lca2007.04.322 (see p. 16).

[117] Curran, M. A.: *Overview of Goal and Scope Definition in Life Cycle Assessment*. In: *Goal and Scope Definition in Life Cycle Assessment*. Ed. by M. A. Curran. LCA Compendium – The Complete World of Life Cycle Assessment. Dordrecht: Springer Netherlands, 2017, pp. 1–62. ISBN: 978-94-024-0854-6. DOI: 10.1007/978-94-024-0855-3{\textunderscore}1 (see p. 16).

[118] Barnhart, C. J. and Benson, S. M.: *On the importance of reducing the energetic and material demands of electrical energy storage*. In: *Energy & Environmental Science* 6.4 (2013), p. 1083. ISSN: 1754-5692. DOI: 10.1039/C3EE24040A (see p. 16).

[119] Joseph, A. and Shahidehpour, M.: "Battery storage systems in electric power systems." In: *2006 IEEE Power Engineering Society General Meeting*. IEEE, 2006, 8 pp. ISBN: 1-4244-0493-2. DOI: 10.1109/PES.2006.1709235 (see p. 17).

[120] Palmer, G.: *A Framework for Incorporating EROI into Electrical Storage*. In: *BioPhysical Economics and Resource Quality* 2.2 (2017). ISSN: 2366-0112. DOI: 10.1007/s41247-017-0022-3 (see p. 17).

[121] Canals Casals, L., Amante García, B., and Cremades, L. V.: *Electric vehicle battery reuse: Preparing for a second life*. In: *Journal of Industrial Engineering and Management* 10.2 (2017), p. 266. ISSN: 2013-8423. DOI: 10.3926/jiem.2009 (see p. 17).

[122] Burke, A.: *Performance, Charging, and Second-use Considerations for Lithium Batteries for Plug-in Electric Vehicles*. 2009. URL: https://escholarship.org/uc/item/2xf263qp (visited on 05/07/2024) (see p. 17).

[123] Rallo, H., Canals Casals, L., La Torre, D. de, Reinhardt, R., Marchante, C., and Amante, B.: *Lithium-ion battery 2nd life used as a stationary energy storage system: Ageing and economic analysis in two real cases*. In: *Journal of Cleaner Production* 272 (2020), p. 122584. ISSN: 09596526. DOI: 10.1016/j.jclepro.2020.122584 (see p. 17).

[124] J. Auger, D., F. Groff, M., Mohan, G., Longo, S., and Assadian, F.: *Impact of Battery Ageing on an Electric Vehicle Powertrain Optimisation*. In: *Journal of Sustainable Development of Energy, Water and Environment Systems* 2.4 (2014), pp. 350–361. DOI: 10.13044/j.sdewes.2014.02.0028 (see p. 17).

[125] Ramoni, M. O. and Zhang, H.-C.: *End-of-life (EOL) issues and options for electric vehicle batteries*. In: *Clean Technologies and Environmental Policy* 15.6 (2013), pp. 881–891. ISSN: 1618-954X. DOI: 10.1007/s10098-013-0588-4 (see p. 17).

[126] Casals, L. C. and Garca, B. A.: *Assessing Electric Vehicles Battery Second Life Remanufacture and Management*. In: *Journal of Green Engineering* 6.1 (2016), pp. 77–98. ISSN: 1904-4720. DOI: 10.13052/jge1904-4720.614 (see p. 17).

[127] DeRousseau, M., Gully, B., Taylor, C., Apelian, D., and Wang, Y.: *Repurposing Used Electric Car Batteries: A Review of Options*. In: *JOM* 69.9 (2017), pp. 1575–1582. ISSN: 1047-4838. DOI: 10.1007/s11837-017-2368-9 (see p. 17).

[128] Hua, Y., Liu, X., Zhou, S., Huang, Y., Ling, H., and Yang, S.: *Toward Sustainable Reuse of Retired Lithium-ion Batteries from Electric Vehicles*. In: *Resources, Conservation and Recycling* 168 (2021), p. 105249. ISSN: 09213449. DOI: 10.1016/j.resconrec.2020.105249 (see pp. 17, 18).

[129] Kampker, A., Wessel, S., Fiedler, F., and Maltoni, F.: *Battery pack remanufacturing process up to cell level with sorting and repurposing of battery cells*. In: *Journal of Remanufacturing* (2020). ISSN: 2210-464X. DOI: 10.1007/s13243-020-00088-6 (see p. 18).

[130] Foster, M., Isely, P., Standridge, C. R., and Hasan, M. M.: *Feasibility assessment of remanufacturing, repurposing, and recycling of end of vehicle application lithium-ion batteries*. In: *Journal of Industrial Engineering and Management* 7.3 (2014). ISSN: 2013-8423. DOI: 10.3926/jiem.939 (see p. 18).

[131] Chen, T., Jin, Y., Lv, H., Yang, A., Liu, M., Chen, B., Xie, Y., and Chen, Q.: *Applications of Lithium-Ion Batteries in Grid-Scale Energy Storage Systems*. In: *Transactions of Tianjin University* 26.3 (2020), pp. 208–217. ISSN: 1006-4982. DOI: 10.1007/s12209-020-00236-w (see p. 18).

[132] Tepe, B., Jablonski, S., Hesse, H., and Jossen, A.: *Lithium-ion battery utilization in various modes of e-transportation*. In: *eTransportation* 18 (2023), p. 100274. ISSN: 25901168. DOI: 10.1016/j.etran.2023.100274 (see p. 18).

[133] Barrera, T. P., Bond, J. R., Bradley, M., Gitzendanner, R., Darcy, E. C., Armstrong, M., and Wang, C.-Y.: *Next-Generation Aviation Li-Ion Battery Technologies—Enabling Electrified Aircraft*. In: *The Electrochemical Society Interface* 31.3 (2022), pp. 69–74. ISSN: 1064-8208. DOI: 10.1149/2.F10223IF (see p. 18).

[134] Killer, M., Farrokhseresht, M., and Paterakis, N. G.: *Implementation of large-scale Li-ion battery energy storage systems within the EMEA region*. In: *Applied Energy* 260 (2020), p. 114166. ISSN: 03062619. DOI: 10.1016/j.apenergy.2019.114166 (see p. 18).

[135] Stecca, M., Ramirez Elizondo, L., Batista Soeiro, T., Bauer, P., and Palensky, P.: *A Comprehensive Review of the Integration of Battery Energy Storage Systems into Distribution Networks*. In: *IEEE Open Journal of the Industrial Electronics Society* (2020), p. 1. DOI: 10.1109/OJIES.2020.2981832 (see p. 19).

[136] Wehner, N. and Daim, T.: *Behind-the-Meter Energy Storage Implementation*. In: *R&D Management in the Knowledge Era*. Ed. by T. Daim, M. Dabić, N. Başoğlu, J. R. Lavoie, and B. J. Galli. Innovation, Technology, and Knowledge Management. Cham: Springer International Publishing, 2019, pp. 71–94. ISBN: 978-3-030-15408-0. DOI: 10.1007/978-3-030-15409-7{\textunderscore}3 (see p. 19).

[137] Rezaeimozafar, M., Monaghan, R. F., Barrett, E., and Duffy, M.: *A review of behind-the-meter energy storage systems in smart grids*. In: *Renewable and Sustainable Energy Reviews* 164 (2022), p. 112573. ISSN: 13640321. DOI: 10.1016/j.rser.2022.112573 (see p. 19).

[138] Müller, M., Viernstein, L., Truong, C. N., Eiting, A., Hesse, H. C., Witzmann, R., and Jossen, A.: *Evaluation of grid-level adaptability for stationary battery energy storage system applications in Europe*. In: *Journal of Energy Storage* 9 (2017), pp. 1–11. ISSN: 2352152X. DOI: 10.1016/j.est.2016.11.005 (see p. 19).

[139] Bereczki, B., Hartmann, B., and Kertesz, S.: “Industrial Application of Battery Energy Storage Systems: Peak shaving.” In: *2019 7th International Youth Conference on Energy (IYCE)*. IEEE, 2019, pp. 1–5. ISBN: 978-1-7281-3923-4. DOI: 10.1109/IYCE45807.2019.8991594 (see p. 19).

[140] Martins, R., Hesse, H., Jungbauer, J., Vorbuchner, T., and Musilek, P.: *Optimal Component Sizing for Peak Shaving in Battery Energy Storage System for Industrial Applications*. In: *Energies* 11.8 (2018), p. 2048. DOI: 10.3390/en11082048 (see p. 19).

[141] Chua, K. H., Lih Bong, H., Lim, Y. S., Wong, J., and Wang, L.: "The State-of-the-Arts of Peak Shaving Technologies: A Review." In: *2020 International Conference on Smart Grid and Clean Energy Technologies (ICSGCE)*. IEEE, 2020, pp. 162–166. ISBN: 978-1-7281-5736-8. DOI: 10.1109/ICSGCE49177.2020.9275637 (see p. 19).

[142] Telaretti, E. and Dusonchet, L.: "Battery storage systems for peak load shaving applications: Part 1: Operating strategy and modification of the power diagram." In: *2016 IEEE 16th International Conference on Environment and Electrical Engineering (EEEIC)*. IEEE, 2016, pp. 1–6. ISBN: 978-1-5090-2320-2. DOI: 10.1109/EEEIC.2016.7555793 (see p. 19).

[143] Uddin, M., Romlie, M. F., Abdullah, M. F., Tan, C., Shafiullah, G. M., and Bakar, A.: *A novel peak shaving algorithm for islanded microgrid using battery energy storage system*. In: *Energy* 196 (2020), p. 117084. ISSN: 03605442. DOI: 10.1016/j.energy.2020.117084 (see p. 19).

[144] Oudalov, A., Cherkaoui, R., and Beguin, A.: "Sizing and Optimal Operation of Battery Energy Storage System for Peak Shaving Application." In: *2007 IEEE Lausanne Power Tech*. IEEE, 2007, pp. 621–625. ISBN: 978-1-4244-2189-3. DOI: 10.1109/PCT.2007.4538388 (see p. 19).

[145] Uddin, M., Romlie, M. F., Abdullah, M. F., Abd Halim, S., Abu Bakar, A. H., and Chia Kwang, T.: *A review on peak load shaving strategies*. In: *Renewable and Sustainable Energy Reviews* 82 (2018), pp. 3323–3332. ISSN: 13640321. DOI: 10.1016/j.rser.2017.10.056 (see p. 19).

[146] Hollinger, R., Diazgranados, L. M., Wittwer, C., and Engel, B.: *Optimal Provision of Primary Frequency Control with Battery Systems by Exploiting All Degrees of Freedom within Regulation*. In: *Energy Procedia* 99 (2016), pp. 204–214. ISSN: 18766102. DOI: 10.1016/j.egypro.2016.10.111 (see p. 19).

[147] Thien, T., Schweer, D., vom Stein, D., Moser, A., and Sauer, D. U.: *Real-world operating strategy and sensitivity analysis of frequency containment reserve provision with battery energy storage systems in the german market*. In: *Journal of Energy Storage* 13 (2017), pp. 143–163. ISSN: 2352152X. DOI: 10.1016/j.est.2017.06.012 (see p. 19).

[148] Zeh, A., Müller, M., Naumann, M., Hesse, H., Jossen, A., and Witzmann, R.: *Fundamentals of Using Battery Energy Storage Systems to Provide Primary Control Reserves in Germany*. In: *Batteries* 2.3 (2016), p. 29. DOI: 10.3390/batteries2030029 (see p. 19).

[149] Fernández-Muñoz, D., Pérez-Díaz, J. I., Guisández, I., Chazarra, M., and Fernández-Espina, Á.: *Fast frequency control ancillary services: An international review*. In: *Renewable and Sustainable Energy Reviews* 120 (2020), p. 109662. ISSN: 13640321. DOI: 10.1016/j.rser.2019.109662 (see p. 20).

[150] Thorbergsson, E., Knap, V., Swierczynski, M., Stroe, D., and Teodorescu, R.: *Primary Frequency Regulation with Li-Ion Battery Based Energy Storage System - Evaluation and Comparison of Different Control Strategies*. In: *Intelec 2013, 35th International Telecommunications Energy Conference, SMART POWER AND EFFICIENCY*. URL: https://ieeexplore.ieee.org/abstract/document/6663276 (visited on 01/10/2024) (see p. 20).

[151] Fleer, J., Zurmühlen, S., Badeda, J., Stenzel, P., Hake, J.-F., and Sauer, D. U.: *Model-based Economic Assessment of Stationary Battery Systems Providing Primary Control Reserve*. In: *Energy Procedia* 99 (2016), pp. 11–24. ISSN: 18766102. DOI: 10.1016/j.egypro.2016.10.093 (see p. 20).

[152] Engels, J., Claessens, B., and Deconinck, G.: *Techno-economic analysis and optimal control of battery storage for frequency control services, applied to the German market.* In: *Applied Energy* 242 (2019), pp. 1036–1049. ISSN: 03062619. DOI: 10.1016/j.apenergy.2019.03.128 (see p. 20).

[153] Chen, A. and Sen, P. K.: "Deployment of battery energy storage system for energy arbitrage applications." In: *2016 North American Power Symposium (NAPS)*. IEEE, 2016, pp. 1–8. ISBN: 978-1-5090-3270-9. DOI: 10.1109/NAPS.2016.7747920 (see p. 20).

[154] Wankmüller, F., Thimmapuram, P. R., Gallagher, K. G., and Botterud, A.: *Impact of battery degradation on energy arbitrage revenue of grid-level energy storage.* In: *Journal of Energy Storage* 10 (2017), pp. 56–66. ISSN: 2352152X. DOI: 10.1016/j.est.2016.12.004 (see p. 20).

[155] Fares, R. L. and Webber, M. E.: *What are the tradeoffs between battery energy storage cycle life and calendar life in the energy arbitrage application?* In: *Journal of Energy Storage* 16 (2018), pp. 37–45. ISSN: 2352152X. DOI: 10.1016/j.est.2018.01.002 (see p. 20).

[156] Schimpe, M., Truong, C. N., Naumann, M., Jossen, A., Hesse, H. C., Reniers, J. M., and Howey, D. A.: "Marginal Costs of Battery System Operation in Energy Arbitrage Based on Energy Losses and Cell Degradation." In: *2018 IEEE International Conference on Environment and Electrical Engineering and 2018 IEEE Industrial and Commercial Power Systems Europe (EEEIC / I&CPS Europe)*. IEEE, 2018, pp. 1–5. ISBN: 978-1-5386-5186-5. DOI: 10.1109/EEEIC.2018.8493717 (see p. 20).

[157] Agnew, S. and Dargusch, P.: *Effect of residential solar and storage on centralized electricity supply systems.* In: *Nature Climate Change* 5.4 (2015), pp. 315–318. ISSN: 1758-678X. DOI: 10.1038/nclimate2523 (see p. 20).

[158] Barcellona, S., Piegari, L., Musolino, V., and Ballif, C.: *Economic viability for residential battery storage systems in grid–connected PV plants.* In: *IET Renewable Power Generation* 12.2 (2018), pp. 135–142. ISSN: 1752-1416. DOI: 10.1049/iet-rpg.2017.0243 (see p. 20).

[159] Weniger, J., Tjaden, T., and Quaschning, V.: *Sizing of Residential PV Battery Systems.* In: *Energy Procedia* 46 (2014), pp. 78–87. ISSN: 18766102. DOI: 10.1016/j.egypro.2014.01.160 (see p. 20).

[160] Hesse, H., Schimpe, M., Kucevic, D., and Jossen, A.: *Lithium-Ion Battery Storage for the Grid—A Review of Stationary Battery Storage System Design Tailored for Applications in Modern Power Grids.* In: *Energies* 10.12 (2017), p. 2107. DOI: 10.3390/en10122107 (see p. 20).

[161] Angenendt, G., Zurmühlen, S., Axelsen, H., and Sauer, D. U.: *Comparison of different operation strategies for PV battery home storage systems including forecast-based operation strategies.* In: *Applied Energy* 229 (2018), pp. 884–899. ISSN: 03062619. DOI: 10.1016/j.apenergy.2018.08.058 (see p. 20).

[162] Khezri, R., Mahmoudi, A., and Aki, H.: *Optimal planning of solar photovoltaic and battery storage systems for grid-connected residential sector: Review, challenges and new perspectives.* In: *Renewable and Sustainable Energy Reviews* 153 (2022), p. 111763. ISSN: 13640321. DOI: 10.1016/j.rser.2021.111763 (see p. 21).

[163] Hoppmann, J., Volland, J., Schmidt, T. S., and Hoffmann, V. H.: *The economic viability of battery storage for residential solar photovoltaic systems – A review and a simulation model.* In: *Renewable and Sustainable Energy Reviews* 39 (2014), pp. 1101–1118. ISSN: 13640321. DOI: 10.1016/j.rser.2014.07.068 (see p. 21).

[164] Cong Nam Truong, Lorenz Viernstein, Michael Schimpe, Rolf Witzmann, Andreas Jossen, and Holger C. Hesse: *Maximizing Solar Home Battery Systems' Contribution to the Energy Transition of the Power System*. In: URL: https://ieeexplore.ieee.org/abstract/document/8421821 (visited on 05/11/2020) (see p. 21).

[165] Komor, P. and Glassmire, J.: *Electricity Storage and Renewables for Island Power: A Guide for Decision Makers*. Bonn, Germany, 2012. URL: https://www.irena.org/-/media/Files/IRENA/Agency/Publication/2012/Electricity-Storage-and-RE-for-Island-Power.pdf?rev=3305b264da6249c3b6e14e7c059720e5 (visited on 04/27/2024) (see p. 21).

[166] Rampazzo, M., Luvisotto, M., Tomasone, N., Fastelli, I., and Schiavetti, M.: *Modelling and simulation of a Li-ion energy storage system: Case study from the island of Ventotene in the Tyrrhenian Sea*. In: *Journal of Energy Storage* 15 (2018), pp. 57–68. ISSN: 2352152X. DOI: 10.1016/j.est.2017.10.017 (see p. 21).

[167] Malhotra, A., Battke, B., Beuse, M., Stephan, A., and Schmidt, T.: *Use cases for stationary battery technologies: A review of the literature and existing projects*. In: *Renewable and Sustainable Energy Reviews* 56 (2016), pp. 705–721. ISSN: 13640321. DOI: 10.1016/j.rser.2015.11.085 (see p. 21).

[168] Fiorentzis, K., Katsigiannis, Y., and Karapidakis, E.: *Full-Scale Implementation of RES and Storage in an Island Energy System*. In: *Inventions* 5.4 (2020), p. 52. DOI: 10.3390/inventions5040052 (see p. 21).

[169] Katsaprakakis, D. A., Dakanali, I., Condaxakis, C., and Christakis, D. G.: *Comparing electricity storage technologies for small insular grids*. In: *Applied Energy* 251 (2019), p. 113332. ISSN: 03062619. DOI: 10.1016/j.apenergy.2019.113332 (see p. 21).

[170] Globisch, J., Plötz, P., Dütschke, E., and Wietschel, M.: *Consumer preferences for public charging infrastructure for electric vehicles*. In: *Transport Policy* 81 (2019), pp. 54–63. ISSN: 0967070X. DOI: 10.1016/j.tranpol.2019.05.017 (see p. 21).

[171] Rivera, S., Goetz, S. M., Kouro, S., Lehn, P. W., Pathmanathan, M., Bauer, P., and Mastromauro, R. A.: *Charging Infrastructure and Grid Integration for Electromobility*. In: *Proceedings of the IEEE* 111.4 (2023), pp. 371–396. ISSN: 0018-9219. DOI: 10.1109/JPROC.2022.3216362 (see p. 22).

[172] Wang, X., Kaleybar, H. J., Brenna, M., and Zaninelli, D.: "Power Quality Indicators of Electric Vehicles in Distribution Grid." In: *2022 20th International Conference on Harmonics & Quality of Power (ICHQP)*. IEEE, 2022, pp. 1–6. ISBN: 978-1-6654-1639-9. DOI: 10.1109/ICHQP53011.2022.9808823 (see p. 22).

[173] Lee, Z. J., Pang, J. Z., and Low, S. H.: *Pricing EV charging service with demand charge*. In: *Electric Power Systems Research* 189 (2020), p. 106694. ISSN: 03787796. DOI: 10.1016/j.epsr.2020.106694 (see p. 22).

[174] Kucevic, D., Englberger, S., Sharma, A., Trivedi, A., Tepe, B., Schachler, B., Hesse, H., Srinivasan, D., and Jossen, A.: *Reducing grid peak load through the coordinated control of battery energy storage systems located at electric vehicle charging parks*. In: *Applied Energy* 295 (2021), p. 116936. ISSN: 03062619. DOI: 10.1016/j.apenergy.2021.116936 (see p. 22).

[175] Wüllner, J., Reiners, N., Millet, L., Salibi, M., Stortz, F., and Vetter, M.: *Review of Stationary Energy Storage Systems Applications, Their Placement, and Techno-Economic Potential*. In: *Current Sustainable/Renewable Energy Reports* 8.4 (2021), pp. 263–273. DOI: 10.1007/s40518-021-00188-2 (see p. 22).

[176] Bryden, T. S., Hilton, G., Dimitrov, B., Ponce de Leon, C., and Cruden, A.: *Rating a Stationary Energy Storage System Within a Fast Electric Vehicle Charging Station Considering User Waiting Times*. In: *IEEE Transactions on Transportation Electrification* 5.4 (2019), pp. 879–889. DOI: 10.1109/TTE.2019.2910401 (see p. 22).

[177] Möller, M., Kucevic, D., Collath, N., Parlikar, A., Dotzauer, P., Tepe, B., Englberger, S., Jossen, A., and Hesse, H.: *SimSES: A holistic simulation framework for modeling and analyzing stationary energy storage systems*. In: *Journal of Energy Storage* 49 (2022), p. 103743. ISSN: 2352152X. DOI: 10.1016/j.est.2021.103743 (see p. 23).

[178] Herbst, A., Toro, F., Reitze, F., and Jochem, E.: *Introduction to Energy Systems Modelling*. In: *Swiss Journal of Economics and Statistics* 148.2 (2012), pp. 111–135. DOI: 10.1007/BF03399363 (see p. 27).

[179] Lopion, P., Markewitz, P., Robinius, M., and Stolten, D.: *A review of current challenges and trends in energy systems modeling*. In: *Renewable and Sustainable Energy Reviews* 96 (2018), pp. 156–166. ISSN: 13640321. DOI: 10.1016/j.rser.2018.07.045 (see p. 27).

[180] Pfenninger, S., Hawkes, A., and Keirstead, J.: *Energy systems modeling for twenty-first century energy challenges*. In: *Renewable and Sustainable Energy Reviews* 33 (2014), pp. 74–86. ISSN: 13640321. DOI: 10.1016/j.rser.2014.02.003 (see p. 27).

[181] Prina, M. G., Manzolini, G., Moser, D., Nastasi, B., and Sparber, W.: *Classification and challenges of bottom-up energy system models - A review*. In: *Renewable and Sustainable Energy Reviews* 129 (2020), p. 109917. ISSN: 13640321. DOI: 10.1016/j.rser.2020.109917 (see p. 27).

List of Figures

Supervised Student Works

a Anand, A.: *Second-Life Lithium Ion Batteries (German: Lithium-Ionen-Batterien im zweiten Lebenszyklus)*, Seminar Report, 2018

b Amer, A.: *System-level Battery Modelling (German: Batteriemodellierung auf Systemebene)*, Seminar Report, 2019

c Gnacy, M.: *Charakterisierung von Second-Life-Batterien für die Anwendung in stationären Energiespeichern (English: Characterization of second-life batteries for application in stationary energy storage systems)*, Master's Thesis, 2019

d Kumar, K.: *An Electro-Thermal Modeling Approach for Thermal Management of Lithium-ion based Stationary Battery Energy Storage Systems (German: Ein elektrothermischer Modellierungsansatz für das thermische Management von Lithium-Ionen-basierten stationären Batterieenergiespeichersystemen)*, Master's Thesis, 2020

e Bhutkar, A.: *Current and Future Development of Lithium Ion Battery Recycling: An Overview (German: Aktuelle und zukünftige Entwicklung des Recyclings von Lithium-Ionen-Batterien: Ein Überblick)*, Seminar Report, 2020

f Schott, M.: *Comparison of Lifetime Emissions of Battery-Assisted High Power Charging Station with Grid Reinforcement Measures (German: Vergleich der Lebensdaueremissionen einer batterieunterstützten Hochleistungsladestation mit Netzausbaumaßnahmen)*, Master's Thesis, 2020

g Gholap, A.: *Aging Modelling Procedure for Lithium-Ion Batteries (German: Alterungsmodellierungsverfahren für Lithium-Ionen-Batterien)*, Seminar Report, 2021

h Velasquez Gomez, G.: *Performance Evaluation Methodologies for Stationary Energy Storage Systems (German: Leistungsbewertungsmethoden für stationäre Energiespeichersysteme)*, Seminar Report, 2021

i Gholap, A.: *ZEC Bike for Smart Cities –Thermal Management of Battery (German: ZEC Bike für Smart Cities – Thermisches Management der Batterie)*, Research Internship, 2021

j Langschartner, P.: *Zeitreihenbasiertes solares Einstrahlungsmodell für einen Batteriespeicher in Containerbauweise (English: Time series-based solar irradiance model for a containerized battery storage system)*, Research Internship, 2021

k Contractor, S.: *Component-wise Cost Evaluation Model of New and Second Life Li-ion Battery Systems for Stationary Applications (German: Komponentenweise Kostenbewertungsmodell für neue und Second-Life-Li-Ionen-Batteriesysteme für stationäre Anwendungen)*, Master's Thesis, 2021

l Hassan, O.: *Battery Swapping for Electric Vehicles (EVs): Opportunities and Challenges (German: Batteriewechsel für Elektrofahrzeuge (EVs): Chancen und Herausforderungen)*, Seminar Report, 2022

m Pankova, B.: *Evaluation methodologies and metrics for stationary energy storage systems and case studies (German: Bewertungsmethoden und Kennzahlen für stationäre Energiespeichersysteme und Fallstudien)*, Research Internship, 2022

n Syed, M.: *Modeling and Analysis of Battery Swapping Technology (German: Modellierung und Analyse der Batteriewechseltechnologie)*, Research Internship, 2022

o Yu, R.: *Data-Driven Understanding and Efficient Prediction of Thermal Behavior for Electric*

Vehicle Battery using Artificial Intelligence (German: Datengetriebenes Verständnis und effiziente Vorhersage des thermischen Verhaltens von Elektrofahrzeugbatterien mithilfe künstlicher Intelligenz), Master's Thesis, 2022

p Renger, V.: *End-of-Life of Electric Vehicle Batteries: a Cost Model and a Review of Business Ideas Along the Remanufacturing, Repurposing and Recycling Value Chains (German: Ende des Lebenszyklus von Elektrofahrzeug-Batterien: Ein Kostenmodell und eine Überprüfung von Geschäftsideen entlang der Wiederaufbereitungs-, Umnutzungs- und Recycling-Wertschöpfungsketten)*, Master's Thesis, 2022

q Narayana, S.: *Energy Management Strategies for Battery Swapping Stations (German: Energiemanagementstrategien für Batteriewechselstationen)*, Seminar Report, 2023

r Malik, A.: *Estimation of the carbon footprint of Battery Energy Storage Systems in typical applications (German: Abschätzung des CO2-Fußabdrucks von Batteriespeichersystemen in typischen Anwendungen)*, Seminar Report, 2023

s Kulkarni, A.: *Roads to Grids: Assessing the Carbon Footprint of Lithium-ion batteries (German: Straßen zu Netzen: Bewertung des CO2-Fußabdrucks von Lithium-Ionen-Batterien)*, Research Internship, 2024

Acknowledgement

It is with immense satisfaction and a deep sense of gratitude that I look back at my time with the Chair of Electrical Energy Storage Technology (EES) at the Technical University of Munich (TUM). This dissertation bears testimony to the vast amount of knowledge and insights I have been fortunate enough to gain during this period. This dissertation also marks the culmination of my association of nearly eight and a half years with TUM, first as a master's degree student and later as a doctoral researcher. I take this opportunity to sincerely acknowledge all those who have supported, guided, and accompanied me through this journey.

I am grateful to my doctoral supervisor, Prof. Dr.-Ing. Andreas Jossen, whom I, and needless to say, the wider scientific community, hold in high regard. My transformation from a second-semester master's degree student enrolled in Prof. Jossen's course Energy Storage EI8033 in the summer of 2016 to assisting Prof. Jossen in conducting the course for four years (2019-2022) was an exceptional honor. I cherish all my scientific discussions and conversations with Prof. Jossen. The role of my doctoral co-supervisor, (now) Prof. Dr.rer.nat. Holger Hesse, in the completion of this dissertation and in my own growth story, can hardly be overstated. Holger gave me a place in the Stationary Energy Storage Systems (SES) research group he led at EES, placed faith in me, mentored me, coached me, and oversaw my progress. Both my doctoral supervisor and co-supervisor have my utmost respect and have helped me become an independent thinker and researcher.

I thank all my EES colleagues and the alumni community for sharing knowledge, insights, and for an environment so conducive to mutual learning and productivity that everyone could effectively grow together. I especially thank my colleagues in the erstwhile SES research group who helped make the mundane everyday grind of doctoral research meaningful and purpose-driven. Stefan Englberger and I shared an office for the longest period, confiding in each other on matters ranging from professional to personal. Benedikt Tepe was a steadfast presence for almost the entirety of my time at EES and was someone I could confide in and turn to. I thank Marc Möller for sharing insights and best practices from his rich experience in the industry, especially with large programming projects. Daniel Kucevic and Nils Collath deserve thanks for their input, support, friendship, and, above all, companionship in our shared journey. Special thanks are due to Carolin Nierwetberg and Dr.rer.nat. Gudrun Rahn-Koltermann for their deft handling of administrative and project management matters. I also thank all my students for their contributions, which are listed in the previous section.

This dissertation is a tribute to my parents (Manjiri Parlikar and Gajanan Parlikar), grandparents, and family, whose sacrifices, untiring encouragement, guidance, blessings, and motivation have carried me to this juncture in life. I especially thank my aunt, Dr. Vasundhara Kamineni, and my uncles, Sanjay Sabnis and Venkatesh Parlikar, who took a special interest in my studies and academic pursuits. My wife, Aditi, is a claimant to substantial credit for the completion of this dissertation through her unwavering support and motivation. I am grateful to my friends, Dr. Shubham Joshi, Dr. Pankaj Madkikar, and Dr. Pushkar Deshpande, who always had an empathetic ear and sound advice on offer. I am fortunate to count Chandan, Himanshu, Florian, Aman, Rene, Sanchay, Ankur, Ayush, and many other brilliant human beings among my friends who shared these years with me.

Appendix

Modeling battery energy storage systems with SimSES

This chapter presents the article ”SimSES: A holistic simulation framework for modeling and analyzing stationary energy storage systems” and introduces SimSES as an advanced simulation framework designed to meet the growing need for comprehensive analysis tools in the realm of stationary energy storage systems. SimSES is a critical tool offering both technical and economic evaluations of various energy storage technologies and their integration into energy systems.

SimSES stands out due to its modular design, allowing for the simulation of diverse storage technologies, including lithium-ion batteries, redox flow batteries, and hydrogen energy chains. This modularity extends to system components and topologies, empowering users to tailor the framework to specific analysis needs. The framework encapsulates the complexity of stationary energy storage systems, incorporating models for EMS, power electronics, and thermal management, which are essential for realistic simulations of energy storage deployment and operation. One of the key strengths of SimSES is its capability to perform detailed technical and economic evaluations. Through a range of key performance indicators (KPIs), SimSES offers insights into the performance, efficiency, degradation, and economic viability of energy storage solutions under various scenarios. Integrating detailed physical models with comprehensive economic analysis interests a broad spectrum of stakeholders, including researchers, industry practitioners, and policymakers. This is showcased through case studies, such as peak shaving and frequency containment reserve applications with different storage configurations and operational strategies.

The highlights of this article include:

- A unified simulation framework to accurately model and analyze various energy storage technologies, such as lithium-ion batteries, redox flow batteries, and hydrogen energy chains
- The impacts of different EMS and operation strategies on the performance and efficiency of energy storage systems
- Evaluation of the technical performance and economic viability of stationary energy storage systems
- The benefits and challenges of integrating hybrid energy storage systems, combining multiple storage technologies, into the power grid

In summary, SimSES is a powerful simulation framework that not only enhances understanding of the technical and economic aspects of stationary energy storage systems but also supports informed decision-making in deploying and optimizing these systems. It contributes to integrating renewable energy sources and the transition towards more sustainable and resilient energy systems. The article also highlights potential expansions of SimSES to include new storage technologies, complex system topologies, and sophisticated operational strategies, underscoring its ongoing relevance and adaptability to the evolving landscape of energy storage integration.

Author contributions

Marc Möller was the lead author of this article and was responsible for the conceptualization, methodology, software, project management, visualization, investigation, and preparation of the original draft and subsequent revisions. Daniel Kucevic contributed to the methodology, software, validation, and the original draft and subsequent revisions. Nils Collath, Anupam Parlikar, and Petra Dotzauer contributed to the methodology, software, and the original draft and its revisions. Benedikt Tepe contributed to the investigation, software, and in the preparation of the drafts. Stefan Englberger assisted with the investigation, validation, and in the preparation of the drafts. Andreas Jossen was instrumental in acquiring funding and resources for the project and reviewing the manuscript. Holger Hesse was involved in the preparation and review of the original manuscript, as well as in supervising the project.

SimSES: A holistic simulation framework for modeling and analyzing stationary energy storage systems

Marc Möller, Daniel Kucevic, Nils Collath, Anupam Parlikar, Petra Dotzauer, Benedikt Tepe, Stefan Englberger, Andreas Jossen, and Holger Hesse

Journal of Energy Storage (49), 103743, 2022

Permanent weblink:
https://doi.org/10.1016/j.est.2021.103743

Journal of Energy Storage 49 (2022) 103743

Contents lists available at ScienceDirect

Journal of Energy Storage

journal homepage: www.elsevier.com/locate/est

Research papers

SimSES: A holistic simulation framework for modeling and analyzing stationary energy storage systems

Marc Möller [a,*], Daniel Kucevic [a], Nils Collath [a], Anupam Parlikar [a], Petra Dotzauer [b], Benedikt Tepe [a], Stefan Englberger [a], Andreas Jossen [a], Holger Hesse [a]

[a] Institute for Electrical Energy Storage Technology, Technical University of Munich (TUM), Arcisstr. 21, 80333 Munich, Germany
[b] Bavarian Center for Applied Energy Research (ZAE Bayern), Department of Energy Storage, Walther-Meiner-Str. 6, 85748 Garching, Germany

ARTICLE INFO

Keywords:
Energy storage system simulation
Lithium-ion battery
Redox flow battery
Hydrogen technology
Storage system design
Stationary application

ABSTRACT

The increasing feed-in of intermittent renewable energy sources into the electricity grids worldwide is currently leading to technical challenges. Stationary energy storage systems provide a cost-effective and efficient solution in order to facilitate the growing penetration of renewable energy sources. Major technical and economical challenges for energy storage systems are related to lifetime, efficiency, and monetary returns. Holistic simulation tools are needed in order to address these challenges before investing in energy storage systems. One of these tools is SimSES, a holistic simulation framework specialized in evaluating energy storage technologies technically and economically. With a modular approach, SimSES covers various topologies, system components, and storage technologies embedded in an energy storage application. This contribution shows the capabilities and benefits of SimSES by providing in-depth knowledge of the implementations and models. Selected functionalities are demonstrated, with two use cases showing the easy-to-use simulation framework while providing detailed technical analysis for expert users. Hybrid energy storage systems consisting of lithium-ion and redox-flow batteries are investigated in a peak shaving application, while various system topologies are analyzed in a frequency containment reserve application. The results for the peak shaving case study show a benefit in favor of the hybrid system in terms of overall cost and degradation behavior in applications that have a comparatively low energy throughput during lifetime. In terms of system topology, a cascaded converter approach shows significant improvements in efficiency for the frequency containment reserve application.

1. Introduction

In former decades, the worldwide energy transition was predominantly driven by introducing more Renewable Energy Sources (RES) capacity to existing power networks, a process strongly supported by both globally declining cost for wind and solar power generation as well as through local legislation support, including subsidy schemes [1,2]. Following these early stage developments, the energy transition in various regions has now started to face new constraints and technical challenges, which demand other and often more site-specific solution approaches. Coupling of the power grid to both heating and electrified transport is certainly a key strategy to increase RES penetration on a global and nationwide level within the power system itself. At the same time, increasing the intermittence of supply that relies more on variable sources like solar and wind generation brings incorporation of grid-tied energy storage into discussion as a technically mature and potentially cost-competitive measure addressing volatility issues [3].

In order to categorize storage integration in power grids we may distinguish among Front-The-Meter (FTM) and Behind-the-Meter (BTM) applications [4]. FTM includes applications such as storage-assisted renewable energy time shift [5], wholesale energy arbitrage [6,7], and Frequency Containment Reserve (FCR) provision [8]. A more distributed and locally coordinated power supply is discussed in the context of BTM applications, e.g., Peak Shaving (PS) for industrial sites or at electric vehicle charging stations [9], or bill-saving at residential sites through Self-Consumption Increase (SCI) with local photovoltaic generation (residential battery storage) [10]. However, before taking a solid investment decision, it is crucial to analyze and optimize the technical parameters, storage dispatch control, as well as cost/revenue streams over the course of the entire project lifetime. Simulation and modeling tools in conjunction with sensitivity analyzes and optimization routines are commonly used to support these crucial steps in the planning and operational phase of grid-integrated storage projects.

* Corresponding author.
E-mail address: marc.moeller@tum.de (M. Möller).

https://doi.org/10.1016/j.est.2021.103743
Received 10 March 2021; Received in revised form 30 August 2021; Accepted 2 December 2021
Available online 24 February 2022

The Simulation Tool for Stationary Energy Storage Systems (**SimSES**) was developed to assist through the aforementioned tasks of storage system planning and operation. Through combining user-defined inputs with pre-parameterized component building blocks, as well as calculation methods and result analysis functions, a reserve is built for research, industry, and policy makers in equal measure to support deployment and enrollment of storage integration to the grid. The approach of **SimSES** is presented within this contribution.

In Section 2, comparable existing tools are reviewed and evaluated before the structure of **SimSES** is elaborated further in Section 3 as well as its detail models for storage technologies (Section 4) and its periphery (Section 5). Afterwards, in Section 6 two case studies are presented to show the capabilities of **SimSES** and concludes with a summary and outlook of further investigations in Section 7.

2. Literature review

Various authors have analyzed sizing and (economically) optimal operation of a specifically chosen storage system in a dedicated application setting, e.g., the usage of redox flow battery (RFB) for industrial PS applications [9] or the usage of lithium-ion battery (LIB) for SCI [11, 12]. Fewer studies exist comparing the suitability of different storage options for a given use case, e.g., refer to Toledo et al. [13] for a suitability comparison of different storage types for conducting residential self-consumption increase. Also, the profitability attainable across different applications was analyzed with a given technology to start off with, e.g., LIB in a wide range of application settings [14]. There is consensus that no uniform ideal candidate to meet all application-specific requirements exists within the storage technologies available to date [15]. In order to predict internal states of a storage system such as the State of Health (SOH) or the storage internal losses, it may become necessary to parameterize and simulate an adequately complex model of a storage system. Furthermore, simulations need to be fed with an operational concept that complies with the application constrains, and may deliver the compatibility of a given configuration as well as provide state predictions for the storage system. From an investor's perspective and ultimately for the most cost-effective integration of storage system to power grids with a high share of Variable Renewable Energy Sources (vRES), it is detrimental to conduct in-depth sensitivity and optimization studies relying on a full spectrum techno-economic model before subsequent tasks of project acquisition, realization, operation, and ultimately disposal are to be considered.

In the following, an overview of a selection of depicted tools for the techno-economic modeling of stationary storage in grid applications is provided. While Table 1 summarizes some of the main characteristics of these tools, it should be noted that this paper does not claim to provide a complete overview of all tools that may be relevant in the context matter.

GridLab-D,[1] developed and distributed via Pacific Northwest National Laboratory (*PNNL*), is a universal tool that allows modeling and analyzing multi-component power system networks. Its strength lies in the ability to simulate physical properties of various components through setting up and solving multiple differential equations, describing all sub-components in the modeling region. While the tool is certainly strong in modeling an entire micro-grid with its numerous grid states, it lacks detailed performance models for energy storage systems as well as application-specific parameterization and is therefore not applicable for detailed techno-economic analysis and optimization of storage project as it is focused in this work.

Other tools like **NAS Battery Simulator**,[2] **PNNL Flow Battery Calculator**,[3] and **H2FAST**,[4] are tools dedicated to specific storage types being sodium sulfur battery (NaS) redox flow, and electrolysis/hydrogen storage, respectively. These tools are developed for conducting rapid cost-revenue calculations for the specific technology of choice and offer limited user-specific input in terms of system parameterization and choice of application use case. Nevertheless, the aforementioned tools are confined to a dedicated storage system technology, rendering them less suitable for cross-technology comparisons. Furthermore, most tools of this kind are distributed as a proprietary code, matching only a dedicated commercial product well, and are not suitable for conducting sensitivity analyzes and adaption to envisioned new storage system control and operation.

More tailored simulations can be conducted using the tool **PerModAC** developed at htw Berlin [16]. Using this open-source software tool, performance and efficiency modeling of PV-coupled residential battery storage systems can be conducted. While the tool is extraordinarily strong in conducting battery storage product-specific performance and efficiency modeling, the model lacks the capabilities to analyze battery degradation. More importantly, the current version of this open-source tool is strictly confined to a specific residential BTM use case and cannot be used directly for cross-application assessments, as is desired for an investor's decision support.

Homer Pro and **Homer Grid** are more versatile modeling tools when it comes to comparing and optimizing the techno-economic performance of storage systems in (micro-)grids. The tools support various storage specific libraries and application-specific modeling capabilities, e.g., storage-supported renewable energy time shift in island grids as well as peak-shaving and solar-plus storage calculations in the current professional versions, and has been used in various scientific publications [17,18]. The software was developed by National Renewable Energy Laboratory (*NREL*), but the license for these tools are distributed solely via *Homerenergy* as a commercial product and cannot be extended/adapted according to the users' desire to address new application scenarios, specific personal needs, or local regulation frameworks. E.g., applications like the provision of frequency containment reserve and arbitrage marketing scenarios are not covered in the current version of the software tools.

Two other tools developed by *NREL* and Sandia National Laboratories (*SNL*) are worth looking at in more detail: **BLAST**[5] (Battery Lifetime Analysis and Simulation Tool) is a powerful software suite programmed using MATLAB® and it is distributed for both vehicle and stationary BTM applications. BLAST-BTM-Lite has powerful modeling capabilities for battery performance and lifetime calculations in stationary BTM applications and it includes both optimization and basic economic calculations. While it is highly recommended that this tool to be looked at closer by users interested in PV self-consumption and PS application, applications (only BTM) and storage systems to be analyzed (only conventional electro-chemical batteries) are clearly limited and confined. Furthermore, its original code structure lies hidden behind a graphical user interface and a proprietary executable file, making it unfeasible for the end-user to adapt parameters, e.g., sample time for peak shaving control.

The System Advisor Model[6] (**SAM**) tool builds up on a PV modeling framework originally set up by *SNL* and is now distributed via *NREL*. In its current version it allows coupling of battery storage with PV systems and incorporates financial models, e.g., for Power Purchase Agreement (PPA) calculations. More importantly, the user interface has been re-factored and is now distributed as an open-source software development kit for the Python programming language, allowing others to contribute with their individual extensions and developments. Nevertheless, on the technology side of its current version only batteries are supported and implemented (no other storage media).

[1] https://www.gridlabd.org/

[2] https://www.ngk-insulators.com/en/product/nas/simulator/

[3] https://github.com/PNNL-OE-Redox-Flow-Battery-Cost-Tool/PNNL-OE-Redox-Flow-Battery-Cost-Tool

[4] https://www.nrel.gov/hydrogen/h2fast.html

[5] https://www.nrel.gov/transportation/blast-btm-lite.html

[6] https://sam.nrel.gov/about-sam.html

Table 1
Overview of technical and economic modeling tools for energy storage in stationary applications.

Tool name	License type	Developer (primary)	Focus
GridLab-D	BSD open license	PNNL	Multi-domain state modeling for power distribution system simulation
NAS Battery Simulator	commercial	NGK-insulators	NGK product-tailored NaS battery simulation in peak shaving application
Flow Battery Calculator	open source	PNNL	Estimation tool of cost for redox flow batteries
H2FAST	open source (Excel sheet)	NREL	Economic assessment of hydrogen fuel stations
PerModAC	open source	htw	Performance and efficiency modeling of PV coupled residential battery storage systems
Homer Pro	commercial	Homerenergy (UL.com)	Residential/Microgrid modeling—multiple storage systems, multiple application scenarios
BLAST-BTM-Lite	commercial freeware (lite version)	NREL	Analysis and modeling of battery degradation
StorageVET	open source	EPRI	Optimization of size and financial evaluation of energy storage
SAM — System Advisor Model	BSD-3-clause	NREL	Modeling and analysis software for renewable energy projects
SimSES	BSD-3-clause	TUM	Physically motivated energy storage component, system and application behavior model

The storage value estimation tool[7] (**StorageVET**) developed mainly by the Electric Power Research Institute (*EPRI*) comes with a documentation, tutorial videos, and a user feedback forum. Since the release of version 2.0 the tool has been available as a Python package and most functional parts are licensed as 3-clause BSD open source. The tools allow conducting cost–benefit analysis and includes various application services like voltage support, retail demand charge reduction, frequency regulation, and even value stacking via aggregating multiple services to be served by one storage system. While the interface to the generation and storage technologies allows multiple options, at present only a very limited number of choices is available (PV/Internal Combustion Engine (ICE) and Battery/Compressed Air Energy Storage (CAES)). Furthermore, performance and degradation modeling is very limited, as it is based on an energy bucket model rather than analyzing the voltage and current specific phenomena of real world electro-chemical devices. Also, there is no thermal model included in the calculations, limiting the value of simulations for temperature sensible parameters like storage system efficiency (including Heating Ventilation Air Conditioning (HVAC) consumption) and storage aging.

Unlike the aforementioned tools, **SimSES** aims to bring together the model precision of tools like **SAM** and **PermodAC** and combine it with an interface to various applications and energy market scenarios. To do so, the model is distributed as open-source code on Gitlab[8] and Python Package Index[9] and builds up on a object-oriented approach programmed in Python language. Several modules are interlinked and interchangeable, and configuration files are used to select the setting of choice for typical time-series evaluations. The program as a whole, or parts of it, can also be integrated into simulation toolchains and modeling environments, making it feasible to be used in sensitivity and optimization studies and at the interface to a super-ordinate multi-instance controlling unit, as is further described in one of the case scenarios (Section 6.1). In order to allow the Energy Storage Systems (ESS) to react directly to states in a distribution grid, **SimSES** can be coupled to grid models, thus making it possible to have a power flow analysis and a detailed simulation of an ESS at the same time. **SimSES** stands out against above-mentionded tools, e.g., **Homer Pro** or **SAM**, by providing various detailed energy storage systems including validated and literature-based degradation models. Furthermore, a plethora of predefined storage-specific application Energy Management System (EMS) like ancillary services and energy trading are implemented and combined with suitable economic parameters, so that end-users are able to test a system of choice for a selected application use case. At the same time, the existent code framework is open-source accessible and open for future contributions from other developers worldwide.

[7] https://www.storagevet.com/
[8] https://gitlab.lrz.de/open-ees-ses/simses
[9] https://pypi.org/project/simses/

3. Simulation framework for stationary energy storage systems

Stationary ESS may become a key component for future energy systems and incorporating various FTM and BTM applications supporting the electricity grid. Simulation tools are needed in order to provide advice for investment decisions and to analyze the impact of a stationary ESS. These tools should be able to model impact of applications on the health status of the ESS and its implications for prospective revenues.

While SimSES aims to allow for techno-economic cross-application and cross-technology comparisons, the tool is designed in a modular fashion and incorporates all technical components necessary for the grid connection of energy storage. Hence, **SimSES** does not only model various technologies, but also their thermal behavior, the corresponding power electronics, as well as the impact of different operating strategies. An integration into other energy simulation frameworks can be easily applied, as shown in project *openBEA*.[10]

The main task of **SimSES** is to determine the effects of the target power provided by the EMS regarding efficiency, temperature, and degradation of the ESS when applied to the storage system. Each implemented component is responsible for modeling its relevant principles. **SimSES** is divided into a simulation part for modeling the physical representation of the ESS and an evaluation part that provides technical and economic results as shown in Fig. 1. The figure also shows the basic working principle of **SimSES**: the time-series based simulation allocates an AC power target provided by the selected EMS to the storage system. After updating all models of the storage system, the current state regarding important variables such as SOC, temperature, SOH, and delivered power is transferred back to the operating strategy on which a new target power is calculated for the next time step.

In order to represent a storage system as a whole, various components need to be taken into account for a storage simulation. Besides the storage technology, power electronics is an important element. For instance, a simple Battery Energy Storage System (BESS) configuration consists of an Alternating Current to Direct Current (ACDC) converter connected to the grid and a battery. Additionally, stationary ESS are usually covered by a housing. These housings need to be thermally controlled in order to keep the ESS within its safety ranges. **SimSES** covers these possibilities with various configurable components and topologies.

More complex topologies can also include Direct Current to Direct Current (DCDC) converter or parallel connected ACDC converters, each connected to an ESS. Various ESS topologies are built with an AC connection to the grid or site location by connecting an ACDC converter to the storage system. However, in recent years Direct Current (DC)-coupled ESS has gained importance, especially in the residential

[10] https://openbeaproject.wordpress.com/

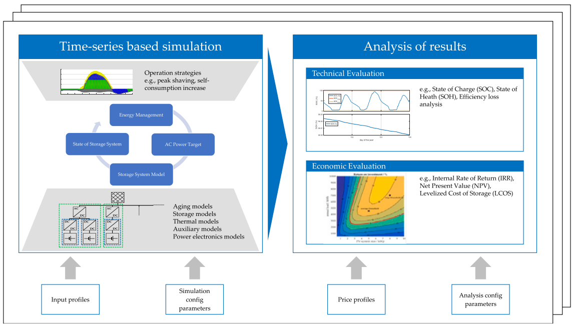

Fig. 1. Graphical overview of **SimSES** showing its simulation and analysis models, including the Energy Management System (EMS), storage system setup, technical and economical evaluation, and its necessary inputs. The state of a storage system includes the most important variables of the storage models, e.g., State of Charge (SOC), temperature, and State of Health (SOH).

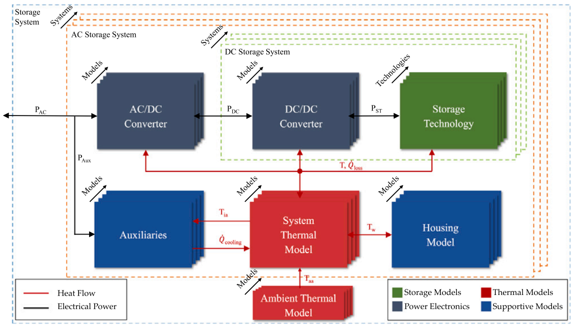

Fig. 2. Main component classes in **SimSES**: Interconnection of electrical and thermal models for ESS including the abstract AC and DC storage systems. Multiple model implementations exist for each component. Possible parallel connections of various AC and DC storage systems are indicated.

sector [19]. Hence, a state-of-the-art storage simulation framework needs to take varying topologies into account. **SimSES** considers these topologies by defining two abstract systems: AC and DC storage systems, which can also be combined in order to meet versatile topology configurations. Every AC storage system consists at least of an ACDC converter and a DC storage system. On the one hand, this allows the connection of several storage systems to the grid in parallel; on the other hand, this allows multiple DC-connected ESS within one storage system. Furthermore, the main ESS model is located inside the DC storage system behind a DCDC converter. These models are depicted in Fig. 2.

In the following sections, each of the **SimSES** packages as well as the underlying models and implementations are described in detail and shown in Fig. 3. *Storage Technology* and *System* provides models to represent physical models of storage system components while *Analysis* focuses on examining the simulation results regarding the technical and economical behavior of the simulated storage systems. All control algorithms and power flow management are handled within the *Logic* package.

Additional packages like *Commons*, *Simulation*, and *Data* deliver supportive functions for **SimSES**. *Config* is tasked to deliver functionality for the mentioned modular configuration of the ESS. In this package, software design patterns like the factory pattern are used to provide a wide range of configurable components [20]. Additionally, the structure allows the use of sensitivity analysis, e.g., by varying either different components or their dimensions. *Simulation* is another package that supports sensitivity analysis by allowing running multiple

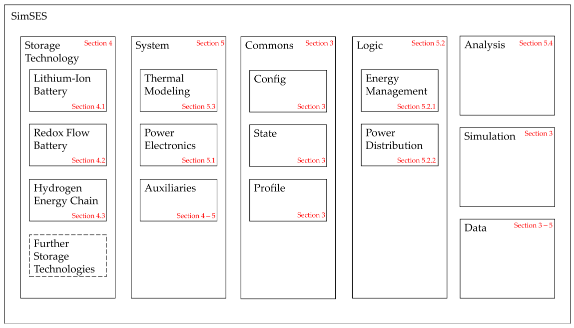

Fig. 3. Structure of **SimSES**: Packages are divided into *Storage Technology*, *System*, *Commons*, *Logic*, *Analysis*, *Simulation*, and *Data*. Within *Storage Technology*, the physical representation of each technology, namely LIB, RFB, and Hydrogen, is located. The *Commons* package delivers general functions for configuration and common features. The periphery is handled in the *System* package. Control algorithm and management is dealt with in the *Logic* package. *Analysis* focuses on the technical and economical evaluation of the simulation results. *Simulation* provides functions for simultaneous simulations, whereas *Data* stores all necessary information.

SimSES instances in parallel, therefore increasing simulation speed. For this purpose, Python's multiprocessing library is used. Further time series functions are implemented, like handling of profiles for power or price time series. These functions are used throughout **SimSES**, for example, by providing power profiles for the EMS. These supportive functions are covered within *Commons*, providing general functionality for time-series based simulations.

4. Storage technology models

Energy storage models represent the core of **SimSES**. In-depth models of various storage technologies are implemented, namely for LIB, RFB, and a hydrogen energy chain represented by electrolyzer, fuel cell and hydrogen storage. Each of these storage technologies have specific implementations regarding their physics and behavior. Due to the modularity of **SimSES**, further technologies can be implemented in future work.

4.1. Lithium-ion battery

ESSs based on LIB have evolved rapidly with a wide range of cell technologies and falling costs in recent years [11,21]. In **SimSES** LIBs are implemented as a distinct storage technology. The target power for this technology P_{st} depends on the storage structure and the power distributor as described in Section 5.

Four subcomponents are implemented in **SimSES** for behavior modeling of LIB. The **Equivalent Circuit Model (ECM)** is used to describe the electrical behavior of a specific cell type providing terminal voltage according to operational input data. The **Battery Management System (BMS)** monitors the cell operation conditions and updates values for the current. The electrical characteristics of LIBs in **SimSES** differ with chemistry and composition of constituent materials and may be fed with predefined manufacturer-specific datasets. Furthermore, various cell-specific degradation models can be selected in **SimSES**. The **aging** calculation is based on the cycle detector selected (e.g., half-cycle detector). These four main components are schematically illustrated in Fig. 4, and explained in detail in the following subsections.

4.1.1. Equivalent circuit model

To describe the electrical behavior, in **SimSES** the battery is implemented as a single-cell ECM. The currently implemented model includes an Open Circuit Voltage (OCV) and an internal resistance R_i, which is depicted in Fig. 4. According to Eq. (1), the terminal voltage

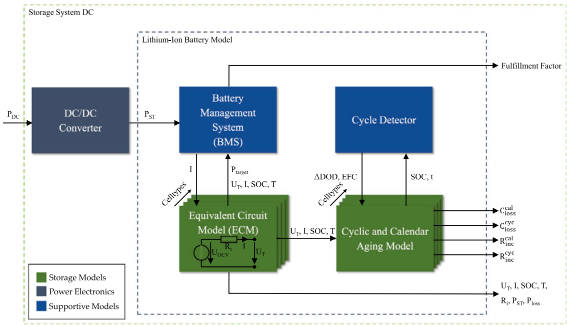

Fig. 4. Package structure of a lithium-ion battery. The battery package in **SimSES** includes four main components: a battery management system, a cell type including a equivalent circuit model, a degradation model, and a cycle detector.

U_T of each cell is calculated from the OCV and the voltage drop ΔU across R_i, due to the cell current I.

The OCVs of all currently implemented cell types are only dependent on the SOC but could be extended with further parameters like temperature and SOH. The internal resistance R_i of all currently implemented cell types takes the cell temperature T_{cell}, I, and the SOC into consideration. For both the SOC as well as R_i, the required data for different cell types are stored as look-up tables in **SimSES**. In between the available data points a linear interpolation is executed. Hence, the result quality relies on the number of data points. To improve performance, the interpolation of the SOC data was replaced by a fitted mathematical function, which is explained in Appendix A.

$$U_T = U_{OCV} - \Delta U = U_{OCV}(SOC) - I \cdot R_i\left(SOC, I, T_{cell}\right) \tag{1}$$

4.1.2. Battery management system

The BMS is linked to the ECM and is responsible for maintaining critical cell parameters within their permissible ranges. In addition to the target power P_{target}, voltage U_T, temperature T_{cell}, SOC, and current I are further input parameter for the BMS. According to the cell-specific parameters (e.g., maximum temperature), the BMS checks the input parameters and indicates whether they are within their limits. If limit violations occur, the current is restricted and returned to the ECM. The other parameters are recalculated accordingly and passed on to the aging models. The fulfillment factor indicates the share of the output power to the target power and will become sub-unity for simulations with boundary violations.

As seen in Eq. (1), the current I and the terminal voltage U_T are interdependent. Differential equations are necessary for calculating these values in the discrete time domain. To avoid these computationally intensive differential equations, an iteration loop is integrated in **SimSES**: the updated current I and terminal voltage U_T are iteratively derived through repetitive numerical approximation. This loop terminates after a predefined maximum number of iterations or as soon as the change in the current I or the terminal voltage U_T falls below a preset limit.

4.1.3. Lithium-ion battery cell types

The LIB cell forms the core of the BESS, and is essential for understanding the electrical and thermal characteristics of an entire system. For a more detailed discussion the reader is referred to [22,23] and for a description of current and future materials for LIBs as well as beyond lithium-based anode materials the reader is referred to [24]. In **SimSES**, three state-of-the-art technologies based on a Carbon-Graphite (C) anode and various cathode materials are currently implemented: two cells with a Nickel-Manganese-Cobalt-Oxide (NMC) cathode and one cell, each with a Lithium-Iron-Phosphate (LFP) and Nickel-Cobalt-Aluminum-Oxide (NCA) cathode, respectively. In addition, a generic cell with linear OCV is implemented in order to run simulations independent of the cell chemistry. Table 2 gives an overview of these cells, including their electrical attributes. The thermal parameters are summarized in Appendix B.

4.1.4. Lithium-ion battery degradation models

LIBs are subject to degradation due to multiple cell-internal aging processes, which can have significant impact on the economics of a BESS project [30]. In **SimSES**, degradation is modeled following a semi-empirical superposition approach of cyclic and calendar aging, as shown in Eqs. (2) and (3).

$$C_{loss}^{total} = C_{loss}^{cal} + C_{loss}^{cyc} \tag{2}$$

$$R_{inc}^{total} = R_{inc}^{cal} + R_{inc}^{cyc} \tag{3}$$

The resulting capacity loss C_{loss}^{total} and resistance increase R_{inc}^{total} are calculated through the addition of the respective calendar aging (C_{loss}^{cal}, R_{inc}^{cal}) and cyclic-aging components (C_{loss}^{cyc}, R_{inc}^{cyc}). Table 3 provides an overview of the primary LIB degradation models that are available in **SimSES** and their dependencies, as well as the sources on which these models are based. Here, t, SOC, T_{cell}, and U_T refer to the simulation time, state of charge, cell terminal voltage, and cell temperature, respectively. ΔDOD, EFC, Q, and $\overline{U_T}$ refer to the delta in depth of discharge for a cycle, the number of equivalent full cycles, the charge throughput, and the average cell terminal voltage over one equivalent cycle. The delta in depth of discharge (ΔDOD), as it is implemented here, is also referenced as depth of cycle or cycle depth in literature by some authors.

While calendar aging is computed once every simulation step, the model routine to calculate increase in cyclic aging is only triggered following the detection of half an equivalent cycle of charge throughput. This decreases the calculation time and allows determining the C-rate as well as DOC for that half equivalent cycle.

4.2. Redox flow battery

Large-scale storage systems are purportedly to be of rising concern in order to ease the growing penetration of RES. Hence, RFBs are of particular interest for multiple hour- and large-scale stationary ESSs because they can be easily and efficiently scaled according to the needs and become cost competitive at an energy range of multiple MWh [31]. To analyze their potential in different applications from small-scale (e.g., residential storage) to large-scale applications (e.g., industrial storage), they are integrated into **SimSES** as an additional storage technology. In an RFB, the liquid storage medium (electrolyte) is stored in external tanks. To charge and discharge the RFB, the electrolyte is pumped through a stack where the electrochemical reactions take place. The electrolyte divided in anolyte and catholyte solutions are separated by an ion-exchange membrane through which the charge carriers are transported. There are several known possible electrolyte combinations, e.g., all-vanadium or vanadium/bromine solutions [32]. As the energy conversion unit and the energy storage medium are decoupled, the power and energy of an RFB can be scaled separately [31, 32].

Fig. 5 shows the structure of the main components modeled in **SimSES** to describe an RFB. The electrochemical model calculates the electrical operating parameters of a specific stack module dependent on the chemical composition of the selected electrolyte system. The control system checks whether the target parameters are within safe operating limits and returns the actual usable values. Different pumps and pump control algorithms can be configured. In the following, the model components are described in more detail.

Table 2
Lithium-ion battery cells currently implemented in **SimSES**, including their electrical parameters.

Manufacturer Model	Acronym in **SimSES**	Anode Cathode	Nom. voltage (V) Voltage range (V)	Capacity (Ah)	C_{rate} Ch. (1/h) C_{rate} Dch. (1/h)	Source
Sony[a] US26650FTC1	SonyLFP	Graphite $LiFePo_4$	3.2 2.0–3.6	3.0	1.0 6.6	[25,26]
Panasonic NCR18650PD	Panasonic- NCA	Graphite $LiNiCoAlO_2$	3.6 2.5–4.2	2.73	0.5 3.5	[27]
E-One Moli Energy IHR18650A	MolicelNMC	Graphite $LiNiCoMnO_2$	3.7 3.0–4.25	1.9	1.05 2.1	[28]
Sanyo UR18650E	SanyoNMC	Graphite $LiNiCoMnO_2$	3.6 2.5–4.2	2.05	1.0 3.0	[27,29]
Generic cell model	GenericCell	–	3.5 3.0–4.0	2.5	2.0 2.0	–

[a]Murata Manufacturing Co. acquired the Sony battery division in 2017.

Table 3
LIB-specific degradation models along with corresponding variable dependencies and literature sources.

Cell acronym	Calendar aging		Cyclic aging		Model based on
	C^{cal}_{loss}	R^{cal}_{inc}	C^{cyc}_{loss}	R^{cyc}_{inc}	
SonyLFP	t, SOC, T_{cell}	t, SOC, T_{cell}	EFC, ΔDOD, C-rate	EFC, ΔDOD, C-rate	[25,26]
PanasonicNCA	t, U_T, T_{cell}	t, SOC, T_{cell}	EFC, U_T, C-rate	EFC, U_T, C-rate	[27]
MolicelNMC	t, SOC, T_{cell}	t, SOC, T_{cell}	Q, ΔDOD, C-rate	Q, ΔDOD, C-rate	[28]
SanyoNMC	t, U_T, T_{cell}	t, U_T, T_{cell}	Q, $\Delta DOD, \overline{U_T}$	Q, $\Delta DOD, \overline{U_T}$	[29]
GenericCell	t	–	EFC	–	–

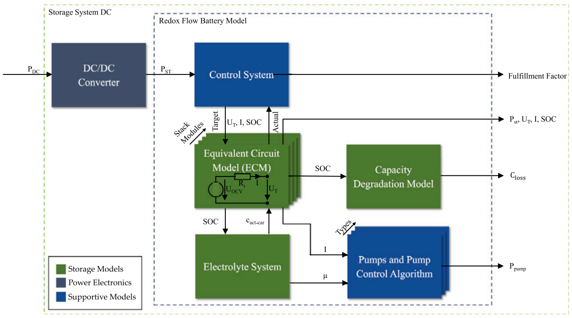

Fig. 5. Package structure for a redox flow battery (RFB). It contains an electrochemical model (equivalent circuit model) with specific parameters for different stack modules, an implemented control system, an electrolyte system, a degradation model, and pumps, with interchangeable control algorithms.

4.2.1. Electrochemical model

As with LIB, the currently implemented electrochemical model of an RFB is based on an equivalent circuit model (cf. Fig. 5). The terminal voltage U_T is directly calculated from the power applied to the RFB. Eq. (4) can be derived from Eq. (1) by using the relation between storage power P_{st}, terminal voltage U_T, and current I ($P_{st} = U_T \cdot I$). U_T is therefore calculated by P_{st}, the OCV, and the internal resistance R_i. Both OCV and R_i are dependent on the SOC and the electrolyte temperature in the stack module T_{stack}.

$$\begin{aligned} U_T &= 0.5 \cdot \left(U_{OCV} + \sqrt{U_{OCV}^2 + 4 \cdot R_i \cdot P_{st}} \right) \\ U_{OCV} &= f\left(SOC, T_{stack}\right) \\ R_i &= f\left(SOC, T_{stack}\right) \end{aligned} \tag{4}$$

Charge effects are taken into account by implementing a current for the charging losses $I_{char\text{-}loss}$ when calculating the change of the system SOC (SOC_{system}) via Eq. (5), considering the simulation time step Δt, the nominal voltage at the stack module U_{nom}, and the total energy of the electrolyte E_{total}. $I_{char\text{-}loss}$ includes coulombic losses due to self-discharge through the transport of reactants over the membrane and shunt currents. Shunt currents occur due to a connection of cells in the stack through an ionic conductive electrolyte distribution system. This creates a bypass current forced by the electric field due to the electrical series connection of the cells [33].

$$\Delta SOC_{system} = \frac{\left(I - I_{char\text{-}loss}\right) \cdot \Delta t \cdot U_{nom}}{E_{total}} \tag{5}$$

A control system is integrated in the electrochemical model, which checks whether U_T, I, and SOC are within safe operating limits. If the values are out of range, they will be adapted and the other parameters are recalculated accordingly.

Additionally, a capacity degradation model including the capacity losses C_{loss} due to hydrogen evolution is implemented in the RFB model. Further research is required to estimate a realistic hydrogen evolution current for industrial-sized stacks to predict the capacity reduction realistically over time. A current approach using experimental data of a laboratory cell from Schweiss et al. [34] overestimates the resulting capacity losses. Whitehead et al. [35] stated a capacity loss of less than 1% per year due to hydrogen evolution. Therefore, a hydrogen current of $5 \cdot 10^{-8}\ \frac{mA}{cm^2}$ is assumed, resulting in a capacity loss of about 1% per year for a system with an Energy-to-Power Ratio (EPR) of 1. As the EPR increases, the loss decreases accordingly.

4.2.2. Stack module and electrolyte system

The calculations in the electrochemical model are based on electrical and geometrical data for a stack. A stack consists of a fixed number of cells electrically connected in series. The data to consider the voltage, charge, and hydraulic losses of a stack can be obtained either from experimental data or from the literature values and models. Stacks can be electrically connected in parallel or in series to a stack module to increase power and voltage of the RFB system. In this configuration the electrolyte flows in parallel through all cells and stacks. The performance parameters of the stack are directly connected to the used electrolyte system. The currently in **SimSES** examined and implemented electrolyte is an all-Vanadium system, consisting of 1.6 mol/l Vanadium solved in an aqueous sulfuric acid (2 mol/l H_2SO_4) from GfE (Gesellschaft für Elektrometallurgie mbH). To reduce side reaction due to high potentials and to prevent performance penalties the electrolyte needs to operate in a limited SOC range. A typical usable SOC range for a RFB lies between 20 and 80% [36]. Based on this SOC

Table 4
Redox-flow battery stack types in **SimSES**.

Acronym in SimSES	Cell number	Cell area (cm^2)	Based on experimental data of	Model based on
CellDataStack5500W	40	2160	Appendix C	[37–39]
DummyStack3000W	20	1000	N/A	N/A
IndustrialStack1500W	18	551	Voltstorage GmbH	[37,38]

range the nominal power of a stack is calculated. An overview of the in **SimSES** implemented stacks is listed in Table 4. The name of the stack includes its nominal power. In addition, some modifications of the described stacks are included, which are up-scaled or simplified versions that are not included in the list.

4.2.3. Pumps and pump control algorithm

The pump control algorithm used to control the flow rate or pressure drop in the system is an important performance-determining factor that affects the operating losses. Two different algorithms to choose from are currently integrated: the constant and the stoichiometric flow rate. It is assumed that the pumps always stop during stand-by to reduce the operating losses. If flow rate $\dot{V}$ or pressure drop Δp is given, the other value is calculated via Eq. (6) from the specific hydraulic, viscosity-corrected resistance $R_{hydraulic,specific}$ and the viscosity μ of the anolyte or catholyte.

$$\Delta p = \dot{V} \cdot R_{hydraulic,specific} \cdot \mu \tag{6}$$

If the pump is operating with a constant flow rate, it must be ensured that the volume flow is sufficiently high so that the stack module is supplied with enough reactants at any time of operation (depending on SOC and I). This is checked by the control system integrated in the electrochemical model.

For the stoichiometric flow rate algorithm $\dot{V}$ is calculated according to Eq. (7) via the stoichiometric factor ν, the total concentration of the active charge carriers in the electrolyte $c_{act\text{-}car}$ (for the implemented Vanadium electrolyte it is 1.6 mol/l), the Faraday constant F, and the still available concentration of reactants in the electrolyte, which is described through the SOC for discharging and (SOC − 1) for charging. If, for example, the RFB is charging at SOC 70%, reactants that can be maximal charged in the Stack are 30% of the total concentration, therefore value is 0.3.

$$\begin{aligned} \dot{V} &= \frac{\nu \cdot I}{F \cdot c_{act\text{-}car} \cdot (SOC - 1)} \qquad \text{for} \quad P >= 0 \\ \dot{V} &= \frac{\nu \cdot I}{F \cdot c_{act\text{-}car} \cdot SOC} \qquad \text{for} \quad P < 0 \end{aligned} \tag{7}$$

The pump losses P_{pump} can be calculated with Δp, $\dot{V}$, and the pump efficiency η_{pump} of a specific pump that can be selected in **SimSES** via Eq. (8) [40].

$$P_{pump} = \frac{\dot{V} \cdot \Delta p}{\eta_{pump}} \tag{8}$$

4.3. Hydrogen energy chain: Electrolyzer, storage, and fuel cell

Hydrogen as an energy carrier is supposed to be one of the major contributors impacting future energy provision, storage, and distribution [41]. The abundance of chemically-bound hydrogen in the form of water as well as its very high-energy density is compelling for its deployment as an energy carrier for large-scale energy storage. However, the efficiency of splitting water into its separate components via electrochemical electrolysis and reverting the process through fuel cells or combustion power plants is comparatively low, in striking contrast to electrochemical storage like LIB [14,42]. As such, hydrogen is thought to complement rather than to compete with LIB and RFB. In order to understand the effects of a hydrogen-based energy chain on a system level including its periphery, models for *electrolyzers*, *fuel cells*, *hydrogen storage*, and its auxiliary components like pumps and compressors are integrated as models within **SimSES**. Within this

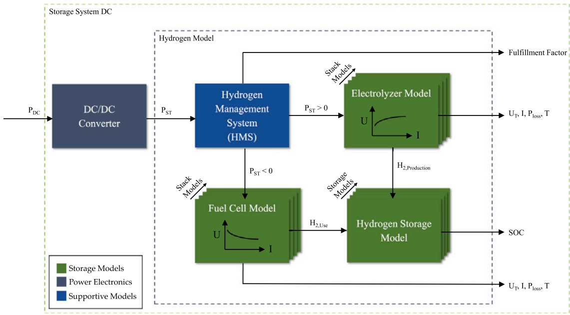

Fig. 6. Package structure for hydrogen in **SimSES** includes four main components: a *hydrogen management system*, an *electrolyzer*, a *fuel cell*, and a *storage model*.

section, implementations of the respective models are explained in detail.

The hydrogen package structure is displayed in Fig. 6, consisting of a *Hydrogen Management System (HMS)*, an *electrolyzer*, a *fuel cell*, and a *H_2 storage model*. The *HMS* supervises the whole hydrogen chain for valid ranges of temperature and SOC and reduces applied power if necessary. The storage model could be a gas pipe with an assumed infinite capacity or a hydrogen pressure tank with a predefined energy capacity. Depending on the pressure of the gas within the storage tank, the gas needs to be compressed to the desired pressure level. The *electrolyzer* and *fuel cell* models are explained in detail in the following sections. It is worth to mention that **SimSES** also allows a single-direction hydrogen energy chain by neglecting either the *electrolyzer* or the *fuel cell* component with special implementations. A summary of all currently implemented models is given in Table 5. Due to the modular structure of **SimSES**, additional models can be implemented in a future release accordingly.

4.3.1. Electrolyzer

A water electrolyzer splits water with the use of electricity into hydrogen and oxygen by passing ions through an electrolyte from one electrode to the other. The pressure and temperature-dependent polarization curve is based on the general equation of Nernst voltage U_{nernst} as well as overpotentials represented by ohmic η_{ohm}, activation η_{act}, and diffusion losses η_{diff} as shown in Eq. (9) [50]. In some implementations mass transport and membrane permeation are also considered.

$$U_{T,EL} = U_{nernst} + \eta_{ohm} + \eta_{act} + \eta_{diff} \tag{9}$$

Depending on the stack technology, e.g., alkaline or polymer electrolyte membranes (PEM), the *electrolyzer* is operated at different pressure and temperature levels, which is taken into consideration by varying polarization curves for each technology [50]. As shown in Fig. 7, the *electrolyzer* model is divided into its stack and corresponding degradation models, pressure and thermal models as well as necessary auxiliaries like a pump, water heater, and gas dryer. The electrical auxiliary power is calculated according to the hydrogen and oxygen generation pressures for the anode and cathode, as well as the stack temperature. A water pump regulates the humidification of the *electrolyzer*, whereas the generated hydrogen gas needs to be dried. These auxiliary models calculate the necessary electrical power in order to provide a temperature and mass equilibrium.

Table 5
Overview of implemented *electrolyzer*, *fuel cell* and *hydrogen storage* models in **SimSES**.

Technology	Acronym in SimSES	Type	Degradation effects	Based on experimental data of	Model based on
Electrolyzer	PemElectrolyzerMultiDimAnalytic	PEM	Resistance increase, Decrease of exchange current	Forschungszentrum Jülich	[43–45]
	PemElectrolyzer	PEM	N/A	N/A	[46]
	AlkalineElectrolyzer	Alkaline	N/A	Hydrogen Research Institute	[47,48]
Fuel Cell	PemFuelCell	PEM	N/A	N/A	[49]
	JupiterFuelCell	PEM	N/A	SFC Energy AG	–
Hydrogen Storage	PressureTank	Pressure Tank	N/A	N/A	–
	SimplePipeline	Pipeline	N/A	N/A	–

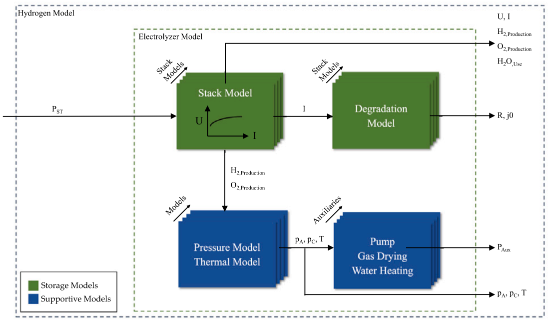

Fig. 7. Package structure for *electrolyzer* in **SimSES** includes a stack, pressure, thermal and degradation model as well as a pump and gas dryer.

Electrolyzer degradation is a field of ongoing research with controversy over underlying mechanisms and influencing factors [51,52]. However, active operation time and applied current density seem to be major impact factors for electrolyzer degradation. For instance, the implemented degradation for the Polymer Electrolyte Membrane (PEM) electrolyzer acquired from the work of Tjarks [43] is based on the findings of Rakousky et al. [44,45] considering a resistance increase and a decrease of the exchange current. Other implementations of electrolyzers are a PEM variant without degradation effects based on the work of Marangio et al. [46] and an alkaline version based on the work of Hammoudi et al. [47] and Henao et al. [48].

4.3.2. *Fuel cell*

As an opposite to *electrolyzers*, *fuel cells* combine hydrogen and oxygen to water while releasing usable energy in the form of electricity [42]. The terminal voltage is calculated by the Nernst voltage subtracted by the voltages due to ohmic, activation, and diffusion losses shown in Eq. (10).

$$U_{T,FC} = U_{nernst} - \eta_{ohm} - \eta_{akt} - \eta_{diff} \tag{10}$$

The *fuel cell* package has a structure that is similar to the *electrolyzer* package, with a stack, pressure, and thermal model. During operation, the water handling especially for PEM fuel cells is crucial and handled by water pumps. An implementation of a PEM fuel cell based on Feroldi et al. [49] as well as a model for the Jupiter PEM fuel cell of SFC Energy AG[11] including a thermal model is available in **SimSES**. However, the implementation of adequate degradation models within SimSES is a task for future action.

5. System periphery, management, and evaluation

Energy storage systems not only consist of the underlying storage technology but also the periphery like power electronic components and thermal behavior as well as an EMS. These elements are crucial for evaluating energy storage systems as a whole. In order to provide insights into the overall system behavior, **SimSES** not only models the periphery and the EMS, it also provides in-depth technical and economical analysis of the investigated ESS.

5.1. *Power electronics*

Besides the storage technology, the power electronic components play a crucial role in terms of system efficiency. Depending on topology and application, power electronics may contribute significantly to the overall system losses [53]. Hence, **SimSES** has to consider these electronic components for an accurate simulation of a storage system like ACDC and DCDC converters. An overview of the implemented models in **SimSES** is given in Table 6. Models of these converters are represented by power and voltage-dependent efficiency curves. In principle, the efficiency of a power electronics module is represented by a given storage power $P_{Storage}$ and the rated power of the power electronics component P_{Rated} as displayed in Eq. (11).

$$\eta_{PE} = f\left(P_{Storage}, P_{Rated}\right) \tag{11}$$

The power applied to the power electronic components is crucial for simulating the efficiency. When considering storage systems, it is possible that these systems do not fully deliver the requested power. These situations occur, for example, if the storage is outside of its temperature limits or the SOC is at its lower or upper limits. Hence, the power is adjusted compared to the target power of the EMS, which leads not only to non-fulfillment, but also to an altered efficiency.

5.2. *Power control*

Every power flow in an ESS has to be monitored and controlled. The power flow is dependent on the application and system topology. In **SimSES**, these two dependencies are handled separately with an EMS, respectively, Power Distribution Strategies (PDS). The EMS defines the target power for the ESS as a function of the application while the PDS allocates the target power to the configured subsystems. These control mechanisms are explained in detail in the following sections.

5.2.1. *Energy management system*

The EMS in an ESS is a system consisting of both hardware and software that allows the user to monitor and control the energy flows within an ESS. In **SimSES**, the function of the EMS is to calculate and supply a target power value for each simulation timestep (Δt) based on the selected operation strategy. This target power value can be dependent or independent of previous system states as well as interfere with various input profiles. In **SimSES** both stand-alone and stacked operation strategies can be simulated. Stacked operation strategies are sorted according to their user-associated priority level. Consequently, the individual stand-alone operating strategies are executed one after another depending on their priority. Additionally, time-discrete serial stacking is already available within **SimSES**. More complex multi-use strategies can be integrated as stand-alone strategies. At present, a handful of

[11] https://www.efoy-pro.com/efoy-pro/efoy-jupiter-2-5/

Table 6
Overview of implemented ACDC and DCDC converter models in **SimSES**.

Converter type	Acronym in SimSES	Based on experimental data of	Model based on
AC/DC	FixEfficiencyAcDcConverter	N/A	N/A
	NottonAcDcConverter	N/A	[54]
	Sinamics120AcDcConverter	Sinamics S120	[55]
	BonfiglioliAcDcConverter	Bonfiglioli RPS TL-4Q	Datasheet[a]
	SungrowAcDcConverter	Sungrow SC 1000 TL	Datasheet[b]
	M2bAcDcConverter	Stable Energy GmbH	[56]
DC/DC	FixEfficiencyDcDcConverter	N/A	N/A

[a] https://www.docsbonfiglioli.com.
[b] https://en.sungrowpower.com.

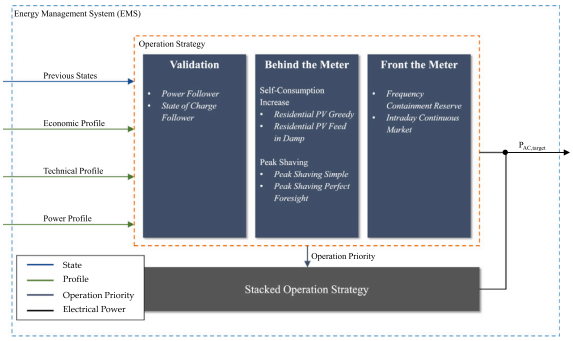

Fig. 8. Structure of the energy management system and overview of available operation strategies and their categorization in **SimSES**.

operation strategies are implemented in **SimSES**. An overview of these operation strategies and their categorization is depicted in Fig. 8.

The *power follower* strategy is a basic operation strategy which aims to get the storage system operation to replicate a given power profile. Similar to the aforementioned strategy, the *SOC follower* converts a given SOC profile to a power profile and attempts to make the storage system fulfill this calculated demand power at each timestep.

Based on the work of Zeh and Witzmann [57], two operation strategies for residential SCI in combination with Photovoltaic (PV) generation units have been implemented. The *residential PV greedy* operation strategy charges the ESS as fast as possible without consideration of the grid by meeting the residual load at all times. To reduce the maximum grid load the *residential PV feed in damp* operation strategy schedules the charging of the ESS according to a PV prediction. It attempts to provide a constant charging power and aims for a fully charged ESS at sundown.

Two strategies have currently been implemented for industrial consumers. The simple *Peak Shaving (PS)* strategy works as follows. As long as the target power is above a specified threshold, the additionally required power is provided by the ESS. In addition, the ESS will recharge itself if the power value is below the PS threshold [58] (used in the case study in Section 6.1). In order to reduce calendar aging for a lithium-ion based ESS, the *PS perfect foresight* strategy operates under the assumption of perfect foresight for the load profile. The ESS will only charge up to the energy that is required for the next load peak, right before the occurrence of that load peak [59].

The EMS strategy for providing *FCR* implemented in **SimSES** is based on the German regulatory framework [60,61]. The requested charging and discharging power is proportional to the frequency deviation. Below 49.8 Hz or above 50.2 Hz the output power is set to the prequalified power. Within the frequency dead band around 50 Hz with +/-10 mHz the output power is set to 0 W. The degree of freedom to exceed the output power by 20% is used, aiming to bring the SOC back to a predefined SOC set-point. The *IDM* operation strategy charges or discharges the ESS by trading energy on the electricity market, in particular on the IDM, if the SOC falls below a predefined lower limit or it exceeds an upper limit [62]. An example for a *FCR* and a *IDM* stacked operation strategy is provided in Section 6.2.

5.2.2. Power distribution strategies

For complex storage system topologies, the power needs to be distributed between the different subsystems of an ESS [63,64]. For this purpose, several power distribution logics are implemented in **SimSES**. These logics distribute the power to the corresponding storage systems, for instance, based on the respective SOH or SOC. In **SimSES**, the ESS is differentiated between an AC and DC storage system (see Section 3). For each node of parallel connected AC systems as well as DC systems, a power flow decision has to be made similar to Bauer [64]. Mühlbauer et al. [63] as well as Bauer [64] define PDS as a simple problem of a distribution factor α as shown in Eq. (12).

$$\mathrm{P_i} = \mathrm{P_{target}} \cdot \alpha_\mathrm{i}, \tag{12}$$

where $\mathrm{P_{target}}$ is the target power provided by the EMS, α_i the power distribution factor for system i, and $\mathrm{P_i}$ the corresponding power of system i on condition that the sum of all α_i equals one. In an optimal case the PDS takes the current limitations of the underlying storage technology for $\mathrm{P_i}$ into consideration in order to be able to fulfill the requested power, e.g., temperature limitations could lead to lower deliverable power. For each node, a PDS can be configured.

Mühlbauer et al. distinguish between static and dynamic categories for PDS while Bauer has more subtle definitions for a dynamical PDS approach with a fixed and variable sequence [63,64]. Bauer also mentions a PDS as an optimization problem currently not considered in **SimSES**. In the following, PDS implemented in **SimSES** are presented.

The most straightforward implementation of a PDS is an equal distribution of the power to all storage systems. This is a static PDS approach with a fixed power distribution factor. Other static PDS-like distribution based on the ESS capacity can be easily added to the PDS set of **SimSES**. In addition, a dynamic PDS is implemented by differentiating between charge and discharge distribution factors depending on the SOC of each system based on [63].

Due to the modularity of **SimSES**, multiple ESSs with different storage technologies can be combined with a hybrid ESS, e.g., a LIB and a RFB system. For this purpose, a novel PDS is introduced prioritizing configured storage technologies by base and peak loads, respectively. While the prioritized system stays within a defined SOC range, e.g., between 25 % and 75 %, it tries to fulfill the target power within its power limits. If either the SOC or the power limit is exceeded, the next highest prioritized system takes over. If the power target is not completely allocated, a second loop distributes the power independent from the defined SOC range. In addition, the logic balances the SOC of the configured ESS if one or more systems are outside of the defined SOC range while other systems are within those ranges. The algorithm also allows a two or one way balancing, e.g., if only the peak load system should be balanced by the base load system (used in the case studies in Section 6).

5.3. Thermal modeling

Performance, efficiency, and aging of all aforementioned storage processes depend not only on charge and discharge currents, but are also highly sensitive to thermal conditions. While for some small-scale storage realizations (e.g., residential battery storage) modeling electricity flows in a fixed temperature setting might be a solution of choice with sufficient accuracy for techno-economic simulations [65], larger storage systems along with investigations about storage efficiency particularly require detailed thermal models [53]. Utility-scale LIB stationary ESS are often designed as free-standing systems, which are installed outdoors and exposed to the environment. The use of standard shipping containers to install entire energy storage systems is the preferred option in the industry today to shield sensitive electric components from adverse environmental conditions. The benefits of such a configuration include modularity, scalability, ease of logistics, conformance with road-transport regulations, and the ability to plan and optimize land usage. Such containers are also specially fitted out with insulation to limit heat flow to/from the environment, and to present a stable operation temperature to the components inside.

Heat is generated in LIBs due to internal resistance to the passage of current during operation. Lithium-ion cell technology is particularly vulnerable to adverse changes in cell temperatures, and degrade faster when operated outside of their optimal temperature ranges. In particular, degradation may result from accelerated kinetics for unwanted side reactions at elevated temperatures resulting in a loss of capacity and an increase in the internal resistance. If the generated heat is not rejected to the environment at a rate greater than the rate of heat generation, overheating and—in extreme cases—a *thermal runaway* may occur. In contrast, for applications with relatively lower current rates (alike most stationary storage use cases), air cooling systems are deemed adequate to aid the heat rejection process to maintain the cell temperatures within the stipulated ranges. It is worth to mention in this context, that in the absence of cooling systems, the capabilities of the cells are severely limited, and under-utilized [66].

In summary, thermal modeling of energy storage systems is a crucial step of the system design process, especially due to the following factors:

- temperature-dependence of the energy conversion efficiency of LIB (dependent on the internal resistance) [67] and other storage technologies,
- temperature-dependence of the degradation mechanisms [68,69],
- dependence of the round-trip efficiency on the energy consumption of auxiliary components, such as the HVAC system [55] and
- operational hazards under extreme temperatures which are too low, or too high [70].

Thermal modeling in **SimSES** follows a zero-dimensional lumped-capacity approach, and consists of a number of component packages which run in tandem to emulate the thermal behavior of a system under the specified operating conditions. Zero-dimensional lumped-capacity approaches are widely used in the reviewed literature and found to be suitable for system models [55,71]. Each of these packages and their core features are presented in this section, along with how they fit into the larger picture within **SimSES** and its architecture. The thermal model and its associated components function at the AC storage system level in **SimSES**. **SimSES** currently supports a container-based housing solution with an air cooling system for LIB stationary ESS. An overview of these packages and their interplay is seen in Fig. 9.

5.3.1. Ambient thermal model

The primary function of the ambient thermal model is to account for the predominant environmental effects that play a role in the thermal behavior of the ESS. The ambient thermal model currently consists of an ambient temperature which supplies a value of ambient air temperature T_{aa} for each simulation timestep Δt at time t. The ambient temperature is available in two variants: a constant temperature model, which supplies a user-specified T_{aa} for each timestep, and a location-specific model, which, depending on the time of day and year, supplies a value of T_{aa} based on recorded temperature time-series data. The ambient temperature datasets currently present in SimSES have been generated with the help of the publicly available simulation tool *greenius*, developed by the German Aerospace Center (DLR) [72]. A solar irradiation model is also envisioned for a future release of SimSES as an extension of the ambient thermal model in order to be able to supply values of incident solar irradiation at a given location at time t to allow for better estimation of the heat load on an ESS. The ambient thermal model is understandably applicable to all AC storage system instances present in a given BESS configuration.

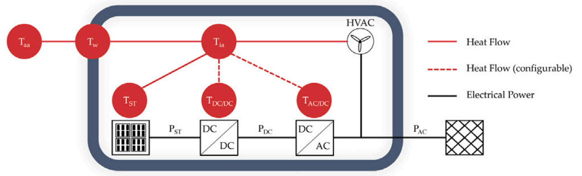

Fig. 9. **SimSES** is thermally interconnected with the thermal nodes of ambient air T_{aa}, wall T_w, inner air T_{ia}, and storage technology T_{ST}. The temperature conjunction of T_{ACDC} and T_{DCDC} can be switched off. The HVAC system controls T_{ia} of the storage system.

5.3.2. Housing model

The housing model emulates the physical attributes of the specified housing type. **SimSES** currently supports system simulations with a standard 20 foot shipping container as the housing. The walls are modeled with three layers of materials, including an insulating layer of Polyurethane (PU) between the outer and inner metal layers. The geometrical dimensions and physical and thermal properties of the walls of the shipping container can be adapted to suit any desired variant. The modular and extendable structure of **SimSES** ensures that the choice is not limited to the presently implemented model, but rather allows for other housing types or installation conditions to be modeled and included in simulations.

5.3.3. Heating, ventilation and air conditioning model

As the temperature inside the housing is to be maintained within a stipulated range to ensure safe and optimal operating conditions, a HVAC unit is necessary to correct temperature deviations. **SimSES** also supports inclusion and modeling of HVAC systems. Two basic HVAC models are currently implemented: one, which uses the internal air temperature T_{ia} deviation from its user-specified set-point to roughly estimate the amount of thermal power required to counter this deviation, and the other, which employs a Proportional-Integral-Derivative (PID) controller logic to arrive at a value of thermal power to counteract the deviation in T_{ia} from its set-point. The corresponding electrical power consumption $P_{electrical}$ of the HVAC, which is related to the thermal power P_{hvac} by the Coefficient of Performance (COP) (see Eq. (13)), is logged in the state of the AC storage system, and influences the round-trip efficiency of the ESS.

$$P_{electrical} = \frac{P_{hvac}}{COP} \tag{13}$$

5.3.4. System thermal model

The system thermal model is central to the thermal modeling process in **SimSES**, in that it emulates the physical phenomenon of heat transfer among the components of the ESS and its environment, as well as integrates the functioning of all aforementioned components. The system thermal model estimates the temperatures of all components of interest after each simulation timestep Δt, based on the various heat loads—both external and internal—that the ESS is subjected to. Each instance of AC storage system has its own system thermal model, and captures the thermal behavior of all components present in each AC storage system. The analysis applies the zero-dimensional lumped capacity approach, and the central assumption is that all the components are treated as lumped isotropic homogeneous objects with heat capacities and heat transfer coefficients. The internal air in the container is assumed to possess a uniform temperature throughout its volume, and flows are not considered. The temperatures of the storage technologies influence important parameters such as efficiency and voltage, as well as the rate at which they degrade. The component models used in **SimSES**, which are explained in the subsequent sections, take these temperature variations into account.

The system thermal model solves a system of first-order coupled differential equations to obtain the temperatures of the storage technologies, the internal air, and components such as the ACDC converter, if they are present within the same housing. This list of components, whose temperatures are of interest, can be expanded as required owing to the modular structure of the system thermal model. As the temperatures at the start of each timestep Δt are known, and the temperatures at the end of each timestep are of interest, an initial value problem can be formulated.

Within each DC storage system, for each instance of storage technology *i* with a mass m_{st} and specific heat c_p^{st}, a differential equation capturing the variation in its temperature T_{ST} under the combined effects of natural convection with the internal air (ia) P_{conv}^{st-ia} and the heat generation within itself on account of energy conversion losses P_{loss}^{st} can be formulated (see Fig. 9). For an AC storage system with a total of *n* storage technology instances within its DC storage systems, a total of *n* differential equations based on Eq. (14) can be formulated.

$$m_{st,i} \cdot c_p^{st,i} \cdot \frac{dT_{st,i}}{dt} = P_{loss}^{st,i} - P_{conv}^{st,i-ia} \tag{14}$$

Similarly, a heat balance equation with a form similar to Eq. (14) can be formulated for other components such as the ACDC converter, which also introduce heat into the housing due to the energy conversion losses (see Fig. 9).

For the internal air with a mass m_{ia} and specific heat c_p^{ia}, a heat balance can also be formulated to determine the variation in its temperature T_{ia}. The heat balance outlines its interaction via natural convection with each storage technology P_{conv}^{st-ia}, other components such as the ACDC converter (if present) $P_{conv}^{acdc-ia}$, and the innermost layer (il) of the housing walls P_{conv}^{il-ia}. The thermal power of the HVAC P_{hvac} is also accounted for in this balance (see Eq. (15)).

$$m_{ia} \cdot c_{p,ia} \cdot \frac{dT_{ia}}{dt} = \Sigma P_{conv}^{st,i-ia} + P_{conv}^{acdc-ia} - P_{hvac} - P_{conv}^{ia-il} \tag{15}$$

The innermost layer of the housing walls, in addition to the convective heat transfer with the internal air, also exchanges heat with the insulation layer adjacent to it via heat conduction, and a heat balance equation can be written.

The insulation layer interacts with both the innermost and outer layers via heat conduction, and a corresponding heat balance equation can be drafted as well. The outer layer exchanges heat with the adjacent insulation layer via conduction, and interacts with the ambient air via natural convection. The outer layer is also subjected to a heat load due to the direct and diffuse solar irradiation incident on its surfaces. A heat balance for the outer layer can be applied by taking into account the heat loads due to the incident solar irradiation, the conduction through the layers, and the natural convection with the ambient air.

Depending on the chosen simulation timestep Δt, the heat balance equations for all considered components are then solved simultaneously at least once, or in the case of very large Δt, the system of equations is solved multiple times in an attempt to obtain a greater degree of accuracy. The solution of this system of equations yields the values of the temperatures at the end of each simulation timestep, which influence the component models.

In case simpler simulations are to be conducted, the thermal model can also be disabled, in which case the storage technologies experience a constant (user-defined) ambient temperature, and the temperatures of the storage technologies and other components are also set to remain at this value and are not updated. **SimSES** currently only offers modeling of thermal behavior for LIB. Augmentation of these capabilities for other storage technologies is planned for future releases.

5.4. Analysis

Following the simulation of ESSs, an analysis of the simulation results is conducted automatically by **SimSES** providing Key Performance Indicators (KPIs) and plots that allow the user to gain insights of the configured ESS. Furthermore, the analysis can be used to compare simulation results of different scenarios quantitatively and qualitatively. While the *Data* subpackage provides relevant parsers and utility functions for processing the time series of simulation results, the *Evaluation* subpackage includes the actual methods for deriving the KPIs and creating plots. Which evaluations should be performed, as well as relevant input data (e.g., electricity prices and storage cost) can be specified by the user. In the following, the technical evaluation and economic evaluation will be explained in more detail.

5.4.1. Technical evaluation

Within the *Technical Evaluation* part of **SimSES**, technical KPIs are determined on the system and storage technology level. Depending on the storage technology used, the respective KPIs are exported at the end of the analysis. Automatically generated plots give the user an impression of the usage and performance of the simulated ESS like time variance of AC and DC power, SOC and capacity. More advanced users can also use the simulation results to calculate characteristic values beyond the displayed KPIs. The technical evaluation's KPIs on system, lithium-ion, redox flow and hydrogen level are summarized in Table 7. As an example, the calculation of two KPIs is shown below.

The Round-Trip Efficiency (RTE) is calculated on the system level using Eq. (17) deviated from Eq. (16). To calculate the RTE, the discharged energy (E_{out}) is divided by the charged energy (E_{in}), from which the change of energy by SOC rise or decrease (ΔE) is subtracted. For simulations over a longer period of time, the efficiency influence on the SOC change can be neglected because charged and discharged energy are substantially larger than the change in energy between the start and end SOC of the simulation. For shorter simulation periods, the influence of efficiency on the SOC change must be considered. For this purpose, the SOC change is divided by the root of the efficiency, since, for example, the additionally charged energy at SOC increase has already passed through the power electronics in one direction and was thus influenced by the efficiency. A symmetrical efficiency for charge and discharge is assumed here.

$$\eta_{RTE} = \frac{E_{out}}{E_{in} - \frac{\Delta E}{\sqrt{\eta_{RTE}}}} \tag{16}$$

with $\Delta E = SOC_{last} \cdot E_{last} - SOC_{initial} \cdot E_{initial}$. Solving Eq. (16) for η_{RTE} leads to:

$$\eta_{RTE} = \frac{E_{out}}{E_{in}} + \frac{\Delta E^2 + \Delta E\sqrt{4E_{out}E_{in} + \Delta E^2}}{2E_{in}^2} \tag{17}$$

Another KPI calculated in the technical analysis is the remaining energy content (e_{rem}) as a percentage of the initial energy (Eq. (18)). For this, the current energy (E_{act}) is divided by the initial energy (E_{nom}).

$$e_{rem} = \frac{E_{act}}{E_{nom}} \tag{18}$$

Table 7
Key Performance Indicators (KPIs) for technical evaluation and the level at which they are calculated. Crosses indicate for which level the respective KPI is calculated.

Selected key performance indicators (KPI)	System	Lithium-ion	Redox flow	Hydrogen
Round-trip efficiency (%)	x	x	x	x
Mean state of charge (%)	x	x	x	x
Number of changes of signs per day (#)	x	x	x	x
Avg. length of resting times (min)	x	x	x	x
Pos. energy between changes of sign (% of capacity)	x	x	x	x
Avg. fulfillment factor (%)	x	x	x	x
Remaining capacity (%)	x	x	x	x
Energy throughput (kWh)	x	x	x	x
Mean power electronics efficiency (%)	x			
Equivalent full cycles (#)		x	x	
Depth of discharges (%)		x	x	
Coulomb efficiency (%)			x	
State of health (%)				x
Energy for heating of water (kWh)				x
Energy for compression of hydrogen produced (kWh)				x
Total mass of hydrogen (kg)				x

5.4.2. Economic evaluation

The economic evaluation of **SimSES** allows assessing the overall profitability of an energy storage project through economic KPIs. These KPIs include the net present value (NPV), internal rate of return, profitability index, return on investment, and levelized cost of storage. Eq. (19) shows the calculation of the NPV as it is performed in **SimSES**.

$$\mathrm{NPV} = -\mathrm{I}_0 + \sum_{n=1}^{N} \frac{\mathrm{CF}_n}{(1+i)^n} \tag{19}$$

I_0 denotes the initial investment cost, i the discount rate, CF the cashflow, and n and N the current and total number of project years, respectively. All parameters apart from the cashflow are derived from the settings in the Configuration File. The cashflow itself is calculated from the time series of logged simulation results. Depending on the selected operation strategy, the cashflows of multiple revenue streams ($\mathrm{CF}_{n,r}$) may be added to obtain the cashflow for a single project year (CF_n), as shown in Eq. (20).

$$\mathrm{CF}_n = -\mathrm{OM}_n + \sum_{r \in R} \mathrm{CF}_{n,r} \tag{20}$$

Here, R denotes the set of applicable revenues streams r for the selected operation strategy and OM the operation and maintenance cost. Table 8 shows the matching of revenue streams and operation strategies, while the following list provides brief descriptions for all currently implemented revenue streams. For stacked operation strategies, such as *FCR* paired with *IDM*, all respective revenue streams will be considered in Eq. (20).

- *Energy Cost Reduction (ECR)*: Reduction of energy-based electricity costs, caused, for example, by increased self-consumption of PV-generated electricity. This is calculated based on the total site load for both with and without the BESS, the electricity purchase price, and the electricity sales price or feed-in tariff.
- *Demand Charge Reduction (DCR)*: Savings generated by a reduction in demand charges, calculated based on the maximum site load with and without the BESS, the applicable billing period, and the demand charge price per unit of power.
- *Frequency Containment Reserve (FCR)*: Revenue that is generated by participating in the FCR market, calculated based on the system's nominal power, the FCR price, and the power allocated to the FCR market.
- *Spot Market Trading (SMT)*: Revenue that is generated through spot market trading, based on the amount of energy traded and the specified time series of prices.

6. Case studies

The following section will focus on **SimSES** from a user perspective. Compared to other solutions and tools in the field of energy system simulation, **SimSES** provides detailed modeling of ESS and applications on a system level during the full investment period. Both the technical properties of different storage technologies and the economic modeling of the components and systems are mapped in detail.

In order to clarify the implementation and adaptability of the tool, two applications are discussed. First, Peak Shaving (PS) for an industrial application comparing a different set of storage technologies—LIB, RFB, and a hybrid system of both technologies. Second, Frequency Containment Reserve (FCR) including an Intraday Continuous Market (IDM) by considering various system topologies are discussed. The underlying system costs are discussed in Appendix D. These case studies can be downloaded and executed as described in Appendix E.

6.1. Case study 1: Peak shaving application

A commonly used application for ESS is Peak Shaving (PS). The tariff model with separate energy- and power-related prices plays an important role here. The PS application aims to cut high power demands from the distribution grid. Since the highest power peak per billing period (usually monthly or annually) is multiplied by the power-related price, it can be economical favorable to cap high demand peaks by using an ESS to provide the necessary power and energy [9].

In this case study, three different storage systems are simulated: a LIB system with 150 kWh, a RFB system with 200 kWh, and a hybrid system with 10 kWh LIB capacity and 180 kWh RFB capacity. More detail on the system configuration chosen for this case study is given in Fig. 10. When investing in a system the user may be interested in deciding upfront which of the three configurations will provide the best economic solution. All systems are dimensioned to provide the peak shaving power even after 20 years, including capacity degradation. In addition, the restriction of a usable SOC range of RFB systems from 20% to 80% is considered [36]. The power electronics is dimensioned with 40 kW rated power. The Sony LFP cell technology for LIB and a scaled *CellDataStack5550W* model (cf. Table 4) as an all-Vanadium RFB system is considered. The assumed system costs for the economic evaluation are provided in Table D.11. As a revenue for reducing the power peak a fixed price of 100 EUR/kW in a yearly billing period is assumed. As an input power profile for the PS application, the Cluster 1 PS power profile from Kucevic et al. [73] is used and scaled to an annual load of 347.55 MWh from which the peak power is reduced to 63.5 kW.

After the simulation has been executed, the analysis and evaluation include both detailed technical and economic evaluations. An extract of the evaluations and results can be seen in the following illustrations:

Table 8
Matching of revenue streams and operation strategies for the cashflow calculation within the economic evaluation.

	ECR	DCR	FCR	SMT
Residential PV Greedy	x			
Residential PV Feed in Damp	x			
Peak Shaving	x	x		
Peak Shaving Perfect Foresight	x	x		
Frequency Containment Reserve			x	
Intraday Continuous Market				x

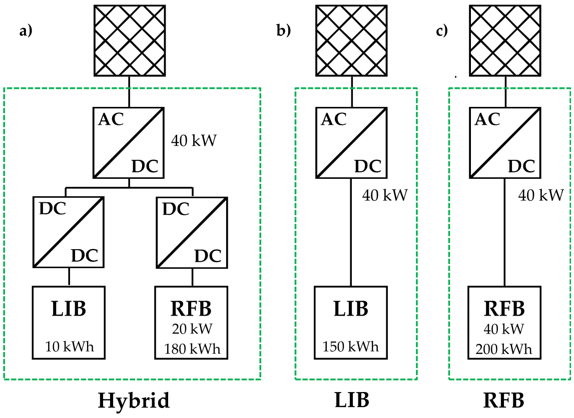

Fig. 10. Three different Energy Storage Systems (ESS) are investigated in the Peak Shaving (PS) case study: **(a)** A hybrid ESS consisting of a DC-coupled LIB and RFB system as well as single storage systems of **(b)** LIB and **(c)** RFB. All systems are dimensioned for providing the PS power even after 20 years of operation. A maximum Depth of Discharge (DOD) for RFB systems of 0.6 is considered. The Power Distribution Strategies (PDS) for the hybrid system performs according to the technology prioritization as described in Section 5.2.2. The DCDC converter is assumed with a fixed efficiency of 98%.

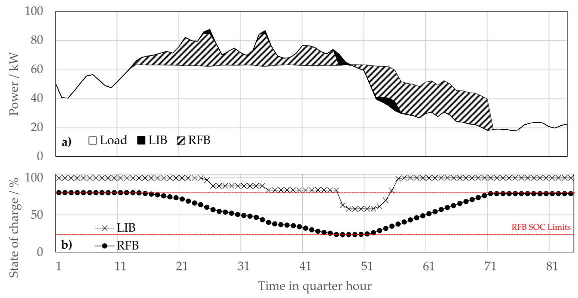

Fig. 11. Peak Shaving (PS) application on a hybrid Energy Storage System (ESS). **(a)** Residual load with and without the PS application with the delivered AC power of the installed ESS as well as the power distribution between the two DC-coupled storage systems. **(b)** State of Charge (SOC) development of the hybrid ESS. LIB systems takes over if target power exceed RFB stack power or if the RFB system hits its SOC limits.

Fig. 11 shows the characteristic curve of the power during the PS application for the hybrid storage system. The residual power can be seen with and without energy storage. It can be seen that the power drawn from the grid does not exceed the value of the PS threshold as was dictated by the operation strategy. Power demand values above the PS threshold are provided by the respective storage unit. This comes in line with charging and discharging power from the ESS and a simultaneous change in the storage-lumped SOC. According to the conditions set, recharging of the storage systems is executed only at times such that the PS threshold is never exceeded. In addition, the power distribution to the corresponding storage technologies of the hybrid system can be seen. The RFB system is prioritized to provide the bulk energy of the PS event while the LIB system covers high power peaks, especially if the RFB systems power capabilities are exhausted.

The remaining capacity (SOH) of the ESS can be seen in Fig. 12. The LIB capacity decreases to 70% during the 20-year simulation, while for the hybrid system as well as for the RFB system the capacity remains higher at 97% and 96%, respectively. Although the integrated degradation models consider both the calendar and the cycle degradation, it is noteworthy that the calendar degradation takes up the largest share in this operation of PS application [59].

In Fig. 12 the difference of the system round-trip efficiency can be observed. The LIB system demonstrates the highest efficiency with 88%, followed by the hybrid system with 68% and the RFB system with 62%. The energy losses of the RFB storage compartments are higher compared to LIB, attributed to a comparably low Coulomb efficiency and additional energy needed for electrolyte pumps.

In addition to the technical evaluation, **SimSES** also provides a comprehensive economic analysis of the simulated time series. In order to show a metric for overall costs, an alternative NPV considering capacity degradation as well is shown in Eq. (21), where c_{ST} represents energy-specific costs of the storage technology and C_{deg} the capacity degradation.

$$NPV_{CD} = NPV - c_{ST} \cdot C_{deg} \tag{21}$$

Fig. 12 shows the overall costs of the ESS operated with baseline cost set to 100% of the LIB system. For the evaluation of the system, not only real tariff models but also the investment costs for the ESS are integrated in the tool resulting in the NPV. In addition, the cost of capacity degradation is added to the NPV in order to take not only the system efficiency into account but also the capacity loss over 20 years (see Eq. (21)). It can be seen that the hybrid system is 5% more cost effective while the RFB system has 81% higher overall costs. The primary reason for these values are the cost of capacity degradation, which is 51% of the overall costs for the LIB system although the NPV for the LIB systems is lowest compared to the other systems. In conclusion, a hybrid system can deliver an overall better solution compared to single storage systems although only a small peak LIB ESS is added to an RFB system, combining the benefits of both techniques, i.e., a higher NPV compared to a single RFB system and a lower capacity degradation compared to a single LIB system. However, with the input parameters chosen herein, none of the three negative storage solutions were able to justify an investment as all resulted in negative NPV_{CD} values. The overall economics of this case study could potentially be improved if the ESS value generation was increased, e.g., by applying multi-use operation and dispatching storage in PS idle times [4,74]. Additionally, results with hybrid storage systems could be improved with optimization and machine learning techniques instead of applying a rule-based algorithm [75,76].

6.2. Case study 2: Frequency containment reserve application

A widely used application of utility-scale ESS is participation in the market for FCR. In this application, the ESS compensate for fluctuations

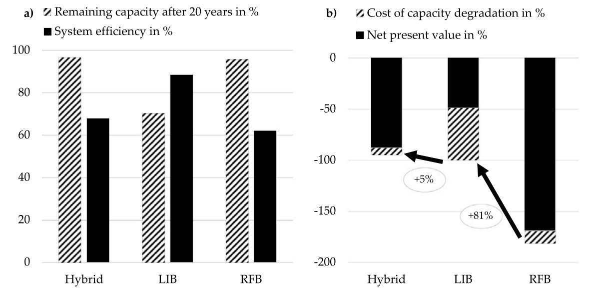

Fig. 12. Economic analysis of the three different Energy Storage Systems (ESS) serving the Peak Shaving (PS) application. **(a)** Comparison of remaining capacity and system efficiency of all simulated ESS after 20 years. **(b)** Overall costs consisting of the NPV and cost of capacity degradation using the LIB system as the baseline. The hybrid system could decrease overall cost by 5%, whereas the RFB system increased the cost by 81%.

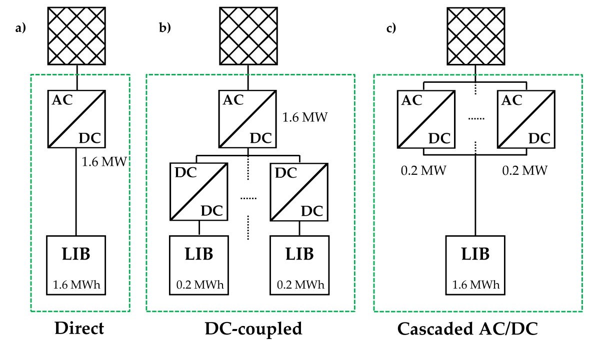

Fig. 13. Three different ESS topologies are investigated in the FCR case study, all with a LIB system of 1.6 MWh and an ACDC connection to the grid of 1.6 MW. The ACDC converter model is the *NottonAcDcConverter* (cf. Table 6). **(a)** A direct-coupled ESS with one ACDC converter. **(b)** Eight parallel DC-coupled systems with an assumed fixed DCDC efficiency of 98%. **(c)** Eight parallel connected ACDC converter with a cascaded activation: The first ACDC converter drives to its nominal power of 0.2 MW before the second ACDC converter is activated.

between consumption and generation in the power grid by reacting accordingly to changes in the grid frequency. The regulations and degrees of freedom for FCR application complying to German regulation criteria are taken into account and are described in detail in [4,8,62,73]. In this operation strategy of **SimSES** the SOC stabilization of the ESS is achieved by support of IDM. FCR and IDM are each basic operation strategies running in a stacked operation. For the simulation a grid frequency profile of 2014 is used to account for the provided stabilizing power [77]. It is assumed that the provided power of 1 MW does not affect the integrated network frequency.

In this case study, three different ESS topologies are simulated (cf. Fig. 13), each with a Sony LFP cell technology providing a capacity of 1.6 MWh and a grid-connection power of 1.6 MW. First, a simple direct approach of connecting a LIB to a grid-connected ACDC converter is investigated. Second, eight parallel DC-coupled systems with a LIB capacity of 0.2 MWh each are simulated. Third, eight parallel connected ACDC converters with a nominal power of 0.2 MW each are activated in a cascaded approach promising a higher efficiency [78]. The assumed system costs for the economic evaluation are provided in Table D.12. The revenue of FCR[12] is taken as a fixed price of 0.2 EUR per kW and day and the IDM[13] price is fixed to 0.04 EUR/kWh, corresponding to a price level of 2020.

The results of the 20-year simulations are displayed in Fig. 14. The cascaded ACDC converter approach shows the best efficiency with 92% compared to the direct approach with 78% and the least efficient topology with DC-coupled systems of 63%. FCR is an application with a high partial-load frequency below 30% of nominal power [55]. Hence, the cascaded ACDC converter are either under a high load compared to their nominal power or deactivated, leading to a higher overall efficiency compared to the direct system. The DC-coupled system shows an overproportional efficiency decrease compared to the direct system. The systems of the DC-coupled ESS are activated similar to the cascade of ACDC converter: one system is ramped up to full power before the second system is activated. Due to relatively high currents in addition to the losses of the DCDC converter, the DC-coupled system shows a comparatively low efficiency. This result suggests that the chosen PDS is inappropriate in terms of efficiency for a FCR application with the given system for the DC-coupled system. Comparing the remaining capacity of the three investigated systems, no large difference can be observed, with a remaining capacity of each system after 20 years of around 80%. One target of the chosen PDS for the DC-coupled system was to reduce the capacity degradation by cycling a few systems more often than other systems in order to get an overall better degradation behavior. However, it can be observed that the chosen strategy shows no improvement in terms of the degradation behavior for this application compared to the other systems.

Analyzing the economics, the high efficiency advantage of the cascaded system could be transferred to a slight monetary improvement compared to the other systems. The cascaded system shows a 4% increase of the NPV compared to the direct system. The DC-coupled system falls behind with a lower NPV of 5% in comparison to the direct system (cf. Fig. 14). This could be explained with IDM recharging cost over the simulation time period since the FCR revenue is the same for all investigated systems (cf. Table 9).

First, the IDM transaction costs are comparatively low: The direct system accounts for 36 kEUR, the DC-coupled system for 64 kEUR and the cascaded system for 14 kEUR, accumulated after 20 years of operation. In comparison, the FCR revenue compensates for around 1,218 kEUR. Second, the low efficiency of the DC-coupled system results in 231 MWh energy sold on the IDM whereas the direct system and the cascaded system could sell 347 MWh and 494 MWh, respectively. This is also reflected in the numbers of bought energy: the DC-coupled system had to buy most energy with 1,829 MWh while the cascaded system had to buy 851 MWh. Although large differences in terms of efficiency exist compared to the direct system (+14% for the cascaded system and -15% for the DC-coupled system) this could only be translated into a 4% increase of the NPV, respectively to a 5% decrease. The economic result of more efficient ESS could be improved by reducing the storage capacity and improving the IDM operation strategy. In conclusion, all three systems have a positive NPV, likely leading to a positive investment decision.

With these case studies a high variety of topologies as well as technology combinations could be investigated. Parameter variations, e.g., for the investment costs or sizing of individual components can easily be made by the user when adapting according initialization files of the case studies available as presented in Appendix E.

7. Conclusion and outlook

Within this work, the simulation and analysis tool for energy storage systems **SimSES** is presented. **SimSES** provides a library of state-of-the-art energy storage models by combining modularity of multiple topologies as well as the periphery of an ESS. This paper summarizes the structure as well as the capabilities of **SimSES**. Storage technology

[12] Prices for the German FCR market can be found at https://www.regelleistung.net.

[13] Prices for the European spot market can be found at https://www.epexspot.com.

Table 9
Overview of the IDM transaction costs for all three investigated ESS.

System	IDM transaction costs/EUR	Energy bought/MWh	Energy sold/MWh
Direct	35,772	1242	347
DC-coupled	63,894	1829	231
Cascaded	14,280	851	494

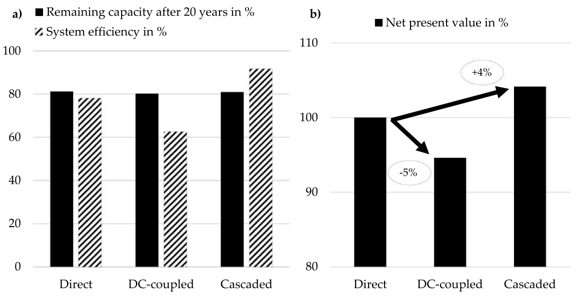

Fig. 14. Technical and economical analysis of the three different Energy Storage Systems (ESS) serving the Frequency Containment Reserve (FCR) application. **(a)** Comparison of remaining capacity after 20 years and system efficiency of all simulated ESSs. **(b)** Economic value consisting of the NPV using the direct system as baseline.

models based on current research for lithium-ion batteries, redox flow batteries, as well as hydrogen storage-based electrolysis and fuel cell are presented in detail. In addition, thermal models and their corresponding HVAC systems, housing, and ambient models are depicted. Power electronics are represented with ACDC and DCDC converters mapping the main losses of power electronics within a storage system. Additionally, auxiliary components like pumps, compressors, and HVAC are considered. Standard use cases like peak shaving, residential storage, and control reserve power provisions through dispatch of storage are discussed in this work, with the possibility to stack these applications in a multi-use scenario. The analysis is provided by technical and economic evaluations illustrated by KPIs.

SimSES' capabilities are demonstrated through the discussion of two case studies mapped to the applications of peak shaving and frequency containment reserve, respectively. It is demonstrated how different energy storage system topologies as well as various performance indicators can be investigated and analyzed with **SimSES**. For the specific cases discussed, the results underline that hybrid storage systems can lead in terms of overall cost and degradation behavior to a beneficial economic results. Special ESS topologies like the cascaded ACDC converter approach can lead to a substantial increase in system efficiency for the FCR application, although the economic benefits are comparatively low.

In the future, more detailed performance and aging models for all types of storage systems will be implemented. This will allow a more detailed cross-technology comparison. For instance, models for bidirectional thermal storage system could be implemented in future versions. Further operating strategies matching internationally renowned and national derivatives of application scenarios could also be investigated. This may allow assessing the value of storage deployment across different regions and convince internationally active investors to reveal best investment scenarios worldwide. **SimSES** has interfaces that can be easily integrated into physically derived and more accurate storage models as well as grid modeling and system analysis tools. While selected validation experiments have already been executed, the authors encourage others in the research community to conduct hardware validation experiments at their sites and contribute to the presented tool. The authors envision interlinking **SimSES** to the vast selection of open-source tools in order to expand on the value chain that storage simulations are capable of covering, e.g., **SimSES** is already a part of the *openMOD*[14] initiative. **SimSES** is open-source available, and the authors encourage users and developers to join in and assist in its further development.

CRediT authorship contribution statement

Marc Möller: Conceptualization, Methodology, Writing - original draft, Writing - review & editing, Software, Project administration, Visualization, Investigation. **Daniel Kucevic:** Writing - original draft, Writing - review & editing, Validation, Software, Methodology. **Nils Collath:** Writing - original draft, Writing - review & editing, Software, Methodology. **Anupam Parlikar:** Writing - original draft, Writing - review & editing, Software, Methodology. **Petra Dotzauer:** Writing - original draft, Writing - review & editing, Software, Methodology. **Benedikt Tepe:** Investigation, Validation, Writing - original draft, Writing - review & editing, Software. **Stefan Englberger:** Investigation, Validation, Writing - original draft, Writing - review & editing. **Andreas Jossen:** Writing - review & editing, Funding acquisition. **Holger Hesse:** Writing - original draft, Writing - review & editing, Supervision.

Declaration of competing interest

The authors declare that they have no known competing financial interests or personal relationships that could have appeared to influence the work reported in this paper.

Acknowledgments

This work was financially supported by the Federal Ministry for Economic Affairs and Energy within the open_BEA project (Grant No. 03ET4072) and the EffSkalBatt project (Grant No. 03ET6148). Both projects are supported by Project Management Juelich. The responsibility for this publication rests with the authors.

We thank Jacob Klinkenberg, Kareem Abo Gamra, and Benedikt Wiesend for their contribution with simulating and implementing models in the hydrogen package, Timo Sandner and Felix Müller for their implementations of ACDC converters, Dang The Phong for his work on the model for a RFB stack as well as Ni Chuanqin and Yuhui Geng for their implementations of two LIB degradation models.

Appendix A. Open circuit voltage curve fitting

The OCV for LIBs (see Section 4.1) is dependent on the cell type. The OCV data for all currently implemented cell types have been measured at the Institute for Electrical Energy Storage Technology at the Technical University of Munich. To improve the performance, the look-up tables of the voltage values are replaced with a mathematical function. These curve-fitting functions are based on the work of Weng et al. [79]. The parameters of this function for the OCV are estimated using the MATLAB® global optimization toolbox. Fig. A.15 shows the OCV in V for the measured data as well as the curve-fitted data and the difference between those in mV.

[14] https://openmod-initiative.org/

Table B.10
Physical parameters for modeling of thermal behavior of lithium-ion batteries (LIBs).

Manufacturer model	Mass (g)	Dimensions (mm)	Specific heat ($Jkg^{-1}K^{-1}$)	Convection coefficient ($Wm^{-2}K^{-1}$)	Source
Sony US26650FTC1	70	dia: 26 len: 65	1001	15	[55,80–89]
Panasonic NCR18650PD	44	dia: 18 len: 65	1048	15	[88–90]
E-One Moli Energy IHR18650A	45	dia: 18 len: 65	965	15	[83,86,89,91–94]
Sanyo UR18650E	46	dia: 18 len: 65	965	15	[83,86,89,92–95]

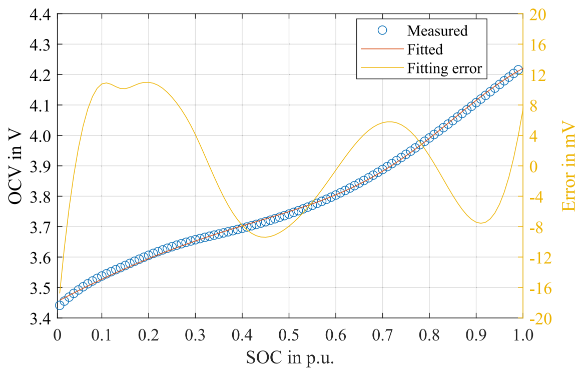

Fig. A.15. Open Circuit Voltage (OCV) curve fitting for the MolicelNMC lithium-ion battery (LIB). The figure shows the OCV in V for the measured data as well as the curve-fitted data and the difference between those in mV.

Appendix B. Thermal parameters

The geometrical and thermal parameters used for modeling the thermal behavior of LIBs are presented in Table B.10. Geometrical parameters such as the dimensions and the weight are obtained from datasheets of the cells. The thermal properties, such as the specific heat capacity for each cell type, are determined from the literature for each cell chemistry, and averaged over several values found in the literature. The value of the convection coefficient is known with the least accuracy, and a value of 15 $Wm^{-2}K^{-1}$ is selected as a "reasonable" value lying between typical values for purely natural convection and forced convection. This is assumed to emulate slow intermittent motion of air around the cells. It is expected that availability of better data in the future will increase the accuracy of the modeling process.

Appendix C. Stack data for a redox flow battery

The parameters are based on single-cell measurements carried out at ZAE Bayern of a cell with a technical representative cell area of 2160 cm^2. To obtain parameters for a stack, the measured values were scaled up with a number of 40 cells. Fig. C.16 shows the data of the internal resistance of the 40-cell stack for charge and discharge. The internal resistance is determined by applying a constant current and measuring the resulting change of voltage. The cell was operating in Vanadium electrolyte (1.6 mol/l V solved in 2 mol/l H_2SO_4) from GfE (Gesellschaft für Elektrometallurgie mbH). Temperature and flow rate were controlled during the procedure. The SOC was determined with an OCV-cell. Due to the relatively high ohmic resistance of the cell and the low possible operation current density (up to approx. 50 mA/cm^2), the cell resistance shows no significant current dependency. The cell resistance R_{cell} was scaled up with the number of cells n_{cell} to receive the stack resistance R_{stack} ($R_{stack} = n_{cell} \cdot R_{cell}$).

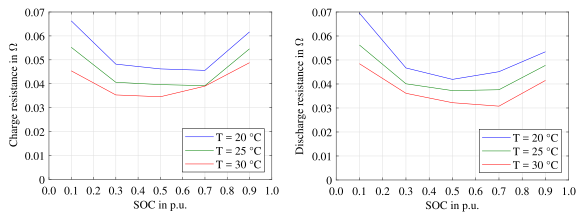

Fig. C.16. Charge and discharge resistance of a stack for a redox flow battery (cell area = 2160 cm^2) dependent on State of Charge (SOC) and temperature (T). The single-cell measurements were scaled up to a stack resistance with a cell number of 40.

Appendix D. Economics for case studies

Assumptions for economical analysis of the case studies are based on Tsiropoulos et al. Minke et al. Figgener et al. and Mongird et al. [96–99]. Challenges for determining energy-specific costs for ESS occur due to a wide range of technology costs as well as various system sizes and designs. In order to distinguish between power and energy system design, Tsiropoulos et al. takes the EPR as an indicator: If EPR is above one, the authors talk about an energy-driven design, otherwise about power-driven design [96]. In addition, it is not always clearly stated which costs for a system design are included, e.g., power electronics, housing, and grid connection [96,98]. For instance, utility scale system costs for LIB in 2017 ranged between 300 EUR/kWh and 1200 EUR/kWh with an average around 570 EUR/kWh [96]. Figgener et al. depicted a similar range for 2018 [98] as well as one reported system for 2019 with an EPR of 1 h and system costs of around 900 EUR/kWh. However, LIB systems with an EPR of 0.125 h show lowest cost with 300 EUR/kWh and costs increase with rising EPR [96]. Mongird et al. have presented system costs for LIB system with an EPR larger than 1 h with falling costs [99]. Interestingly, the system costs of [99] show a lower average system cost price than those of [96,98] representing European costs' levels (a USD to EUR conversion of 0.82 is assumed). In contrast, a broad cost database does not exist for RFB systems. However, Minke et al. investigated various RFB projects from 2004 to 2017 by determining system prices for different EPR, similar to Tsiropoulos et al. [97]. The authors also found an even broader range of system costs for RFB from 155 EUR/kWh to 1738 EUR/kWh, especially due to different electrolytes, stack modules, sizing, and system definition. RFB system costs decrease with a rising EPR with average system costs of 717 EUR/kWh for an EPR of 2 h and 166 EUR/kWh for a ratio of 15 h. These findings are also in agreement with the results of Mongird et al. [99].

For the following case studies, system cost curves depending on EPR are assumed for LIB and RFB systems with the prices and ratios

Table D.11
Economics for Case Study 1.

Storage technology	Power/kW	Capacity/kWh	EPR/h	Specific system cost/EUR kWh^{-1}	System cost/EUR	Overall system cost/EUR
LIB	40	10	0.25	584	5,839	
RFB	20	180	9.00	329	59,216	65,055
LIB only	40	150	3.75	367	55,089	55,089
RFB only	40	200	5.00	451	90,247	90,247

Table D.12
Economics for Case Study 2.

Storage technology	Power/kW	Capacity/kWh	EPR/h	Specific system cost/EUR kWh^{-1}	System cost/EUR
LIB	1,600	1,600	1	473	756,800

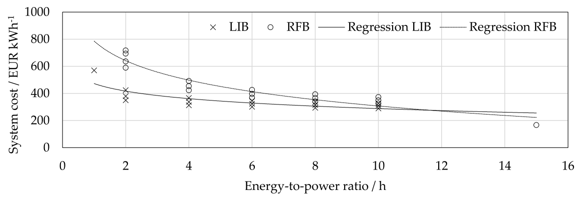

Fig. D.17. System costs curves depending on EPR for LIB and RFB systems based on [96,97,99].

given represented by regression curves in Eqs. (D.1) and (D.2). From an EPR of 1 h up to 15 h, this cost curve has a realistic cost range with decreasing cost over EPR. The system costs, however, have a high uncertainty attached, as shown in the previous analysis. The used price curves are shown in Fig. D.17. It is worth mentioning that the cost assumptions for RFB systems are based on a usable SOC range of 20% and 80%, which reduces the gross capacity configured by 40% [97].

$$c_{LIB} = -80 \cdot \ln(EPR) + 473 \quad \text{and} \tag{D.1}$$

$$c_{RFB} = -208 \cdot \ln(EPR) + 786, \tag{D.2}$$

where c represents the energy specific costs of LIB, respectively RFB.

Using Eqs. (D.1) and (D.2) the system costs for the two case studies discussed in Section 6 are calculated as provided in Tables D.11 and D.12.

Appendix E. Availability of SimSES

SimSES is available as open source[15] and is part of the open-source simulation and optimization toolchain of the Institute for Electrical Energy Storage Technology at the Technical University of Munich.[16] A *readme.md* helps with the first steps in order to get **SimSES** running. An installed Python environment is mandatory as well as the required packages installed automatically if you run *setup.py*. With executing *main.py*, a default configured simulation could be started directly. This file offers also all necessary interfaces in order to connect it to other simulation programs. The case studies presented within this paper are conducted with the open-source release version 1.0.4.

For configuring a simulation, there are two important configuration files: *simulation.ini* and *analysis.ini*. These configuration files are documented and offer all possible settings for setting up a simulation and the consequent evaluation. These config files follow a pattern for a *default* and *local* configuration. The *default* configuration inherits all possible settings, in the *local* file: only the changed settings are necessary. This allows a quick exchange of configuration settings between users.

The *Simulation* package allows multiple simultaneous simulations, which are also used for the presented case studies. In here, the configurations and code could be found with the case study configs in *case_studies*. In order to execute the case studies, the configuration needs to be copied to the config location and renamed to *simulation.local.ini*.

[15] https://gitlab.lrz.de/open-ees-ses/simses
[16] http://www.simses.org

References

[1] V. Lauber, S. Jacobsson, The politics and economics of constructing, contesting and restricting socio-political space for renewables – the German renewable energy act, Environ. Innov. Soc. Transitions 18 (2016) 147–163, http://dx.doi.org/10.1016/j.eist.2015.06.005.

[2] H.E. Murdock, D. Gibb, T. André, F. Appavou, A. Brown, B. Epp, B. Kondev, A. McCrone, E. Musolino, L. Ranalder, Renewables 2019 global status report, REN21, https://www.ren21.net/wp-content/uploads/2019/05/gsr_2019_full_report_en.pdf.

[3] P. Denholm, E. Ela, B. Kirby, M. Milligan, The Role of Energy Storage with Renewable Electricity Generation, Technical Report NREL (2010), 2010, http://dx.doi.org/10.2172/972169.

[4] S. Englberger, A. Jossen, H. Hesse, Unlocking the potential of battery storage with the dynamic stacking of multiple applications, Cell Rep. Phys. Sci. 1 (11) (2020) http://dx.doi.org/10.1016/j.xcrp.2020.100238.

[5] A. Evans, V. Strezov, T.J. Evans, Assessment of utility energy storage options for increased renewable energy penetration, Renew. Sustain. Energy Rev. 16 (6) (2012) 4141–4147, http://dx.doi.org/10.1016/j.rser.2012.03.048.

[6] D. Zafirakis, K.J. Chalvatzis, G. Baiocchi, G. Daskalakis, The value of arbitrage for energy storage: Evidence from European electricity markets, Appl. Energy 184 (2016) 971–986, http://dx.doi.org/10.1016/j.apenergy.2016.05.047.

[7] R.H. Byrne, R.J. Concepcion, C.A. Silva-Monroy, Estimating potential revenue from electrical energy storage in PJM, in: IEEE Power and Energy Society General Meeting (2016), 2016, http://dx.doi.org/10.1109/PESGM.2016.7741915.

[8] T. Thien, D. Schweer, D. vom Stein, A. Moser, D.U. Sauer, Real-world operating strategy and sensitivity analysis of frequency containment reserve provision with battery energy storage systems in the german market, J. Energy Storage 13 (2017) 143–163, http://dx.doi.org/10.1016/j.est.2017.06.012.

[9] A. Oudalov, R. Cherkaoui, Sizing and optimal operation of battery energy storage system for peak shaving application: Lausanne, Switzerland, 1 - 5 july 2007, IEEE Lausanne Power Tech. (2007) http://dx.doi.org/10.1109/PCT.2007.4538388.

[10] J. Hoppmann, J. Volland, T.S. Schmidt, V.H. Hoffmann, The economic viability of battery storage for residential solar photovoltaic systems – A review and a simulation model, Renew. Sustain. Energy Rev. 39 (2014) 1101–1118, http://dx.doi.org/10.1016/j.rser.2014.07.068.

[11] H. Hesse, R. Martins, P. Musilek, M. Naumann, C. Truong, A. Jossen, Economic optimization of component sizing for residential battery storage systems, Energies 10 (7) (2017) 835, http://dx.doi.org/10.3390/en10070835.

[12] S. Englberger, H. Hesse, D. Kucevic, A. Jossen, A techno-economic analysis of vehicle-to-building: Battery degradation and efficiency analysis in the context of coordinated electric vehicle charging, Energies 12 (5) (2019) 955, http://dx.doi.org/10.3390/en12050955.

[13] O.M. Toledo, D. Oliveira Filho, A.S.A.C. Diniz, Distributed photovoltaic generation and energy storage systems: A review, Renew. Sustain. Energy Rev. 14 (1) (2010) 506–511, http://dx.doi.org/10.1016/j.rser.2009.08.007.

[14] H. Hesse, M. Schimpe, D. Kucevic, A. Jossen, Lithium-ion battery storage for the grid—A review of stationary battery storage system design tailored for applications in modern power grids, Energies 10 (12) (2017) 2107, http://dx.doi.org/10.3390/en10122107.

[15] B. Dunn, H. Kamath, J.-M. Tarascon, Electrical energy storage for the grid: A battery of choices, Science 334 (2011) http://dx.doi.org/10.1126/science.1212741.

[16] J. Weniger, T. Tjaden, Performance-Simulationsmodell für AC-gekoppelte PV-Batteriesysteme (PerModAC): Dokumentation | Version 1.0, Hochschule für Technik und Wirtschaft H.T.W. Berlin, Berlin, 2017, URL https://pvspeicher.htw-berlin.de/wp-content/uploads/2017/03/PerModAC_doku.pdf.

[17] N.-K.C. Nair, N. Garimella, Battery energy storage systems: Assessment for small-scale renewable energy integration, Energy Build. 42 (11) (2010) 2124–2130, http://dx.doi.org/10.1016/j.enbuild.2010.07.002.

[18] U. Sureshkumar, P.S. Manoharan, A.P.S. Ramalakshmi, Economic cost analysis of hybrid renewable energy system using HOMER, in: IEEE-International Conference on Advances in Engineering, Science and Management, ICAESM -2012, 2012, pp. 94–99.

[19] J. Figgener, P. Stenzel, K.-P. Kairies, J. Linßen, D. Haberschusz, O. Wessels, G. Angenendt, M. Robinius, D. Stolten, D.U. Sauer, The development of stationary battery storage systems in Germany – A market review, J. Energy Storage 29 (2020) http://dx.doi.org/10.1016/j.est.2019.101153.

[20] E. Gamma, R. Helm, R. Johnson, J.M. Vlissides, Design Patterns: Elements of Reusable Object-Oriented Software, first ed., Addison-Wesley Professional, 1994.

[21] B. Nykvist, M. Nilsson, Rapidly falling costs of battery packs for electric vehicles, Nature Clim. Change 5 (4) (2015) 329–332, http://dx.doi.org/10.1038/nclimate2564.

[22] G. Zubi, R. Dufo-López, M. Carvalho, G. Pasaoglu, The lithium-ion battery: State of the art and future perspectives, Renew. Sustain. Energy Rev. 89 (2018) 292–308, http://dx.doi.org/10.1016/j.rser.2018.03.002.

[23] M. Yoshio, R.J. Brodd, A. Kozawa, Lithium-Ion Batteries, Springer New York, New York, NY, 2009, http://dx.doi.org/10.1007/978-0-387-34445-4.

[24] A.M. Divakaran, M. Minakshi, P.A. Bahri, S. Paul, P. Kumari, A.M. Divakaran, K.N. Manjunatha, Rational design on materials for developing next generation lithium-ion secondary battery, Prog. Solid State Chem. 62 (2021) 100298, http://dx.doi.org/10.1016/j.progsolidstchem.2020.100298.

[25] M. Naumann, F.B. Spingler, A. Jossen, Analysis and modeling of cycle aging of a commercial LiFePO4/graphite cell, J. Power Sources 451 (2020) 227666, http://dx.doi.org/10.1016/j.jpowsour.2019.227666.

[26] M. Naumann, M. Schimpe, P. Keil, H.C. Hesse, A. Jossen, Analysis and modeling of calendar aging of a commercial LiFePO4/graphite cell, J. Energy Storage 17 (2018) 153–169, http://dx.doi.org/10.1016/j.est.2018.01.019.

[27] P. Keil, S.F. Schuster, J. Wilhelm, J. Travi, A. Hauser, R.C. Karl, A. Jossen, Calendar aging of lithium-ion batteries, J. Electrochem. Soc. 163 (9) (2016) A1872–A1880, http://dx.doi.org/10.1149/2.0411609jes.

[28] S.F. Schuster, T. Bach, E. Fleder, J. Müller, M. Brand, G. Sextl, A. Jossen, Nonlinear aging characteristics of lithium-ion cells under different operational conditions, J. Energy Storage 1 (2015) 44–53, http://dx.doi.org/10.1016/j.est.2015.05.003.

[29] J. Schmalstieg, S. Käbitz, M. Ecker, D.U. Sauer, A holistic aging model for li(NiMnCo)o2 based 18650 lithium-ion batteries, J. Power Sources 257 (2014) 325–334, http://dx.doi.org/10.1016/j.jpowsour.2014.02.012.

[30] M.M. Rahman, A.O. Oni, E. Gemechu, A. Kumar, Assessment of energy storage technologies: A review, Energy Convers. Manage. 223 (2020) 113295, http://dx.doi.org/10.1016/j.enconman.2020.113295.

[31] G. Kear, A.A. Shah, F.C. Walsh, Development of the all-vanadium redox flow battery for energy storage: a review of technological, financial and policy aspects, Int. J. Energy Res. 36 (11) (2012) 1105–1120, http://dx.doi.org/10.1002/er.1863.

[32] A.Z. Weber, M.M. Mench, J.P. Meyers, P.N. Ross, J.T. Gostick, Q. Liu, Redox flow batteries: a review, J. Appl. Electrochem. 41 (10) (2011) 1137–1164, http://dx.doi.org/10.1007/s10800-011-0348-2.

[33] N. Hagedorn, M.A. Hoberecht, L.H. Thaller, NASA redox cell stack shunt current, pumping power, and cell performance tradeoffs, U.S. Department of Energy / NASA Technical Memorandum, 1982, URL https://ntrs.nasa.gov/citations/19820011459.

[34] R. Schweiss, A. Pritzl, C. Meiser, Parasitic hydrogen evolution at different carbon fiber electrodes in vanadium redox flow batteries, J. Electrochem. Soc. 163 (9) (2016) A2089–A2094, http://dx.doi.org/10.1149/2.1281609jes.

[35] A.H. Whitehead, M. Harrer, Investigation of a method to hinder charge imbalance in the vanadium redox flow battery, J. Power Sources 230 (2013) 271–276, http://dx.doi.org/10.1016/j.jpowsour.2012.11.148.

[36] M. Skyllas-Kazacos, L. Cao, M. Kazacos, N. Kausar, A. Mousa, Vanadium electrolyte studies for the vanadium redox battery-a review, ChemSusChem 9 (13) (2016) 1521–1543, http://dx.doi.org/10.1002/cssc.201600102.

[37] A. Tang, J. Bao, M. Skyllas-Kazacos, Studies on pressure losses and flow rate optimization in vanadium redox flow battery, J. Power Sources 248 (2014) 154–162, http://dx.doi.org/10.1016/j.jpowsour.2013.09.071.

[38] E.A. Kaminski, R.F. Savinell, A technique for calculating shunt leakage and cell currents in bipolar stacks having divided or undivided cells, J. Electrochem. Soc. 130 (5) (1983) 1103–1107.

[39] fumatech, in: fumatech (Ed.), Redox-Flow-Batteries: data sheet: fumasep® membrane types, URL https://www.fumatech.com/NR/rdonlyres/6E4FA7B9-0AAA-42B9-98E4-BF756C23F981/0/FUMATECH_BWT_GmbHRedoxFlowBatteries.pdf.

[40] C. Blanc, R. Alfred, Understanding the vanadium redox flow batteries, in: InTech (Ed.), Paths to Sustainable Energy, InTechOpen, 2010, pp. 333–358.

[41] M. Robinius, P. Markewitz, P. Lopion, D. Stolten, Cost-efficient and climate-friendly transformation strategies for the german energy system up to 2050, in: Forschungszentrum JÜLich: Energy & Environment, 499, 2019.

[42] R.P. O'Hayre, S.-W. Cha, W.G. Colella, F.B. Prinz, Fuel cell fundamentals, third ed., John Wiley & Sons Inc, Hoboken New Jersey, 2016.

[43] G. Tjarks, PEM-electrolysis-systems for the integration in power-to-gas applications, (Ph.D. thesis), Lehrstuhl für Brennstoffzellen, RWTH Aachen, Aachen, 2017, http://dx.doi.org/10.18154/RWTH-2017-04470.

[44] C. Rakousky, U. Reimer, K. Wippermann, M. Carmo, W. Lueke, D. Stolten, An analysis of degradation phenomena in polymer electrolyte membrane water electrolysis, J. Power Sources 326 (2016) 120–128, http://dx.doi.org/10.1016/j.jpowsour.2016.06.082.

[45] C. Rakousky, U. Reimer, K. Wippermann, S. Kuhri, M. Carmo, W. Lueke, D. Stolten, Polymer electrolyte membrane water electrolysis: Restraining degradation in the presence of fluctuating power, J. Power Sources 342 (2017) 38–47, http://dx.doi.org/10.1016/j.jpowsour.2016.11.118.

[46] F. Marangio, M. Santarelli, M. Cali, Theoretical model and experimental analysis of a high pressure pem water electrolyser for hydrogen production, Int. J. Hydrogen Energy 34 (3) (2009) 1143–1158, http://dx.doi.org/10.1016/j.ijhydene.2008.11.083.

[47] M. Hammoudi, C. Henao, K. Agbossou, Y. Dubé, M.L. Doumbia, New multi-physics approach for modelling and design of alkaline electrolyzers, Int. J. Hydrogen Energy 37 (19) (2012) 13895–13913, http://dx.doi.org/10.1016/j.ijhydene.2012.07.015.

[48] C. Henao, K. Agbossou, M. Hammoudi, Y. Dubé, A. Cardenas, Simulation tool based on a physics model and an electrical analogy for an alkaline electrolyser, J. Power Sources 250 (2014) 58–67, http://dx.doi.org/10.1016/j.jpowsour.2013.10.086.

[49] D. Feroldi, M.S. Basualdo, Description of PEM Fuel Cells Systems, Springer, London and New York, 2012, http://dx.doi.org/10.1007/978-1-84996-184-4_2.

[50] A. Buttler, H. Spliethoff, Current status of water electrolysis for energy storage, grid balancing and sector coupling via power-to-gas and power-to-liquids: A review, Renew. Sustain. Energy Rev. 82 (2018) 2440–2454, http://dx.doi.org/10.1016/j.rser.2017.09.003.

[51] Q. Feng, X.-Z. Yuan, G. Liu, B. Wei, Z. Zhang, H. Li, H. Wang, A review of proton exchange membrane water electrolysis on degradation mechanisms and mitigation strategies, J. Power Sources 366 (2017) 33–55, http://dx.doi.org/10.1016/j.jpowsour.2017.09.006.

[52] A. Ursúa, E.L. Barrios, J. Pascual, I. San Martín, P. Sanchis, Integration of commercial alkaline water electrolysers with renewable energies: Limitations and improvements, Int. J. Hydrogen Energy 41 (30) (2016) 12852–12861, http://dx.doi.org/10.1016/j.ijhydene.2016.06.071.

[53] M. Schimpe, N. Becker, T. Lahlou, H.C. Hesse, H.-G. Herzog, A. Jossen, Energy efficiency evaluation of grid connection scenarios for stationary battery energy storage systems, Energy Procedia 155 (2018) 77–101, http://dx.doi.org/10.1016/j.egypro.2018.11.065.

[54] G. Notton, V. Lazarov, L. Stoyanov, Optimal sizing of a grid-connected PV system for various PV module technologies and inclinations, inverter efficiency characteristics and locations, Renew. Energy 35 (2) (2010) 541–554, http://dx.doi.org/10.1016/j.renene.2009.07.013.

[55] M. Schimpe, M. Naumann, N. Truong, H.C. Hesse, S. Santhanagopalan, A. Saxon, A. Jossen, Energy efficiency evaluation of a stationary lithium-ion battery container storage system via electro-thermal modeling and detailed component analysis, Appl. Energy 210 (2018) 211–229, http://dx.doi.org/10.1016/j.apenergy.2017.10.129.

[56] M. Förstl, N. Truon, M. Möller, H. Hesse, A. Singer, T. Weyh, The efficiency and profitability of the modular multilevel battery for frequency containment reserve, Atlantis Highlights Eng. 6 (2020) 80–85, http://dx.doi.org/10.2991/ahe.k.210202.012.

[57] A. Zeh, R. Witzmann, Operational strategies for battery storage systems in low-voltage distribution grids to limit the feed-in power of roof-mounted solar power systems, Energy Procedia 46 (2014) 114–123, http://dx.doi.org/10.1016/j.egypro.2014.01.164.

[58] D. Kucevic, C.N. Truong, A. Jossen, H.C. Hesse, Lithium-ion battery storage design for buffering fast charging stations for battery electric vehicles and electric buses, in: D. Schulz (Ed.), NEIS 2018, VDE VERLAG GMBH, Berlin, 2019, pp. 1–6, URL http://ieeexplore.ieee.org/stamp/stamp.jsp?tp=&arnumber=8669466&isnumber=8669446.

[59] N. Collath, S. Englberger, A. Jossen, H. Hesse, Reduction of battery energy storage degradation in peak shaving operation through load forecast dependent energy management, in: D. Schulz (Ed.), NEIS 2020, VDE VERLAG GMBH, 2020, pp. 250–254, URL https://ieeexplore.ieee.org/stamp/stamp.jsp?tp=&arnumber=9273426.

[60] D. Übertragungsnetzbetreiber, Eckpunkte und Freiheitsgrade bei Erbringung von Primaerregelleistung (in German): Leitfaden für Anbieter von Primaerregelleistung, Berlin, Germany, 50Hertz Transmission GmbH and Amprion GmbH and TenneT TSO GmbH and TransnetBW GmbH, https://www.regelleistung.net/ext/download/eckpunktePRL.

[61] D. Übertragungsnetzbetreiber, Anforderungen an die Speicherkapazitaet bei Batterien für die Primaerregelleistung (in German), Berlin, Germany, 50Hertz Transmission GmbH and Amprion GmbH and TenneT TSO GmbH and TransnetBW GmbH, https://www.bves.de/wp-content/uploads/2015/08/2015_08_26_Anforderungen_Speicherkapazitaet_Batterien_PRL.pdf.

[62] A. Zeh, M. Müller, M. Naumann, H. Hesse, A. Jossen, R. Witzmann, Fundamentals of using battery energy storage systems to provide primary control reserves in Germany, Batteries 2 (3) (2016) 29, http://dx.doi.org/10.3390/batteries2030029.

[63] M. Mühlbauer, O. Bohlen, M.A. Danzer, Analysis of power flow control strategies in heterogeneous battery energy storage systems, J. Energy Storage 30 (2020) 101415, http://dx.doi.org/10.1016/j.est.2020.101415.

[64] M. Bauer, System Design and Power Flow of Stationary Energy Storage Systems, (Ph.D. thesis), ETH Zurich, 2019, http://dx.doi.org/10.3929/ETHZ-B-000374736.

[65] C.N. Truong, M. Naumann, R.C. Karl, M. Müller, A. Jossen, H.C. Hesse, Economics of residential photovoltaic battery systems in Germany: The case of teslas powerwall, Batteries 2 (2) (2016) 14, http://dx.doi.org/10.3390/batteries2020014.

[66] A.M. Divakaran, D. Hamilton, K.N. Manjunatha, M. Minakshi, Design, development and thermal analysis of reusable li-ion battery module for future mobile and stationary applications, Energies 13 (6) (2020) 1477, http://dx.doi.org/10.3390/en13061477.

[67] D. Wang, Y. Bao, J. Shi, Online lithium-ion battery internal resistance measurement application in state-of-charge estimation using the extended Kalman filter, Energies 10 (9) (2017) 1284, http://dx.doi.org/10.3390/en10091284.

[68] C.R. Birkl, M.R. Roberts, E. McTurk, P.G. Bruce, D.A. Howey, Degradation diagnostics for lithium ion cells, J. Power Sources 341 (2017) 373–386, http://dx.doi.org/10.1016/j.jpowsour.2016.12.011.

[69] T. Waldmann, M. Wilka, M. Kasper, M. Fleischhammer, M. Wohlfahrt-Mehrens, Temperature dependent ageing mechanisms in lithium-ion batteries – a post-mortem study, J. Power Sources 262 (2014) 129–135, http://dx.doi.org/10.1016/j.jpowsour.2014.03.112.

[70] S. Ma, M. Jiang, P. Tao, C. Song, J. Wu, J. Wang, T. Deng, W. Shang, Temperature effect and thermal impact in lithium-ion batteries: A review, Prog. Nat. Sci. Mater. Int. 28 (6) (2018) 653–666, http://dx.doi.org/10.1016/j.pnsc.2018.11.002.

[71] B. Shabani, M. Biju, Theoretical modelling methods for thermal management of batteries, Energies 8 (9) (2015) 10153–10177, http://dx.doi.org/10.3390/en80910153.

[72] Deutsches Zentrum für Luft- und Raumfahrt (DLR) / German Aerospace Centre, greenius: Green Energy System Analysis, Deutsches Zentrum für Luft- und Raumfahrt (DLR) / German Aerospace Centre, Köln, Germany, 2018, URL https://www.dlr.de/sf/en/desktopdefault.aspx/tabid-11688/20442_read-44865/.

[73] D. Kucevic, B. Tepe, S. Englberger, A. Parlikar, M. Mühlbauer, O. Bohlen, A. Jossen, H. Hesse, Standard battery energy storage system profiles: Analysis of various applications for stationary energy storage systems using a holistic simulation framework, J. Energy Storage 28 (2020) 101077, http://dx.doi.org/10.1016/j.est.2019.101077.

[74] S. Englberger, H. Hesse, N. Hanselmann, A. Jossen, SimSES multi-use: A simulation tool for multiple storage system applications, in: 2019 16th International Conference on the European Energy Market, EEM, 2019, pp. 1–5, http://dx.doi.org/10.1109/EEM.2019.8916568, URL https://ieeexplore.ieee.org/abstract/document/8916568/.

[75] L. Gerlach, T. Bocklisch, Experts versus algorithms? Optimized fuzzy logic energy management of autonomous PV hybrid systems with battery and H2 storage, Energies 14 (6) (2021) 1777, http://dx.doi.org/10.3390/en14061777.

[76] L. Desportes, I. Fijalkow, P. Andry, Deep reinforcement learning for hybrid energy storage systems: Balancing lead and hydrogen storage, Energies 14 (15) (2021) 4706, http://dx.doi.org/10.3390/en14154706.

[77] 50Hertz Transmission GmbH, Archive of mains frequency of ENTSO-e, 2021, URL https://www.50hertz.com/de/Transparenz/Kennzahlen/Regelenergie/ArchivNetzfrequenz.

[78] A. Parlikar, H. Hesse, A. Jossen, Topology and efficiency analysis of utility-scale battery energy storage systems, Atlantis Highlights Eng. 4 (2019) 119–131, http://dx.doi.org/10.2991/ires-19.2019.15.

[79] C. Weng, J. Sun, H. Peng, A unified open-circuit-voltage model of lithium-ion batteries for state-of-charge estimation and state-of-health monitoring, J. Power Sources 258 (2014) 228–237, http://dx.doi.org/10.1016/j.jpowsour.2014.02.026.

[80] Akkuplus.de, Panasonic - UR18650e - 3,7 volt 2150mah Li-Ion - EOL, 2020, URL https://akkuplus.de/Panasonic-UR18650E-37-Volt-2150mAh-Li-Ion-EOL.

[81] N. Damay, C. Forgez, M.-P. Bichat, G. Friedrich, Thermal modeling of large prismatic LiFePO 4 /graphite battery. Coupled thermal and heat generation models for characterization and simulation, J. Power Sources 283 (2015) 37–45, http://dx.doi.org/10.1016/j.jpowsour.2015.02.091.

[82] C. Forgez, D. Vinh Do, G. Friedrich, M. Morcrette, C. Delacourt, Thermal modeling of a cylindrical LiFePO4/graphite lithium-ion battery, J. Power Sources 195 (9) (2010) 2961–2968, http://dx.doi.org/10.1016/j.jpowsour.2009.10.105.

[83] B. Lei, W. Zhao, C. Ziebert, N. Uhlmann, M. Rohde, H. Seifert, Experimental analysis of thermal runaway in 18650 cylindrical li-ion cells using an accelerating rate calorimeter, Batteries 3 (4) (2017) 14, http://dx.doi.org/10.3390/batteries3020014.

[84] M.S. Rad, D.L. Danilov, M. Baghalha, M. Kazemeini, P.H.L. Notten, Thermal modeling of cylindrical LiFePO4 batteries, J. Mod. Phys. 04 (07) (2013) 1–7, http://dx.doi.org/10.4236/jmp.2013.47A2001.

[85] L.H. Saw, K. Somasundaram, Y. Ye, A. Tay, Electro-thermal analysis of lithium iron phosphate battery for electric vehicles, J. Power Sources 249 (2014) 231–238, http://dx.doi.org/10.1016/j.jpowsour.2013.10.052.

[86] A. Lidbeck, K.R. Syed, Experimental Characterization of Li-ion Battery cells for Thermal Management in Heavy Duty Hybrid Applications, (Ph.D. thesis), Department of Energy and Environment - Division of Electric Power Engineering, Chalmers University of Technology, 2017, URL http://publications.lib.chalmers.se/records/fulltext/252994/252994.pdf.

[87] K.K. Parsons, Design and Simulation of Passive Thermal Management System for Lithium-Ion Battery Packs on an Unmanned Ground Vehicle, (Ph.D. thesis), Faculty of California Polytechnic State University, 2012, URL https://digitalcommons.calpoly.edu/cgi/viewcontent.cgi?article=1961&context=theses.

[88] M.W. Tahir, Thermal characterization, multi-scale thermal modeling and experimental validation of lithium-ion batteries for automobile application, (Ph.D. thesis), University of Stuttgart, 2016, http://dx.doi.org/10.18419/OPUS-8775.

[89] A. Greco, Numerical and Analytical Modelling of Battery Thermal Management using Passive Cooling Systems, (Ph.D. thesis), Faculty of Science and Technology, Lancaster University, 2015, URL https://eprints.lancs.ac.uk/id/eprint/78600/1/2016AngeloGrecophd.pdf.

[90] akkuteile.de, Panasonic NCR18650 3,6v 2900mah (flat top) ungeschützt, 2020, URL https://www.akkuteile.de/lithium-ionen-akkus/18650/panasonic/panasonic-ncr18650_100605_1206.

[91] E-One Moli Energy, Molicel IHR18650c, 2020, URL https://www.custompower.com/documents/MOLICELIHR18650CDataSheetV1.0LC.pdf.

[92] A. Awarke, M. Jaeger, O. Oezdemir, S. Pischinger, Thermal analysis of a li-ion battery module under realistic EV operating conditions, Int. J. Energy Res. 37 (6) (2013) 617–630, http://dx.doi.org/10.1002/er.2884.

[93] A. Hales, L.B. Diaz, M.W. Marzook, Y. Zhao, Y. Patel, G. Offer, The cell cooling coefficient: A standard to define heat rejection from lithium-ion batteries, J. Electrochem. Soc. 166 (12) (2019) A2383–A2395, http://dx.doi.org/10.1149/2.0191912jes.

[94] P.E. Roth, Thermal Abuse Performance of MOLI, Panasonic and Sanyo 18650 Li-Ion Cells, Sandia National Laboratories, https://prod-ng.sandia.gov/techlib-noauth/access-control.cgi/2004/046721.pdf.

[95] Akkuplus.de, Sony - US26650FTC1 - 3,2 Volt 3000mah LiFePO4, 2020, URL https://akkuplus.de/Sony-US26650FTC1-32-Volt-3000mAh-LiFePO4.

[96] I. Tsiropoulos, D. Tarvydas., N. Lebedeva, Li-ion batteries for mobility and stationary storage applications - Scenarios for costs and market growth, JRC Science for Policy Report, 2018, http://dx.doi.org/10.2760/87175.

[97] C. Minke, T. Turek, Materials, system designs and modelling approaches in techno-economic assessment of all-vanadium redox flow batteries – A review, J. Power Sources 376 (2018) 66–81, http://dx.doi.org/10.1016/j.jpowsour.2017.11.058.

[98] J. Figgener, P. Stenzel, K.-P. Kairies, J. Linßen, D. Haberschusz, O. Wessels, M. Robinius, D. Stolten, D.U. Sauer, The development of stationary battery storage systems in Germany – status 2020, J. Energy Storage 33 (2021) 101982, http://dx.doi.org/10.1016/j.est.2020.101982.

[99] K. Mongird, V. Viswanathan, J. Alam, C. Vartanian, V. Sprenkle, Energy Storage Grand Challenge Cost and Performance Assessment 2020, U.S. Department of Energy / Pacific Northwest National Laboratory, 2020, DOE/PA-0204, URL https://www.pnnl.gov/sites/default/files/media/file/Final20-20ESGC20Cost20Performance20Report2012-11-2020.pdf.